A 3-Dimensional Analysis and Assessment of the Natural Gas Hydrate System in the Kumano Forearc Basin, Offshore Japan, from NanTroSEIZE Drilling and 3D Seismic Data

A THESIS SUBMITTED TO THE GRADUATE DIVISION OF THE UNIVERSITY OF HAWAIʻI AT MĀNOA IN PARTIAL FULFILLMENT OF THE REQUIREMENTS FOR THE DEGREE OF

MASTER OF SCIENCE

IN

GEOLOGY AND GEOPHYSICS

July 2015

By

Katie B. Taladay

Thesis Committee

Gregory F. Moore (Chairperson)
Stephen Masutani
Gregory Ravizza

Keywords: gas hydrates, Kumano Basin, NanTroSEIZE, heat flow, resource assessment

Acknowledgements

This research would not have been possible had it not been for the extraordinary efforts of my adviser Greg Moore to open the door to graduate school for a nontraditional student with little previous knowledge in the geological sciences. I am tremendously grateful for all of the opportunities he has given me to conduct meaningful research, and to engage with the marine science community through workshops, conferences, and his recommendations that helped pave the path to participating in an IODP expedition. These experiences have provided me with a strong foundation in marine geology and the behind the scene efforts that go into science proposals and planning. I will carry each memory and lesson with me always. I am further immensely thankful for the support and wisdom of Dr. Stephen Masutani who graciously opened the door to his laboratory and provided me with financial support which saved me from homelessness and starvation during the beginning and ending of this research. I was a curious student who just really wanted to learn. He gave me that chance, and my world is forever brighter. Dr. Greg Ravizza has also opened doors for me into new worlds of knowledge by introducing me to the field of energy and mineral resource geology. He has been a consistent source of stimulating questions and critiques that have helped to make the research presented herein better.

A project of this scope demands many areas of expertise, and this thesis benefits from the help of Dr. Masataka Kinoshita at JAMSTEC who provided heat flow derivations and Ph.D. candidate Matteo Paganoni at University of Oxford who provided the BGHS equations. Dr. Brian Boston at the University of Hawaii is also credited for his assistance with making the GMT maps, and the many scientists who help to collect the NanTroSEIZE data.

Lastly, I could not have completed this thesis without the support of my friends and family. Despite disappearing for weeks on end you were each always ready to greet me with open arms, dinner, or a phone conversation whenever I needed a break. It was a selfish life phase, but you were tolerant and encouraging. I am blessed. Yet, my deepest gratitude goes to

my mom who taught me that no dream is out of reach so long as you are willing to work hard enough. Whenever I feel I can go no further I think of her, and I push onward.

Abstract

Natural gas hydrates are crystalline inclusion compounds that form within the pore space of marine sediments along continental margins worldwide. These hydrate deposits host highly compressed gas molecules, most commonly methane, and are proposed to be the largest dynamic reservoir of organic carbon on this planet. As such, it is tremendously important for both climate scientists and countries in need of energy security to understand the controls on hydrate formation, stability, and decomposition in response to natural and manmade environmental stresses. This study utilizes industry quality 3-dimensional (3D) seismic reflection data combined with Integrated Ocean Drilling Program (IODP) drilling data collected during the NanTroSEIZE project in the Kumano Forearc Basin, offshore Japan. Our aim is to investigate natural gas hydrate occurrence, the 3D distribution and behavior of the base of gas hydrate stability (BGHS) in response to surface and underlying deformation processes, fluid flow patterns, zones of concentrated hydrate deposits, and a gas in place resource estimate for hydrate concentration zones near the BSR.

Three types of BSRs including upper, lower, and a primary gas hydrate related BSRs were identified and mapped a across a region of 27 km by 11 km. The primary BSR, inferred to be the BGHS, is a widespread, continuous feature, and the depths of the primary BSR clearly show the complex controls that underlying basement deformation from compressional tectonics, and surface sedimentation and mass wasting events exert on the BGHS. Upper BSRs mark paleo-BGHS in the seaward regions, as well as the top of hydrate concentration zones above the BSR in two regions of the basin. Mixed gas, BGHS modeling provides compelling evidence that the lower BSRs could mark a Structure-II methane-ethane gas hydrate BGHS below a Structure-I methane hydrate BGHS. While 3D BSR-derived heat flow values were found to range from 42 -54 mWm^{-2} , which indicates that focused fluid advection is not presently active, drilling and seismic data provide evidence for thermogenic gas migration from depth up into basin sediments. Gas charged fluids are identified in the seismic data as high amplitude reflections (HARS) and low velocity zones beneath the BGHS, and migration appears to proceed as diffuse flow up landward dipping permeable strata, through short-range hydrate recycling in

response to BGHS repositioning and up/laterally outward from deep cutting normal faults. Deep fluids potentially charge the four zones of concentrated gas hydrate deposits identified above the BSR. The hydrate concentration zones (HCZs) presented in this study are analogous to the confirmed methane HCZs in the eastern Nankai Trough, and should be considered highly prospective reservoirs.

Table of Contents

List of Tables

List of Figures

List of Abbreviations

BSR	Bottom Simulating Reflection
BHSZ	Base of gas Hydrate Stability Zone
GH	Gas Hydrate
GTG	Geothermal gradient
HF	Heat flow
IODP	Integrated Ocean Drilling Program; International Ocean Discovery Program
LBSR	Lower Bottom Simulating Reflection
MbBSR	Meters below primary BSR
MBSF	Meters below seafloor
MBSL	Meters below sea level
MTD	Mass transport deposit
NGH	Natural Gas Hydrate – Distinguished from gas hydrates which is often used in short for Methane hydrate. Because the gas hydrate in our system could be composed of other gas, we adopt the term Natural Gas Hydrate.
UBSR	Upper Bottom Simulating Reflection
sI	Structure I methane hydrate
sII	Structure II mixed gas hydrate
WMSF	Wireline meters below seafloor

Chapter 1

Introduction

1. Introduction

1.1 Background and History

Marine sediments host enormous volumes of organic carbon in the form of natural gas, much of which is locked up in dynamic natural gas hydrate (NGH) reservoirs. These reservoirs are formed as a product of a complex biogeochemical system that is not only fascinating from the perspective of scientific inquiry, but is also remarkably important to understand in order to accurately assess and model earth's carbon budget, among other relevant science issues. NGH deposits have primarily enticed global interest because they represent a potentially lucrative, unconventional energy resource (Collett, 2002; Boswell et al., 2009) particularly for countries currently lacking significant indigenous energy reserves, such as Japan and India. Others motives driving NGH research are related to the industrial and societal hazards associated with hydrate formation or decomposition in marine sediments. It is has been proposed that hydrate dissociation could: be a trigger mechanism for inducing tsunamigenic submarine slope failure (McIver, 1982; Sultan et al., 2007; Maslin et al., 2010; Kim et al., 2013); compromise borehole stability (Birchwood et al., 2008); plug natural gas pipelines (e.g., Wenqing et al., 2013); produce a gas kick potentially resulting in industrial blowouts such as the Macondo well, Deepwater Horizon blowout of 2010 (McConnell et al., 2012; Helgeland et al., 2012). On the climate front, NGH deposits could serve as a host reservoir for carbon sequestration (Ota et al., 2005; Komatsu et al., 2013); however, the release of gas from such deposits is a potential contributing factor to ocean acidification (Milkov et al., 2003; Hautala, et al., 2014) and/or climate change (Kennet et al., 2000; Archer, 2007; Archer, 2009). It is essential for both offshore production planning and climate models to understand the conditions of hydrate stability and the kinetics of hydrate equilibration following perturbations. Looking beyond our own planet, planetary scientists studying icy planets, comets and even potential human habitation of Mars have much to gain by studying NGH behavior on earth as a terrestrial analogue (Blake et al., 1991; Max, 2001; Duxbury, et al., 2004; Mousis and Alibert, 2005; Prieto-Ballesteros et al., 2005; Mousis et al., 2010; Sohl, 2010; Zahnle et al., 2014; Day et al., 2015. Mousis et al., 2015).

The product of dissociation of NGH is pure water and natural gas; two key ingredients for life and energy. Thus, understanding the formation, distribution and response behavior of NGHs to perturbations in marine sediments have far-reaching, and worthwhile implications.

NGHs are crystalline inclusion compounds technically known as clathrates that are thermodynamically stable at certain pressure-temperature-salinity conditions for a particular liquid+gas+hydrate three-phase equilibrium boundary, depending on the composite fluid and gas chemistry and surrounding host sediments (Sloan and Koh, 2007; Miyoshi et al., 2007). They are composed of hydrogen-bonded water molecules that form a rigid lattice framework (host), with highly compressed, unbounded gas molecules (guests) inside the cages of the lattice structure (Carroll, 2009) (Fig 1.1). There are a variety of NGH formers found in marine sediments including methane, ethane, pentane, propane, hydrogen, hydrogen sulfide, and carbon dioxide, and the species of gas or gas mixture is very important because it will affect the crystallographic structure of the hydrate and corresponding phase stability. Cubic structure-I (sI) methane hydrates, are by far the most common type of NGH encountered in nature, however cubic structure-II (sII) NGHs, hosting higher order hydrocarbons, have been recovered from the Gulf of Mexico (Macelloni et al., 2015), the Caspian Sea (Diaconescu and Knapp, 2002;) and are hypothesized to exist in other regions.

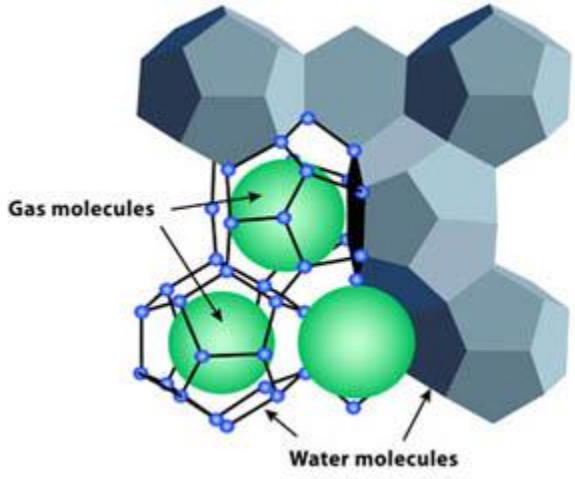

Figure 1.1 - Schematic drawing of a structure I methane hydrate with the gas molecules inside the water lattice structure. Image from http://archive.noc.ac.uk/IPY/background.html

The first documentation of gas hydrates came from the laboratory analyses of Sir Humphrey Davy, a Cornish chemist, in 1810 where he noted that, “The solution of oxymuriatic gas in water freezes more readily than pure water, but the pure gas dried by muriate of lime undergo undergoes no change whatever at a temperature of 40 below 0° of Fahrenheit” (Davy, 1811). In

the 1930s, hydrates became a nuisance to the oil and gas industry because their role in clogging natural gas pipelines (Anderson et al., 2012; Rao et al., 2013). However, it was not until the 1970s, coinciding with the WWII boom in seismic profiling, that submarine NGHs were discovered and associated with bottom simulating reflectors, the seismic expression at the interface between hydrate-bearing and free gas-bearing sediments at Blake Ridge and in the Caspian Sea (Yefremova and Zhizhchenko,1974; Bryan, 1974; Shipley et al., 1979).

Over the past four decades specialized volumes about natural gas hydrates have been written (Henriet and Mienert, 1998; Sloan, 1998; Paull and Dillon, 2001; Max and Johnson, 2006; Sloan and Koh, 2007; Collett et al., 2009; Carroll, 2009; Long et al., 2009; Riedel et al., 2010; Thakur and Rajput, 2010; Giavarini and Hester, 2011; Ojha, 2012; Max and Johnson, 2013), research programs such as the German SUGAR (Submarine Gas hydrate Reservoirs) and the Norwegian CAGE (Centre for Arctic Gas Hydrate, Environment and Climate) have been established, and a series of international field programs led by scientific ocean drilling and industry exploration projects have been conducted. Scientific ocean drilling by the International Ocean Discovery Program and its predecessors (IODP, DSDP, and ODP) has made enormous contributions to our understanding of submarine NGHs- particularly from data collected during ODP legs 66 (Mexico), 76 (Blake Outer Ridge), 84 (Middle America Trench), 96 (Ocra Basin), 112 (Peru Margin), 141 (Chile Triple Junction), 146 (Cascadia), 164 (Blake Outer Ridge), 201 (Peru Slope), 204 (Hydrate Ridge), and IODP Expedition 311 (Cascadia margin). There are more than eight pending active IODP proposals for studying gas hydrates in nature, including: 635-Full3, 781A-Full, 791-APL2, 797-Pre, 806-Pre, 811-Full, 836-APL, 841-APL2 (proposals available online at: http://www.iodp.org/active-proposals). These expeditions have sought (and seek) to define the geological controls, occurrence, abundance, and chemical processes involved in regulating NGH systems. Additionally, industry and government projects including the U.S. Department of Energy (DOE) supported Gulf of Mexico Gas Hydrate Joint Industry Project (JIP) Legs I (2005) (Ruppel et al., 2008) and II (2009) (Frye et al.), the Indian NGHP Expeditions I (2006) (Collett et al., 2015)and II (2015), Ulleung Basin UBGH1 (2007) (Bahk et al., 2011) and UBGH2 (2010) (Ryu et al., 2012; Bahk et al., 2013), Shenhu GH drilling in the Northern South China Sea GMGS-1

(2007) (Wu et al., 2011), and the 2013 gas hydrate production trials offshore in eastern Nankai Trough, Japan (Fujii et al., 2013; Egawa et al., 2015; Fujii et al., 2015; Jun et al., 2015; Kida et al., 2015; Konno et al., 2015a; Konno et al., 2015b.; Ito et al., 2015; Santamarina et al., 2015; Yamamoto, 2015). Each of these research efforts has provided invaluable data that have broaden our knowledge substantially.

From these varied research efforts to study gas hydrates in nature combined with a host of laboratory investigations, it is now well known that NGHs are found worldwide in arctic permafrost regions (10%) and precipitate within the pore space and fracture networks of marine sediments (90%) along continental shelves under favorable conditions of relatively high pressure, low temperature, with a sufficient supply of water and flux of natural gas (usually methane) in excess of solubility (Kvenvolden and Lorenson, 2001; Klauda and Sandler, 2005; Lu and Sultan, 2008). NGH deposits exist in a variety of morphologies including pore-filling, grain-cementing, fracture-filling, massive/nodular forms, and disseminated in fine-grained sediments (Holland et al., 2008; Boswell et al., 2012; Dai et al., 2012). Current consensus is that the largest reservoir for marine hydrates is fine grained sediments where hydrate forms as a diffuse, un-economical deposit (Boswell and Collett, 2011). In terms of modeling carbon fluxes to better understand earth's climate both past and present, the abundance of organic carbon locked up in disseminated NGHs in fine grained sediments is likely the most significant reservoir. However, NGHs in fines has not drawn substantial research attention largely because there is no potential economic benefit from these deposits, they are difficult to synthesize in a laboratory setting, and the disseminated nature makes them difficult to constrain using geophysical methods given the limitations in seismic resolution and imaging capabilities. Potential economic deposits exist in large sand reservoirs (Boswell and Collett, 2011) however, the Japanese production trial of 2013 showed that methane can be recovered from submarine hydrate reservoirs using current technology, but considerable technological advancements, and longer duration production trials are needed to test if NGH reservoirs can be exploited for economic gain or considered for energy security reserves.

Equilibrium of the hydrate phase reflects a dynamic balance between hydrate formation and dissociation, which occurs when the chemical potentials of the hydrate components are uniform across all phase boundaries. Important controls on NGH occurrence and stability are functions of not only the geothermal gradient, pore pressure, and pore water salinity, but also of the amount of total organic carbon (TOC) supply and burial, flux of natural gas from depth, *in situ* gas production, gas solubility with depth, ambient pore water gas saturation, pore water availability, porosity, permeability, sediment grain size, effective stress, sediment thermal conductivity, host mineralogy, and perhaps even the morphology of the hydrate itself (e.g., Weinberger, 2005; Shankar et al., 2010; Sloan et al., 2010; Bahk et al., 2011; Bahk et al., 2013; Bahk et al., 2013b). For a detailed summary of the current state of gas hydrate research, readers are referred to The Consortium Ocean Leadership's (2013) marine methane hydrate field research plan drafted by a consortium of NGH experts.

Despite substantial advances in fundamental scientific knowledge, there is still much progress to be made particularly in regards to gas in place budget estimates and the kinetics of GH formation, dissociation, and dissolution in the natural environment. It is undisputable that NGHs host one of the largest carbon reservoirs on earth, yet there is a pressing need to continue to constrain gas in place estimates with ground-truth data. The global resource estimates of the amount of methane (CH_4) sequestered in dynamic NGH reservoirs controversially range across several orders of magnitude between 1 to 100 trillion m^3 (Boswell and Collett, 2011); however, it is most commonly cited at 20,000 trillion standard m^3 (scm)-, compared to the 368 trillion scm of conventional natural gas reserves remaining on the planet (Buffett and Acher, 2004; Milkov, 2004; Boswell, 2009; Burwicz et al., 2011). Researchers also need to develop a more mature understanding of how NGH reservoirs respond to perturbations to account for the effects of stress from offshore installations, production efforts, climatic changes, and tectonic activity on NGH systems. This will require collaboration across fields to constructively synthesize multidisciplinary datasets in order to build more intricate, dynamic, geological models that can better predict distribution patterns, the geologic conditions

favorable for methane source/production, migration pathways, trapping mechanism, and the physical chemistry and kinetics of NGH stability over time in comparison to laboratory analyses.

The Kumano Forearc Basin, overlying a heavily faulted accretionary prism in an active subduction region of the western Nankai Trough is a superb location to assess a basin scale NGH system by integrating geochemical, geophysical, and geological datasets. The Nankai Trough is arguably the most rigorously studied subduction zone in the world providing a wealth of publically accessible scientific data, and this region is particularly notorious in the NGH community for being home to intensive gas hydrate exploration and characterization efforts costing over 1 billion US dollars (Collett, 2002; Max et al., 2006; Nagakubo, 2009; Fujii et al., 2013). In 2013, the first-ever offshore NGH production trial conducted at Daini Atsumi Knoll in the eastern Nankai Trough succeeded in producing 120,000 m^3 of methane from a gas hydrate concentration zone (Fujii et al., 2015). The reserve of methane locked up in gas hydrates in the eastern Nankai Trough is estimated to be 1.14 trillion m^3 (Fujii et al., 2008) which is roughly equivalent to about 9 years' worth of natural gas supply based on Japan's 2014 consumption levels. Analogous concentration zones are mapped and evaluated in this study.

Concentrated hydrate deposits tend to form at the base of NGH stability which results in a sharp contrast in mechanical properties between NGH saturated layers overlying a zone where free gas and water occupy the pore space. The contrast in properties is expressed in seismic data as a reversed polarity reflection, relative to the seafloor, known as a bottom simulating reflection (BSR). The general consensus is that BSR amplitude strengths are more a product of the occurrence and amount of free gas below the base of gas hydrate stability (BGHS) BGHS than the amount of hydrate above (Holbrook, 2001). Nevertheless, these reflections help researchers to infer the presence of gas hydrate and can be used to evaluate the heat flow of the basin and to guide exploration for potential hydrate concentration zones (HCZs).An industry quality 3D seismic dataset collected across the Kumano Basin in 2006 reveals continuous BSRs, the most robust indicator of hydrate occurrence, over tens of kilometers across the basin. The presence of gas hydrates in the Kumano Basin has already been confirmed in drill cores and at

several seep sites (Ashi et al., 2001; Takahashi et al., 2001; Baba et al., 2004).In addition to the industry quality 3D seismic data, seven NanTroSEIZE drilling expeditions in the Kumano Basin (Tobin and Kinoshita, 2006) have provided theborehole databases needed to constrain seismic interpretations.

The aim of the research presented in this thesis is to utilize the broad spectrum of results from nearly a decade of scientific drilling in the Kumano Forearc Basin, along with supporting evidence from other gas hydrate-bearing margin studies, to constrain new, regional seismic interpretations of the NGH system in this region. To meet this objective we use the combined datasets to extract BSR-derived heat flow estimates, gas source analysis, fluid flow mechanisms and pathways, and the spatial distribution of hydrate concentration zones above the BSR, and perform a volumetric resource estimate for gas in place in the HCZs. We further explore the regional extent and character of several different types of BSRs, and attempt to employ the BSRs as a proxy for environmental/tectonic disturbances with the end goal of answering the following questions:

1. How do subsurface heat flow, tectonic activity, sedimentation patterns, and surface processes associated with mass wasting and erosion affect the base of hydrate stability and correlative BSR depths and distribution?

2. Is there any active migration of free gas or fluid advection from depth? If so, then can we identify these pathways and their relationship to gas hydrate occurrence?

3. What is the cause of the double BSRs in the Kumano Basin? Are double BSRs paleo-boundaries of gas hydrate stability, active hydrate boundaries out of thermal equilibrium, the base of a thick gas layer, or a structure-II NGH boundary coexisting with an overlying structure-I NGH boundary?

1.2 Thesis Outline

This thesis is divided into 8 chapters:

Chapter 1- introduces the history and current status of natural gas hydrate research, the motivations behind this study, and the research objectives to be addressed herein.

Chapter 2- provides a regional geologic framework surrounding our study region. This includes the tectonic environment, observations of the stratigraphic architecture as revealed in the seismic data, a composite outline of reported significant events that have contributed to the formation of the Kumano Forearc Basin, and the importance of each of the aforementioned to gas hydrate formation and stability evolution.

Chapter 3- lays out the methods of data collection, processing, interpretation, and modeling employed throughout this study.

Chapter 4 - presents both shipboard and shore-based gas hydrate-relevant data results from the many NanTroSEIZE drilling expeditions at Sites C0002 and C0009 organized by data type including: pore fluid geochemistry, gas geochemistry, core material evidence for hydrates, downhole logging evidence for hydrates, documented free gas occurrence, and downhole lithology. New 3D seismic maps and observations regarding the extent and various classes of BSRs are also presented in this chapter.

Chapter 5 - discusses the implications of the data results outlined in Chapter 4, and further considers some of the potential data errors, possible interpretations, and clearly states which points of interpretation are unable to be confirmed, we reject, or we accept and use in our modeling and hydrate petroleum system analyses in Chapters 6 and 7.

Chapter 6 – extrapolates the data results interpretations outlined in Chapters 4 and 5 to 3D space by employing models. We first model the BGHS using Sloan's publicly available CSMHYD software using drilling defined parameters. Eight different scenarios for gas mixtures and geothermal gradients are modeled and compared to the primary BSR and the double BSRs to determine the nature of the BSRs (sI or sII) and to identify discrepancies between the modeled BGHS and the observed BSR. We then utilize the mapped primary BSR as a proxy for heat flow and potential fluid flow pathways. The heat flow derivation map is presented and the spatial distribution of high and low heat flow relative to surface and subsurface structures is explored using the 3D seismic amplitude volume.

Chapter 7 - integrates data results, interpretations, and modeling results from Chapters 4 through 6 to construct a basin-scale natural gas hydrate system assessment using a petroleum system approach. This assessment considers gas source, migration mechanisms and pathways, zone of free gas and gas hydrate accumulation, and a first order volumetric gas in place resource estimate for the hydrate concentration zones mapped in the basin. Ultimately, the goal is to constrain the controls on gas hydrate stability, the overall thickness of the gas hydrate stability zone (GHSZ) based on BSR depths, BSR response to environmental disturbances, and the volume of gas sequestered in hydrate concentration zones immediately above the BSR where hydrates are most susceptible to perturbations- each of which are important input parameters for carbon-cycling models, resource estimates, and geo-hazard assessments.

Chapter 8 - concludes this research with a summary of the significant findings.

Chapter 2

Geologic Setting

2. Geologic Setting

2.1 Tectonic Environment

The Kumano Forearc Basin (FAB) is a ridge FAB (e.g., Dickinson, 1995) off Kii Peninsula, Japan. It overlays a late Miocene aged accretionary prism within an active subduction complex in the Nankai Tough- which is formed by the oblique subduction of the ~15 Ma aged Philippine Sea Plate beneath the Eurasian Plate at a rate of about 4.0-6.5 cm/year (Seno et al., 1993; Miyazaki and Heki, 2001). Sediments are being incorporated into the thickening accretionary prism that is presently >100 km wide by means of compaction (Taira, 2001; Strasser et al., 2014). Underwood and Moore (2012) reported that broadly similar conditions are encountered in the Cascadia Basin, Aleutian Trench, Sunda Trench and Southern Chile which are also known gas hydrate-bearing regions.

NGHs are widely distributed in such accretionary prism and overlying forearc basins settings because subduction zone compressional tectonics produce fracture and fault networks that can act as fluid migration pathways from depth enabling the delivery of gas-charged fluids into the hydrate stability zone (Booth et al., 1998; Kastner, 2001; Yamada et al., 2014). These fluids are often rich in chemical compounds including methane and potentially other higher C_2+ hydrocarbons such as ethane and pentane (Saffer and Tobin, 2011; Kastner et al., 2015). The Nankai Trough is the largest known methane hydrate bearing zone offshore Japan, and has a history of enormous, megathrust earthquakes (M>8.0) with a recurrence interval of 100 to 200 years and concomitant fluid expulsion generation potential as a result of compressive stress induced compaction (increases pore pressure) and mineral dehydration (Ando, 1975; Baba and Cummins, 2005; Saffer and Tobin, 2011; Fischer et al., 2013). Seismic surveys across the Nankai Trough have shown extensive reversed polarity BSRs suggesting widespread occurrence of gas hydrate with free gas accumulation below (Fig. 2.1 and 2.2)

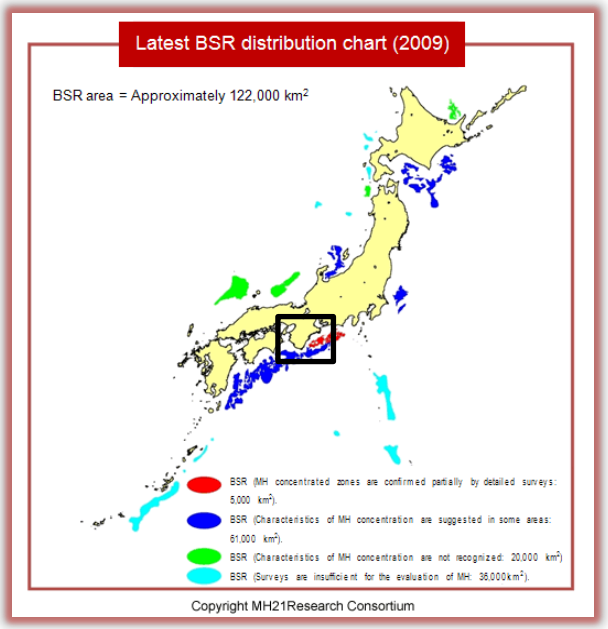

Figure 2.1 - Most recent offshore BSR distribution map from the MH21 Research Consortium. Kii peninsula and the Kumano Basin is outlined in black. Blow up of the black box with seafloor bathymetry and survey locations is presented in fig. 2.2

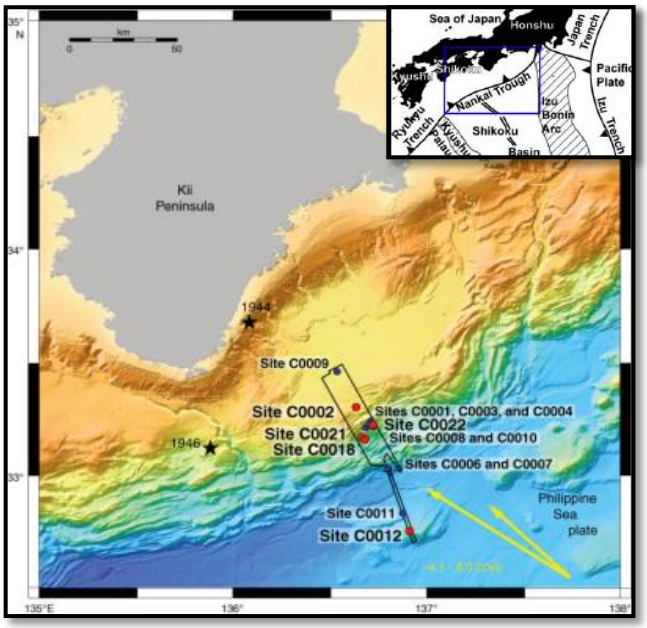

Figure 2.2 - A bathymetric map of a portion of the Nankai Trough with the 57 km by 12 km 3D seismic survey area outlined (black rectangle). This study focuses on the landward half of the survey in the forearc basin region. IODP NanTroSEIZE drill sites are indicated by red dots. Drilling data to support this study are taken from IODP Sites C0002 and C0009.

2.2 Basin Morphology and Evolution

Understanding the structural and stratigraphic evolution of a basin and the complex interplay between sediment delivery and basin architecture is essential for deducing fluid and solid material budgets, and for constraining potential hydrocarbon source, maturation, migration pathways, and trapping mechanisms. The Kumano Basin's evolutionary history is complicated, and not yet fully resolved, but it is generally accepted that the accommodation space was formed when uplift along the megasplay fault created a barrier to sediment delivery to the trench at around ~1.95 ma (Moore et al., 2007; Strasser et al., 2009; Gulick et al., 2010; Moore et al., in press). At present, the basin is filled with ~2 km of pelagic and hemipelagic muds intercalated with clastic turbidites and thin ash layers (Strasser et al., 2014). Basin strata

are severed by a series of recently active, deep-cutting normal faults with offsets of 5 -30 meters (Moore et al., 2013). Small scale faults in the accretionary wedge have been determined to be the youngest deformational structures (Hayman et al., 2012).

The morphology of the basin is controlled by accretionary, strike-slip tectonics, while the basin fill is characterized by a submarine fan turbidite depositional system delivering sediments from Kii Peninsula via large submarine canyons (Fig. 2.3). There have been significant fluctuations to sediment provenance and shifts in delivery pathways and rerouting since the basin's initiation (Fergusson, 2003; Clift et al., 2013 (zircon and apatite thermochronology); Usman et al., 2014; Buchs et al., 2015 (detrital pyroexenes). A margin-wide assessment conducted by Takano et al. (2013) shows that the submarine fans have transformed over time from a braided channel-dominated system to a small fan dominated system with shrinking separated small basins; to a trough-fill turbidite system; to a channel-levee system. These changes in depositional processes undoubtedly affect the spatio-temporal delivery of organic matter. While sedimentation rates are not well constrained, we do have some biostratigraphic age constraints obtained at Sites C0009 and C0002 which tag these sediments as Quaternary to modern in age (Saffer et al., 2010; Ramirez, et al 2015, Moore et al., 2015). At present, the basin extends from about 70 km north to south and 100 km east to west (Tobin et al., 2009).

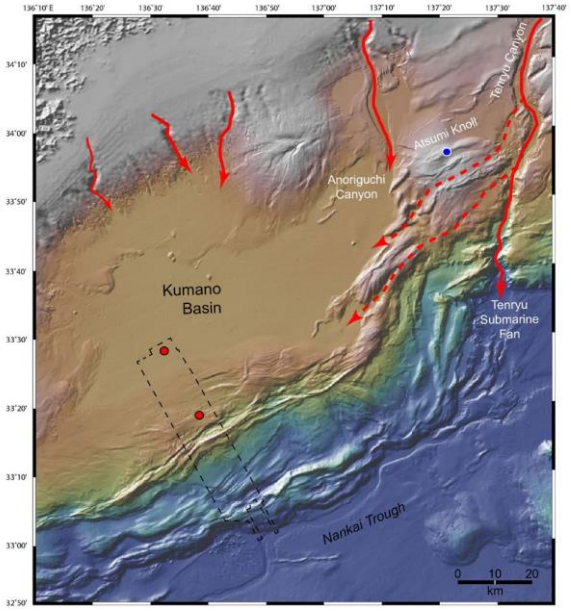

Figure 2.3 - Kumano Basin area with major sediment dispersal pathways shown in red (present = solid line, possible past pathways = dashed lines; Egawa et al., 2013; Noguchi et al., 2011; Takano et al., 2013; Usman et al., 2014). Red dots are IODP drill sites, blue dot is Atsumi Knoll drill site. Figure from Moore et al., 2015.

The 3D seismic data reveal an archive of complex interactions between sedimentation and deformation processes that together controls not only the stratigraphic architecture of the basin, but also the evolution of hydrate stability conditions. Currently, the seafloor is relative flat at ~2000 m water depth and has been well imaged by side-scan sonar, swath bathymetry, and seismic surveys (Ashi et al., 2002; Morita et al., 2004; Taira et al., 2005). The surface morphology shows several large scale mass transport deposit (MTD) scars, while the seismic data reveals that buried MTDs, all locally sourced, are common throughout the basin in depths between 140-700 meters below seafloor (mbsf) (Moore and Strasser, 2015). These MTDs undoubtedly affect GH occurrence, fluid flow behavior, and GH recycling processes.

The basin has been divided into 12 sequences based on the seismic sequence stratigraphy work of Gulick et al. (2010) and Moore et al. (2015) which can more broadly be grouped into two major units each with three subunits (Ramirez et al., 2015): Upper Basin Sediments – UB1, UB2, UB3 and Lower Basin Sediments LB1, LB2, LB3 (Fig. 2.4). Major unconformities and facies changes imaged in the 3D seismic volume points to specific phases of Kumano's basin development (Bangs et al. 2004; Gulick et al. 2010; Taladay et. al 2014; Ramirez et. al 2015; Moore et. al 2015). These phases can be divided into 7 stages of events (Table 1)

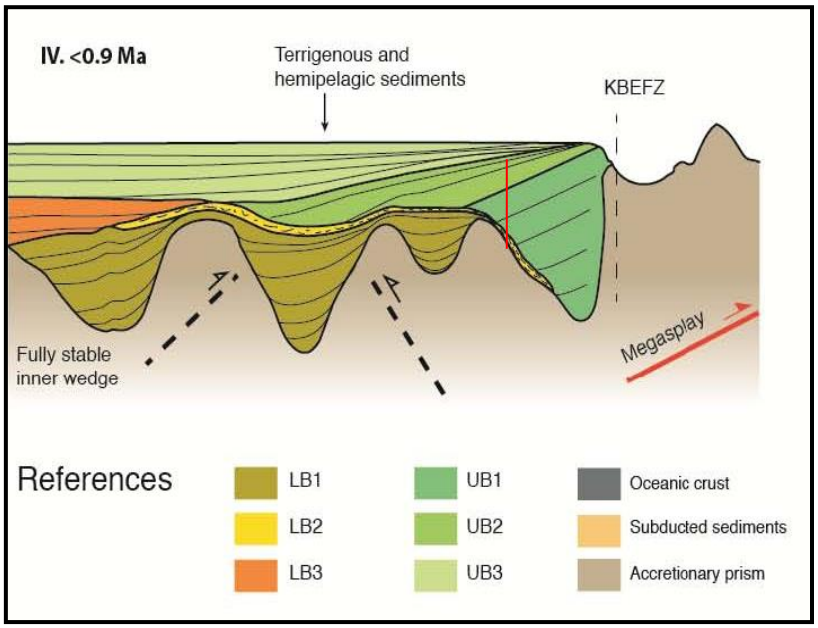

Figure 2.4 - Modified Schematic drawing from Ramirez et al., 2015. Highlights the thick organic rich lower basin sediment sequences (LB1-LB3) which are very thin (condensed slope sediment section) at Site C0002 (red line)

Table 1 - Chronological summary of significant geologic events during the evolution of the Kumano Basin

Stage	Process	Timing	Description
1	*Accretionary Prism Development*	8.0 – 6.0 Ma	Izu-Bonin Arc collided with the Honshu Arc at 12 Ma with four major episodes of accretion occurring at 8-6, 5-3, an 1 Ma (Usman, 2014)
			Subduction Initiation (Yoshioka et al., 2013)
		7.0 Ma Late Miocene	The accretionary prism is formed by offscraping and underplating of materials from trough fill turbidites and hemipelagic sediments of the Shikoku basin on the subducting plate; a former back-arc basin related to the adjacent Japan subduction zone (Baba and Yamada, 2004).
			Margin-parallel shortening to margin-oblique shortening caused by changes in plate motion from >5.6 Ma: Northward direction with thrust-sense shear zones to <3.8 Ma: Northwestward direction with faults and block rotation (Hayman et al., 2012).
2	*Incipient Slope Basin*	Early-Late Pliocene	*Depositional Style:* Braided Channel Type With large amounts of clastic supply (Noguchi et al., 2011)
3	Forearc Basin Initiation		Synchronous with uplift along the megasplay fault: creating a damn that provides the accommodation space for sediments to accumulate (Moore et al., 2007).
			Increase in subduction rate (Kimura et al., 2005)
		4 Ma	Slow hemipelagic sedimentation (Underwood and Moore, 2012).
		3.8-1.67 Ma	Change in direction of motion of the Philippine Sea Plate (Takahashi, 2006)
		3.0 Ma	Trench-Slope basin (Buchs et al.,2015). Variable relief in basement provided space for turbidite accumulation (Ike et al., 2008)

		1.93 Ma	
4	*Early Trench Slope Sedimentation*	Early Pliocene	Compressional Stage, folding *Depositional Style*: Shrinking Small Fans (debris fans & MTDs) Takano et al.
		Mid Pleistocene	Relaxation phase, variable subsidence over space and time, overall widening of the basin (Hayman et al., 2012). Simultaneous lower and upper basin deposition (Ramirez et al., 2015).
		Late Pleistocene	Gently inclined slope basin. Trench slope sedimentation and early accumulation of forearc basin strata. Burial of woody organic material, Glauconite (Ramirez et al., 2015). *Style:* Channel Levee System (lobes, sandy sheet turbidites) (Takano et al., 2013)
5	*Upper Basin Sedimentation and Progressive Tilting*	Early Quaternary	Compressional Stage, shortening, slip along the megasplay fault.
		Mid Pleistocene	Relaxation phase, variable subsidence over space and time, overall widening of the basin (Hayman et al., 2012). Simultaneous lower and upper basin deposition (Ramirez et al., 2015).
		1.6 Ma	Turbidite deposition began
		1.55-1.24 Ma	Splay fault inactive 1.55-1.24 Ma. Reactivated at ~1.24 Ma (Strasser et al., 2009).
		1.3-1.0 Ma	5-8 degrees of tilting, migration of the depocenter (Gulick et al., 2010) indicative of an uplift regime.
		1.0 Ma	Decoupling of sediment routing pattern from transvers to long-distance axial flow (Usman et al., 2014). Buried thrust fault activated (Boston et al., 2011).
		0.9 Ma	*Depositional Style:* Trough-Fill Turbidites

			(muddy sheet fans) (Takano et al., 2013)
6	Faulting	Late Quaternary to Modern	Northward tilted sequences are truncated by an erosional surface and cut by normal faults (Park et al., 2002). Normal Faults from gravitational response to uplift or as a by-product of sediment underthrusting (Bangs et al., 2009; Byrne et al., 2009) NE trending: initial uplift; ENE trending: later phase (ongoing) (Gulick et al., 2010).
		0.44 Ma	Oldest of three phases of normal faulting. 70% of total fault populations are landward-dipping (Sacks et al., 2013)
		0.43 Ma	Buried thrust fault activity ceases (Ramirez et al., 2015). Four phases of normal faulting. Horizontal extension <2% concentrated at the seaward edge (Moore et al., 2013)
7	Present Day Configuration		Kumano Basin Edge Fault Zone- A right-lateral transtensional. Appears as a topographic notch in the 3D seismic data (Moore et al., 2009; Tsuji et al., 2014)

The segregation of fault activity into three phases may have implications for fluid expulsion events, fluid migration, heat flow, and hydrate precipitation. The topic of fault behavior is explored more in Chapter 6.

Sea level changes in the late Pleistocene and Holocene affect sediment transport (Omura and Ikahara 2010; Strasser,) which is important because highstands are generally associated with lower turbidite disposition and thus a low delivery of organic matter. While turbidite deposition at Site C0009 appears to be cyclic in nature, the biostratigraphy is too coarse to pinpoint if depositional cycles are controlled by Milankovich forcing (Moore et al., in Press). Most important for this study, however, is that sea level changes are insignificant in terms of affecting the base of gas hydrate stability (BGHS) in the Kumano Basin because the

seafloor is at ~2,000 m water depth; so even 100 m of sea level rise or fall would have a negligible effect on pressure at the BGHS.

In addition to the geomorphology, and the structural and stratigraphic architecture, the sedimentary fabric is a key reservoir parameter; turbidites, ash layers, and channel fill sediments are each prime targets for NGH and free gas reservoirs in marine environments, and in the absence of enough total organic carbon (< 0.5 wt%) migration of gas from depth through either focused or diffuse fluid flow, or hydrate recycling instigated by rapid changes in sedimentation or tectonic uplift/subsidence is vital to support a concentrated gas hydrate system (Fujii et al., 2009a,b; Takano et al., 2009, Johnson et al., 2014). Each of the geologic elements necessary to support a robust NGH system, including deep water (high pressure), cold bottom waters (2°C), turbidite depositional system, gas hydrate recycling provocations via tectonic perturbations, and potential fluid expulsion events with gas migration routes from depth are present in our study region.

The presence of mud volcanism, bright spots over anticlinal structures and ethane in increasing concentrations with depth are supportive evidence of thermogenic gas migration upward into the basin sediments which, in high enough concentrations, could lead to the formation of DBSRs by virtue of variable phase stabilities unique to sI and sII gas hydrates

Chapter 3

Data Acquisition and Interpretation Methods

3: Data Acquisition and Interpretation Methods

3.1 IODP Borehole Data

Borehole data collected onboard the drillship D/V Chikyu, provides essential constraints for the regional seismic interpretations presented in this study including standard geochemical, geophysical, and sedimentological analyses along with post expedition research results from Sites C0002 and C0009 (Fig. 3.1).

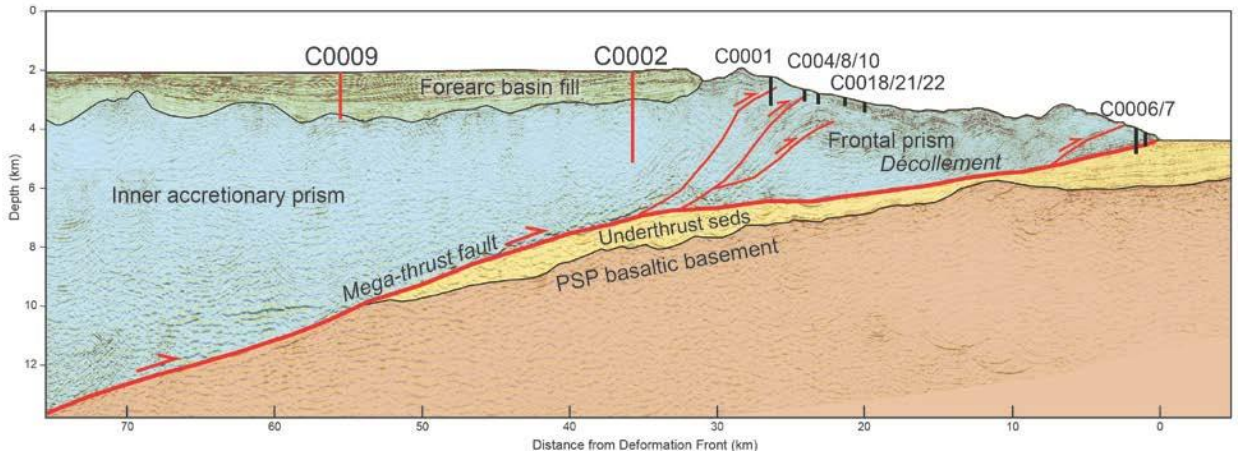

Figure 3.1 - Regional 2-D seismic line KR0108-5, showing IODP Sites studied in this paper (red) in relation to all other NanTroSEIZE drill sites along the Kumano transect (black). PSP = Philippine Sea Plate. Modified from Park et al (2002), Nakanishi et al. (2008), and Moore et al. (2014).

3.1.1 Natural Gas Hydrate Proxies

Because of the ephemeral nature of NGHs, without pressure cores to recover deposits under nearly *in situ* pressure, temperature, and effective stress conditions (e.g., Santamarina et al., 2015), studies have had to rely on a number of now established proxies for detecting and estimating the volume of NGH pore space occupancy (saturation) in marine sediments (e.g., Riedel et al., 2005). These proxies are rooted in geochemical (e.g., Dickens et al., 1997; Milkov et al., 2003), geophysical (e.g., Kumar et al., 2009; Collett, 2001), and sediment physical property data (e.g., Piñero et al., 2007).

The most commonly used geochemical indicator for NGH occurrence is a Cl- freshening anomaly in interstitial water (IW) samples relative to seawater values, or some defined baseline (e.g., Kastner et al., 1995; Ussler and Paull, 2001; Kim et al. 2013). This method is based on the premise that NGH formation excludes ions. By assuming that the fresh water pulse detected in shipboard IW ion chromatography measurements reflects a 1:1 relationship to GH dissociation in recovered cores (e.g. Ussler and Paull, 2001; Tréhu et al., 2004; Torres et al., 2008) via

$$M_{\mathrm{cl}} = 1 - \mathrm{Cl}_m/\mathrm{Cl}_b$$

whereby M_{cl} is the volume of pure water from dissociated hydrate, Cl_m is the measured chloride concentration and Cl_b is the chloride baseline, hydrate saturation can be determined. However, there are a number of diagenetic processes that also result in pore fluid freshening and, thus, it is essential that Cl- data is supplemented by oxygen and hydrogen isotopic data to confirm that the freshening is from GH dissociation versus, say, clay dewatering or other hydrous silica dehydration reactions (Kastner, 1995b.; Malinverno et al., 2008; Solomon et al., 2014; Kinoshita et al., 2015). During hydrate formation $\delta^{18}O$, is preferentially incorporated into the hydrate structure while the surrounding pore fluids become depleted in $\delta^{18}O$ relative to VSMOW (e.g., Solomon et al., 2014). In the case of hydrate-fractionated released waters, $\delta^{18}O$ and δD will follow the same trend (not magnitude) of relative enrichment, whereas in the case of freshening from silica dehydration reactions, $\delta^{18}O$ and δD will exhibit an inverse relationship with more enriched $\delta^{18}O$ and values coinciding with more depleted values for δD.

Gas chromatography is another tool used to infer the presence of gas hydrates and to estimate the composition of hydrate-bound gases (e.g., see Pape et al., 2010). Headspace (routine) and void space (select scenarios) gases are analyzed for the molar ratio of C_1/C_2+ hydrocarbons to determine gas origins and hydrate thermodynamic stability (Bernard et al., 1976). The stable carbon isotopic composition of gas samples is used to distinguishing whether the gas source is from biogenic (highly fractionated) or thermogenic (less fractionated) production; however, there are potential errors with this method which are discussed in more detail in Chapter 7.

The Kumano basin expeditions are unique compared to other hydrate related expeditions because of the drilling vessel used. The D/V Chikyu operates a riser system. This means that IODP Expeditions 319, 338 and 348 also had the opportunity to engage with mud gas monitoring data which, like headspace measurements, is useful for making *qualitative* assessments about *in situ* gas composition (Erzinger et al., 2006), assuming the mud is circulated properly to avoid contamination from passing through gas rich zones.

An important limiting factor of NGH precipitation is the amount of TOC in marine sediments. Johnson et al. (2014) estimates that at least 5 wt% of TOC is needed to support a hydrate system without any additional gas input from recycling or advection. The bioavailability of organic carbon is necessary for microbial production of methane and also, the more organic carbon buried to deep depths, the greater the potential amount of hydrocarbon production becomes from thermal cracking. TOC is measured on the ship using a Thermo Finnigan Flash elemental analysis (EA) 1112 carbon-hydrogen-nitrogen-sulfur analyzer (see methods section Strasser et al., 2014).

Borehole logging offers a window into *in situ* hydrate distribution and abundance; however, this method of geophysical detection is contingent on the type of tool used, whether logs were collected through logging while drilling (LWD) tools or after drilling with wireline logs (WL), and further depends on hydrate morphology, pore space saturation relative to the surrounding sediment matrix, and borehole conditions (Goldberg and Saito, 1998; Bahk et al., 2013). The most commonly used suite of geophysical logs for estimating hydrate saturation are electrical resistivity logs, gamma ray density logs and temperature measurements, and sonic velocity logs with P-wave values of 2000-3,800 m/s (Lee and Collett 2001) as compared to the velocity of a gas saturated layer at ~1000-1500 m/s and seawater saturated sediments at ~1500 m/s. Because gas hydrates are electrically more resistant than their surrounding host sediments, their presence produces high resistivity spikes, along with an increase in P-wave velocities because the sonic velocity through hydrate saturated sediments is higher than water saturated sediments (e.g. Zhang and Han, 2010). To affirm that the log response is from gas hydrate occurrence, the density and porosity logs should also be investigated because hydrate

occurrence will result in a slight increase in density and neutron porosity, and a decrease in nuclear magnetic resonance porosity (Fujii et al., 2009b). Well log quantification of gas hydrates has also become a common practice (e.g. Kumar et al., 2009); however, there are often disagreements between well log and pore water saturation estimates (Paull et al., 2000b; Lee and Collett, 2006; Kumar et al., 2009). Downhole logs are particularly prone to higher estimation errors with decreasing hydrate saturations (Lee and Collett, 2001). Another geophysical detection method exploits the endothermic nature of hydrate dissociation by using thermal infrared scanning to detect cold spot anomalies in recovered cores (e.g., Ford et al., 2003; Tréhu et al., 2004; Riedel et al., 2011). Infrared scanning measures the thermal radiation of the core, which is a function of its surface temperature.

A lithological proxy for NGH occurrence in sediment cores is the presence of soupy or moussey textural fabric as a result of the release of water and gas expansion during core retrieval (Tréhu et al., 2003; Peñero et al., 2007) (Fig. 3.2).

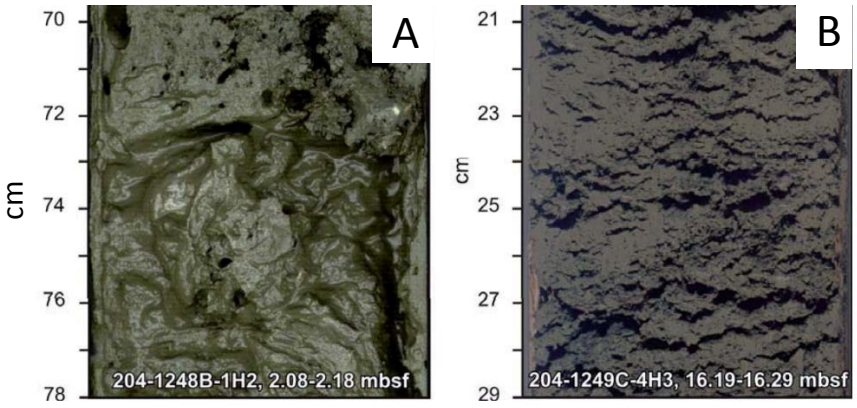

Figure 3.2 - Sedimentary disturbance fabrics attributed to hydrate dissociation from Hydrate Ridge, ODP Leg 204. A= Soupy, B= Mousse like. Figure modified from Tréhu et al., 2003. Cores are from hydrate-bearing sediments offshore Cascadia.

It is important to keep in mind that a key source of error for each proxy assessment is related to baseline assumptions which are often elusive and require an intimate understanding of the background geologic and chemical environment.

3.2 3D Seismic Data

Seismic imaging is an important exploration tool for identifying gas hydrates (Riedel et al., 2010; Spence et al., 2010) because both gas hydrates (high p-wave velocity) and free gas (low p-wave velocity) alter the physical properties of sediments which affects the travel path and attenuation of the seismic wavelet. Industry quality, 3D reflection seismic data are used in this study to map geologic horizons, bottom simulating reflections, and to evaluate gas hydrate and free gas occurrence using seismic amplitude and attribute analyses. Localized high amplitude reflections (HARs) serve as direct hydrocarbon indicators for free gas when below the hydrate stability zone, and likely indicators of gas hydrate when occurring within the GHSZ (Saeki et al., 2008; Tsuji et al., 2009; Spence et al., 2010). Hydrate within the GHSZ in low concentrations may also appear as a "blank" zone, but these zones are not target reservoir prospects. The sub-surface distribution of free gas and corresponding gas hydrates is further evidenced by the complex distribution of BSRs, variable BSR amplitude strength, and phase reversals in dipping beds crossing the BSR (see Fig. 3.3). Free gas is known to significantly attenuate the seismic wavelet, and blank zones below the BSR can appear if there is a thick free gas zone below the BSR (Matsushima, 2006).

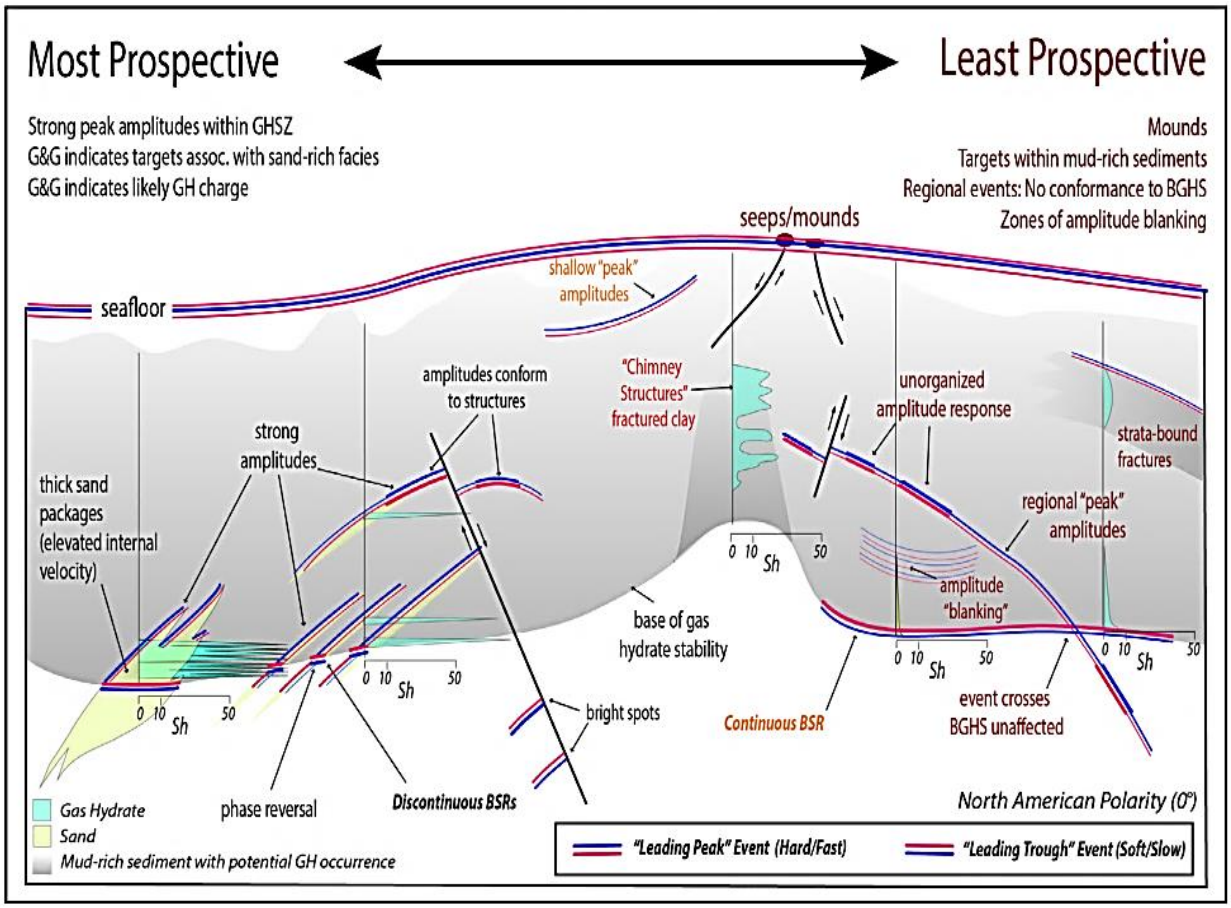

Figure 3.3 - Schematic of geophysical features commonly observed in the shallow subsurface and their relationship to most to least prospective for gas hydrate reservoirs. The concepts illustrated above were successfully tested during the 2009 Gulf of Mexico Hydrates Joint Industry Project. In addition to IODP borehole constraints, we adopt this gas hydrate exploration seismic interpretation model from Boswell et al., 2014.

3.2.1 Acquisition

The 3D seismic reflection survey was carried out by Petroleum GeoServices (PGS) in 2006 (Moore et al., 2009) in preparation for NanTroSEIZE drilling and site selection. The resulting volume is of unparalleled quality in academia, covering a geographical area of 12X 56 km with 12.5 meters between inlines (oriented NW-SE) and 18.75 meters between crosslines (SW-NE) with excellent shallow resolution of 5-7 m (Moore et al., 2009). Two arrays of 28 Sodera G-guns fired alternatively at 37.5 m intervals, and four 4500 m long hydrophone cables with 360 receivers grouped at 12.5 m spacing received the seismic source. This setup of 4-

streamers per 2-sources produced 8 common midpoint (CMP) profiles per sail line with a spacing of 37.5 m and 30-fold data. Frequency range was 40-50 Hz for the BSR depths. The entire survey area is oriented at 330.1^{o}

3.2.2 Data Processing

The data were processed by CGG geophysical services and was corrected for noise and gain. Normal moveout was applied and binned traces were stacked following velocity analysis. The data was migrated using 3D anisotropic Kirchhoff pre-stack time migration (PSTM) with 4 km aperture to migrate the reflections to the correct position in both inline and crossline directions. Later the data underwent 3D pre-stack depth migrated (PSDM). The PSDM volume, with 12.5m between crosslines and 18.75 m between inlines is used in this study.

3.2.3 BSR Horizon Picking and Mapping

High resolution 3D seismic data enabled identification and mapping of three types of BSRs presented herein, including a GH related boundary referred to as the primary BSR. Interestingly, these reflections were barely identifiable in earlier 2D surveys (e.g. Park et al., 2002) which is a significant point, because it is possible that other margin surveys may have also missed imaging BSRs given the frequency used during 2D seismic acquisition. Seismic interference from the presence of a complex fault network in the center of the survey made automatic tracking of the primary-BSR impossible. It was therefore necessary to manually pick BSRs in the inlines and to confirm correct picks by cross-checking picks in the crosslines. BSR horizons were manually picked on every inline in the PSDM 3D seismic amplitude volume (IL2150-IL2720) across an area of ~ 27 km by 12 km. In regions where BSRs were difficult to see in the amplitude volume because of fault interference, picking was guided by use of a Signal Envelope attribute volume (Taladay and Moore, 2015). Interpolation of the BSR was made in one region across a syncline where no BSR was imaged. All picks were made using Paradigm 3D Canvas Seismic Software, and the BSR maps were created using Generic Mapping Tools

software (GMT) (Wessel and Smith, 2013). The specifics regarding any applied smoothing in GMT are noted in figure captions.

3.2.4 Attribute Analysis

Seismic attributes with well control can be translated into petrophysical properties making attribute analysis a powerful tool for revealing subtle features that might be lost in the amplitude volume, and thus attributes can enhance the insight behind an interpretation (e.g., Chopra and Marfurt, 2006). A seismic signal is composed of three properties: amplitude (energy), phase, and frequency. Attributes exploit one or more of these properties by breaking up the seismic waveform into components of frequency, energy and phase (explained by Taner, 2001). To supplement the amplitude analyses, this study employs the Signal Envelope (E) (also known as reflection strength) attribute which is a complex trace attribute calculated by the formula: $E(t)=SQRT\{T^2(t)+H^2(t)$) (Subrahmanayam and Rao, 2008) where E(t) = the signal envelope, *T(t)* = seismic trace, *H(t)* = Hilbert's transformation of T(t) which is a 90° phase shift of T(t). It is proportional in magnitude to the reflection coefficient and represents the instantaneous energy of the signal. This serves to highlight acoustic impedance as a result of gas accumulation, or significant hydrate accumulation.

3.2.5 Velocity Analysis

The velocity volume was generated as a step in the processing stage, but is also very useful as a standalone for interpretation. The minimal interval velocity is set at 1200 ms^{-1} to 3000 ms^{-1}. GH compressional velocity (Vp) is typically between 2000-4500 ms^{-1}, whereas Vp through free gas is rather low at ~1450 ms^{-1} (Rajput et al., 2010). The typical Vp of sediments common beneath the seafloor fall within the 1600-1800 ms^{-1} range.

3.3 Base of Gas Hydrate Stability (BGHS) Modeling

We computed an estimated BGHS surface using laboratory-derived stability conditions of Sloan (1998) using the CSMHYD software for a 0-30°C (273-303 K) temperature range,

constant seawater salinity of 35‰ and four gas mixture compositions, three of which produce sI hydrate and one sII hydrate (Table 2). Pressure was then converted to depth considering 33° latitude gravity and standard atmospheric and hydrostatic pressures with a water density of 1024 kb/m^3. A 5^{th} or 6^{th} degree polynomial equation (temperature vs. depth) was developed for each gas composition (R^2>0.99998) (Table 2). Intersections between the four temperature vs. depth stability functions and two geothermal gradient functions (40° C/km from Expedition 338 (Strasser et al., 2014) and 43° C/km from Expedition 315 Scientists (2010)) were measured each 100 m for an interval of 500-5000 m water depth and two 6^{th} degree polynomial equations (seabed vs. BGHS depth) were obtained for each composition (Table 2). The resulting eight seabed vs. BGHS depth equations were imported into Paradigm 3D Canvas and compared to the interpreted BSRs.

Table 2 - Seabed depth vs BGHS depth for 4 different gas compositions each at 2 geothermal gradients. x= seabed depth (meters below sea level); y = BGHS depth

VENT GAS COMPOSITION \ GEOTHERMAL GRADIENT	40 ˚C/km	43 ˚C/km
100% C_1 **(Structure I hydrate is formed)**	$0.000000000000000000730247329081x^6+$ $0.000000000000013544910335046 2x^5+$ $0.000000000101343440392194x^4+$ $0.000000392681482336927x^3+$ $0.00084555792753603 7x^2+$ 2.06036992993061x+ 207.763089463891 R^2 = 0.999999052282181	y = $0.000000000000000000378375532849x^6+$ $0.000000000000007446179445506 25x^5+$ $0.000000000596424704818147x^4+$ $0.000000250421952762 24x^3+$ $0.00059391845857299x^2+$ 1.84050026151520x+ 163.082602106908 R^2 = 0.999993782550491
98%C_1, 2%C_2 **(Structure I hydrate is formed)**	y = $0.000000000000000000574637317252x^6+$ $0.000000000000010684268728 1814x^5+$ $0.000000000802252114315739x^4+$ $0.000000312652958598879x^3+$ $0.00068055973259207 7x^2+$ 1.88051593476179x+ 111.047775785852 R^2 = 0.99999943569754	y = $0.000000000000000000547332427029x^6+$ $0.000000000000010178597718 5618x^5+$ $0.000000000764448130296091x^4+$ $0.000000297976113840931x^3+$ $0.00064857594251954 8x^2+$ 1.83745397907127x+ 115.532667737074 R^2 = 0.999999489358172
96%C_1, 4%C_2 **(Structure I hydrate is formed)**	y = $0.000000000000000000465168768332x^6+$ $0.000000000000008669841189927 21x^5+$ $0.000000000653309360177785x^4+$ $0.000000256063105566708x^3+$ $0.00056328408660190 6x^2+$ 1.75114291839257x+ 37.9016099512337 R^2 = 0.999999646542576	$0.000000000000000000449157661805x^6+$ $0.000000000000008369589043712 55x^5+$ $0.000000000630455591423943x^4+$ $0.000000246940382529728x^3+$ $0.00054242394189038 8x^2+$ 1.71967056943482x+ 48.2304416274674 R^2 = 0.999999667384746000000000000
95%C_1, 4%C_2, 1%C_3 **(Structure II hydrate is formed)**	y = $0.000000000000000000204424757 41x^6+$ $0.000000000000003853242444618x^5+$ $0.000000000029511445443014 8x^4+$ $0.000000011870591634575x^3+$ $0.00027342585095133 3x^2+$ 1.41483864923126x- 154.126038500236 R^2 = 0.999999946665675	y = $0.000000000000000000248809095130x^6+$ $0.000000000000004528963642682 15x^5+$ $0.000000000334429757812929x^4+$ $0.000000129528363309127x^3+$ $0.00028682127679226 3x^2+$ 1.41465110542043x- 130.088248652232 R^2 = 0.999999819844402

In Sloan's equation, the maximum depth of hydrate stability depends on the temperature of the seawater at the seafloor, and the geothermal gradient within the sediment column, pressure at any point, pore water salinity, and the gas mixture composition (Field and Kvenvolden, 1985; Sloan 1998). The gas fraction is an important input parameter, because even just small percentage of higher hydrocarbons relative to methane will shift the phase boundary to be stable at higher temperatures for equal pressures, and therefore deeper in marine sediments (Carroll, 2009)(Fig. 3.4). The purpose of modeling the BGHS is to compare the results with the observed depths of the BSRs. We want to test if they are: (1) in good agreement, and (2) if it is possible that the lower BSR is a sII mixed-gas hydrate boundary beneath a sI methane hydrate boundary. Any mispicks during BSR interpretation in geologically complicated regions where the BSR was difficult to determine would introduce a source of error between modeled and observed BSR.

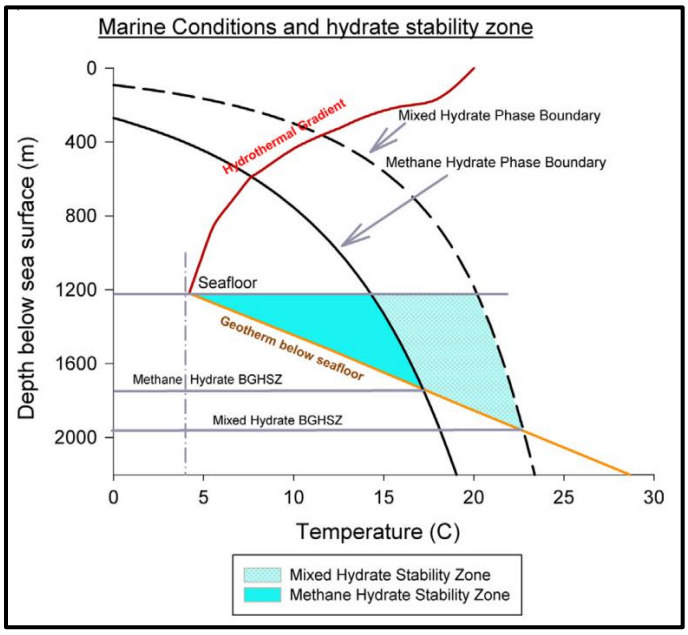

Figure 3.4 - Hydrate phase diagram for marine conditions. Mixed hydrate and methane hydrate equilibrium data are computed via CSMGem (Sloan, 2008) with a model natural gas mixture consisting of 93% methane, 5% ethane and 2% propane. Hydrothermal and geothermal gradients for marine setting were retrieved from Birchwood et al. 2008. Figure from Chong et al., 2015.

Bale et al. (2014) proposed the concept of "BSR Stability Envelope". This study does not adopt Bale's envelope theory, but we do recognize as Bale demonstrates, that discrepancies between seismic and theoretical BSR depths can occur as a result of the particular stability equation applied (e.g. Tinivella and Guistiniani, 2013). For example, the equation of Dickens and Quinby-Hunt (1994) is only good for pressures between 2.5 and10 MPa (Sloan, 1998; Bale et al., 2014), and thus is inappropriate for a deep water setting such as the Kumano Basin. Variations in sediment mineralogy, grain size, pore size (>100nm), pore networks and the resulting

capillary effects of marine sediments are also parameters that influence methane solubility and the dissociation point of hydrates which typically are not included in most stability relationships (Henry et al., 1999; Peltzer and Brewer, 2000; Uchida et al., 2004; Anderson et al., 2009; Liu et al., 2011; Daigle and Dugan, 2011, Bahk et al., 2011).

3.4 BSR-derived Heat Flow Modeling

Heat flow is a response to geothermal gradients established by the thermal conductivity and advective characteristics of the media, and is an essential input parameter for estimating GHSZ thickness. Indirectly, heat flow maps indicate zones of temperature perturbations, possibly from focused fluid advection or surface sedimentation/erosional processes. Our heat flow model assumes 1D conductive, steady-state heat transfer. To estimate the heat flow through the forearc using the primary-BSR, we first assume the BSR coincides with the sI, methane hydrate phase boundary in a region of approximately constant pressure, and therefore represents an isothermal contour. Because the Kumano Forearc sediments are overlain by >2000 meters of water, the primary factor that determines the loci of the hydrate stability boundary in our study region is the geothermal gradient. Using a hydrostatic pore pressure model, pressure at any particular depth is calculated as the sum of the overburden load from the water and sediment column. This assumption of hydrostatic pressure is validated by MDT data collected at Site C0009 (Expedition 319 Proceedings) and consolidation test results at Site C0002 (Guo et al., 2011) We use the BSR's thermobaric nature in conjunction with NGH phase boundary conditions of Maekawa et al. (1995) to derive, and analyze an intricate map of heat flow variations throughout the basin.

This method of using BSR depths to estimate heat flow was first introduced by Yamano et al. (1982), and has since been adopted to model geothermal regimes around the world including: in Makran accretionary prism (Kaul et al., 2000); the Voring Plateau near the Storrega Slide (Bouriak et al., 2000); the Black Sea (Ludmann et al., 2004); the Svalbard margin (Vanneste et al., 2005); throughout the Chile Triple Junction (Bangs et al., 2010); in the Nankai Trough

forearc slope region offshore, Japan (Kinoshita et al., 2011); the Nankai Trough (Hamamoto et al., 2011; Harris et al., 2013); the Andaman Sea (Shankar et al., 2013); at Hydrate Ridge in the Cascadia accretionary complex (Crutcheley et al., 2013); in the Trujillo Basin, Peru (Herbozo et al., 2013),around Cucumber Ridge, north Cascadia (Hong-Li et al., 2014); in the Krishna-Godavari (KG) Basin offshore India (Uma et al.,2010; Mandal et al., 2014); in the South China Sea near Taiwan (Liao et al., 2014), and at Woosley Mound in the Gulf of Mexico (Macelloni et al., 2015). BSR-derived values have been found to be consistent with probe measurements within a 10–20% error range at worst (Hyndman et al., 1992; Martin et al., 2004; Riedel, 2010). Probe measurements, however, are not without error, and an advantage of BSR-derived heat flow measurements is that they are less affected by disturbances at the seafloor such as short-term bottom water temperature variation, which has been shown to introduce significant noise into probe measurements (Hamamoto et al., 2011; Yamano et al., 2014)

3.4.1 Heat Flow Derivation

The seismic BSR is assumed to be in equilibrium and marks the phase boundary of the sI gas hydrate stability. While the BSR is assumed to be the BGHS for the purpose of heat flow modeling, it is important to note that BSR and BGHS are not used interchangeably in this study. Heat flow anomalies can serve as a proxy for warm fluids migrating up from depth via advection, or identify non-equilibrium zones. The manually picked BSR data were exported to a xyz file and then converted to a grid using GMT. We did not smooth the BSR because we assume that any small scale BSR variations could reflect local phenomena of potential interest. The BSR grid was then subtracted from the seafloor depth grid to create an isopach map between the BSR depths and the seafloor. The isopach map is converted back into a xyz file for use in our heat flow derivation whereby BSR depths below seafloor are converted to pressure assuming hydrostatic conditions with a water density of 1024 kg/m^3. This process yielded an *in situ* pressure of 23.46 MPa at the BSR. Temperature is calculated using Maekawa's (1995) P-T conditions for methane hydrate stability in sodium chloride solutions under high pressure

conditions, which takes into account that dissolved ions in interstitial water, inhibits hydrate formation and thus shifts the phase boundary.

$$\mathrm{Ln}(p/p^0) = -926.815 + 31979.3/T + 144.909 \ln T + 5847.92x + 3220.26x^2 + 5840.50 \ln(1-x)$$

Where p is the pressure (MPa) of methane hydrate dissociation, p^0 is the atmospheric pressure (MPa), T is the temperature (K) of methane hydrate dissociation and x is the mole fraction of sodium chloride in the liquid phase. This stability equation is appropriate for the hydrostatic pressure conditions and pore water salinity values found in the Kumano Basin. This same hydrostatic pressure model was successfully used to predict the temperature gradients in the Muroto and in the Tokai area (ODP leg 131 wells westward of Kumano and MITI wells eastward of Kumano) which agreed with *in situ* borehole measurements (Hyndman et al., 1992; Takahashi et al., 2001; Martin et al., 2004; Kinoshita et al., 2011). We can confidently assume that the temperature (T) at the seafloor (z=0) is equal to 2°C throughout the region based on CTD measurements collected during submersible "Shinkai" dives and from annual mean water temperature profile from the Japan Oceanographic Data Center (JODC, http://www.jodc.go.jp/) in the Kumano region. Variations in bottom water temperature are small, ~0.15 K (Hamamoto et al., 2011), and have an insignificant effect at BSR depths because there is simply not enough time for annual cyclic temperature variations to diffuse more than ~10 m into the sediments (Martin et al., 2004).

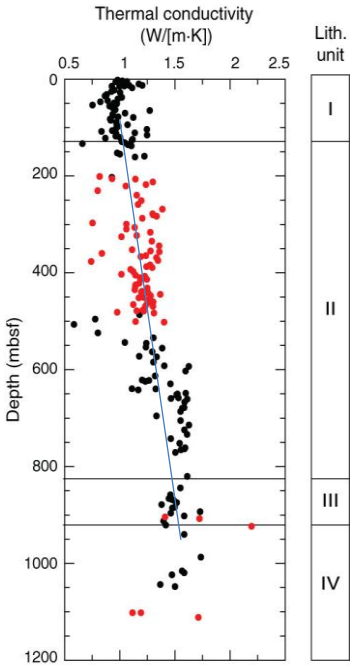

Figure 3.5 - Thermal conductivity measurements taken at Site C0002. Red = Expedition 338 data, black = Expedition 315 data. Modified from figure F87, IODP Expedition 338 Proceedings, Moore et al., 2014.

The average thermal conductivity (K) was estimated from the empirical relationship between Vp and K at nearby boreholes (C0002) for all BSR points (Fig. 3.5). K generally increases

from 1 W/[m·K] at depth (z) = 0 mbsf to 1.2 W/[m·K] at z= 400 mbsf. The linear relationship was set at K(z)=(1.0 + (0.2/(400*z))). Therefore:

$$\text{Heat flow } (q) = K_{avg} * GTG$$

Whereby K=avg is the average thermal conductivity of sediments from physical property data of Site C0002 and GTG= ((TBSR-TSF)/(zBSR-zSF)).

A thermal-resistance method was applied for a steady-state, 1D conduction regime with varying thermal conductivity. The steady-state assumption is an adequate approximation given the thickness of the plate at <15 km results in a short time scale for thermal diffusion (e.g. Hamamoto et al., 2011). To exclude any topographic high-frequency artifacts on the heat flow data (Blackwell et al., 1980), spatial smoothing was applied to the seafloor topographic data to eliminate short wave length of ~0.2m (~400m) using a box-car averaging with the GMT block mean command, -10.2/0.2m. A topographic relief less than ~400 m, the typical depth to the BSR, should not affect the temperature at the BSR. Martin et al. (2004) applied similar smoothing to the BSR in their study on the eastern Nankai Margin. The final heat flow map was also generated using GMT.

3.4.2 Uncertainties in BSR-derived Heat Flow

BSR-derived heat flow can have errors up to 10-20% because of potential uncertainties in seismic time-depth conversions, seafloor temperature, sediment thermal conductivity, limitations from 1D analysis, and possibly fromvariations in sediment pore size because of the Gibbs-Thomson effect whereby the BGHS would appear at a lower temperature than would be predicted (creating larger than true heat flow values) (Kinoshita et al., 2011; Goto et al., 2012; Dugan and Daigle, 20XX). Grevemeyer and Villinger (2001) compared geothermal gradients predicted from BSR depths with borehole temperature measurements at ten locations around the world with results showing that BSR-derived values can exceed borehole derived values by up to 8.5^{o}C. We also assume an interstitial salinity of 35g/L (3.5 wt%). Lower than 3.5 wt%

salinity could contribute to heat flow errors by shifting the phase curve of methane + seawater to higher temperatures, or lower temperature for higher salinity such as in the case of very recent gas hydrate formation (He et al., 2007). Uncertainty due to the resolution limit of the seismic data is very minor in the shallow portion of the Kumano sediments. The seismic resolution is 5-7 meters, corresponding to a heat flow uncertainty of ~1 mW/m^2. Further, excellent correlation between the seismic BSR depths and the drop in borehole resistivity values at the BGHS were found at Site C0002 which gives us confidence in the accuracy of our velocity model to the BSR. We are also confident in the seafloor bottom water temperatures; however the thermal conductivity is dependent on mineral compositions, porosity, and the type of pore fluid, thus the assumption of borehole derived average thermal conductivity extrapolated across a large region could introduce error.

3.5 Gas In Place (GIP) Resource Estimate

For consistency, we adopt the volumetric gas in place estimation method used by the MH21 Research Consortium to evaluate the eastern Nankai Trough hydrate concentration zones (Fujii, et al., 2008).

$$GIP = GRV * Net/Gross\ ratio * P * MH_{sh} * VR * CO$$

Whereby GIP represents the gas in place [units], GRV is the total rock volume [units], p is the net to gross porosity ration, MH_{sh} is the methane hydrate saturation, which is the volumetric fraction of hydrates pore space occupancy, VR is the void ratio at STP and CO is the hydrate cage occupancy which is defined as the ratio of hydrate cages occupied by a natural gas molecules/the total number of cages(Uchida et al., 1999) . Assumptions regarding and details of these parameters are provided in Chapter 6.

Chapter 4

Data Results

"Data! Data! Data!" he cried impatiently. "I can't make bricks without clay!" – Sherlock Holmes,

The Adventure in the Copper Beaches, Sir Arthur Conan Doyle

4 Data Results

4.1 NGH Indicators from NanTroSEIZE Drilling Data and Post Cruise Analyses

IODP shipboard analyses along with numerous post-expedition studies have investigated and reported NGH indicators and GH saturation estimates using a variety of datasets collected at both sites C0002 and C0009. These results are synthesized here and used later in this study to support seismic interpretations and the NGH system analysis.

4.1.1 Site C0002

Site C0002 includes twelve boreholes drilled during IODP Expeditions 314, 315, 332, 338, and 348. Holes A, F, N, P were logged using the logging while drilling (LWD) approach, and Holes C, B, D, H, J, K, L, M were cored (Expedition 348 Scientists, 2014) (Fig. 4.2). The seafloor depth is 1936 mbsl (Expedition 314 Scientists, 2009). Expedition 315 had good recovery in the upper and lower sections; however, they failed to retrieve sediments from 203.5 mbsf to 479.4 mbsf which is essentially the core region of methane hydrate occurrence (Expedition 315 Scientists, 2009). Expedition 338 was able to core this missing interval in holes K and L (Moore et al., 2013). Combining data from 314, 315 with 338 provide seamless downhole measurements (Fig. 4.1) which are further supplemented by repeat logging during 332 and deeper coring and logging operations conducted during Expedition 348. Expedition 348 scientists (2014) provided information about changes in pore water and gas geochemistry all the way into the accretionary prism which could be providing overlying sediments with a source of gas charged fluids. With age constraints provided by biostratigraphy, the sedimentation rate within the GHSZ is 3.08 cm/Kya (Strasser et al., 2014). The pore pressure in the accretionary prism near the seaward side of the basin was reported by Tsuji et al., 2014 to be abnormally high, which could result in gas expulsion from depth.

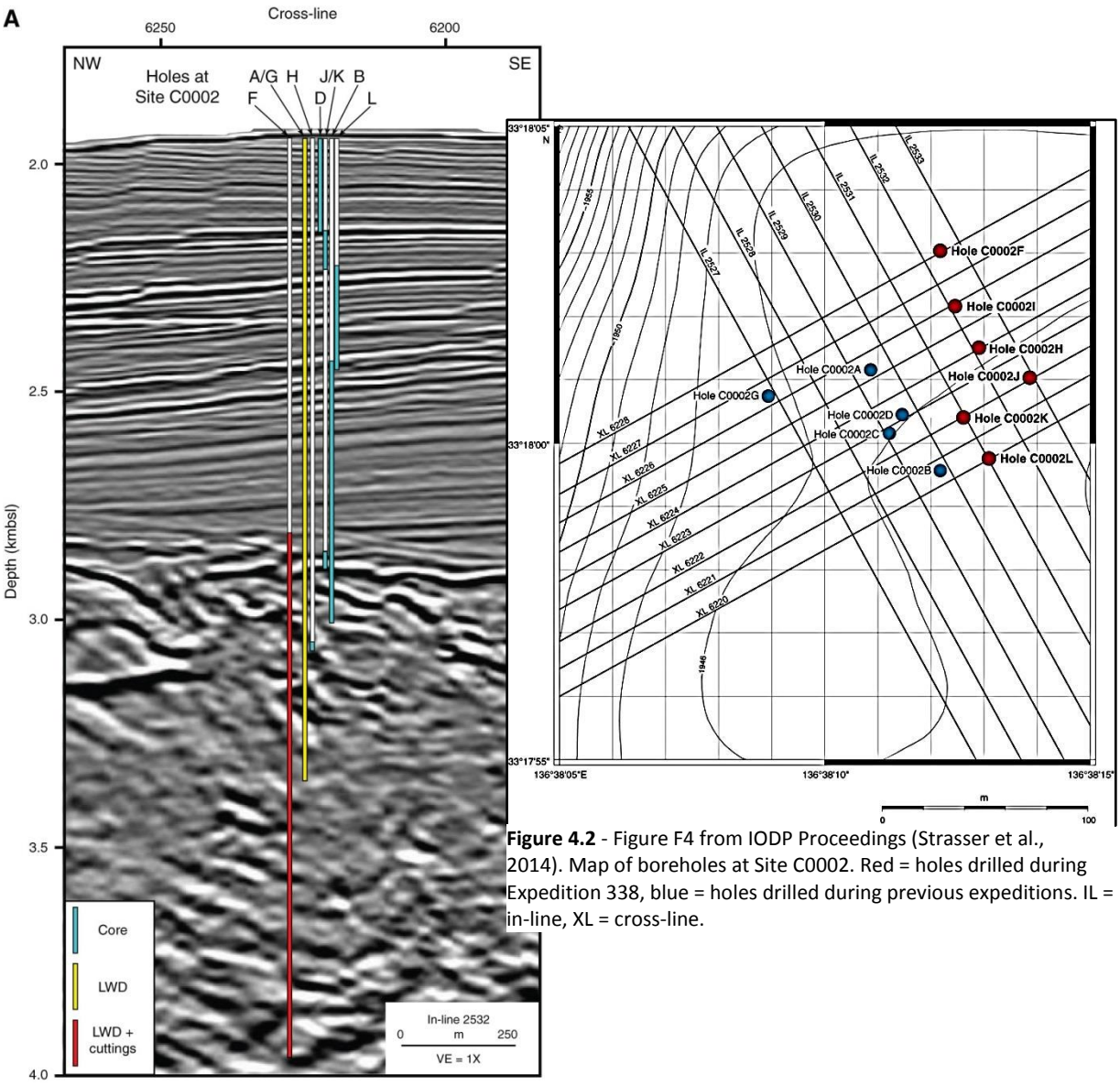

Figure 4.2 - Figure F4 from IODP Proceedings (Strasser et al., 2014). Map of boreholes at Site C0002. Red = holes drilled during Expedition 338, blue = holes drilled during previous expeditions. IL = in-line, XL = cross-line.

Figure 4.1 - Figure F3 from IODP 338 Proceedings (Strasser et al., 2014). Seismic Inline 2532 showing relative locations of holes drilled at Site C0002. LWD = logging while drilling, VE = vertical exaggeration

4.1.1.1 NGH Geochemical Indicators

Standard ship-board geochemical analyses were conducted on pore fluids, headspace gas, void space gas and sediment samples collected from cores and cuttings during Expeditions 315 and 338 (see methods chapter Strasser et al., 2014) and together provide important

information about gas composition and hydrate saturation. The sulfate-methane transition zone (SMTZ) occurs at ~9 mbsf while the downhole Na+ and Cl- baseline decreases with depth until it reaches a minimum at the BSR then increases with depth until returning to seawater values at ~800 mbsf (Fig. 4.3). High SO_4^{2-} concentrations were detected between 200 and 500 mbsf during Expedition 338, with no evidence from other chemical profiles to suggest contamination.

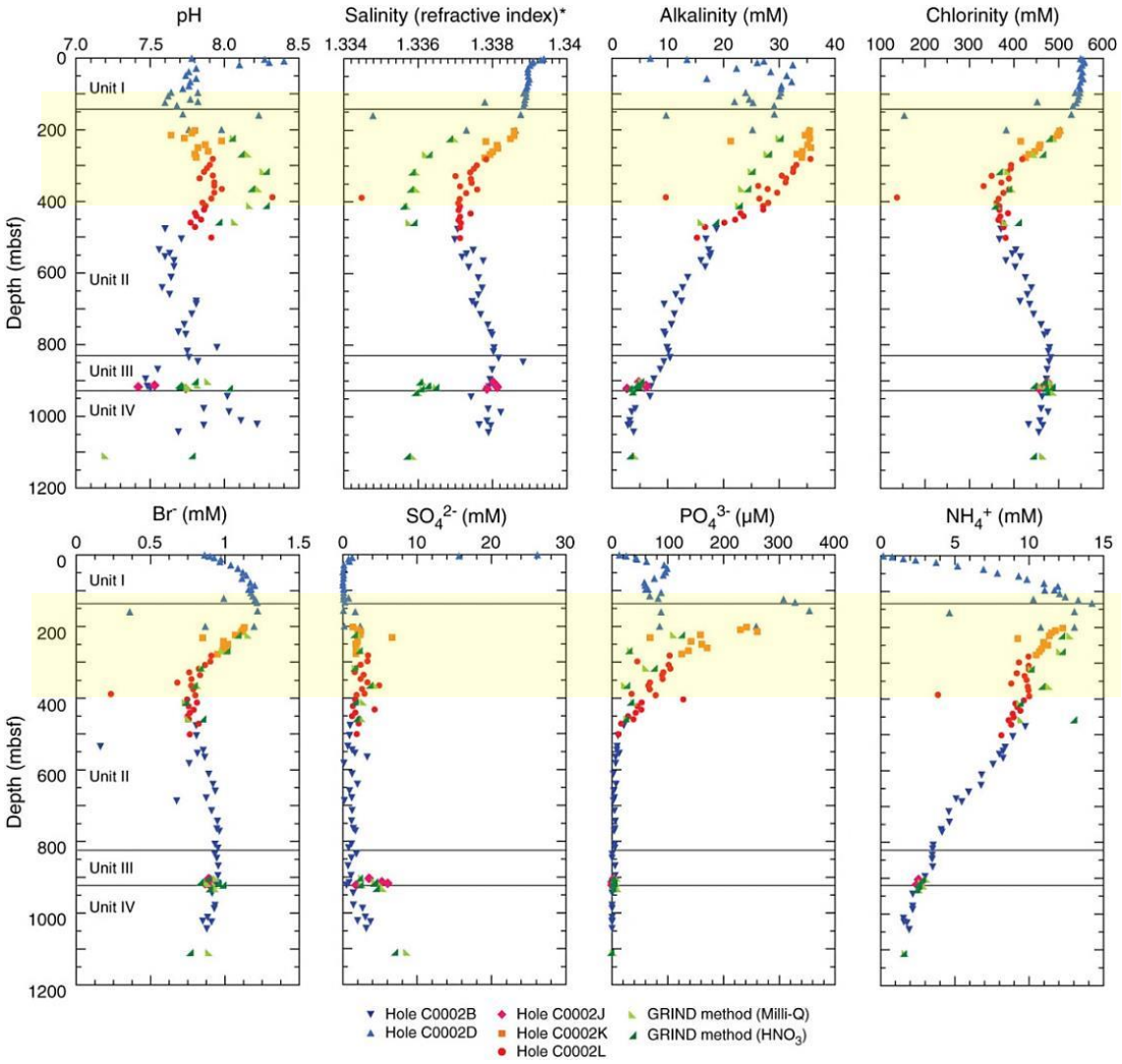

Figure 4.3 - Variation of geochemical parameters and concentrations of dissolved salt in interstitial water samples. Discrete chloride anomalies are from GH dissociation during core recovery. The background freshening is likely from silica dehydration fluid delivery from depth. Modified Figure from Strasser et al. 2014, IODP 338 Proceedings.

Discrete, negative Cl- excursions are concentrated between ~125 mbsf to 400 mbsf with the lowest measured value of 136.5 mM at the BSR depth (389 mbsf). These discrete intervals can confidently be attributed to pore fluid freshening from gas hydrate dissociation during core recovery and interestingly, indicate a broader gas hydrate occurrence zone (GHOZ) than detected by logging data sonic and resistivity spikes (see 4.1.1.2). The background chlorinity trend reverses to less fresh values at 500 mbsf.

Jia et al., (In Review) used Cl- measurements to estimate GH saturation from both a baseline curve and from a constant background of 560 mM which together resulted in a similar trend but with higher GH saturation values associated with the fixed 560 mM background. The highest GH concentration was found to occur at 388 mbsf which was calculated to be 81.6% and 84% GH_{sh} based on the two different methods employed, respectively. However, they may have overestimated GH occurrence by assuming the incorrect baseline. The isotopic composition of the pore water was not considered not consider and the baseline freshening could be the result of fresh water migration from diagenetic processes mixing with NGH dissociation released waters. Water molecules that construct the gas hydrate lattice are enriched in both ^{18}O and D relative to V-SMOW, while clay mineral dehydration reactions fluids are enriched in ^{18}O, but not D. Expedition 315 shipboard data show 3 possible hydrate occurrences in the upper 200 meters (Fig. 4.4), but the $\delta^{18}O$ and δD values are not publically available from expedition 338.

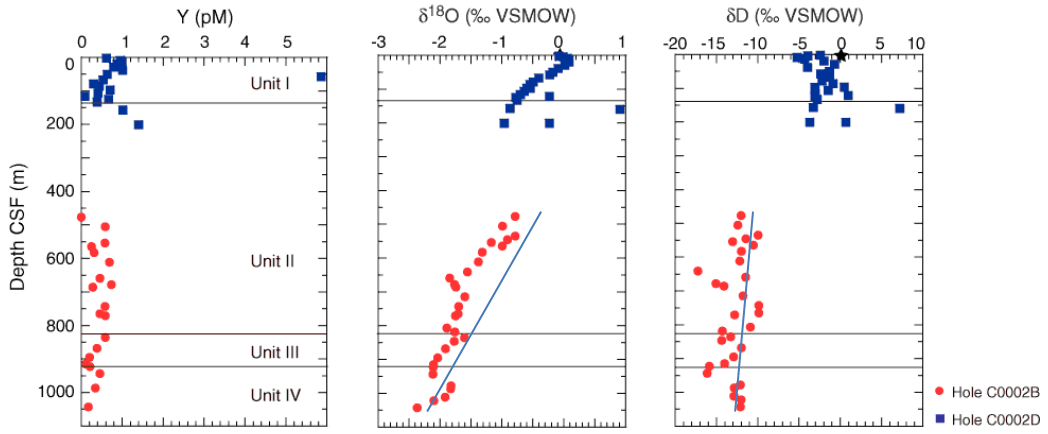

Figure 4.4 - Concentration of Y and oxygen and hydrogen isotopic composition of interstitial water, Site C0002. Star = standard seawater value. CSF = core depth below seafloor. The data gap spans most of the hydrate occurrence zone. Modified from F23 315 Proceedings (Strasser et al., 2014).

A recent study by Tomaru and Fehn (2015) measured $^{129}I/I$ concentrations and used methods of iodine geochronology to date the ^{129}I of pore waters from across the Kumano transect. They found at Site C0002 iodine ages between collected at 36.3, 111.9, 741.3 and 984.2 mbsf were 31.2, 41.0, 28.5 and 28.8 Ma, respectively, which is dramatically older than the surrounding sediments. Further, iodine enrichment up to >400 mM was not accompanied by higher total organic carbon (TOC) but is accompanied by a similar behavior in methane. They concluded that iodine (and methane) was transported by upward lateral migration of fluids originating from deeper layers in the upper plate from 6-8km deep over later distances > 10 km from Eocene aged and older sediments present in the backstop (Waseda and Uchida, 2004).

TOC was only measured below 200 mbsf during Expedition 338. It ranged from 0.21 – 0.97 wt% peaking at 800 mbsf, with an average value of ~ 0.58 wt% (Strasser et al., 2009) (Fig. 4.6). Woody material (Fig. 4.5) was discovered in the lower basin sequences which is very thin at C0002, but thickens at C0009. Toki et al. (2012) reported that the NH_4^+ concentration was highest at Site C0002 in comparison to C0001, C0004, and C0008 meaning that organic matter degradation is more active at this site than further seaward, likely because the higher sedimentation rates at C0002 prevent aerobic degradation of organic matter.

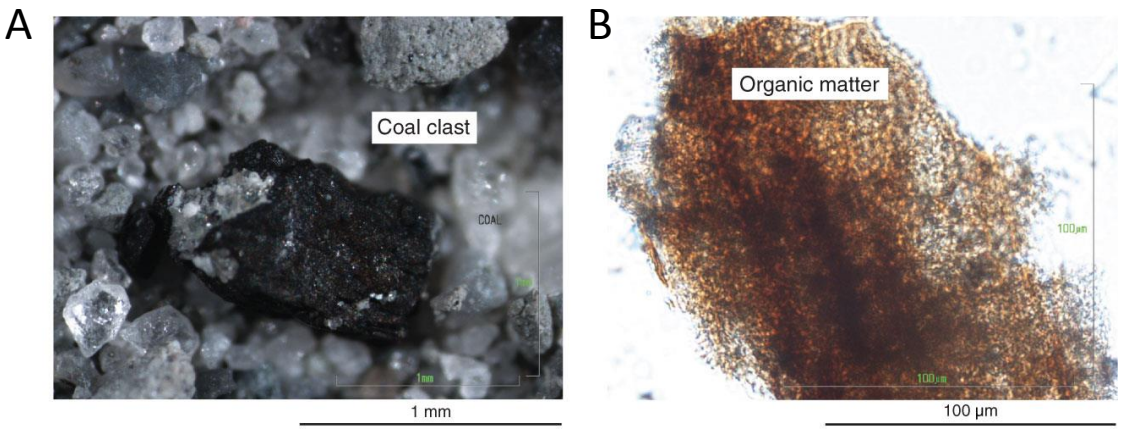

Figure 4.5 - Smear slide and binocular microscope plates of mineralogy and fossils in cuttings samples. (A) coal clast (Sample 338-C0002F-96-SMW; 1255.5 mbsf). D–F. Smear slides under PPL of (B) organic matter (Sample 338-C0002F-26-SMW; 950.5 mbsf) Organic material/wood/lignite is common between 1140.5-1600.5 mbsf Modified Figure F26 from Strasser et al., 2014, IODP 338 Proceedings Volume.

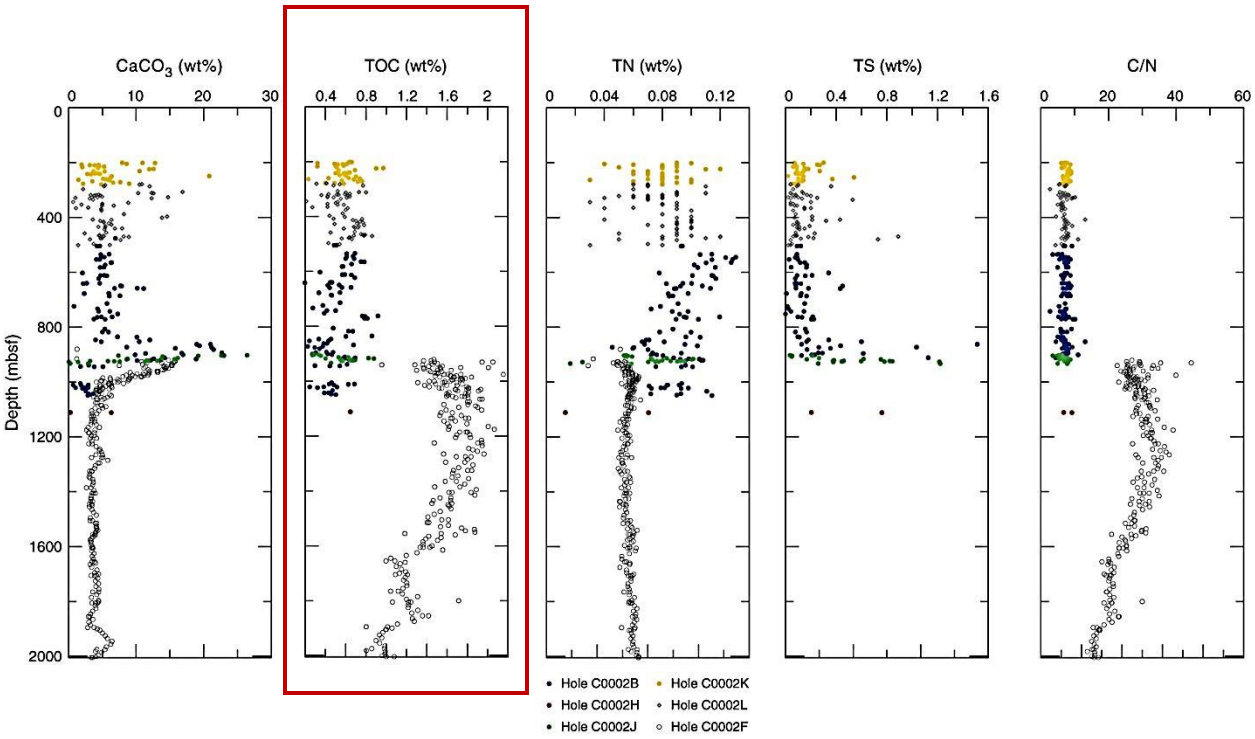

Figure 4.6 – Organic geochemistry profiles. $CaCO_3$, total organic carbon (TOC) (red box) is generally low at <0.8 wt%, total nitrogen (TN), total sulfur (TS), and C/N from Holes C0002B, C0002H, C0002J, C0002K, C0002L, and C0002F. Modified Figure F84 (Strasser et al., 2014).

Methane concentrations in headspace gas measurements range from nearly 0 to 50,000 ppm with high variability downhole. Peaks in methane concentration occur at 30 mbsf, are clustered between 250 mbsf to 450 mbsf, with deeper peaks at 920 mbsf and 1050 mbsf (Fig. 4.7). Higher molecular weight hydrocarbons, including pentane and ethane, were found in low concentrations with ethane peaks between 390-400 mbsf, at 920 mbsf and at 1050 mbsf. Expedition 338 scientists noted that ethane concentrations are affected by extraction methods (Organic Geochemistry section In Strasser et al., 2014). Pentane peaks occur at 200 mbsf and 380 mbsf. Despite the presence of ethane and pentane within the GHSZ, isotopic analysis of $\delta^{18}C$ of CH_4 determined that the gas had microbial origins (Strasser et al., 2014). The $\delta^{13}C$ of CH_4 ratio is most enriched at -50‰ at 500 mbsf and becomes more depleted with depth down to -60‰ (Toki et al., 2012). Thermogenic gas is prevalent below 1700 mbsf with C_1/C_2 ratios between 300 and 400 (Moore et al., 2013; Hammerschmidt et al., 2014). Void space gas measurements were richer in methane than headspace gas measurements. Void gas samples tend to capture the more volatile components which are dissolved in interstitial waters

(methane less soluble than ethane), compared to headspace measurements which tend to be enriched in less volatile components and reflect the gas composition within sediments.

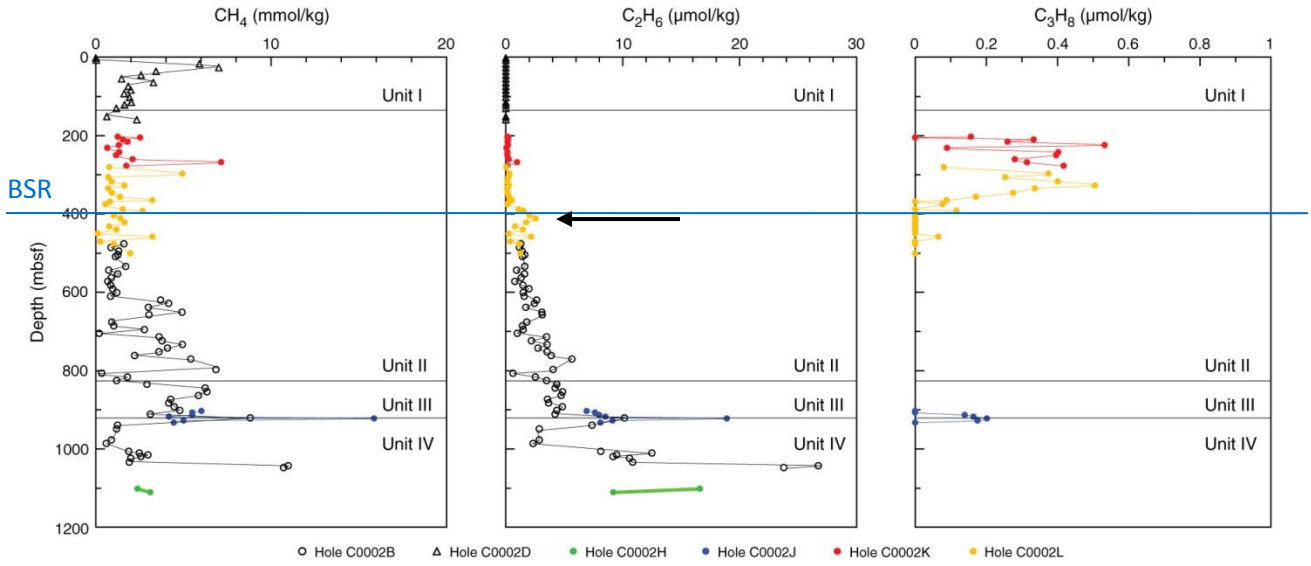

Figure 4.7- Vertical profiles of methane, ethane, and propane concentrations in headspace gas samples, Site C0002. Horizontal lines = Hole C0002B lithologic unit boundaries. Small ethane spike (black arrow) observed just beneath the BSR (blue line). Methane, ethane and propane are measured in ppmv using a flameionization detector. Modified F74 (Strasser et al., 2014).

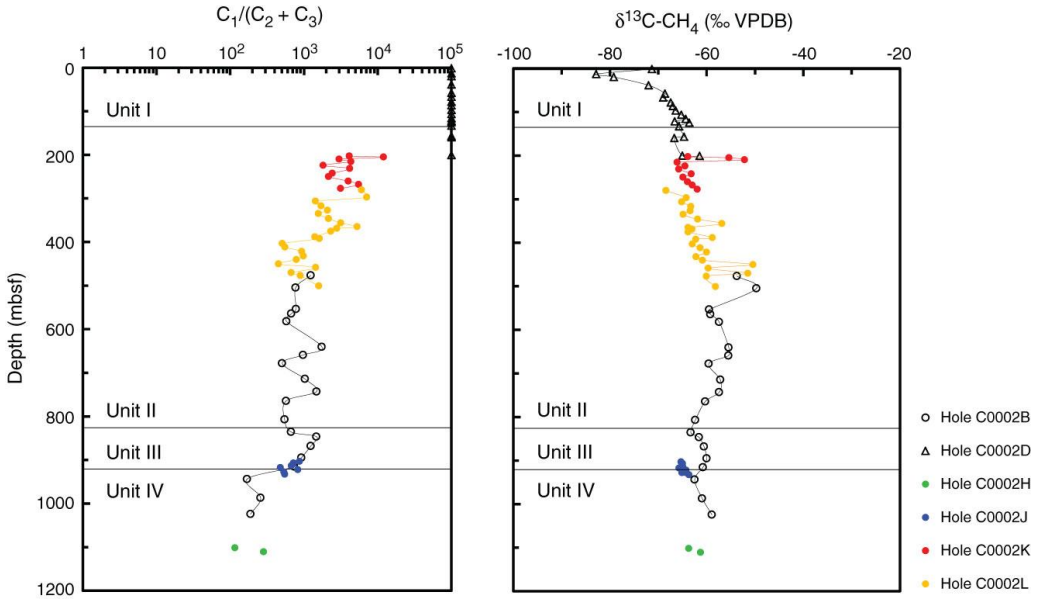

Figure 18: Vertical profiles of $C_1/(C_2 + C_3)$ ratios as well as $\delta^{13}C\text{-}CH_4$ calculated from headspace gas samples (solid symbols). Site C0002. VPDB = Vienna Peedee belemnite. Horizontal lines = Hole C0002B lithologic unit boundaries. Carbon isotopic composition was measured using a methane carbon isotope analyzer. Modified Figure F76 (Strasser et al., 2014) .

4.1.1.2 NGH Well Log Data

LWD data were collected during Expeditions 314, 332, 338 and 348. Expedition 314 collected a continuous LWD log from the seafloor down to 1400 mbsf at a resolution of 1 sample/4 cm (Fig. 4.11). Shipboard scientists noted numerous elevated resistivity values between 218.1-400.4 mbsf correlating with sand horizons (Expedition 314 Scientists, 2009) which was further supported by Expedition 338 results showing distinct resistivity spikes at 270, 295, 370, and 390 mbsf (Fig. 4.10) (Strasser et al., 2014). These resistivity peaks are interpreted to indicate gas hydrate occurrences (Expedition 314 Scientists, 2009; Strasser et al., 2014). Further investigation by 314 Scientists (2009) found that the high resistivity peaks correlate to the base of asymmetric gamma ray log lows representing fining upward, gradational tops.

Zone B in Unit II from 481.6-547.1 mbsf (Expedition 314 Scientists, 2009) is a sand rich interval with elevated free gas (P-wave velocity drop) that correlates to a strong negative polarity reflection in the seismic data (Fig. 4.9). This gas-bearing zone occurs ~80 m below the BSR. The caliper log which is used to determine borehole conditions was poor in Zone B (gas-bearing zone) which likely indicates washout units comprising unconsolidated sands. Gamma ray logs indicate that Zone B is sandwiched between two clay rich intervals (Expedition 314 Scientists, 2009).

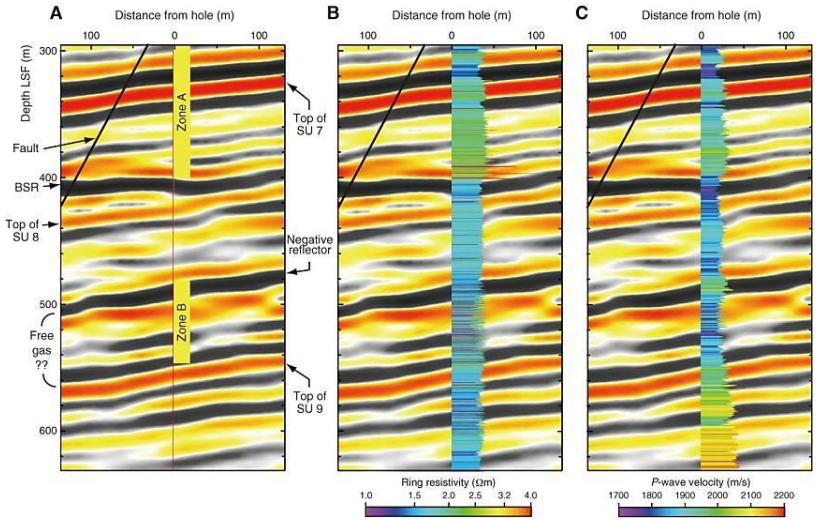

Figure 4.9 - Resistivity log curves tied to local seismic section (variable density display method; red = positive, black = negative) at depths of Zones A and B. Data superimposed over Inline 2529 near Hole C0002A. Figure F47 from 314 Proceedings (Expedition 314 Scientists, 2009).

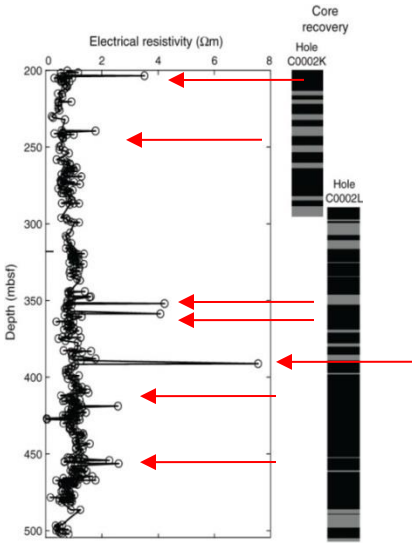

Figure 4.10 -Electrical resistivity data from four-pin electrodes, Holes C0002K and C0002L. Spikes (red arrows, inferred to be hydrates in sands. Modified F89 from Strasser et al., 2014.

Expedition 332 drilled Hole C0002F down to 868.5 mbsf, and their LWD data results were largely consistent with Expedition 314 (Expedition 332 Scientists, 2011). Unit boundaries were situated at analogous depths. Zone A (gas hydrate-bearing) zone was slightly thinner (2018.1 to 400.4 mbsf) while Zone B (gas bearing zone) was thicker (481.6 to 547.1 mbsf).

LWD data has been analyzed for gas hydrate occurrence and saturation estimates by Barnes (2013), Miyakawa et al. (2014), Malinverno and Goldberg (2015), and Jia et al., (In Review). Barnes (2013) determined hydrate saturation using Archie's equation to peak at 80% at the depth of the BSR, but noted that uncertainties in the parameters used could result in over estimations. Miyakawa et al. (2014) used logs and sediment porosity data from core samples collected during Expeditions 314 and 315 to calculate gas hydrate saturations (pore fraction) from the resistivity and P-wave velocity logs. Using eight different equations for a robust quantitative analysis, the resulting hydrate saturation baseline ranged from 0-35% and 0-30% for resistivity and P-wave velocity logs, respectively (Miyakawa et al., 2014). P-wave data indicates GH occurrence between the 218.1 mbsf and 404.4 mbsf (*LWD depths*) and several high resistivity spikes were found in sandy units below 260 mbsf which recorded hydrate saturations > 60%. A discrepancy between P-wave velocity and resistivity derived GH saturation was attributed to the presence of free gas above the BSR. We can confirm that free gas also appears above the BSR as a low velocity zone in our seismic velocity volume (Fig. 5.1) and likely reflects a large flux of gas into the GHSZ.

Malinverno and Goldberg's (2015) analysis of the downhole logs found NGH occurrence in 166 sand layers between 108 and 401 mbsf and defined this as the gas hydrate occurrence zone (GHOZ) with increasing hydrate content with depth approaching the BSR and a maximum saturation of 70%. Jia et al. (In Press) applied a first-principle-based effective medium model to predict GH saturation from the sonic data collected at Hole C0002A considering both a pore-filling model and a matrix supporting model. Results were compared to those derived from Archie's equations (85.6% at highest peak). Background resistivity of water saturated sediments was calculated to be 1.17-1.18 ohm.m and resistivity of the pore water was determined to

range from 0.21-0.22 ohm.m above the BSR. The pore filling model indicated higher saturations than the matrix-supporting model with a maximum difference of 21.1%.

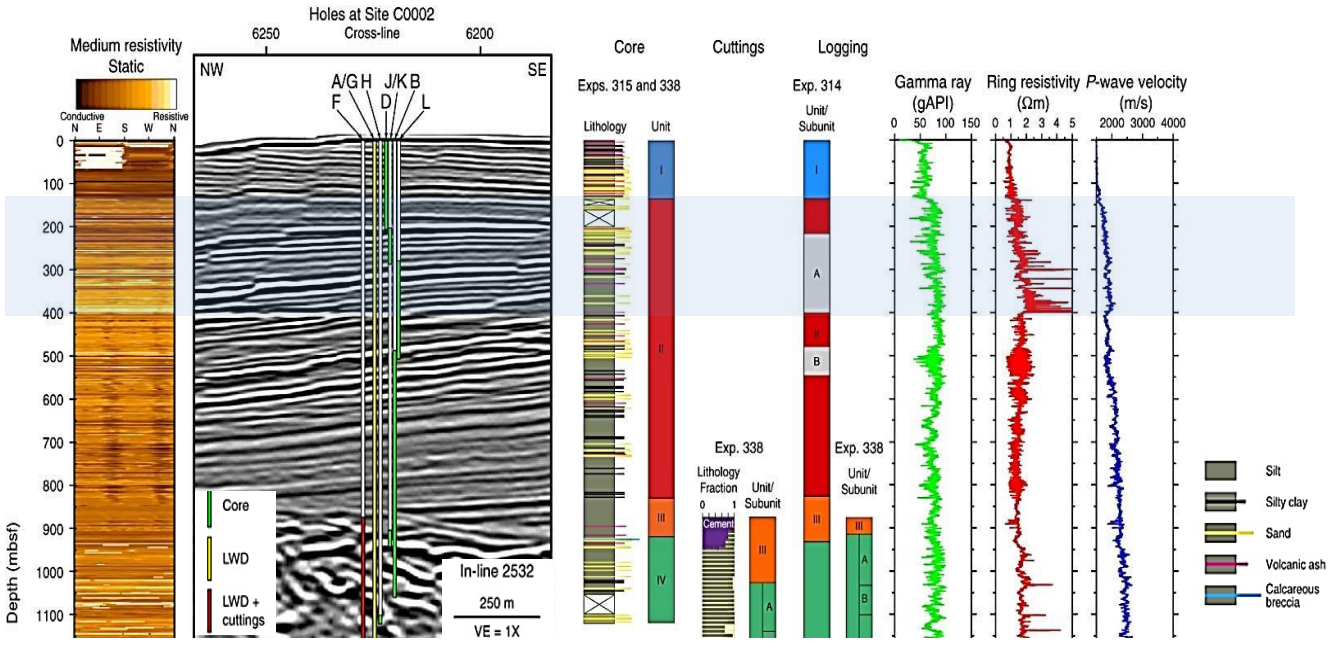

Figure 4.11: Cuttings-core-log-seismic integration, Site C0002 with all holes projected onto seismic data from In-line 2532 of the Kumano 3-D PSDM volume (Moore et al., 2009). Composite medium button static resistivity image, All Site C0002 holes projected onto the seismic line, composite core lithology plot, cuttings-derived unit boundaries, logging-while-drilling (LWD) unit boundaries, and composite LWD data. The composite LWD data comprise Hole C0002A data from 0 to 900 mbsf and Hole C0002F data below 900 mbsf. VE = vertical exaggeration. Gamma ray baseline set at 75 gAPI and corrected for K rich drilling mud. Sand <75 gAPI and clay rich >75 gAPI. Sudden drop below resistivity spike of ~5.0 ohm at 400mbsf correlating to the BSR in the seismic data. Modified F115 (Strasser et al., 2014).

4.1.1.3 Lithological NGH Indicators

The dominant lithology at C0002 is dark, olive-gray, silty, claystone with minor lithologies including sandstone, sandy siltstone, silty claystone, calcareous claystone, and fine ash. Most sediment samples are dominated by a siliciclastic assemblage of clay, quartz, and feldspar, with variable amounts of pelagic carbonate and a minor, but persistent, component of volcanic glass widely distributed (Fig. 4.12).

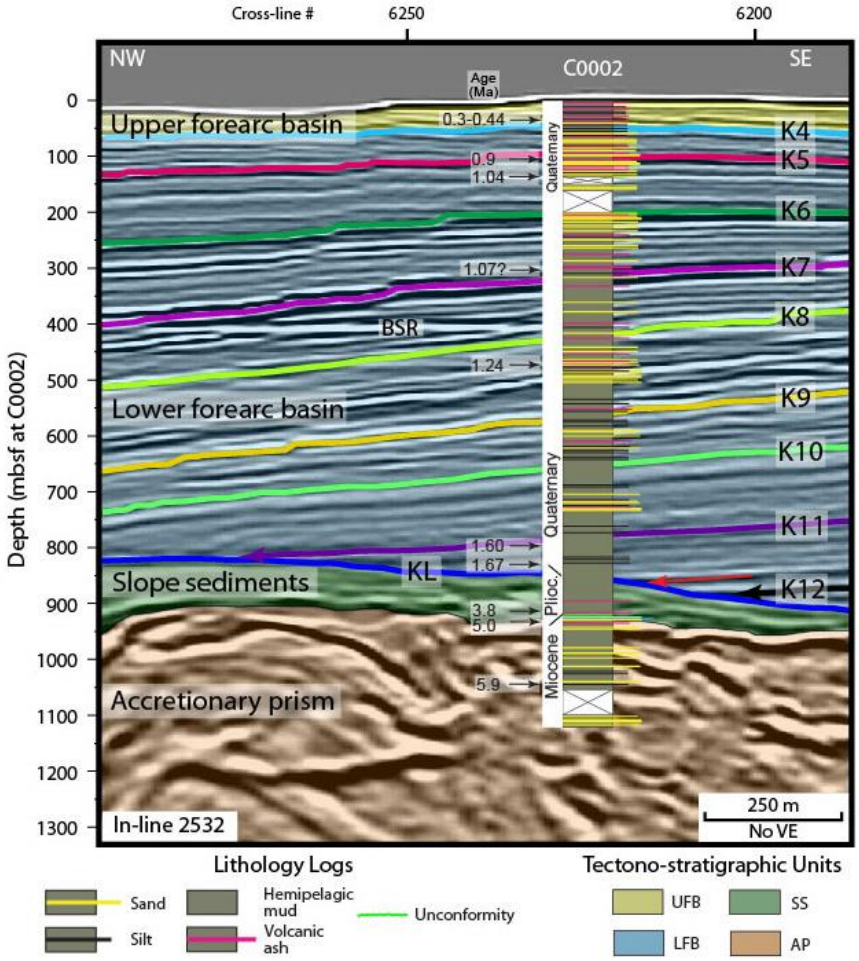

Figure 4.12 - Lithostratigraphic summary column of site C0002 overlain on a 3-D seismic in-line. Seismic sequence boundaries are from Gulick et al. (2010). Labeled seismic horizons are the tops of sequence boundaries as defined by Gulick et al, (2010); e.g., KL = top of "Kumano Lower", K11 = top of "Kumano 11".VE = vertical exaggeration. Figure from Moore et al., 2015.

Figure 4.13: C0002K_9X_8. Three cycles of turbidite deposition with finning upward sequences

The cores have clearly documented stacked turbidite deposits (Fig. 4.13), which supports the seismic interpretations of turbidite deposition based on alternating positive and negative events. A thick >3 m sand bed was found just above the BSR at about 386 mbsf (Strasser et al., 2014), corresponding to the highest hydrate saturation estimated from Cl- and resistivity logs. Zones of poor recovery were likely unconsolidated sand units. This is a common problem in ocean drilling and is unfortunate for gas hydrate research because these sands could have hosted unaccounted for NGHs.

From 286.53 to 499.76 mbsf, 66 occurrences of soupy fabric were identified during shipboard analyses of Holes C0002K and C0002L (Table 2). Compositionally, 33 soupy structures (example in Fig. 4.14) were found in muds-silt, 29 in sands, one occurrence in an ash/mud mixture, one sand/mud mixture, and three occurrences in an unidentified lithology. These data showing soupy structures predominant in the fine-grained sediment is in direct conflict with the logging data that shows no occurrence of gas hydrates in the fine grained sediments (Kinoshita et al., 2009) and with the common interpretation that gas hydrates predominantly form in the coarse-grained units. Noteworthy, according to shipboard data (Strasser et al., 2014) most of the core at Hole C0002L Core 23X, interval 486-486.405 mbsf (a sand rich interval occurring at the base of a fining upward package) was lost after an explosion caused by gas hydrates expansion. This occurrence of hydrate is *86 meters below the BSR,* and no mention of it was included in the proceedings. This piece of data has important implications for understanding the double BSR on the seaward edge of the margin.

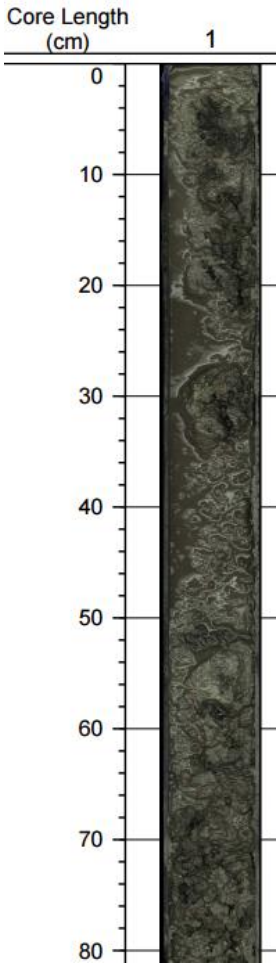

Figure 4.14 - C0002K, core 6T. Showing 80 cm of a 1.5 m soupy interval between 229.5 to 232.9 m CSF-A taken from Expedition 338 core images database.

Table 3 - Documented Soupy Sediments, a potential GH proxy, in Holes C0002K and C0002L.

Physical Properties of Soupy Sediments in Holes C0002K and C0002L							
Core,Section, Interval (cm)	Depth (mbsf)	Electrical Resistivity	Formation Factor	MAD Porosity %	Archie m exponent	Archie Tortuosity	Notes
338-C0002K-2X-1, 3.0	286.53	0.577	2.129	48.63	1.05	4.38	Soupy mud
3X-1, 32.0	296.32	0.742	2.738	56.78	1.78	4.82	Soupy silty mud
5X-1, 79.0	315.79	0.718	2.649	54.23	1.59	4.88	Soupy silty

							mud
5X-4, 73.0	318.425	0.966	3.565	49.02	1.78	7.27	Dark soupy sand
5X-5, 56.0	319.31	1.366	5.041	49.41	2.29	10.20	Dark soupy sand
5X-5, 81.0	319.56	1.071	3.952	44.08	1.68	8.97	Dark soupy sand
5X-6, 50.0	320.485	1.053	3.886	45.18	1.71	8.60	Dark soupy sand
5X-7, 21.0	321.305	1.086	4.007	43.67	1.68	9.18	Dark soupy sand
5X-7, 21.0	321.305	1.086	4.007	43.67	1.68	9.18	Dark soupy sand
6X-1, 65.0	325.15	0.843	3.205	44.8	1.45	7.15	Soupy silty mud
6X-2, 68.0	325.995	1.358	5.163	49.85	2.36	10.36	Soupy silty mud
6X-5, 103.0	328.475	1.199	4.559	54.34	2.49	8.39	Soupy silty mud
8X-2, 28.0	344.085	1.392	5.273	50.02	2.40	10.54	Soupy dark sand
8X-5, 73.0	347.43	1.603	6.072	50.28	2.62	12.08	Soupy dark sand
9X-1, 10.0	353.1	0.83	3.132	46.37	1.49	6.75	Soupy mud
9X-3, 25.0	354.53	0.762	2.875	49.32	1.49	5.83	Soupy mud
9X-3, 55.0	354.83	0.68	2.566	51.14	1.41	5.02	Soupy mud
9X-8, 75.0	359.455	0.67	2.528	55.78	1.59	4.53	Soupy mud
9X-8, 95.0	359.655	0.96	3.623	44.66	1.60	8.11	Soupy silty mud
10X-1, 99.0	363.49	0.381	1.432	60.17	0.71	2.38	Soupy mud
10X-1, 99.0	363.49	0.381	1.432	60.17	0.71	2.38	Soupy mud
10X-7, 122.0	368.66	0.645	2.425	47.31	1.18	5.13	Soupy sand
11X-1, 83.0	372.83	0.828	3.09	52.14	1.73	5.93	Soupy dark sand
11X-3, 20.0	374.83	0.455	1.698	56.18	0.92	3.02	Soupy silty mud
11X-6, 13.0	376.345	0.705	2.631	55.71	1.65	4.72	Soupy sand
12X-1, 103.0	382.53	0.641	2.392	49.48	1.24	4.83	Soupy
13X-5, 32.0	396.455	0.801	2.989	52.7	1.71	5.67	Soupy sand
15X-7, 44.0	415.205	0.686	2.569	59.92	1.84	4.29	Soupy sand
15X-7, 70.0	415.465	0.616	2.307	59.92	1.63	3.85	Soupy sand
15X-8, 130.0	417.465	0.946	3.543	48.65	1.76	7.28	Soupy sand
16X-2, 44.0	420.915	0.959	3.578	51.94	1.95	6.89	Soupy sand
16X-7, 38.0	426.785			42.41			Soupy mud
16X-7, 105.0	427.455			47.76			Soupy mud

17X-1, 107.0	430.07	0.631	2.354	48.65	1.19	4.84	Soupy mud
17X-6, 25.0	433.775	0.872	3.254	45.6	1.50	7.14	Soupy mud
17X-7, 25.0	435.155	0.988	3.687	49.42	1.85	7.46	Soupy mud
17X-7, 68.0	435.585	0.936	3.493	47.51	1.68	7.35	Soupy mud
18X-5, 123.0	443.33	1.566	5.779	38.74	1.85	14.92	Soupy sandy laminae
19X-5, 6.0	452.225	0.942	3.476	45.47	1.58	7.64	Soupy mud and ash
19X-7, 5.0	454.8	0.67	2.472	44.12	1.11	5.60	Soupy black sandy laminae
19X-7, 48.0	455.23	0.67	2.472	46.25	1.17	5.34	Soupy mud
20X-1, 34.0	457.84	0.906	3.356	46.82	1.60	7.17	Soupy mud
21X-1, 19.0	467.19	0.375	1.404	50.53	0.50	2.78	Soupy mud
21X-1, 54.0	467.54	0.72	2.697	50.53	1.45	5.34	Soupy mud
21X-1, 88.0	467.88	0.738	2.764	50.53	1.49	5.47	Soupy silt
21X-1, 104.0	468.04	0.678	2.539	49.59	1.33	5.12	Soupy sand
21X-1, 112.0	468.12	0.65	2.434	49.59	1.27	4.91	Soupy sand
21X-2, 11.0	468.525	0.96	3.596	51.24	1.91	7.02	Black layer in mud
21X-2, 14.0	468.555	0.815	3.052	51.24	1.67	5.96	Soupy sand
21X-2, 30.0	468.715	0.608	2.277	51.24	1.23	4.44	Soupy sand
21X-2, 36.0	468.775	0.689	2.581	51.24	1.42	5.04	Soupy sand
21X-2, 78.0	469.195	0.563	2.109	48.14	1.02	4.38	Soupy sand
21X-2, 95.0	469.365	0.597	2.236	48.14	1.10	4.64	Soupy sand
21X-3, 28.0	469.895	0.688	2.577	47.37	1.27	5.44	Soupy mud
21X-7, 13.0	473.915	0.599	2.243	54.38	1.33	4.12	Soupy mud
21X-7, 44.0	474.225	0.558	2.09	55.38	1.25	3.77	Soupy mud
22X-2, 22.0	477.38	0.722	2.714	49.22	1.41	5.51	Soupy sand
22X-3, 14.0	477.725	0.65	2.444	49.22	1.26	4.97	Soupy sand
22X-5, 52.0	479.74	0.619	2.327	53.3	1.34	4.37	Soupy sand
22X-5, 97.0	480.19	0.49	1.842	53.3	0.97	3.46	Soupy sand
22X-8, 16.0	481.39	0.579	2.177	48.34	1.07	4.50	Soupy sand
24X-1, 35.0	495.85	0.59	2.177	48.79	1.08	4.46	Soupy mud
24X-1, 100.0	496.5	0.351	1.295	45.04	0.32	2.88	Soupy mud
24X-2, 85.0	497.745	0.41	1.513	52.37	0.64	2.89	Soupy mud
24X-3, 30.0	498.56	0.421	1.554	49.58	0.63	3.13	Soupy mud
24X-4, 10.0	499.76	0.369	1.362	46.12	0.40	2.95	Soupy mud
338-C0002L-2X-1, 3.0	286.53	0.577	2.129	48.63	1.05	4.38	Soupy mud
3X-1, 32.0	296.32	0.742	2.738	56.78	1.78	4.82	Soupy silty mud
5X-1, 79.0	315.79	0.718	2.649	54.23	1.59	4.88	Soupy silty mud

5X-4, 73.0	318.425	0.966	3.565	49.02	1.78	7.27	Dark soupy sand
5X-5, 56.0	319.31	1.366	5.041	49.41	2.29	10.20	Dark soupy sand
5X-5, 81.0	319.56	1.071	3.952	44.08	1.68	8.97	Dark soupy sand
5X-6, 50.0	320.485	1.053	3.886	45.18	1.71	8.60	Dark soupy sand
5X-7, 21.0	321.305	1.086	4.007	43.67	1.68	9.18	Dark soupy sand
5X-7, 21.0	321.305	1.086	4.007	43.67	1.68	9.18	Dark soupy sand
6X-1, 65.0	325.15	0.843	3.205	44.8	1.45	7.15	Soupy silty mud
6X-2, 68.0	325.995	1.358	5.163	49.85	2.36	10.36	Soupy silty mud
6X-5, 103.0	328.475	1.199	4.559	54.34	2.49	8.39	Soupy silty mud
8X-2, 28.0	344.085	1.392	5.273	50.02	2.40	10.54	Soupy dark sand
8X-5, 73.0	347.43	1.603	6.072	50.28	2.62	12.08	Soupy dark sand
9X-1, 10.0	353.1	0.83	3.132	46.37	1.49	6.75	Soupy mud
9X-3, 25.0	354.53	0.762	2.875	49.32	1.49	5.83	Soupy mud
9X-3, 55.0	354.83	0.68	2.566	51.14	1.41	5.02	Soupy mud
9X-8, 75.0	359.455	0.67	2.528	55.78	1.59	4.53	Soupy mud
9X-8, 95.0	359.655	0.96	3.623	44.66	1.60	8.11	Soupy silty mud
10X-1, 99.0	363.49	0.381	1.432	60.17	0.71	2.38	Soupy mud
10X-1, 99.0	363.49	0.381	1.432	60.17	0.71	2.38	Soupy mud
10X-7, 122.0	368.66	0.645	2.425	47.31	1.18	5.13	Soupy sand
11X-1, 83.0	372.83	0.828	3.09	52.14	1.73	5.93	Soupy dark sand
11X-3, 20.0	374.83	0.455	1.698	56.18	0.92	3.02	Soupy silty mud
11X-6, 13.0	376.345	0.705	2.631	55.71	1.65	4.72	Soupy sand
12X-1, 103.0	382.53	0.641	2.392	49.48	1.24	4.83	Soupy
13X-5, 32.0	396.455	0.801	2.989	52.7	1.71	5.67	Soupy sand
15X-7, 44.0	415.205	0.686	2.569	59.92	1.84	4.29	Soupy sand
15X-7, 70.0	415.465	0.616	2.307	59.92	1.63	3.85	Soupy sand
15X-8, 130.0	417.465	0.946	3.543	48.65	1.76	7.28	Soupy sand
16X-2, 44.0	420.915	0.959	3.578	51.94	1.95	6.89	Soupy sand
16X-7, 38.0	426.785			42.41			Soupy mud
16X-7, 105.0	427.455			47.76			Soupy mud
17X-1, 107.0	430.07	0.631	2.354	48.65	1.19	4.84	Soupy mud

17X-6, 25.0	433.775	0.872	3.254	45.6	1.50	7.14	Soupy mud
12X-1, 103.0	382.53	0.641	2.392	49.48	1.24	4.83	Soupy

No authigenic carbonates were identified. Between 205.97- 496.75 mbsf, there were 17 intervals with pyrite abundances of >0.1-1%, and 10 intervals where pyrite was common at >1-10% (Table 3, Fig. 4.15). High pyrite accumulation could be recording fossilized sulfate-methane transitions zones (Borowski et al., 2013). There was also no progressive clay mineral diagenesis (Guo and Underwood 2012). Authigenic pyrites were also recovered during IODP Expedition 316 at Site C0008C located trenchward near the megasplay fault (Kars and Kodama, 2015).

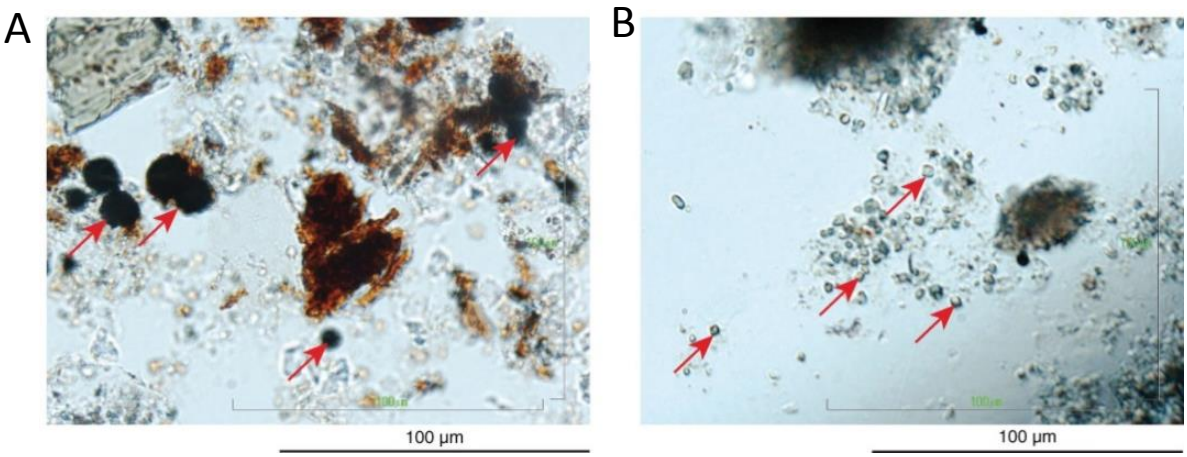

Figure 4.15 - Examples of petrographic features including A. Red-brown organic matter (kerogen) of terrestrial origin (Sample 338-C0002H-2R-3, 70 cm; PPL). Red arrows = pyrite framboids. B Possible microdolomite crystals (red arrows) in a calcareous silty claystone (Sample 338-C0002H-1R-1, 102 cm; XPL). Modified Figure F34 from Strasser et al., 2014.

Table 4 - Authigenic Pyrite Occurrences at C0002. Abundant pyrite accumulation may record buried paleo-SMTZ. With precise sedimentation rates and age constraints, you could theoretically determine times of active methane venting.

Authigenic Pyrite Occurrences C0002 Expedition 338 D: dominant (>50%), A: abundant (>10-50%), C: common (>1-10%), F: few (>0.1-1%), R: rare <0.1				
Core Identification	Depth mbsf	Lithology	Abundance	Notes
C0002K-3T-1 47.0	205.97	silty clay	F	
C0002K-3T-2 41.0	206.81	silty clay	F	
C0002K-3T-2 60.0	207.00	silty clay	F	

C0002K-3T-4 60.0	209.08	silty clay	F	
C0002K-3T-4 85.0	209.33	Sand	C	
C0002K-6T-4 109.0	232.74	silty sand	F	
C0002K-8X-3 117.0	251.57	Sand	C	
C0002K-8X-4 80.0	252.45	silty clay	F	
C0002K-9X-1 20.0	258.20	sandy silty clay	F	
C0002K-9X-2 80.0	259.81	silty clay	F	
C0002K-9X-4 45.0	260.84	fine sand	F	
C0002K-10X-1 37.0	267.87	silty sand	C	
C0002L-5X-1 30.0	315.30	silty clay	F	
C0002L-5X-4 20.0	317.90	silty clay	F	
C0002L-6X-1 15.0	324.65	silty clay	F	
C0002L-10X-2 14.0	363.78	silty clay	F	
C0002L-12X-2 89.0	383.62	Sand	C	
C0002L-14X-2 39.0	402.29	sandy silt	C	
C0002L-14X-2 50.0	402.40	silty sand	F	
C0002L-15X-10 37.0	418.85	silty sand	C	Tiny framboids and as grain coatings
C002L-20X-4 22.0	460.68	silty clay	C	
C0002L-17X-1 18.0	429.18	silty clay	F	
C0002L-17X-6 28.0	433.81	sandy silt	C	
C0002L-18X-4 74.0	441.44	sand 100%	C	Microcrystalline grain coated and framboids
C0002L-20X-CC 46.0	467.17	Sand	C	Microcrystalline grain coated and framboids
C0002L-22X-5 120.0	480.42	silty clay	F	
C0002L-24X-1 125.0	496.75	sandy silt	F	

Porosity measurements from Expeditions 338 and 315 were compiled into a single chart and shows a generally decreasing trend with depth at approximately 60% near the top of the hole decreasing to about 30% at 1000 mbsf. At the BSR depth of 400 mbsf, porosity is approximately 50% (Fig. 4.16).

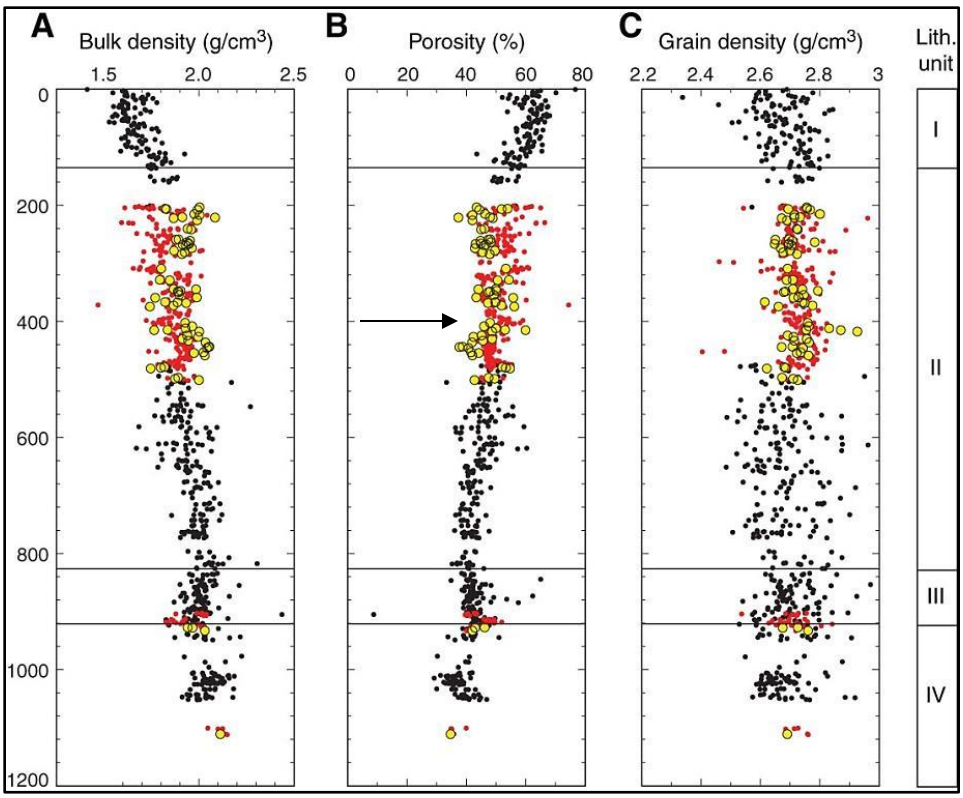

Figure 4.16: MAD measurements on core samples, Site C0002. Red = Expedition 338 mud samples, yellow = Expedition 338 sand samples, black = Expedition 315 data. A. Bulk density. B. Porosity. C.Grain density. Average porosity at the BSR depth of 400 mbsf (black arrow) is ~ 50%. Modified Figure F86 from Strasser et al., 2014

4.1.2 Site C0009

Site C0009 is located 20 km northeast of Site C0002 with a seafloor depth at 2054 mbsl. To meet the specific science objectives of Expedition 319, LWD was given priority over coring within the basin sediments, and the available data relevant to gas hydrate occurrence is abbreviated compared to the datasets provided by cores collected at Site C0002. However, the logging data, cutting analyses, mud gas chemistry, and analyses conducted on 34 cores collected between 1510 and 1594 m core depth below seafloor (CSF) (well below the gas hydrate occurrence zone (GHOZ)) do provide important clues for understanding the basin's gas source and migration pathways, and further provide sedimentological constraints for interpreting seismic horizons.

4.1.2.1 NGH Geochemical Indicators

Mud gas samples were collected during all phases of drilling and analyzed throughout the hole. CH_4 concentrations were high in the lower forearc basin sediments (791-1285 mbsf) reaching up to 14 vol% (Fig xx) (Exp. 319 Scientists, 2010). Higher order hydrocarbons including ethane (C_2H_6) and pentane (C_3H_8) were also detected at 16 ppmv and 3 ppmv respectively (Fig. 4.17) (Exp. 319 Scientists, 2010; Doan et al., 2011).

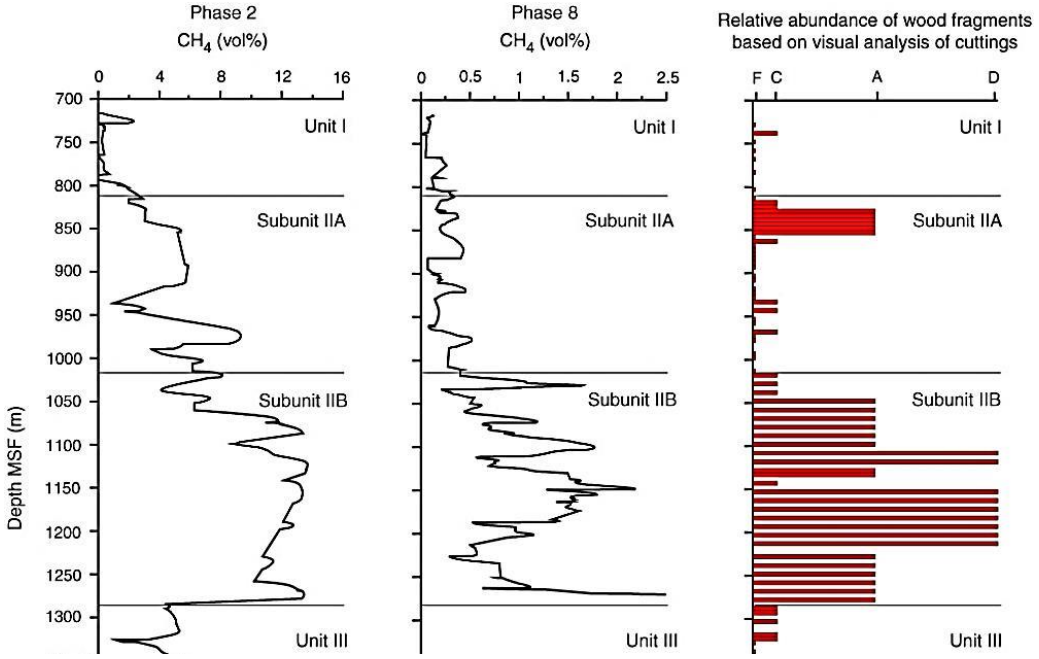

Figure 4.17 - Methane distribution in drilling mud gas during Phase 2 and Phase 8 plotted next to relative abundance of woody fragments from visual observations of drill cuttings. D = dominant, A = abundant, C = common, F = few. Figure from Expedition 319 Scientists (2010).

TOC was only measured from cuttings collected between 1038 and 1588 mMSF and from core samples collected from 1509.8 to 1591.5 mCSF. No data exist for upper basin sediments. TOC was, on average, 2.51 wt% in comparison to 0.55 avg. wt% at C0002. Notably, TOC content reached peaks as high as 8.7 wt% at 1088 and 1183 MSF likely from high wood and coal (lignite) content in the lower forearc sediments (as shown in Fig. 4.18). 5 wt% is enough TOC to support hydrocarbon production of natural gas in situ and thus, we can consider this zone a source region. However, the geothermal gradient at C0009 is lower than at C0002, and

the temperature here is <40°C at 1200 mbsf which is not high enough for *in situ* thermal cracking (Doan et al., 2011). Thus, as Doan et al, (2011) concludes, if methane is being sourced from this region, then it is produced through biogenic pathways.

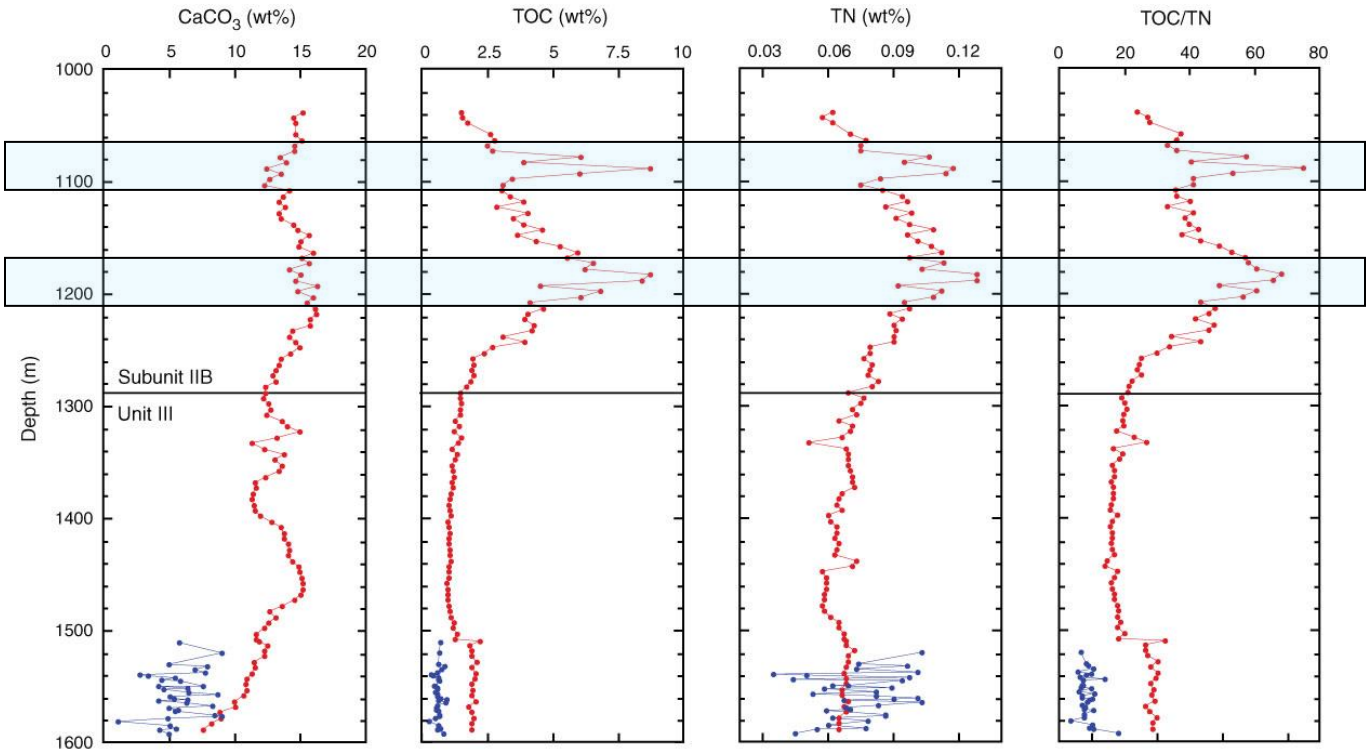

Figure 4.18 - $CaCO_3$, total organic carbon (TOC), total nitrogen (TN), and TOC/TN ratio, Site C0009. Red = cuttings samples, blue = core samples. Cuttings depths are in MSF, core depths are in CSF. Modified F51 from Expedition 319 Scientists (2010).

4.1.2.2 NGH Well Log Indicators

Logging data were collected using both measurement while drilling (MWD) and wireline logging (WL) techniques. Five WL log runs and three phases of MWD provide a continuous downhole record (Expedition 319, 2010). The hole was divided into four logging units primarily based on interpreted changes in lithology (Fig. 4.19, Units I-III shown). There is an excellent correlation between drops in p-wave velocity and increased methane and wood content in Unit IIIB (black box).

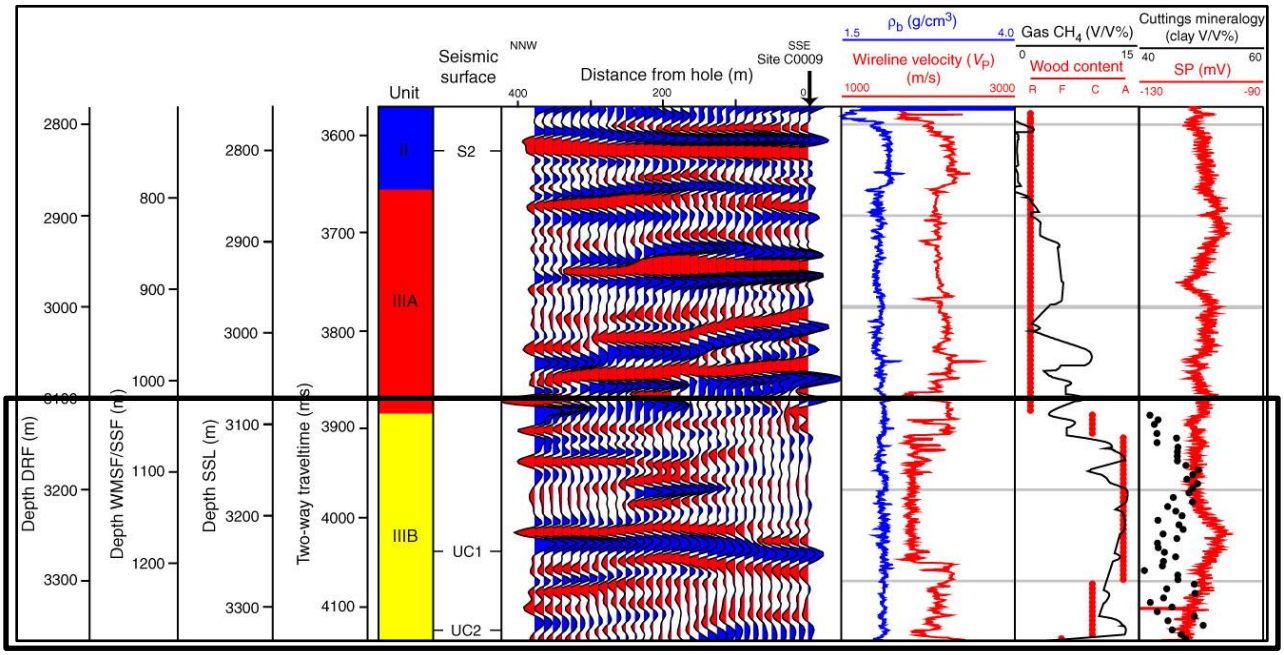

Figure 4.19: Seismic data correlated to well data from 700 to 1500 m WMSF, Site C0009. Vertical arrow = Site C0009 location on seismic data. Low wireline sonic velocity (V_P) is correlated to zones where cuttings had abundant wood fragments and elevated methane concentration from mud gas. Unit III/IV boundary is marked by an increase in clay fraction observed in cuttings from XRD and a decrease in spontaneous potential (SP). R = rare, F = few, C = common, A = abundant. Note abrupt increase in wood at 1037-1047 m MSF. Modified Figure F114 from Expedition 319 Proceedings (2010).

Sonic data was evaluated by Doan et al. (2011) to estimate the total porosity, amount of free gas, and gas distribution downhole using Brie equations for clay. They proposed that in situ biogenic gas produced from the organic-rich sediments of the lower forearc is able to migrate upward along dipping permeable strata and accumulates within coarse grain rich strata towards the seaward edge of the basin.

4.1.2.3 Lithological NGH Indicators

Four lithologic units were defined on the basis of WL, cutting, and geochemical data. Unit I (0-467 mbsf) and Unit II (upper forearc basin 467-791 mbsf) comprise ofsilty mudstone with cyclical sand rich layers 10-50 m in thickness and unconsolidated silty mud with silt and sand interbeds and minor interbeds of volcanic ash respectively (Fig. 4.21). Unit I is noted to be

turbidit-rich with sandier units than found at C0002, while Unit II sands are finer than Unit I, but overall coarser than sands recovered at C0002 and in Units III and IV of C0009. Unit III is distinguished from Unit II by an increase in silt content and overall is composed of silty clay and poorly lithified silty claystone with interbeds of silt and fine sand layers (Expedition 319 Scientists, 2010). Unit III is further broken down into Subunit IIIA and Subunit IIIB. IIIB is characterized by a sharp increase in the abundance of organic woody material (Fig. 4.20). Because the organic material of a source rock is mostly wood, kerogen type III, the hydrocarbon produced upon maturation will be natural gas, versus a type I or II kerogen, primarily composed of algae and marine plankton, respectively, which would generate oil and natural gas (McCarthy et al., 2011). This sedimentary package thickens towards the center of the basin and thins out near C0002 where very little organic matter was found constrained to this unit Unit IV (1287.7 to 1603.7 m MSF) is finer-grained than previous units dominated by silty claystone with some silt interbeds and poorly consolidated sands and the rare fine vitric tuff. The wood content is decreased. According to the biostratigraphy, this unit is 5.6 to 7.9 Ma and is separated from Unit III by a 1.8 Ma hiatus between 3.8 and 5.6 Ma (Expedition 319 Scientists, 2010).

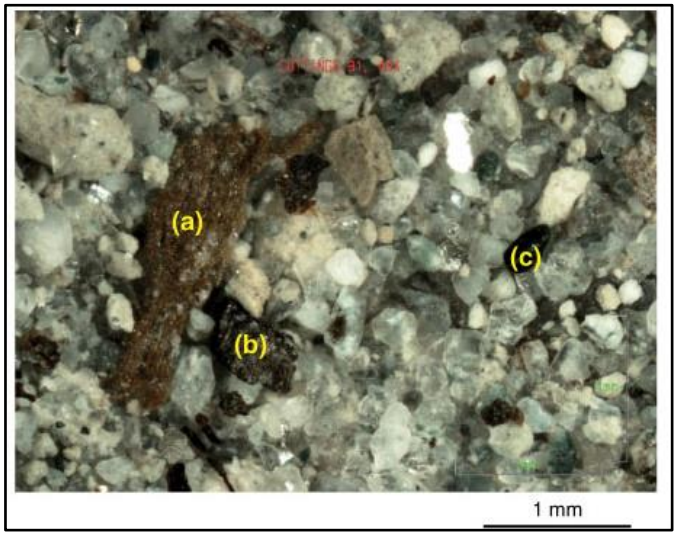

Figure 4.20 - Binocular photographs of fine-grained cuttings samples, 319-C0009A-81-SMW (1067.7–1072.7 m MSF, Subunit IIIB) with (a) pyritized wood, (b) wood/lignite, and (c) rounded Glauconite. Modified Figure F15 from Expedition 319 Scientists (2010).

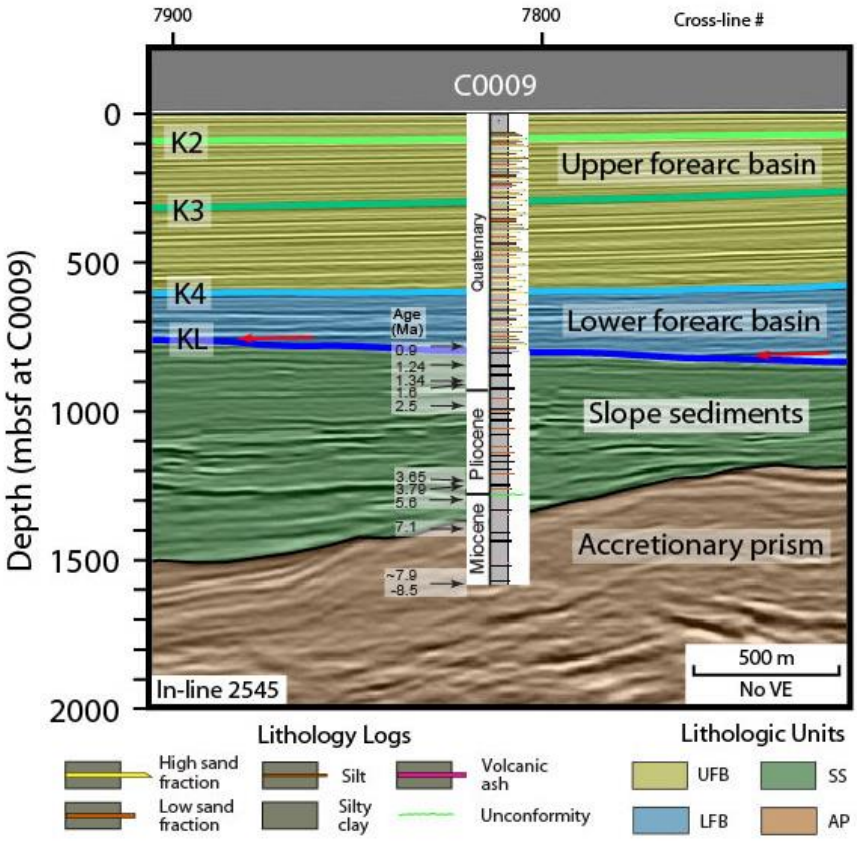

Figure 4.21 -Lithostratigraphic summary column of site C0009 overlain on a 3-D seismic in-line. Seismic sequence boundaries are from Gulick et al. (2010). VE = vertical exaggeration. Taken from Moore et al., 2015.

4.2 Seismic Data

The 3D PSDM seismic volume reveals a complicated geology as a result of complex faulting, tilting of beds from tectonic uplift of the basin's seaward margin, and numerous events of mass wasting. The dominant acoustic character of the basin's strata consists of landward-tilted (on the seaward end) to planar parallel (landward end), high-amplitude, laterally-continuous reflections interpreted as onlapping turbidite sequences. The basin-fill architecture shows that continuation of the uplift, along with growth of the accretionary wedge, migrated the locus of sedimentation landward, expanding the basin from ~10 km in width to > 30 km. A

topographic high, formed by continued motion along thrusts in the underlying prism, is onlapped by deformed basin strata. Channel deposits occur throughout, indicating changes in depositional environment over time (Fig. 4.22). High amplitude reflections (HARs) correlating with gas charged sands are common beneath the primary BSR (e.g., Fig. 4.22 and 4.23). Blanking is observed in a thick sequence above the BSR and is inferred to indicate gas hydrate occurrence, (e.g., Ecker et al., 2000) (Fig 4.24). Drilling in the GoM has demonstrated that blanking is related to GH occurrence, but reflects only minor hydrate saturations and is not considered a prospective resource zone (Boswell et al., 2014).

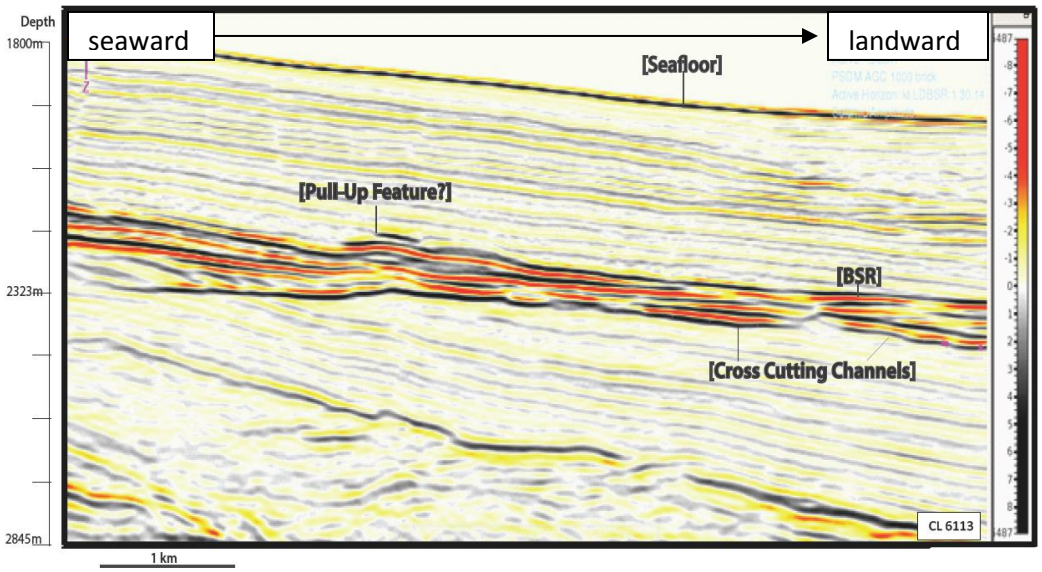

Figure 4.22 - HARS just above and below the BSR in crossline 6113 looking landward indicating gas hydrate and free gas occurrence respectively. Gas related HARs are highly concentrated in erosional or potential channel features. Sequences containing hummocky strata characteristic of slumps and MTDs are observed near the seafloor. Hydrate dissolution or dissociation could contribute to the formation of MTDs by reducing the shear strength of the surrounding host sediments. Reduced permeability in the MTDs may act as a cap overlying the free gas below the GHSZ.

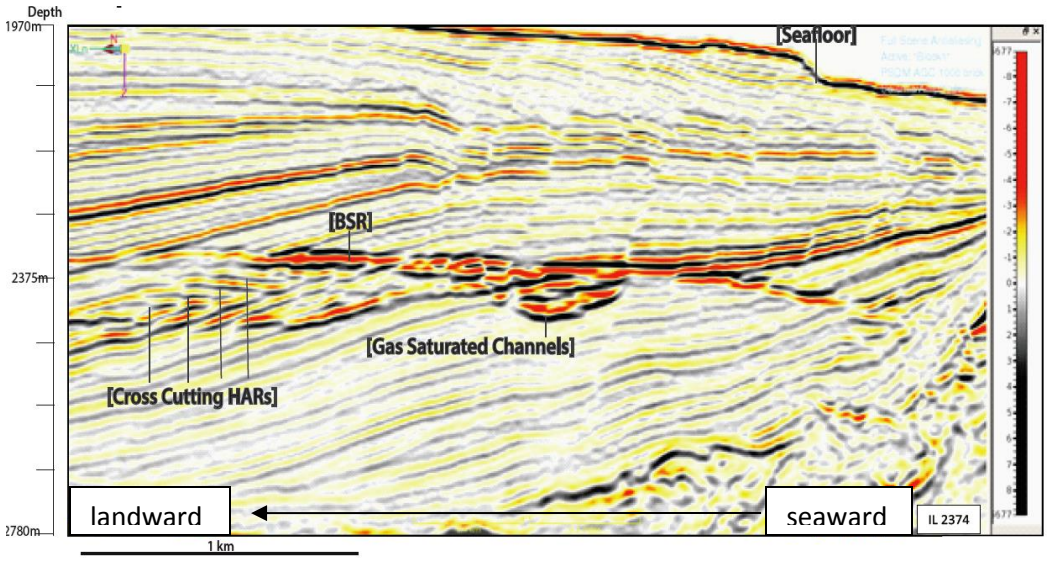

Figure 4.23 - Inline 2374 view of HARs beneath the BSR and strong HARs within the erosional channel feature near the margin of the basin.

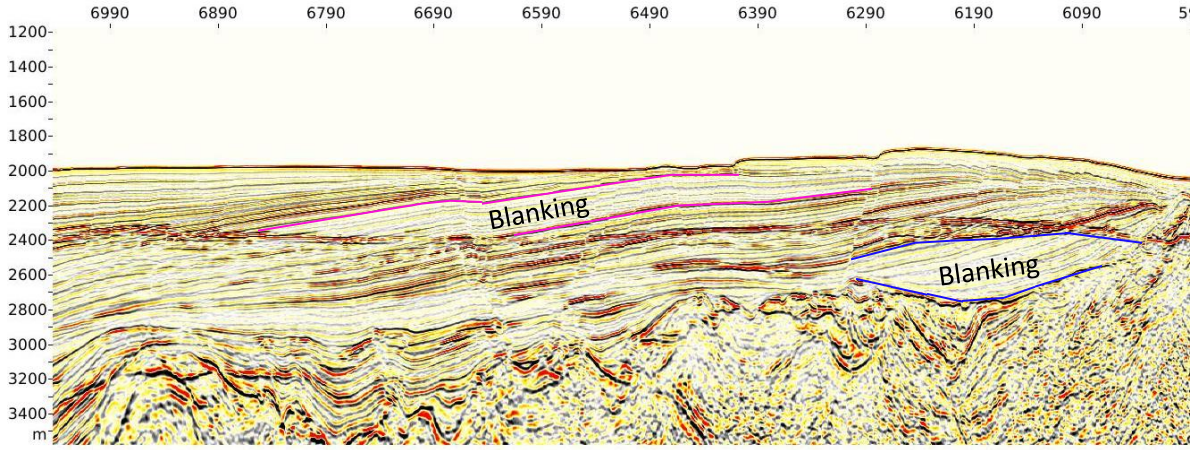

Figure 4.24: Inline 2312 Acoustic Blanking above the BSR attributed to low gas hydrate saturations. Blanking below the BSR could be from either gas saturated muds, or acoustic attenuation of the seismic wave as it passes through a thick free gas zone.

MTDs are common sedimentary features in the Kumano seismic data (e.g. Moore et al., 2015) and are important because the can affect the geometry and distribution of free gas, gas hydrates, and alter fluid flow pathways. There are abundant small to large scale MTDs throughout the basin which seem to have slid along bedding planes during uplift. These

features are characterized by chaotic seismic reflections with an underlying basal sliding plane and an overlying bounding surface (e.g., Fig. 4.25). It is hypothesized that the large release of gas and water from large-scale hydrate dissociation could result in excess pore pressure, mechanical weakening, and a reduction in effective stress which together can directly initiate large scale sediment failure (Sultan et al., 2004; Ellis et al., 2010; Mountjoy et al., 2013; Vanneste et al., 2014) However, excess pore pressure can also be triggered by rapid sediment loading, and the vertical effective stress can be decreased by lateral flow along permeable pathways (Dugan and Flemings, 2000). Alternatively, Yelisetti et al. (2014) proposed that gas hydrate-strengthened sediments could act as a glide plane for overlying sediments lacking the extra stability provided by hydrates. While we do know that the MTDs in the Kumano Basin do not have a recurrence interval in agreement with the seismicity recurrence interval (Moore and Strasser, 2015), to determine whether MTDs are triggered by hydrate dissociation, differential loading, lateral fluid flow, or from the contrast in sediment physical properties between hydrate filled and non-hydrate filled sediments requires further investigation.

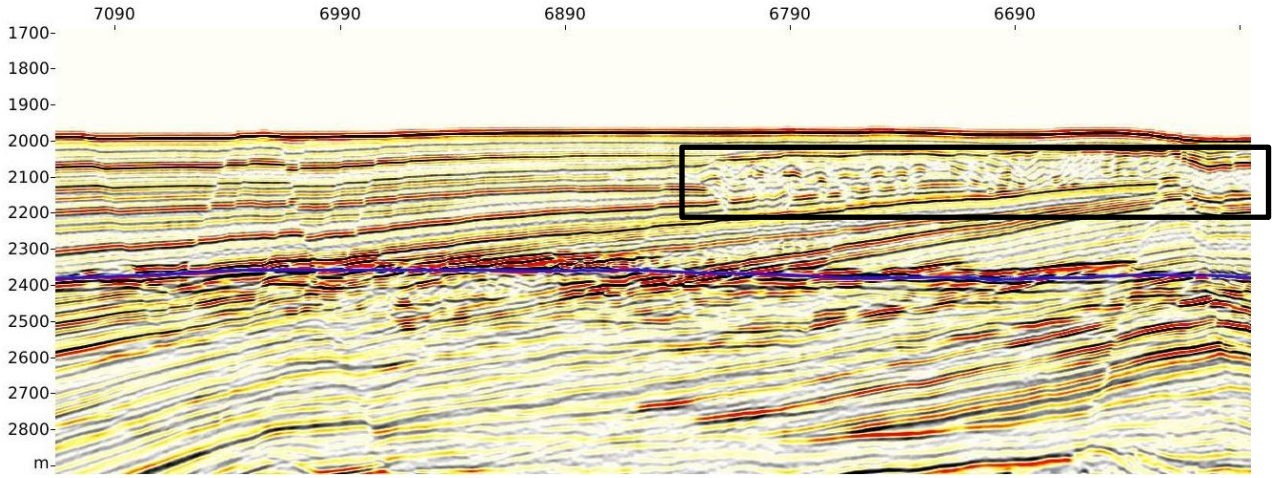

Figure 35: Inline 2435. An example of a very large MTD in the center of the basin is framed in black. It measures 3125 km across, and >100 m thick.

4.2.2 Multiple BSRs

There are 3 BSRs, referred to here as the primary BSRs (BSRs), upper BSRs (UBSRs) and lower BSRs (LBSRS) and each are abundant throughout the survey region. Since not all BSRs are associated with gas hydrates (e.g. Somoza et al., 2014), it is necessary to distinguish between the different types of BSRs in order to understand what these seismic events mean in terms of the geology (e.g. Berndt, 2004). The primary BSR, representing the current base of hydrate stability was identified as a crosscutting reflection that closely mirrors the seafloor and is opposite polarity to the seafloor (red). Because the primary-BSR is a gas hydrate related BSR, the amplitude strength is strongly affected by the amount of free gas below (Golmshtok and Soloviev, 2006; Yi et al., 2011). UBSRs and LBSRs are crosscutting reflections that occur above and below the primary BSR and are generally the same polarity as the seafloor (black) with the exception of one lower double BSR which appears as a second reversed polarity reflection (red).

4.2.2.1 Primary BSRs

The primary BSR is a prevalent, continuous feature across the basin (Fig. 4.26 and 4.27). It generally exhibits a strong high amplitude character, suggesting a continuous free gas zone is present beneath. It is parallel or sub-parallel to the seafloor, occurring between a minimum depth of ~320 mbsf and a maximum depth of ~520 mbsf with an average depth at 400 mbsf. We have determined that this seismic event is a GH related BSR that generally marks the three-phase (water+gas+hydrate) equilibrium boundary based on its depths below seafloor, which nearly coincides with estimated BGHS depths (Chapter 6). Further, it is a crosscutting reflection with reversed polarity (red) relative to the seafloor (black) (e.g. Spence et al., 2010), and logging data at C0002 shows a resistivity peak followed by a drop right at the BSR boundary indicating the presence of hydrate immediately above the BSR with a lack of hydrate below (Strasser et al., 2014). The depth at the base of the GH layer at Site C0002 at 400 mbsf perfectly matches the BSR depths in our 3D seismic volume data (Tobin et al., 2009); this gives us confidence in the accuracy of the BSR depths in this study. However, it is important to note that “BSR” and

"BGHS" are not interchangeable terms; in some instances, the BSR could be in a transitory state, unaligned with the current BGHS.

Further evidence to support that the primary BSR is a GH related phase boundary is the frequent occurrence of seismic phase changes in dipping beds crossing BSRs. Drilling in the Gulf of Mexico has confirmed that this type of phase change occurs as a result of changes in physical properties when a hydrate saturated layer is buried beneath the BGHS and becomes a water-gas saturated unit (Boswell et al., 2012). Barnes et al. (2013) noted this phase change character and proposed that higher amplitude horizons above the BSR may be associated with gas hydrate accumulation while high amplitudes below the BSR could be associated with gas. Her research further found that BSR amplitude strengths were strongest when intersecting sand layers.

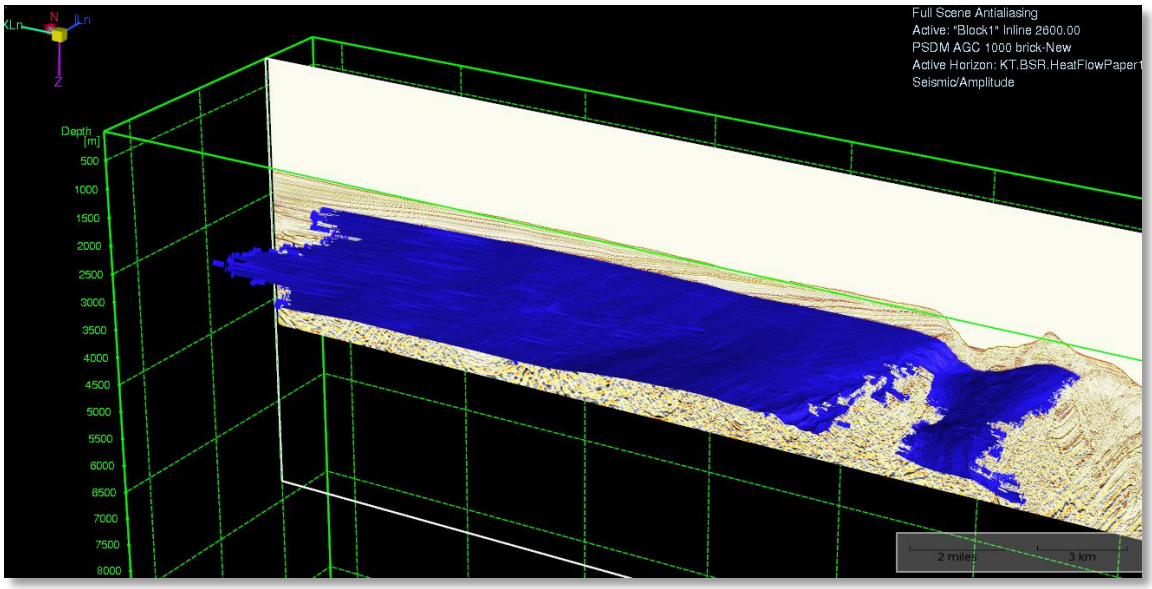

Figure 4.26 - Tridimensional view of the interpreted BSR in Paradigm 3D Canvas.

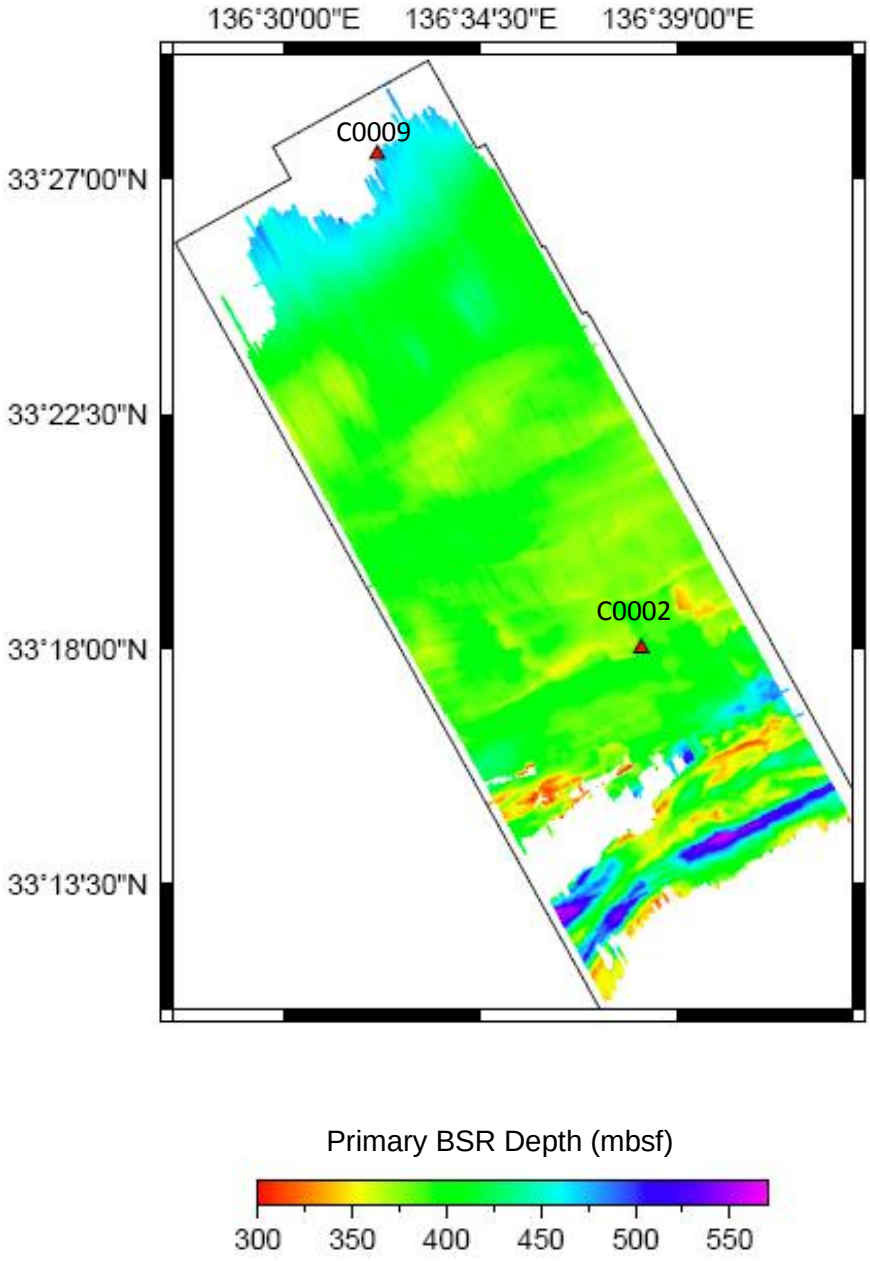

Figure 4.27- Primary BSR depth map in meters below seafloor. Red triangles represent drill Sites C0009 and C0002.

The relationship of the BSR relative to faults can tell us about the timing of faulting if the BSR is offset, or about fluid flow if the BSR shoals upward/downward surrounding a fault indicating the of upward migration of warm fluids or the downward migration of cold fluids, respectively. There are no significant offsets of the BSR across faults in our seismic data, which was similarly observed to be the case in the Makran region (Smith et al., 2014). On occasion, however, the amplitude of the primary BSR weakens when crossing faults as was the case in the KG Basin offshore India (Wang et al., 2014) and in the Trujillo Basin, Peru (Herbozo et al., 2013)(Fig. 4.28).

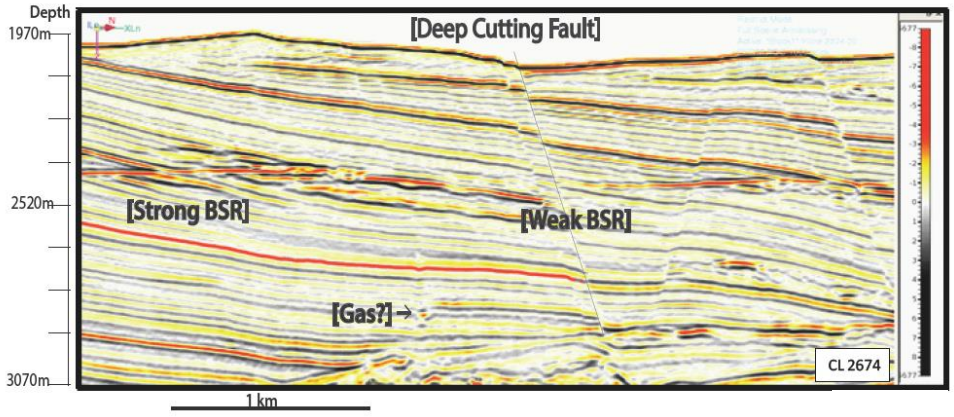

Figure 4.28 - Seismic crossline 2674 (seaward to the left, landward to the right) showing weak BSR amplitudes on the hanging wall. The shift from strong to weak BSR amplitudes across deep cutting normal faults could indicate an active gas escape route.

The BSR is clearly sub-parallel to the seafloor in various regions, indicating local perturbations or variable conditions in the ambient environment. Shedd et al. (2012), refers to up-warped BSRs as “pluming” BSRs which shoal upward in response to heat from below. The primary BSR in this study region warps both upward relative to the seafloor in response to elevated heat transport from below, and downward in response to seafloor erosion and subsequent exposure to cold bottom waters and a cooling in the surrounding environment Noteworthy is the very deep BSR that does not mirror the seafloor at the outer notch. Detailed investigation of BSR anomalies is the topic of Chapter 6.

There are four zones where the primary BSR is not apparent in the seismic data. The first occurs across a fold in the accretionary prism which is technically outside of the Kumano Basin boundary (Fig. 4.29). The second is a small circular region associated with a vent feature (see Cartwright and Santamarina, 2015 for an excellent overview of fluid escape features) in the seaward edge of the basin near the outerarc high, interpreted to be an active mud volcano. Here the BSR deflects upward (pluming BSR) before terminating across the chaotic reflections of the vent. The third region crosses a syncline feature in the landward half of the margin. Here it was necessary to infer the BSR depths. Two ends of a continuous BSR were extrapolated across and connected across the syncline. This means that there could be some errors associated with the picks in this region. Lastly the BSR fades out in the parallel dipping strata on the landward most edge of the survey which results in the irregular BSR truncations along strike in the BSR map.

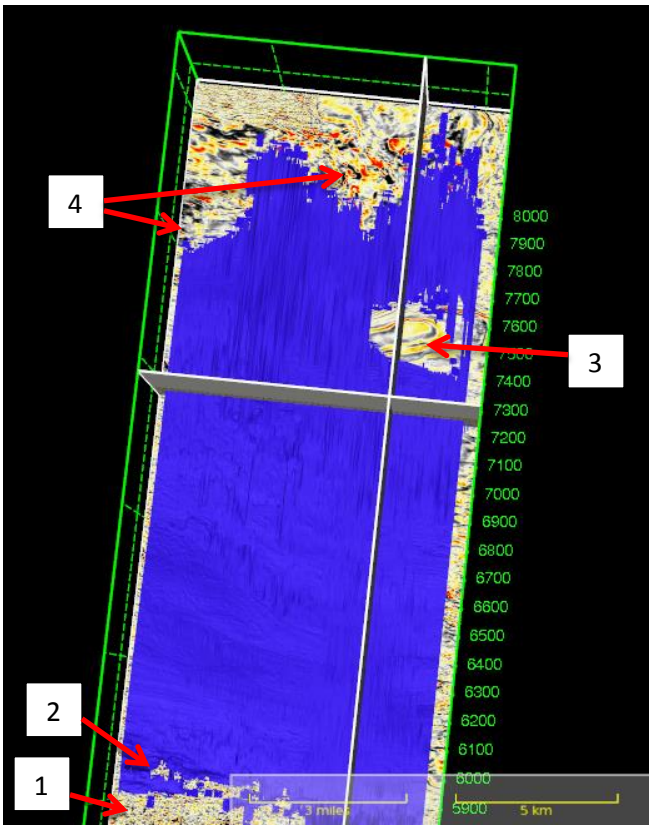

Figure 4.29 Tridimensional map view of the primary BSR highlighting the four regions where BSRs were not imaged in the seismic data. Region 3 was interpolated for the purpose of deriving heat flow values.

4.2.2.2 Lower BSRs

Lower BSRs are commonly referred to as “double BSRs” (Inamori and Hato, 2004; Foucher et al., 2002; Rajput et al., 2012). However, we adopt the term “lower BSR” to distinguish its spatial relationship to the primary BSR. LBSRs appear in localized regions, the seismic amplitude volume beneath the primary BSR, as patchy, discontinuous reflections of variable thickness and amplitude strength (Fig. 4.30 and 4.31). We discriminate two distinct types of LBSRs based on their amplitude polarity relative to the seafloor and their velocity character in the seismic velocity volume.

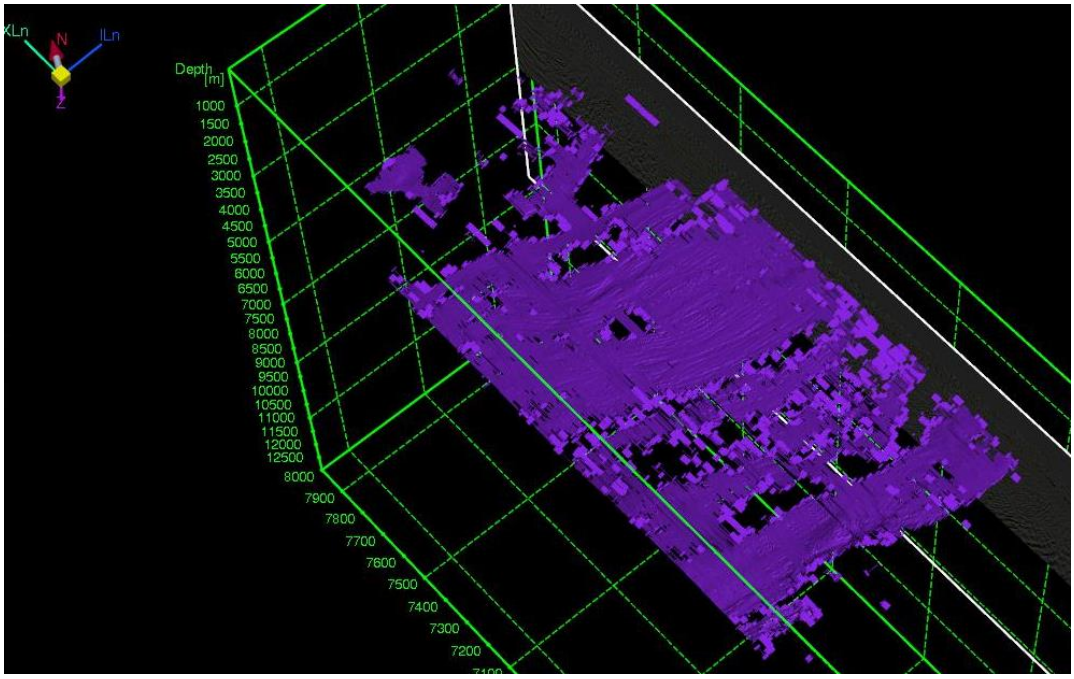

Figure 4.30 - Tridimensional, map view of the interpreted lower BSRs distributions in Paradigm 3D Canvas.

LBSR-1s are prominent positive polarity reflections falling between 25 m -100 m deeper than the primary BSR. They are strongest in the seaward half of the basin where successive activations of the megasplay fault has resulted in uplift and ~5-8 degrees of tilt over a period of 300,000 years (Gullick et al., 2010). Here, gas from depth is observed in the seismic data to be

migrating updip via landward dipping strata corresponding to C0002 Zone B (Fig. 4.31). The amplitude character of the LBSR-1s is very strong, and appears to be segmented laterally by non-permeable dipping beds. Similar segmented BSRs are found beneath some thrusts on the Hikurangi Margin (Navalpakam et al., 2012) and in the Gulf of Mexico (Shelander et al., 2010) and are believed to represent a zone of higher gas or hydrate saturations in higher porosity sediments which has been confirmed by drilling (Shelander et al., 2010). As opposed to the LBSR-2s discussed next, these LBSR-1s are not associated with a low velocity zone (Fig.44)

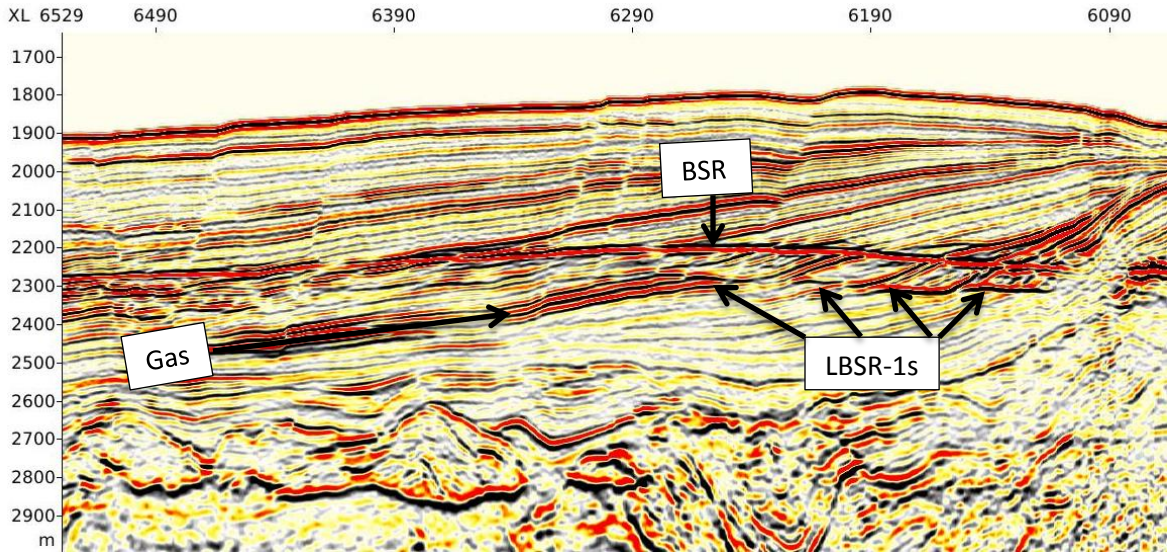

Figure 4.31: Inline 2185 displaying lower HARs, HAR in dipping strata below lower BSRs and overlying primary BSR

LBSR-2s are common in the heavily faulted central regions of the basin, particularly above a buried thrust fault (Fig. 4.32, black arrows). They are segmented laterally but are continuous for long distances along the strike parallel to the trench (see LBSR map Fig. 4.30). There are additional BSR-like reflections beneath the LBSR-2s (Fig. 4.32) with the same regional pattern, however, they are more disperse and display weaker amplitude strengths than overlying LBSR-2s (Fig. 4.32). The LBSR-2s are reversed polarity reflections, and lack the lateral

continuity of the primary BSR. These acoustic boundaries fall within a think low velocity zone (Fig. 45).

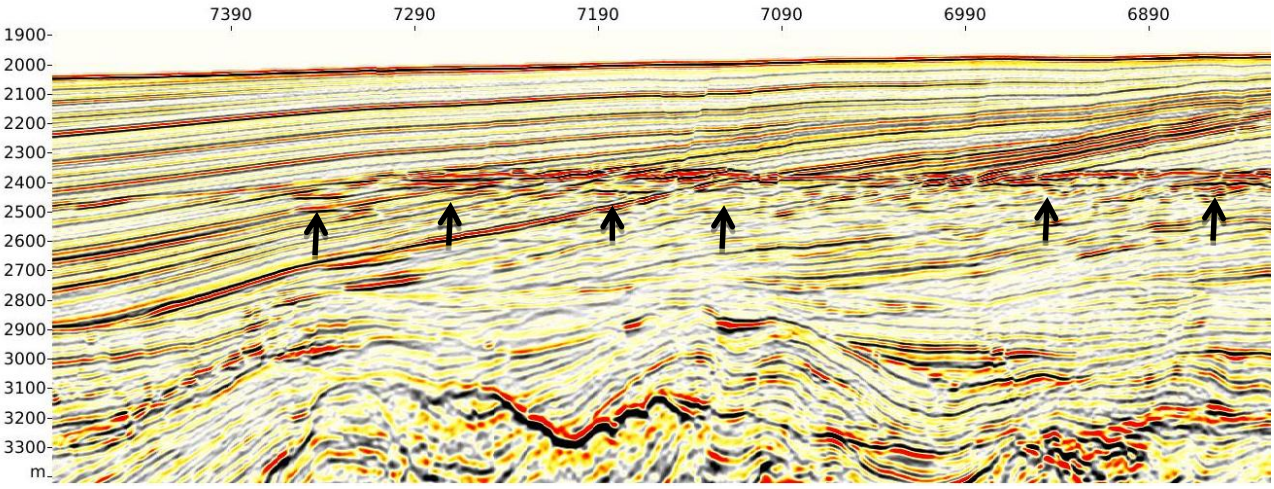

Figure 4.32 - Lower BSRs-2 in the central region of the basin overlying a 0.43 Ma reactivated thrust.

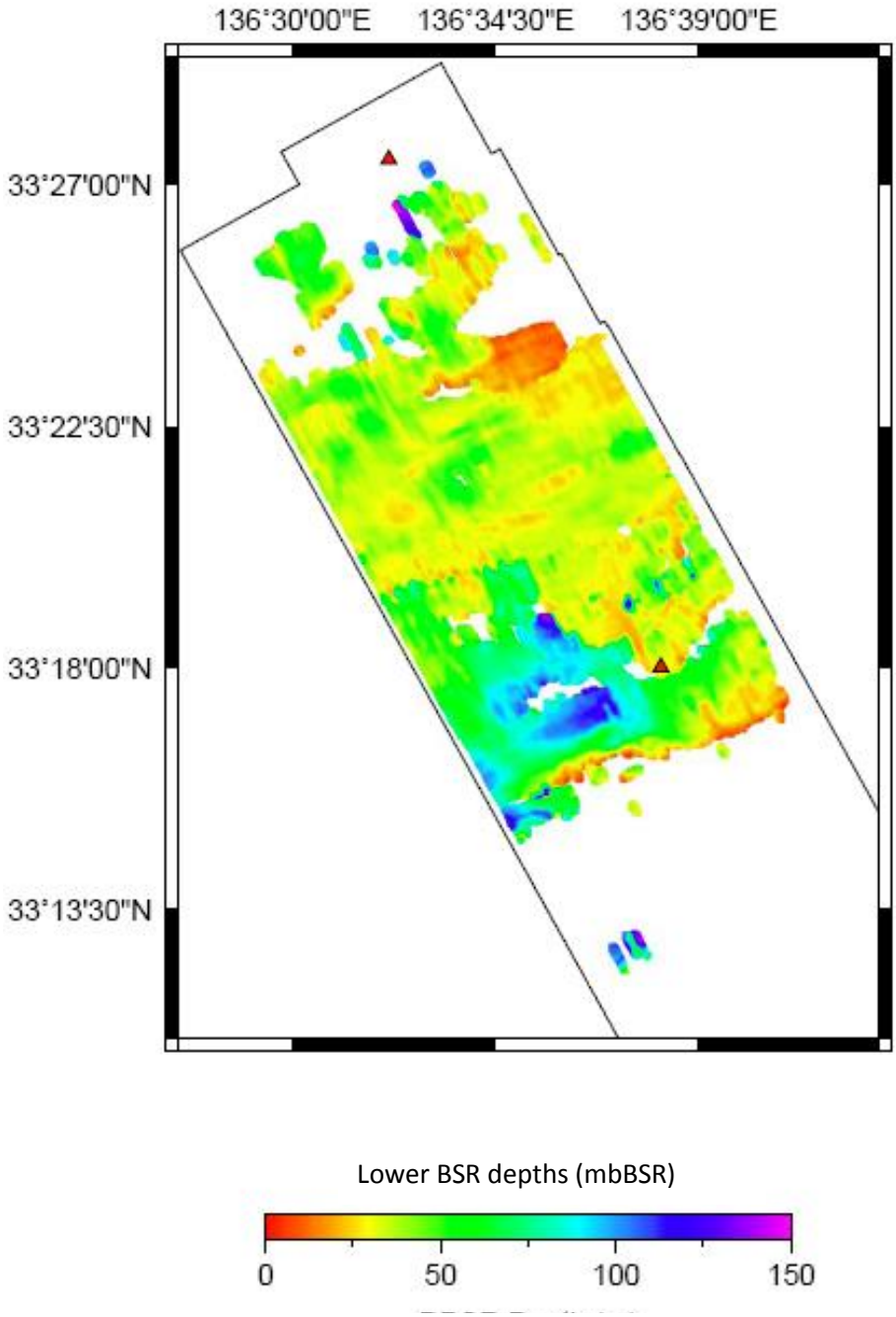

Figure 4.33 - Map of Lower BSR depths below the primary BSR.

4.2.2.3 Upper BSRs

Positive polarity, crosscutting reflections indicating an increase in impedance contrast appear above the primary BSR in two regions of the basin: UBSR-1 is in the central region associated with numerous normal faults and fractures, and UBSR-2 is near the uplifted outer arc on the seaward end (Fig. 4.34). UBSR-1s are patchy, sub-parallel to the seafloor, and clearly terminate against regional normal faults particularly in the center of the basin. They are located between 10-100 m above the primary BSR, but on average are ~40 m higher. UBSR-2s are less frequent and are limited to the seaward edge of the basin where uplift has occurred along the outerarc. These UBSR-2s are nearly parallel to the seafloor, and appear to crosscut sandy units only. They show a steeper gradient than the UBSR-1s and are up to 90 meters above the primary BSR.

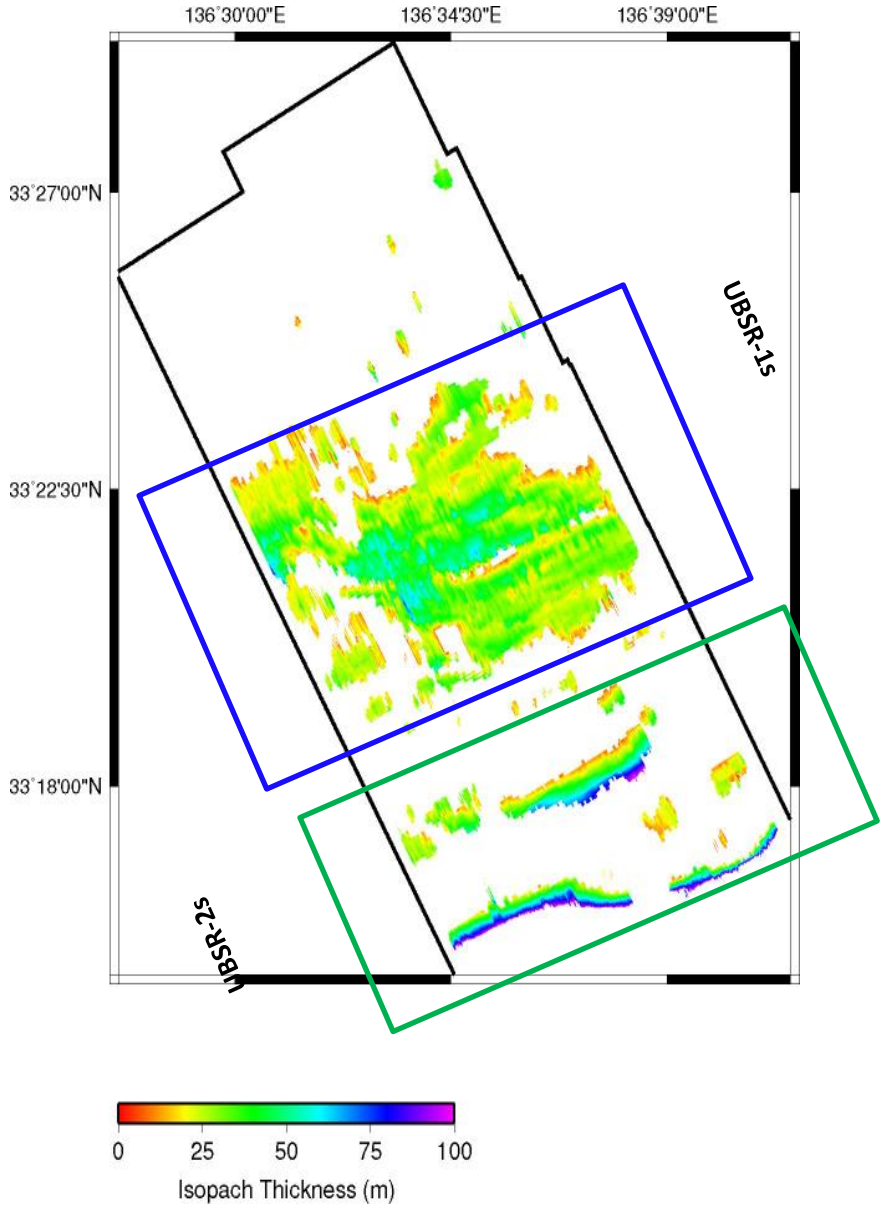

Figure 4.34 - Distribution of Upper BSRs. Isopach thickness values illustrates thickness between the UBSRs and the underlying primary BSR. This surface serves as the upper boundary for hydrate concentration zones for the GIP resource estimate in Chapter 8.

Chapter 5

Data Interpretation and Discussions

"In solving a problem of this sort, the grand thing is to be able to reason backward. That is a very useful accomplishment, and a very easy one, but people do not practice it much. In the everyday affairs of life it is more useful to reason forward, and so the other comes to be neglected. There are fifty who can reason synthetically for one who can reason analytically."

-Sherlock Holmes, A Study in Scarlet, Sir Arthur Conan Doyle

5: Data Interpretation and Discussions

5.1 NanTroSEIZE Drilling Data

Geochemical, geophysical and sedimentological data from Sites C0002 and C0009 clearly document abundant gas hydrate occurrences within the GHSZ above 400 mbsf, preferentially accumulating in sand units and notably one gas hydrate related explosion approximately 86 m below the BSR. There are discrepancies in quantitative GH saturation estimations depending on the proxy used. Errors are likely the result of inaccuracies in proxy assumptions related to baselines, which is not uncommon in hydrate estimations. For example, the use of Archie equations to estimate gas hydrate saturations from resistivity logging data has been proven to overestimate hydrate saturations (Max,2012; Lee and Collett, 2001; Shankar 2011; Pandey et al., 2013). While other margin studies have found that Cl- measurements provide more accurate estimates (e.g., Kumar et al, 2009) than logging data, without data from pressure cores (e.g., Schultheiss et al., 2010) there is no way to determine at this stage which method of hydrate saturation estimation is the most accurate in predicting in situ conditions in the Kumano Basin.

The predominant chemical reaction pathways involved in the production of natural gases in marine sediments include microbial mediated decay of organic carbon, anaerobic oxidation of methane, sulfate reduction, and thermal cracking of organic matter following deep burial (Kaplan, 1972). It has been recognized that *in-situ* processes related to particulate organic carbon (POC) degradation is not efficient enough to support a robust gas hydrate system without some form of upward fluid transport via focused migration up faults and facture networks, or through the process of hydrate recycling (e.g., Burwicz et al., 2011; Johnson et al. 2014). Site C0002 cores hosted low TOC concentrations but high GH saturations, suggests that the gas incorporated into hydrate reservoirs on the seaward end of the basin is migrating from an external source. Doan et al. (2011) proposed that the external source is from regions where organic carbon rich lower basin sediments (found at Site C0009) are thickest

within basin synclines. This is possible, but additionally we propose a component of gas contribution from the accretionary prism because low velocity signatures of gas are not associated with syncline features, but rather stem off of fractured basement anticlines (Fig. 5.1 and 5.2) as do high amplitude reflections in the amplitude volume and strong reflection strength anomalies in the signal envelope volume.

The pore water profiles show discrete Cl- freshening anomalies that are undoubtedly related to hydrate dissociation in the core. IODP Expedition 311, Hydrate Ridge, showed that only discrete Cl- outliers could be attributed to gas hydrates (Riedel et al., 2010). What is unclear about the Site C0002 Cl- trend is the cause of the background freshening with depth and assumptions about the Cl- baseline can result in very large errors in gas hydrate saturation estimates (e.g., Matsumoto and Borowski, 2000). Analogous Cl- baseline freshening with depth trends have been found at Hydrate Ridge Site U1327 (Riedel et al., 2010) and at IODP Expedition 353 Site U1445 offshore the Indian margin (Clemens et al., 2015). Isotopic oxygen and hydrogen analyses of the pore waters collected at Site U1445 determined that the background freshening trend is a result of advection of fresh fluids from depth related to clay mineral dehydration reactions (Taladay et al., 2015). Similar observations were made by Kastner et al. (1995b) regarding Cascadia convergent margin pore fluids. It is likely that at Site C0002, there is a component of fluid mixing, and the background baseline for calculating hydrate saturation should not be a constant seawater value, but rather the observed freshening with depth trend. Therefore, we favor the lower hydrate saturation estimates of Jia et al. (In Press)

We are reluctant to accept the fluid flow and migration pathway analysis of Tomaru and Fehn's (2015) based on their iodine ages, because geologically it is implausible that fluids would migrate laterally such far distances through a very low permeability, heavily faulted accretionary prism given the tortuous path that such fluids would have to travel through. The iodine enrichment is possibly associated with the high TOC content buried down-dip in the lower basin sediments as was detected at Site C0009. The high TOC elsewhere in the basin was not considered in Tamaru and Fehn's analysis. Postulates about errors in Tamaru and Fehn's

assumptions or Iodine ages are beyond the scope of this study. While the seismic data does provide evidence for gas and fluid migration from the accretionary prism into basin sediments, it is unlikely that these fluids have traveled from as far as 6-8 km away (as proposed by Tamaru and Fehn).

Another pore water peculiarity is the occurrence of sulfate well below the methane-sulfate transition zone. Sulfate is not expected to be present in pore water below the SMTZ. The presence of deep SO_4^{2-} suggests pore fluid contamination; however, there is no evidence to support contaminated fluids in any of the other geochemical profiles (Strasser et al., 2014). It has been proposed by Bottrell et al. (2000) that anoxic-oxidation of pyrite involving Fe3+ in marine sediments can release sulfate into deep pore water such that:

$$FeS_2 + 14Fe^{3+} + 8H_2O \rightarrow 15Fe^{2+} + SO_4^{2-} + 16H^+$$

Given the abundant pyrite occurrence in the sediment cores, we are inclined to think that this is a plausible mechanism for SO_4^{2-} formation in the basin and consider the SO_4^{2-} to represent in situ conditions.

Sedimentary intervals with abundant authigenic pyrite deposits are important because they could be recording paleo-sulfate methane transition zones (SMTZ), periods of active methane flux from depth, and abrupt changes to SMTZ depths (Raiswell and Canfield, 1998; Borowski et al., 1996; Borowski et al., 1999; Dickens, 2001; Peckmann et al., 2001; Lim et al., 2011; Peketi et al., 2012; Antler et al., 2013; Xie et al., 2013; Hong et al., 2014; Zhang et al., 2015). Enhanced delivery of methane to the SMTZ is necessary to form large deposits of sulfide minerals like pyrite (e.g., Borowski et al, 2013). Framboidal pyrite morphology as noted in C0002 core descriptions is particularly consistent with sulfate reduction and pyrite precipitation related to anoxic microbial activity, and an upward flux and oxidation of methane (Jiang et al., 2006; Chen et al., 2007 more). If sedimentations rates are well constrained and accompanied by high resolution biostratigraphy it would be possible to determine paleo-SMTZ depths and burial rates, which could help us to pinpoint the timing of active methane venting. However, the biostratigraphy age constraints are too coarse to employ this strategy at this site. Nevertheless

we can say that from the frequent occurrence of abundant pyrite samples that methane venting has been active during periods in the past.

One occurrence of dolomite is determined from cuttings at Site C0002. The precipitation of dolomite is favored when dissolved sulphate is absent and where supersaturation helps to overcome the low-temperature kinetic barriers (Ritger et al., 1987; Aloise et al., 2000; Magalhaes et al., 2012). Dolomite is an authigenic mineral, and the precipitation of dolomite at these depths is likely a product of subduction-induced dewatering, silicate alteration (buffers acidification) and advection of methane-enriched pore fluids following structural deformation (e.g. Ritger et al., 1987; Meister et al., 2011). The presence of dolomite at C0002 near the accretionary prism likely precipitated from hydrothermal fluids, which akin to pyrite occurrences, suggests significant venting from depth at some point in the geologic past.

In terms of the soupy structure proxy, while it is commonly accepted that GH preferentially forms in higher porosity sands and ash, the presence of soupy structures in fines at Site C0002 suggests that in addition to pore-filling GH in sand reservoirs, disseminated GH in fine-grained muds are also common. Notably, if soupy structures are used as a proxy for gas hydrate occurrence then these data provide further evidence that hydrates may exist below 400 mbsf. Table 2 shows that soupy disturbance fabrics were found down to nearly 500 mbsf in Hole C0002K. It should be noted that soupy structures could also be the product of drilling disturbance, and it is important that shipboard scientists document when such disturbance structures might be related to drilling or core handling (for example: if the core was plunged on the catwalk). No such documentation is noted in any of the C0002 core descriptions.

5.2 Seismic Interpretations

5.2.1 Primary BSRs

BSRs are the most commonly used seismic proxy for NGHs in marine sediments, but not all BSRs are related to gas hydrate occurrence, nor is gas hydrate occurrence restricted to regions with BSRs (Paull et al., 2000; Collet et al., 2008). Generically, BSRs are crosscutting reflections marking a sharp acoustic impedance contrast as a result of a sudden change in

lithology, sediment physical properties, or pore fill constituents such as fluids and gas. Therefore, they can be produced by a number of geologic processes including GH related BSRs as well as diagenetic boundary BSRs which are also controlled by T-P conditions (e.g. Berndt, 2004).

The appearance of GH related BSRs in seismic data is dependent on the seismic frequency used during acquisition (Chapman et al., 2002; Hardage and Roberts, 2010; Mosher et al., 2011) and the dip angle of sedimentary beds (e.g. Shedd et al., 2012). Their distributions depend significantly on the presence of free gas below and depths are controlled by the many parameters already outlined in the introduction. The BGHS can vary with local or regional changes to heat flow, tectonic uplift, subsidence, salinity pulses, sedimentation rates, and sediment physical/geotechnical properties (e.g., Hutchinson et al., 2008; Ashi et al., 2009; Kinoshita et al., 2011; Winters et al., 2014) and may or may not correspond to observed BSR depths. The wide range in depths of the primary BSR in our seismic data, along with the fact that it does not everywhere mirror the seafloor indicates that the BGHS is highly sensitive to local conditions, and thus the evolution of the BGHS is incongruent across the basin. It is well accepted that the amplitude strength of the BSR is related to amount and distribution of free gas below rather than the amount of GH above (e.g., Navalpakam et al., 2012). The low amplitude character of the BSR on the hanging wall of several normal faults suggests that the gas layer is either very thin, or has escaped. Most faults do not offset the BSR meaning that there has been sufficient time since fault activity for BSR relaxation. The continuous nature of the BSR is characteristic of a diffusive system supported primarily by gas hydrate recycling processes (Haacke et al., 2007; Wang et al., 2014). The very thick low velocity zones in the center of the basin also (Fig. 5.1) support the widespread occurrence of gas beneath the BSR.

We can assume that GH at or nearly above the BSR are acting as an effective seal.

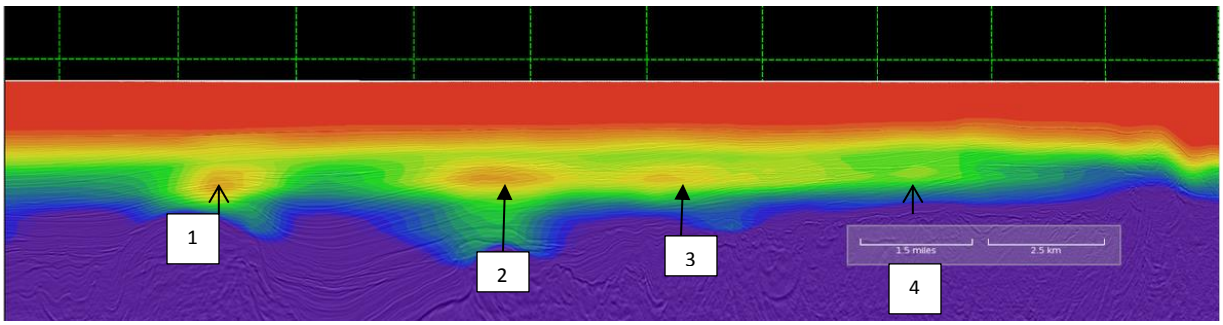

Figure 5.1 - Three prominent low velocity zones representing trapped gas beneath the BSR within basin sediments above anticlinal structure in the underlying accretionary prism. Inline 2483 Red = low velocity to purple = high velocity. Red in the upper part of the figure is the sea water. The four regions appear as very strong amplitude reflections in the amplitude data and is also interpreted to be zones where deeply sourced gas is migrating into basin sediments.

Regarding the four regions where there is no apparent BSR (Fig. 4.29), there are several possible explanations. The first is related to fluid flow patterns in the basin. For example, the upward deflection of the BSR and the termination of a BSR in the presence of chaotic horizons across the inferred mud volcano (Fig. 4.29 Zone 2) can be interpreted to be a fluid escape vent where pulses of warm fluids from earthquakes or the release of overpressure conditions can be transported from the subduction interface to the seafloor. If this migration of fluids is sufficiently strong, it will cause gas hydrates to dissociate releasing gases and result in heat flow anomalies. The seismic evidence supports that this is an active or recently active vent delivering fluids from depth. The use of the primary BSR in analyses of heat and fluid flow is explored in detail in Chapter 6 and further elaborated on in the hydrate system analysis of Chapter 7.

Across the syncline feature in the center of the basin (Fig. 4.29 Zone 3), the apparent lack of a BSR could simply be a matter of interference due to the nearly horizontal strata (Shedd et al., 2012). Alternatively, the channeling away of fluids and gas in the up dip direction may be suppressing the formation of an overlying gas hydrate seal by virtue of a lack of gas supply from depth. Holbrook et al.'s (1996) study showed that a BSR will not appear in the absence of free gas which cannot accumulate without a trap and seal. The seismic velocity data does not reveal a low velocity zone beneath this BSR discontinuity, but it does reveal a low velocity zone on

each side of the BSR discontinuity where high amplitude BSR reflections are observed (Fig. 5.2). Thus, we favor the interpretation that gas is being channeled away from the synclinal feature.

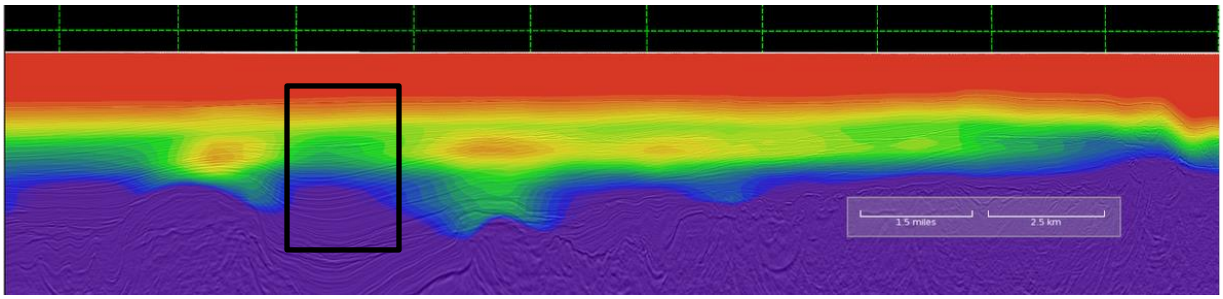

Figure 5.2 - Inline 2483. No low velocity signature beneath the third un-imaged BSR corresponding to a thick syncline.

Selective increases in BSR amplitudes indicate the important role of sand layers as a conduit for upward migration of gas-bearing fluids (Moore, 1989; Pecher et al., 2001; Baba and Yamada, 2004; Barnes, 2013) (Fig. 5.3). Preferential occurrence of BSRs in sand units as opposed to the non-expression in mud units was also observed in the 3D seismic data collect across the northern Gulf of Mexico (Shedd et al., 2012).

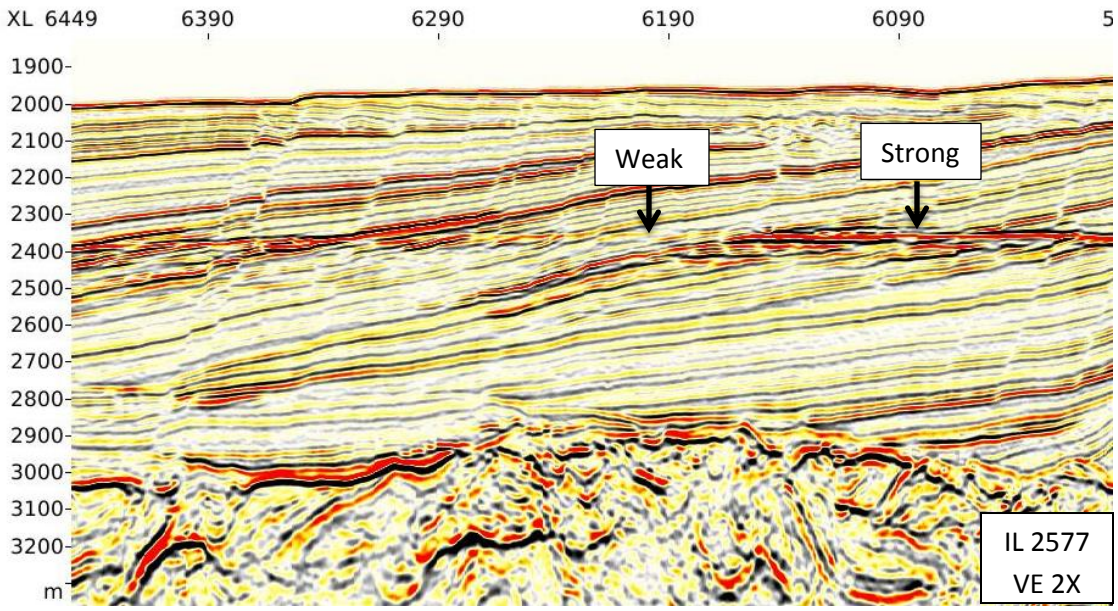

Figure 5.3 - Seismic Inline 2577 displaying an example of variable BSR amplitude strengths across sandy units (strong) and clay rich units (weak)

5.2.2 Double BSRs

Double BSRs are perplexing features, and interpretations of these seismic events remain an unresolved issue (Posewang and Mienert, 1999; Popescu et al., 2006; Rajput, 2008; Geletti et al., 2011) largely because they have not been sampled by scientific drilling efforts. Therefore, what these seismic boundaries represent in terms of geology must be inferred or modeled. Several hypothesis have been proposed in which double BSRs are: (1) the bottom of a thick free gas zone (Gomshtok and Soloviev, 2006); (2) a silica diagenetic boundary such as an opal-A to opal-CT transition, or an illite to smectite transition (Hein et al., 1978; Kuramoto et al., 1992; Berndt et al., 2004; Somoza et al., 2014); (3) an authigenic carbonate layer imprinted on the sediments following rapid hydrate dissociation (Ritger et al., 1987; Bohrmann et al., 1998; Pierre et al, 2000; Bahr et al., 2010); (4) the top of thick gas hydrate occurrence zone particularly above the BSR (Saeki et al., 2008); (5) a remnant BGHS with remnant GH and/or free gas (Posewang and Meinert, 1999; Andreassen et al., 2000; Matsumoto et al., 2000; Matsumoto et al., 2004; Bangs et al., 2005 Crutchley et al., 2015); or (6) two stacked active phase boundaries (Poswang and Mienert, 1999; Foucher et al., 2002). If even just a small fraction of H_2S or higher hydrocarbons such as ethane or pentane exists in the pore spaces in excess of solubility, then the phase boundary for hydrate stability would favor a sII system whereby ethane and pentane would preferentially be taken up in the hydrate lattice over methane (Carroll, 2009; Macelloni et al., 2015). These sII hydrates would be stable at higher temperatures for equal pressures, and thus deeper in marine sediments than a sI phase boundary (Carroll, 2009).

5.2.2.1 Lower BSRs

Lower BSRs are common throughout the Nankai Trough region (Baba and Yamada, 2004), and have also been recognized at Blake Ridge where the two BSR levels are believed to have been caused by erosion (Gorman et al., 2002); near Norway (Posewang and Mienert, 1999); on the Nankai Slope (Foucher et al., 2002); the Danube deep-sea fan in the Black Sea (Popescu et

al., 2006); Cascadia (Bangs et al., 2005); and in the Mohican Channel area of the central Scotian Slope (Mosher et al., 2008). Generally, most of these studies attributed double BSRs to environmental disturbances during glacial to interglacial transitions whereby the double BSRs represent an acoustic impedance contrast from preserved physical or chemical alteration to the surrounding sediments, or free gas left behind during the gas hydrate recycling process (Posewant et al., 1999; Andreassen et al., 2000; Foucher et al., 2002; Baba and Yamada 2004; Bangs et al., 2005; Popescu et al., 2006; Golmshtok and Soloviev, 2006; Laird and Morely, 2011). For the Nankai Slope, Matsumoto et al. (2004) and Foucher et al. (2002) both favor the idea that rapid tectonic uplift of 100 m at a rate of 1 cm/year would produce the lower BSR. Kim and co-authors (2011) discovered double BSRs (upper and lower) in the Ulleung Basin and inferred both BSRs are related to residual hydrates following the rising and lowering of the BGHS.

The glacial-interglacial disturbance hypothesis cannot be applied to explain the LBSRs in our survey region, because it would demand a sea level change far greater than 100 m or bottom water temperature increases by >7.2°C (not accounting for the counteracting effect of pressure increase from sea level rise) in order to affect the BGHS in our study region (Golmshtok et al., 2006). Each of these scenarios is highly improbable. As far as the Opal-A/Opal-CT hypothesis, theoretical modeling has shown that an Opal-A/Opal-CT boundary will form deeper in marine sediments than the base of gas hydrate stability under a variety of parameters (Somoza et al., 2014); however, Opal-A/Opal-CT transition tend to occur around 25°C (Hein et al., 1978; Pisciotto, 1981) which would be equivalent to ~625 mbsf assuming a geothermal gradient of 40°C/km as recorded at C0002 (Strasser et al., 2014). At ~515 mbsf the LBSR is too shallow to be explained as a diagenetic front unless the geothermal gradient was significantly higher at some point in the past.

Considering all available evidence, including gas composition data from Sites C0002 and C0009, and the seismic character of these lower cross-cutting reflections, we propose that LBSR-1s are a product of rapid migration of the BGHS representing relict BGHS which are often referred to in the literature as “remnant BSRs” and are currently zone of residual hydrates

supported by a thick free gas zone (helps to prevent dissolution). The LBSR-1 and LBSR-2s could also both potentially be a second layer of sII hydrates formed from the fractionation of thermogenic gas to form a sII hydrate boundary. This process is analogous to mineral crystal formation whereby heavier molecules are the first to precipitate out of a multicomponent fluid leaving the remaining solution enriched in the lighter molecules, which in our case would be methane. The idea here is that the nucleation of sII hydrates formed with heavier gas molecules would proceed until the heavier molecules (ethane and pentane) are depleted from the gas mixture and then followed by later a later stage precipitation of sI methane hydrates. This process has been observed in the laboratory and is called staged nucleation (Uchida, 2004; Osegovic et al., 2006).

Returning to the idea of relict BGHS zones, GHs are in a constant state of dynamic re-equilibration in response to sedimentation rates and tectonic activity. If we assume that the BSR tracks the BGHS, high sedimentation rates would result in repositioning the BGHS above previously precipitated hydrates. As mentioned in Chapter 2, as the basin evolved, the depocenter of sedimentation migrated landward over the region where the stacked LBSR-1s are observed. Additionally, these features are associated with a zone of acoustic turbidity (gas) overlying a buried, reactivated thrust (potential tectonic disturbance and period of fluid advection) (Boston 2011, Moore et al., 2015). We interpret the closely stacked LBSRs as recording phases of upward migration of the BGHS, and any hydrates remaining beneath the current BGHS exist in a metastable state. The discontinuous nature of LBSR-1 reflections could be echoing patchy residual hydrate distributions. The implication here is that gas from the thick low velocity zone is likely a mixture of new gas migrating from depth, and released gas from hydrate decomposition. If the BGHZ were to lower as a result of rapid subsidence or overburden removal, this gas mixture would then be recycled to form new gas hydrates. Thus gas could remain in the system for long periods of time. These remnant BSRs may serve as a record of significant tectonic events or pulsed changes in sediment load between times of steady state P-T conditions.

There are two possible explanations for LBSR-2s. The positive polarity character of LBSR-2 could be indicating the bottom of a thick free gas zone; however the high velocity nature of LBSR-2 near the seaward edge provides compelling evidence that this seismic feature is illuminating a sII hydrate stability boundary as does the fact that hydrates were found at C0002 86 meters below the BSR. Mud volcanism, bright spots deep beneath the BSRs and documented ethane and propane in increasing concentrations with depth as reported in mud gas analyses from Sites C0002 and C0009 are all supportive evidence that thermogenic gas containing higher order hydrocarbons migrates up dip into the GHSZ. Numerical models and full-wave from inversion efforts have shown that multiple BHSZs can coexist as a direct consequence of the presence of thermogenic gas in the free gas phase (Andreassen et al.2000; Rajput et al., 2010; Macelloni et al., 2015). Rajput et al. (2010) created a full-wave model using a finite-difference solution for the vector wave equation utilizing parameters from seismic data from Green Canyon, Gulf of Mexico that showed that the presence of a low velocity layer (fluid, gas) sandwiched between two NGH filled layers would generate a double BSR response similar to that of which we observe. Experimental studies using methane-ethane mixed gas to form GHs found that clathration reactions favor the sII phase enriched in ethane first prior to sI formation (Murshed et al., 2009). The fact that the LBSR-2s do not occur at equal depths beneath the primary BSR could reflect lateral variability in the composition of the gas mixture. At Woolsey Mound, Northern Gulf of Mexico, multi-gas systems showed an apparent preferential fractionation of higher hydrocarbon gases – ethane and propane- in the hydrate phase (L. Macelloni, 2015). Further, trace amounts of heavier hydrocarbons found in pressure cores in the eastern Nankai Tough provided evidence that heavier hydrocarbons are indeed preferentially trapped into the hydrate phase over the vapor phase (Kida et al., 2015). Kida et al. (2015) found that a small amount of hydrate crystals collected from hydrate-bearing sediments in the eastern Nankai Trough were different than sI; however, they did not specifically state this structure to be a sII hydrate. BGHS modeling in Chapter 6 further explores the possibility that LBSR-2s are the product of sII GHs.

5.2.2.2 Upper BSRs

The same hypotheses employed to explain the LBSRs have also been evoked to describe BSRs within the HSZ along other margins. Again we can rule out the option of an opal-A to opal-CT transition, which is dependent on temperature of ~25°C, based on the shallow depths of these UBSRs in relation to the geothermal gradient in the basin. There is also no evidence in C0002 or C0009 cores to suggest the presence of an authigenic carbonate layer. As mentioned previously, gas hydrates are associated with stimulated microbial activity which results in the production of magnetic iron sulfides from sulfate reduction (Housen and Musgrave, 1996Musgrave et al., 2006). Preservation of greigite and pyrrhotites is favored in regions with disseminated gas hydrates and will transform to pyrite once gas hydrates decompose (Kars and Kodama, 2015). A concentrated layer of pyrite could represent a "fossilized" gas hydrate horizon (Kars and Kodama, 2015) possibly from a GHCZ above the BSR. However, it is unlikely that a concentrated pyrite deposit would be thick enough for seismic detection.

Zones of high amplitude reflections occurring above the BSR similar in nature to our UBSR-1s were found in the Nankai prism (Inamori and Hato, 2004), the eastern Nankai Trough (Baba and Yamada, 2004), and in the Gulf of Mexico (Boswell and Saeki, 2010; Boswell et al. 2012). Core analysis determined these reflections marked the top of highly concentrated gas hydrate zones (Baba and Yamada, 2004; Boswell et al., 2014). Similar thin, positive amplitude reflections above the BSR have also been interpreted to represent the top of a concentrated gas hydrate zone along the Chilean margin (Rodrigo et al., 2009). The UBSRs are very irregular, do not mirror the seafloor, and are clearly offset by faults (Fig. 5.4). We interpreted the UBSR-1s to mark the top of gas hydrate concentration zones and these boundaries are used in conjunction with the BSR to extract a volumetric gas in place estimate presented in Chapter 7.

The UBSR-2 was interpreted by Bangs et al. (2010) to be a paleo-BSR above the present-day BSR, near a V-shaped notch where a large amount of material was rapidly removed resulting in significant perturbation to the BGHS (Fig. 5.5). It on average falls between 420-410

mbsf, and is a continuous feature. It is clearly offset by faults, and this boundary may mark a long standstill of steady state conditions prior to a deepening of the BGHS and gas hydrate accumulation above the paleo-BGHS may still be present in these sediments; however, this largely depends on unknown temporal factors including the timing of the perturbation and the kinetics of hydrate dissolution. This upper BSR is also further discussed in Chapter 6 under BGHS modeling.

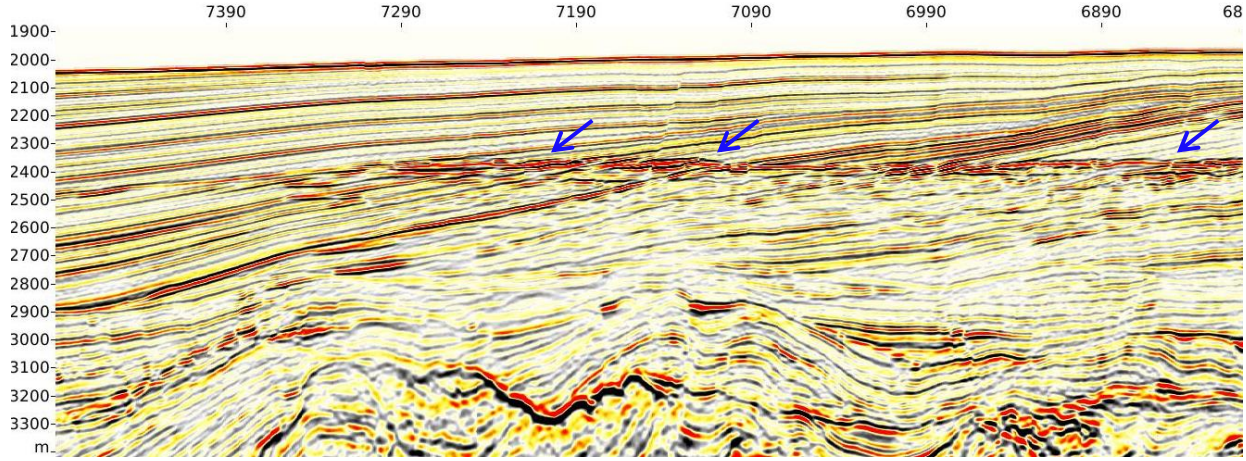

Figure 5.4 - Inline 2200 showing representative cross section through UBSR-1s

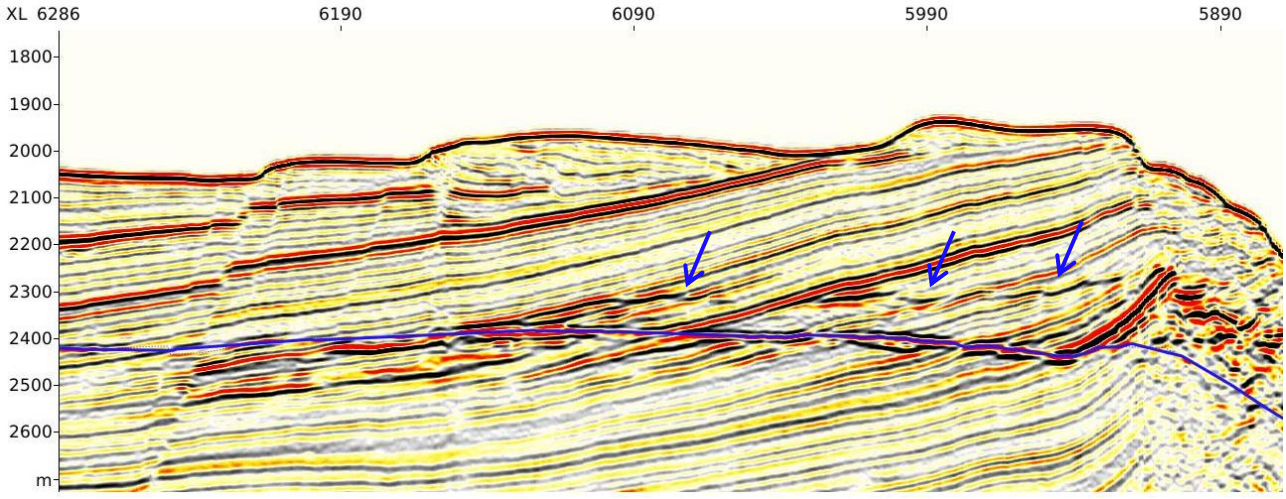

Figure 5.5 - Inline 2693 showing representative cross section of the UBSR-2s.

Chapter 6

BGH Stability and Heat Flow Modeling

"It is a capital mistake to theorize before you have all the evidence. It biases the judgment."
-Sherlock Holmes, A study in Scarlet, Sir Arthur Colan Doyle

6. BGH Stability and Heat Flow Modeling

6.1 BGHS Modeling: Predicted vs. Observed BSR

The modeled BGHS is determined using the input parameters outlined in the methods section of this manuscript and is referred to herein as the modeled BSR. Eight scenarios were run with variable input parameters for gas composition and geothermal gradient in order to determine the best fit for the primary BSR, and to test if the lower BSR might be reflection a sII phase boundary. All other parameters were fixed. In each case, the modeled BSR perfectly mirrors the seafloor and thus does not reflect any in situ perturbations to heat flow, salinity anomalies, variable GTG, or regions where the BSR exists in a transient stability state. At C0002, a geothermal gradient of 40°C/km was estimated by Expedition 338 Scientists (Strasser et al., 2014), while a 43°C/km GTG was estimated by Expedition 315 Scientists (2009).

Primary BSR

Scenario 1a: 100% methane, 40°C/km
Scenario 1b: 100% methane, 43°C/km

Lower BSRs

Scenario 2a: 98% methane, 2% ethane, 40°C/km
Scenario 2b: 98% methane, 2% ethane, 43°C/km

Scenario 3a: 96% methane, 4% ethane, 40°C/km
Scenario 3b: 96% methane, 4% ethane, 43°C/km

Scenario 4a: 95% methane, 4% ethane, 1% propane, 40°C/km
Scenario 4b: 95% methane, 4% ethane, 1% propane, 43°C/km

Scenario 1a produces a modeled BSR that is consistently shallower than the observed primary BSR by 25-55 meters, implying a thicker GHSZ than what is revealed by the BSR in the seismic data (Fig. 6.3). Scenario 1b at 43°C/km provides the best match with the observed

primary BSR (Fig 6.1). However, it is important to avoid jumping to quick conclusions. Discrepancy between the modeled BGHS and the observed BSR could be related to any number of errors in assumptions related to variations in sediment thermal conductivity across the basin, or in the assumed model parameters. The fact that Scenario 1b with a GTG of 43°C/km provides a better fit with the observed BSR does not necessarily mean that the estimated GTG of 43°C/km as reported by the expedition 315 Scientists is more precise than Expedition 338's estimate. It is possible that the GTG of 40°C/km is more accurate, and that the reason for a consistently deeper modeled BSR relative to the observed BSR is the result of capillary controls on methane solubility from the Gibbs-Thomson effect has on BSR depths (e.g., Daigle and Dugan, 2014). However, BSRs along the Canadian margin in the Atlantic also tended to be shallower than the theoretical base (Mosher, 2011); as did BSRs throughout the South China Sea (He et al., 2009) and at Blake Ridge. Using a GTG of 43°C/km, the observed LBSR is best matched by Scenario 3b with a 96% methane, 4% ethane gas mixture (Fig. 6.2, 6.5).

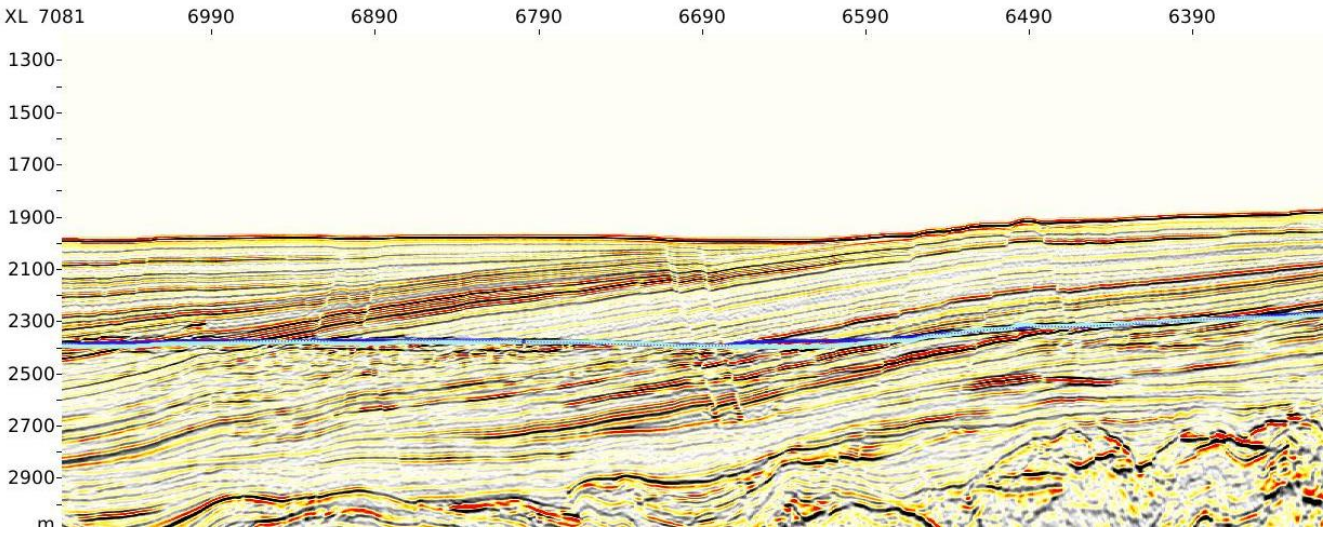

Figure 6.1 - Inline 2264. Observed BSR in dark blue. The light blue horizon is the modeled BSR under Scenario 1b - 100% methane and a GTG of 43°C/km and are generally in good agreement.

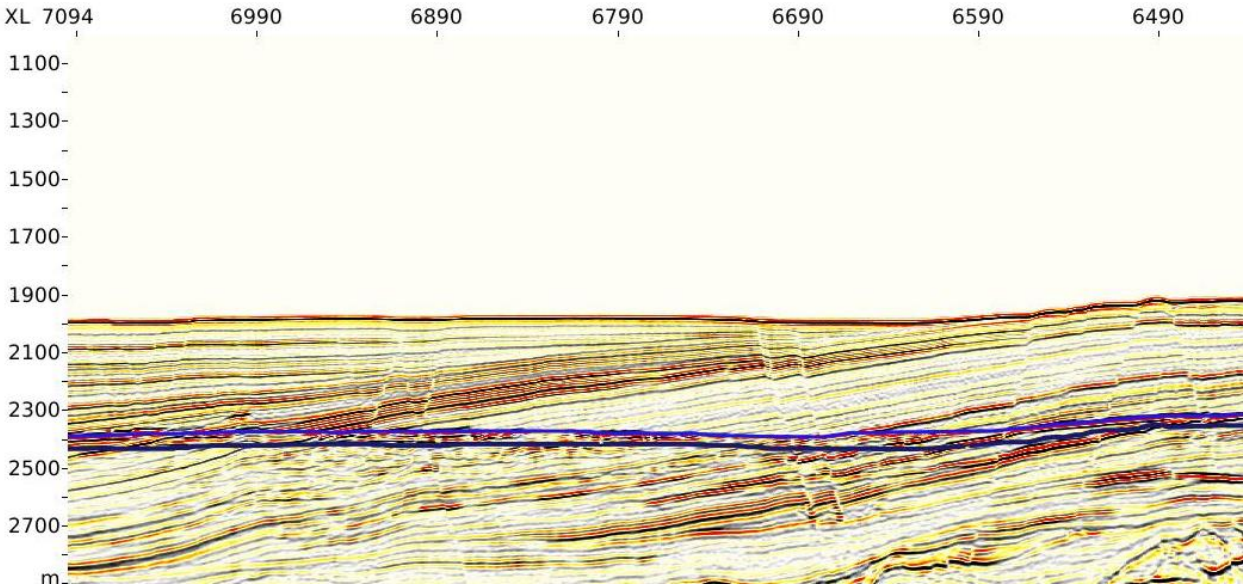

Figure 6.2 - Inline 2264. Best fit double BSR in darker blue beneath the primary BSR. Scenario 4b: 96% methane, 4% ethane at 43°C/km.

If the BGHS does reside beneath the observed BSR because of the Gibbs-Thomson effect as proposed by Dugan and Daigle, (2014) then BSR-derived heat flow estimates would be underestimated. Discrepancies between the modeled and observed BSR could also be explained by localized elevated heat flux shifting the pressure-temperature boundary defining the BGHS to shallower depths than what the model can account for ("pluming" BSRs). A BSR above the BGHS could also indicate a limited supply of methane (Kastner, 2001), however an expansive seismically imaged gas cloud beneath the BSR does not support this hypothesis. Alternatively, some BSR regions may not have adjusted yet to recent sedimentation, erosional, and/or tectonic perturbations. These ideas are explored in further detailed in Chapter 6.2.

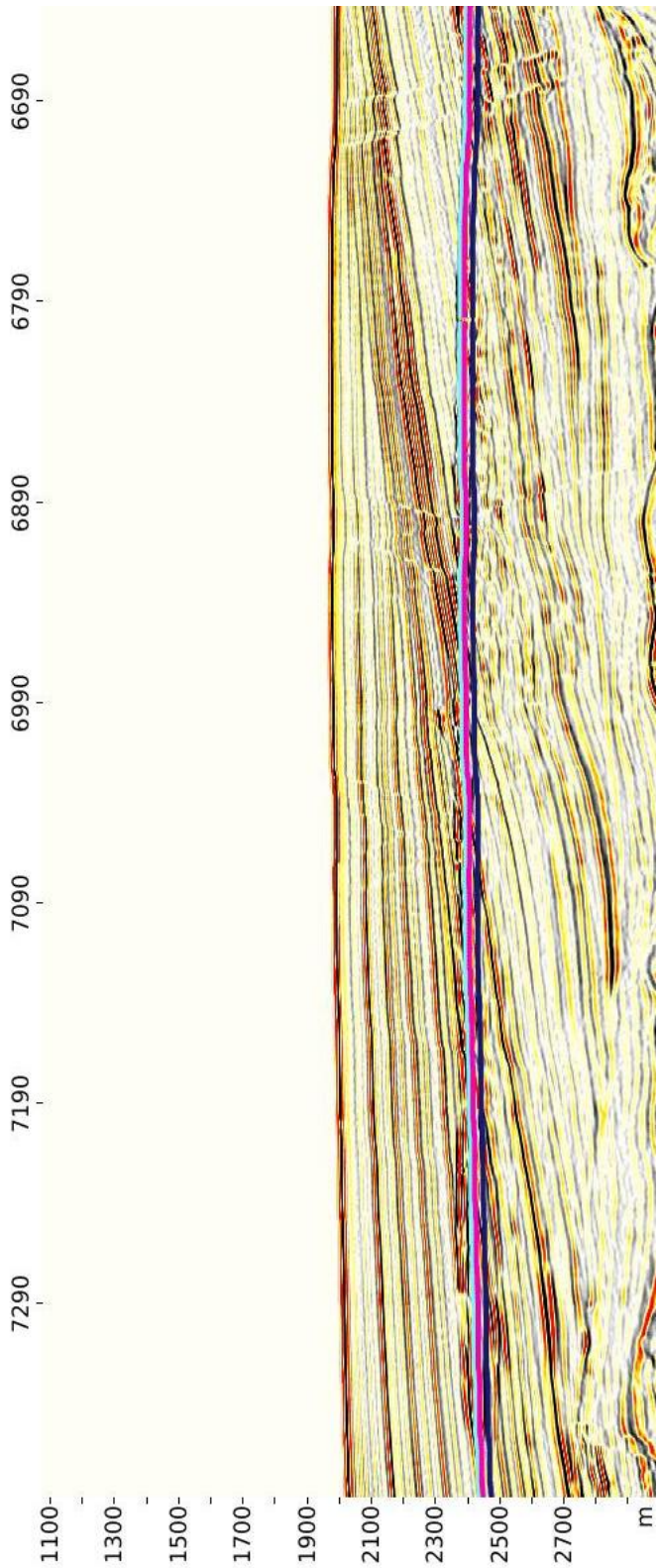

Figure 6.3 - Inline 2264. Modeled BSR using a 43°C/km GTG. Baby blue - 100% CH_4 is in good agreement with the observed BSR. Pink – 96% CH_4, 4% C_2H_6, Dark Blue - 95% CH_4, 4% C_2H_6, 1% C_5H_{12}. 98% CH_4, 2% C_2H_6 horizon is not shown because covered by other modeled horizons.

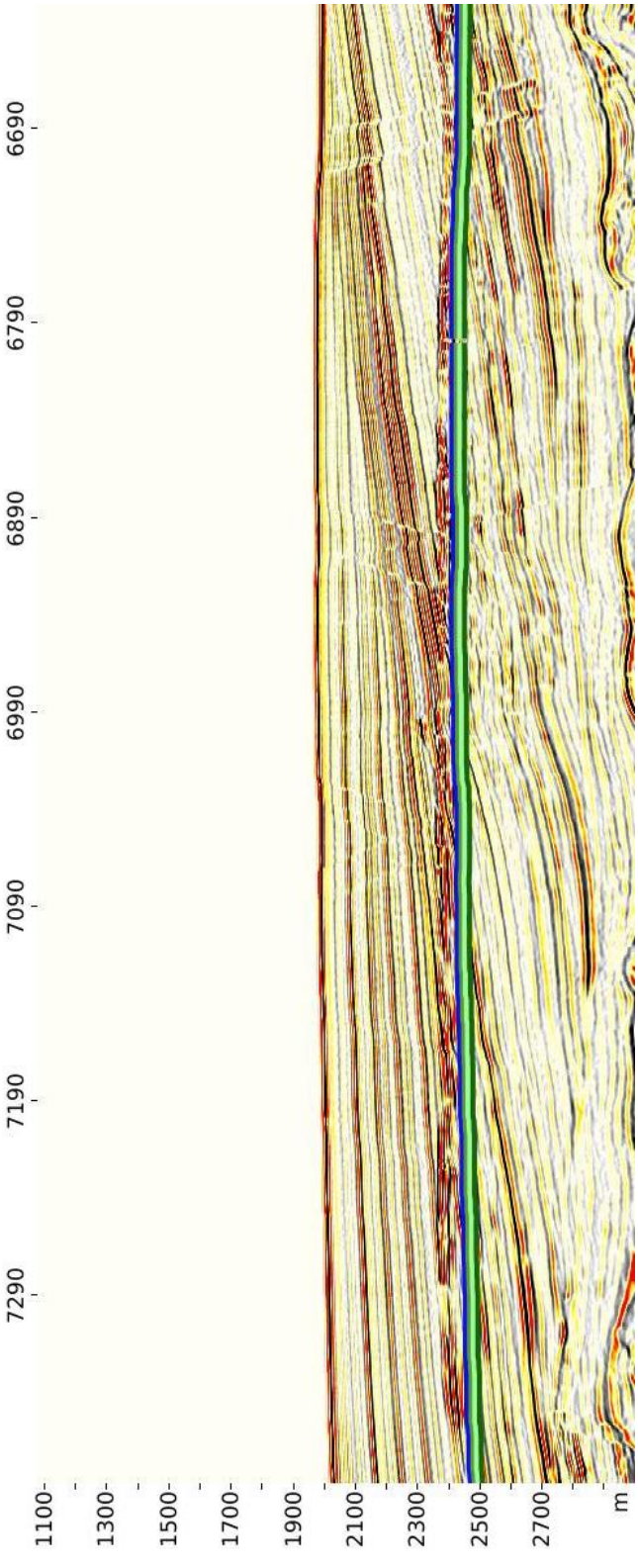

Figure 6.4 - Inline 2264. Modeled BSR using a 40°C/km GTG. Dark blue - 100% CH_4 is consistently 25-55 m the observed BSR. Gray green – 96% CH_4, 4% C_2H_6, Bright green -98% CH_4, 2% C_2H_6, Dark green - 95% CH_4, 4% C_2H_6, 1% C_5H_{12}.

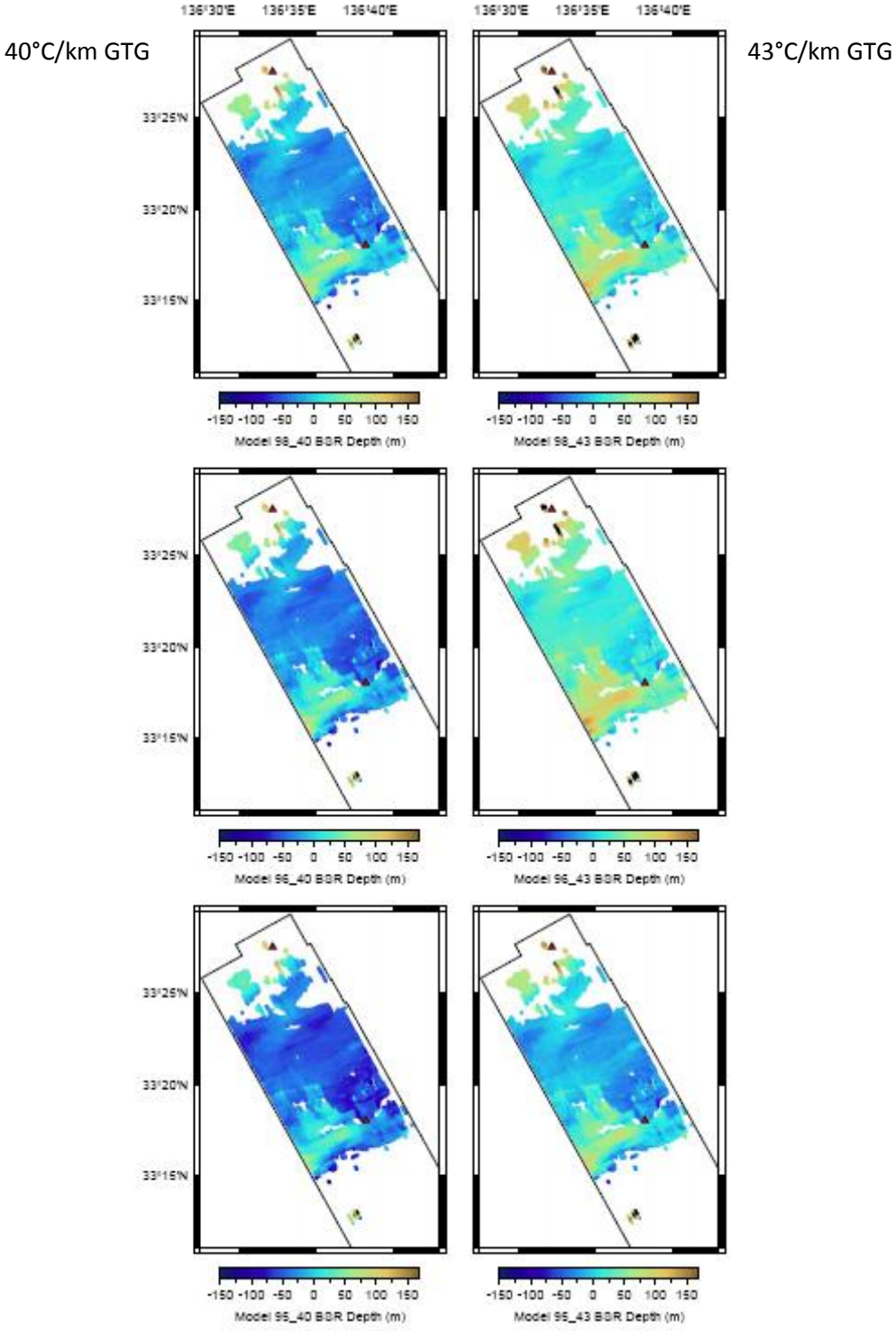

Figure 6.5 - Modeled vs observed LBSR Depths. Negative values are depths of the model in meters below the observed LBSR while positive value are depths in meters above the observed LBSR. Zero values mean the modeled and observed depths are in agreement.

6.2 BSR-derived Heat Flow from the Primary BSR

The BSR-derived heat flow values range between 42 -54 mWm^{-2} with an average value of 48 mWm^{-2}. These values fall at the lower end of the predicted values for the Kumano region compared to the model presented by Harris et al. (2011; 2013) (Table 5), and indicate conductive heat transfer as the primary control on heat transport through the forearc . Using the formula, Heat flow (q) = Kavg * GTG whereby Kavg = 1.1 W/[m·K] and GTG = ((TBSR-TSF)/(zBSR-zSF). The background heat flow is considered to be 48 mW/m^2 based on the average heat flux value in the flattest regions. Because heat flow in flat areas is not affected by topography, it should roughly represent the background value. This same approach for estimating the background heat flow was employed by Li et al. (2013) in their heat flux/fluid flow model for Cucumber Ridge off Vancouver Island.

Table 5 Modeled heat flow values reported in Harris et al. (2013) in black. Our modeled heat flow values are plotted in blue for comparison. The min and max values are presented as a function of distance from the trough axis. Heat flow from below (equilibrated) should be reduced by 10-20% at BSR depth, thus, what we compare is the (modeled heat flow)*(0.8~0.9) vs. BSR-derived heat flow.

Dist(km)	min	max	20%	10%	BSR
30	50	62	40.0 - 49.6	45.0 - 55.8	42-52
40	48	64	38.4 – 51.2	43.2 - 57.6	48-52
50	49	66	39.2 – 52.8	44.1 - 59.4	46-48
60	50	66	40.0 – 52.8	45.0 – 59.4	42

In comparison with borehole measurements, IODP Expedition 315 Scientists (2009) reported an estimated heat flow value of ~40 mWm^{-2} at Site C0002 (crosshairs on our heat flow map) (Fig. 6.6). Long-term temperature monitoring at 900 mbsf at C0002 reports a heat flow value of 56 ±1 mWm^{-2} (Sugihara et al., 2014) which is equivalent to the heat flow estimate of Harris et al. (2013). Discrepancy between the shipboard and post cruise analysis likely arise as a result of variations in sediment thermal conductivity with depth and corrections for sedimentation were not applied during shipboard operations. Our BSR model shows a value of ~48 mWm^{-2} which is in excellent agreement with Sugihara et al. (2014) assuming an avg. 15% correction for BSR depths (47.6 mWm^{-2}). For the purposes of this research however, we are not

we are primarily concerned with the qualitative, relative spatial distribution of heat flow rather than actual heat flow values.

While all heat flow models for the Kumano transect project a decrease in heat flow with increasing distance from the trench (Hamamoto et al., 2011; Harris et al., 2013) our results show considerable spatial variability compared to an idealized, 2-dimensional understanding. There are seven zones that appear to have high BSR-derived heat flow defined as values 52 mWm^{-2} or higher, and five zones expressing low BSR-derived heat flow values of 44 mWm^{-2} or less. The spatial distribution pattern in the regional geothermal regime allows us to pinpoint potential geothermal anomalies, and to investigate the cause of apparent high and low values. The objective here is to establish connections between BSR depths, tectonic and sedimentary features, and potential fluid flow pathways in order to explore how these processes might be related to gas hydrate accumulation and/or perturbations to the hydrate stability zone. To illustrate this point, we provide a representative seismic inline through each zone of high and low heat flow zone and proceed to consider the origins for these modeled values.

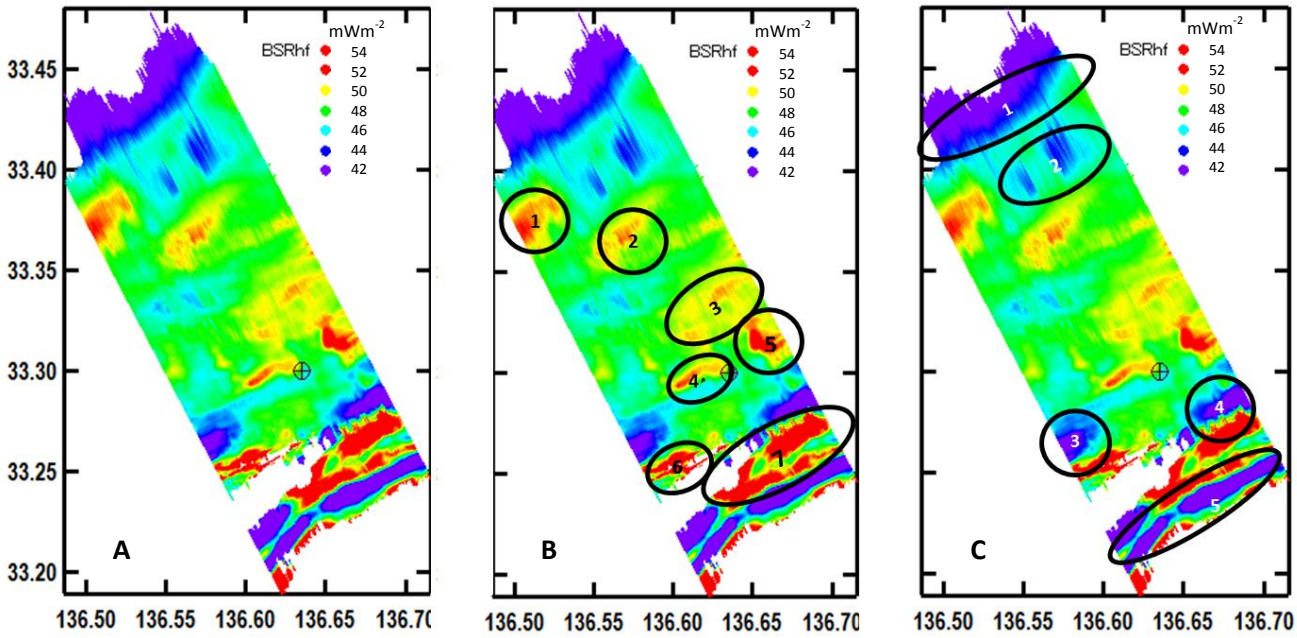

Figure 6.6 - Heat flow distribution. A. BSR-derived heat flow map. B. Seven high heat flow regions. C. Five low heat flow regions.

6.2.1 Analysis of High Heat Flow Regions

High heat flow regions correspond to shallow BSR depths, and thinner GHSZs. The first high heat flow zone occurs in the northwestern-most region of our study area, between 33.36-33.9 lat. and 136.50-136.55 lon. (Fig. 56B) This large, circular anomaly is associated with shallow BSR depths of ~375.5 mbsf relative to a flat seafloor and thus, the corresponding high heat flow values are not related to surface activity. The seismic data reveal an underlying anticlinal feature in the accretionary prism, with numerous flat spots occurring in the overlying sediments indicative of gas beneath the BSR. At least two additional BSR-like events occur beneath the primary BSR that appear as the same polarity as the seafloors. These LBSRs are possibly relict bases of hydrate stability (refer back to Chapter 5). Much of the region below the BSR is characterized by apparent discontinuous reflections, pull-down artifacts, and a decrease in amplitude reflection strength (blanking), each of which are characteristic seismic responses to the presence of gas. We attribute the shoaling of the BSR in this region to the concentration of heat in underlying topographic high within the accretionary prism which is characterized by higher thermal conductivity (see Hamamoto et al. 2011 for discussion about accretionary prism

thermal conductivity), and potential fluid migration from the prism up into the basin sediments along the associated fracture network (Fig. 6.6). The high amplitude reflections above the BSR in this zone are interpreted to be large NGHs deposits (see Chapter 6). The seismic data does not provide evidence for high velocity focused fluid expulsion through the deep-seated normal faults. The breath (wide reaching) and magnitude (low) of this heat flow anomaly is characteristic of heat transport by diffusion. This is not to say that focused advection has not occurred in this region in the past, but based on the present BSR character, any focused advection of fluids from depth in this region must be episodic.

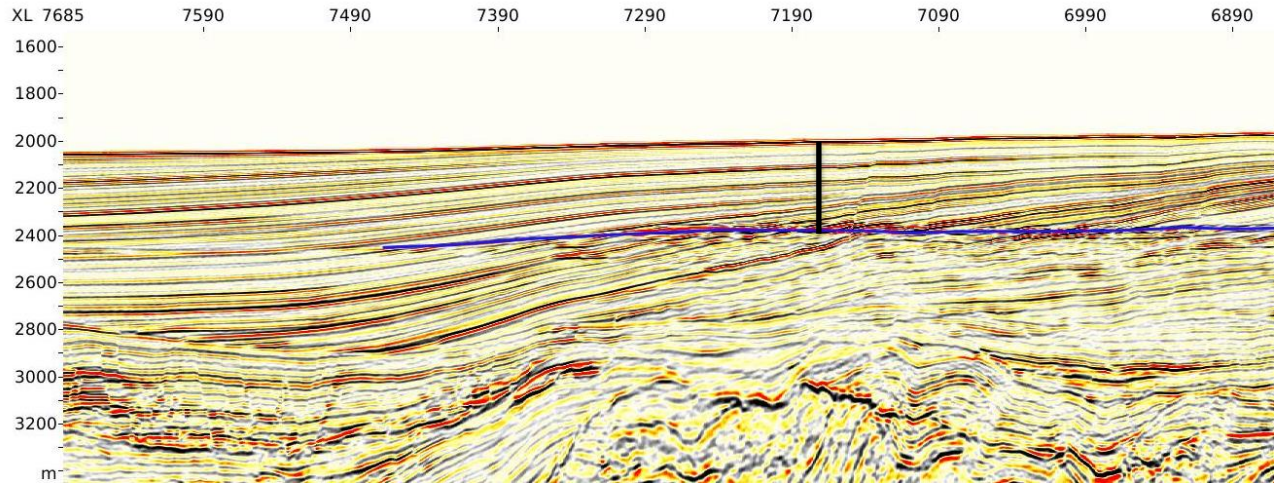

Figure 6.6 - High HF 1 IL2168 BSR (interpreted in blue) depth at 375.5 mbsf (black line)

The second high heat flow zone occurs in the north central region between 33.35 – 33.38 lat. and 136.55 - 133.60 lon. It is more linear in form than High HF Zone 1. The seismic data shows the BSR at 361.93 mbsf directly beneath a normal fault at the point where the hanging wall and foot wall meet at the fault plane along the seafloor (Fig. 6.7). Looking at the heat flow map (Fig. 6.5), the landward perimeter of this zone closely follows the normal fault distribution. The pressure effect on the BGHS is likely insignificant, and the fact that the BSR is not offset across the fault suggests that the BSR has already adjusted to any perturbations from the fault activity. There is no break in the BSR, and shoaling of the BSR does not occur equally on each side of the fault, thus there is no seismic evidence to suggest that this fault is acting as

a focused conduit for warm or cold fluids. The high heat flow modeled along this fault is likely from the focusing of heat at the fault piercing point. There is also a topographic high in the underlying accretionary prism below this zone, with significant fracturing in the overlying sediments with a corresponding diffuse, high heat flow circular pattern similar to High HF Zone 1. The fracture network which cuts into the accretionary prism could be facilitating diffuse fluid flow and methane migration into the hydrate stability zone.

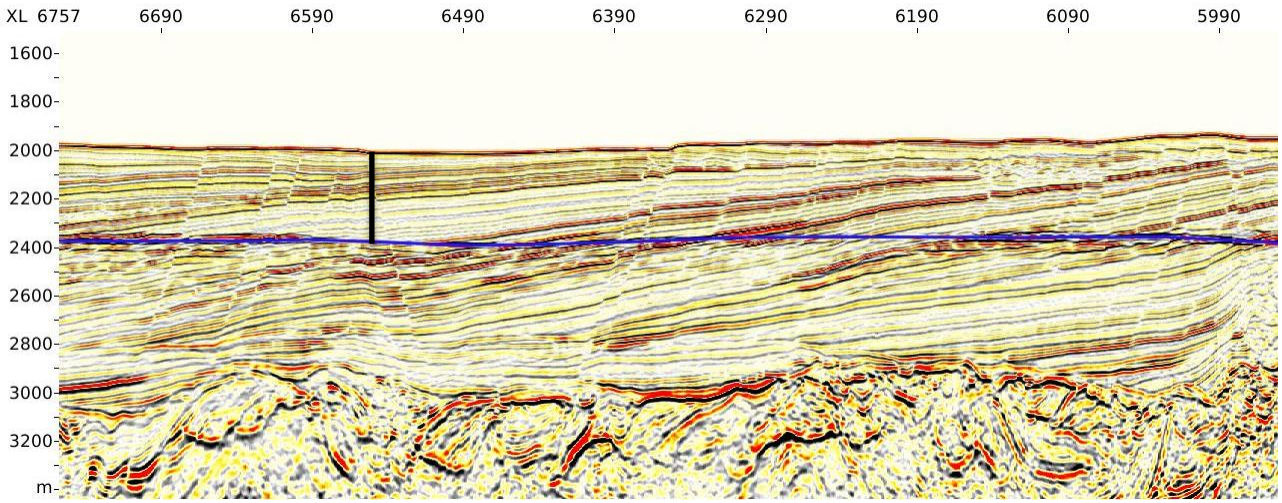

Figure 6.7: High HF Zone 2 IL2577 BSR depth (black line) 361.93 mbsf

High HF 3 appears between 33.32-33.35 lat. to 136.60 - 136.65 lon. and is patchy in nature. The underlying accretionary prism in this zone is flat. The seismic data clearly shows that the upper, surface sediment layers have been truncated meaning that a large volume of sediment has recently been eroded and carried away. There is no nearby evidence of re-deposition of this missing material (Fig. 6.8). The depth of the BSR across this zone is on average ~335.35 mbsf. The BSR in this region has not yet adjusted to the recent removal of material, likely because the thermal perturbation has not propagated down to the BSR depths. The high heat flow in this region is likely the result of erosion which transiently increases heat flow until the unroofed material has had enough time to come to thermal equilibrium (Harris et al., 2013). The patchy nature of the heat flow values here could be indicating differential BSR rebound, perhaps from compositional variations in under and overlying sediments, or variances in the

amount of material that was removed at the surface. Unfortunately, we do not have a good age constraint on when the surface sediment was removed, and thus cannot comment on the kinetics of BSR adjustment.

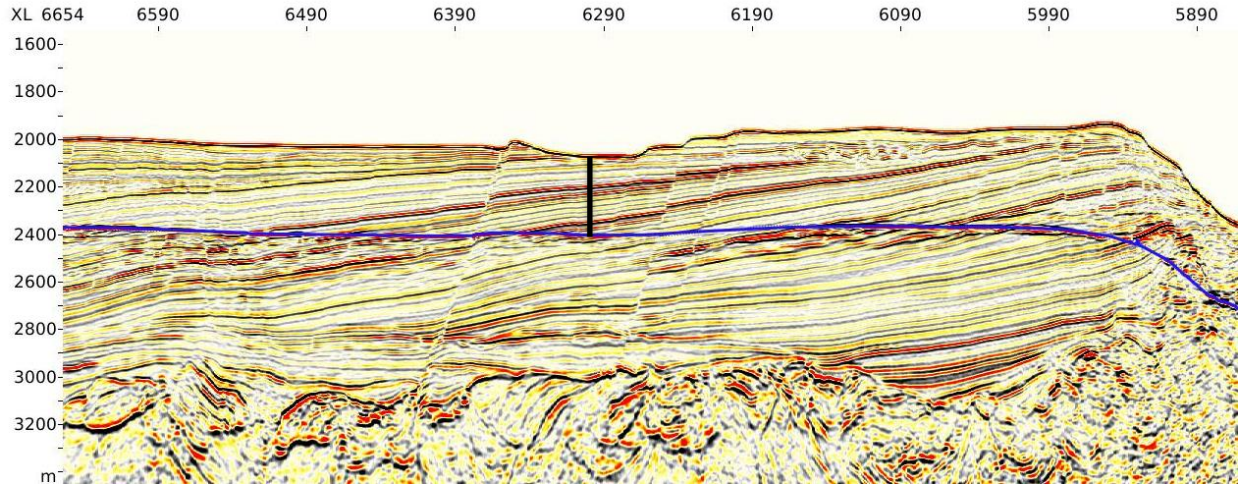

Figure 6.8 - High HF Zone 3 IL2638 BSR depth (black line) 335.35 mbsf

High HF Zone 4 is similar to High HF Zone 2 in that a shallow BSR is observed beneath the seafloor intersection of the hanging wall and footwall of a large normal fault, with a relatively flat underlying accretionary prism (Fig. 6.9). This high HF region is well defined, linear in form, and occurs between 33.28 – 33.30 lat. and 136.58-136.65 lon. The BSR does not deflect upward at any of the surrounding faults, nor is it offset across the faults. Thus it is unlikely that the BSR is out of equilibrium or that warm fluids are actively migrating up these faults.

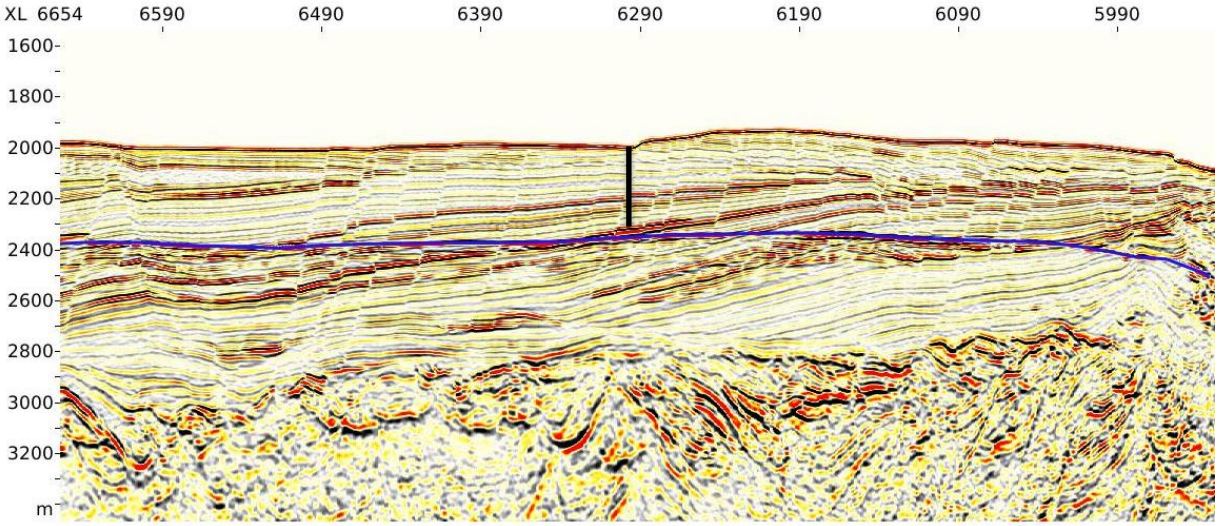

Figure 6.9 - High HF 4 IL2435 BSR depth (black line) 353.31 mbsf

High HF Zone 5 appears in the southeastern portion of the survey region, from 33.30 – 33.33 lat. to 136.65 – 136.68 lon. It is a well-defined, oblate feature, with a shallow BSR at ~ 360 mbsf. This zone of high heat flow occurs over toe, on the flanks of a large surface slump (Fig. 58 and 59) suggesting a strong defocusing of heat away from the slump towards the toe. The slump appears as a package of discontinuous reflections with a tilt opposite in character (seaward) compared to nearby horizons with landward tilts. The primary BSR does not appear to have fully responded to the change in seafloor geometry. We would expect a seafloor disturbance of this magnitude to affect the BGHS given enough time for the temperature perturbation to diffuse to the depth of the BSR. Below the primary BSR here, a second BSR appears in the seismic data as a strong, reversed polarity reflection. It is possible that the BSR is in the process of relaxing and migrating downward to the present BGHS.

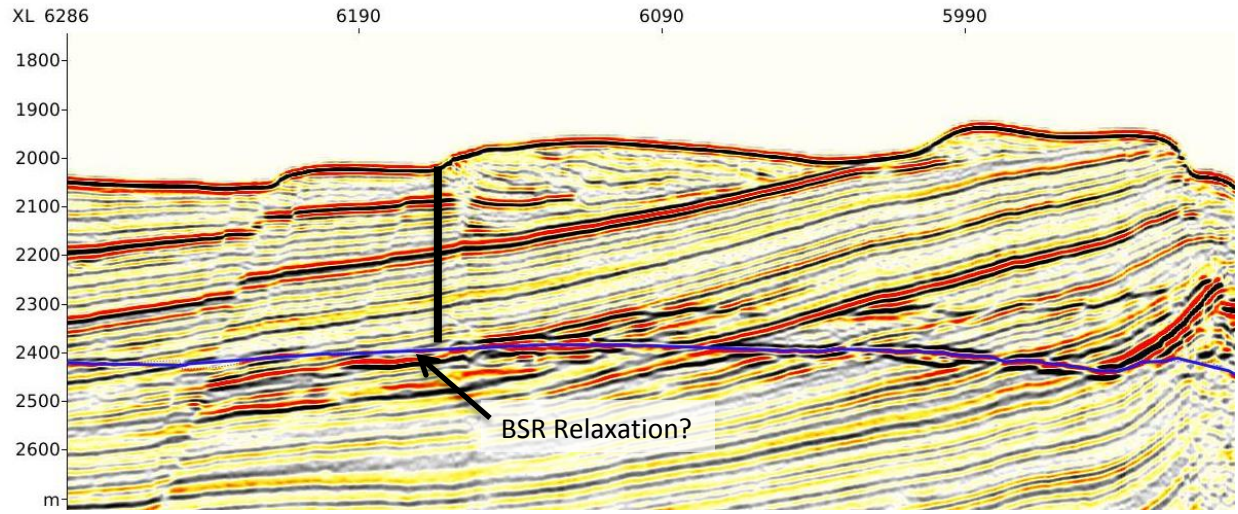

Figure 6.10 - High HF Zone 5a IL2693 X6154 BSR depth 360.33 mbsf

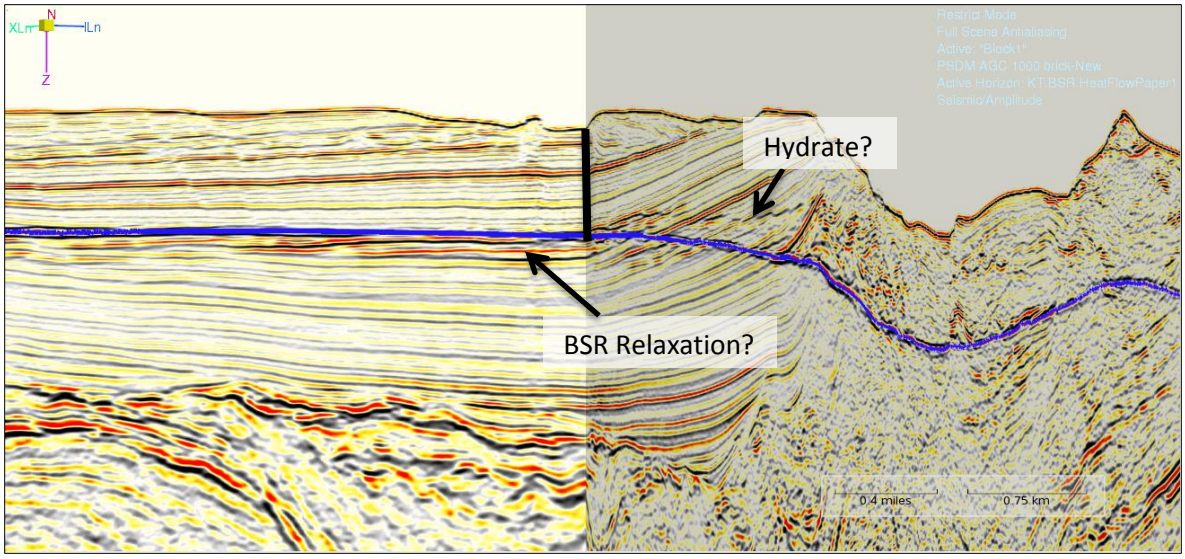

Figure 6.11 - High HF Zone 5b Inline 2715 and Crossline 6145, BSR 363.75 mbsf

High HF Zone 6 is a strong, linear feature from 33.24-33.26 lat. to 136.58 – 136.64 lon. The BSR here mirrors the seafloor at a depth of ~359 mbsf. The seismic data shows this region is highly deformed by accretionary tectonics (Fig. 6.13), and the upper sediments column has been altered by erosion which would increase surface heat flow (e.g., Hamamoto et al., 2011) A mud volcano is observed about 500 meters away (Fig. 6.14). Laterally across the mud volcano, the BSR deflects upward on both sides and disappears across the central vent which is

characterized by chaotic reflections. The lack of a BSR across the vent feature suggests that this vent is active, and the upward migration of warm fluids is prohibiting hydrate formation. The upward deflection of the BSR to each side of the BSR gap is consistent with the active transport of heated fluids and/or sediment from depth (Cartwright and Santamarina, 2015; Crutchley et al., 2015). Mud volcanoes are not uncommon across the Kumano forearc (Morita et al., 2002; Hamamoto et al., 2011; Pape et al., 2014). Other mud volcanoes in the Kumano Basins were found to have higher thermal conductivity values than surrounding regions (Hamamoto et al., 2011), and were associated with shallow BSRs (Baba and Yamada, 2004). Because conductive heat flow is the product of vertical temperature gradient and the thermal conductivity, an increase in thermal conductivity would result in more efficient heat transfer and overall higher heat flow.

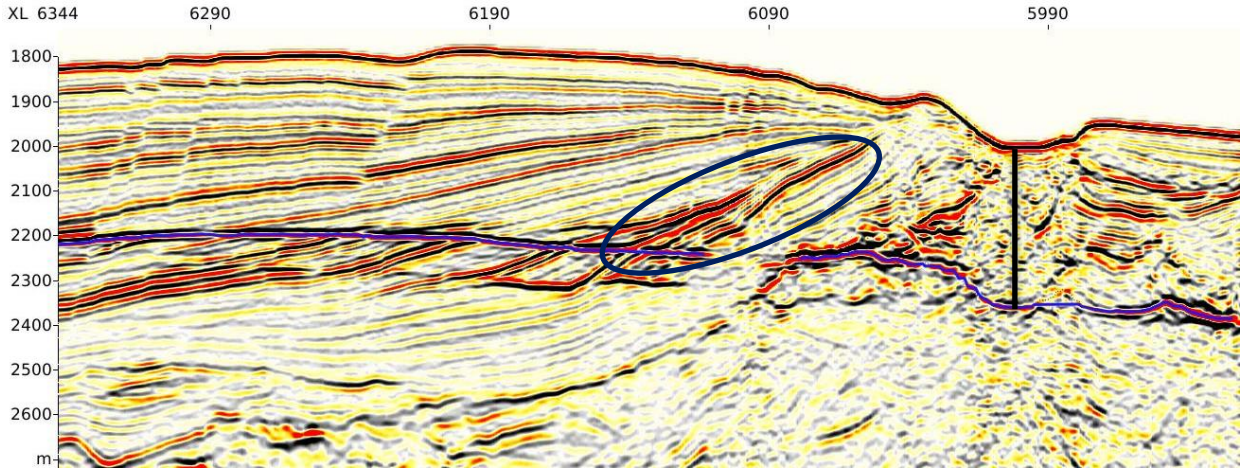

Figure 6.13 - High HF Zone 6a IL2175 BSR depth 359.30 mbsf

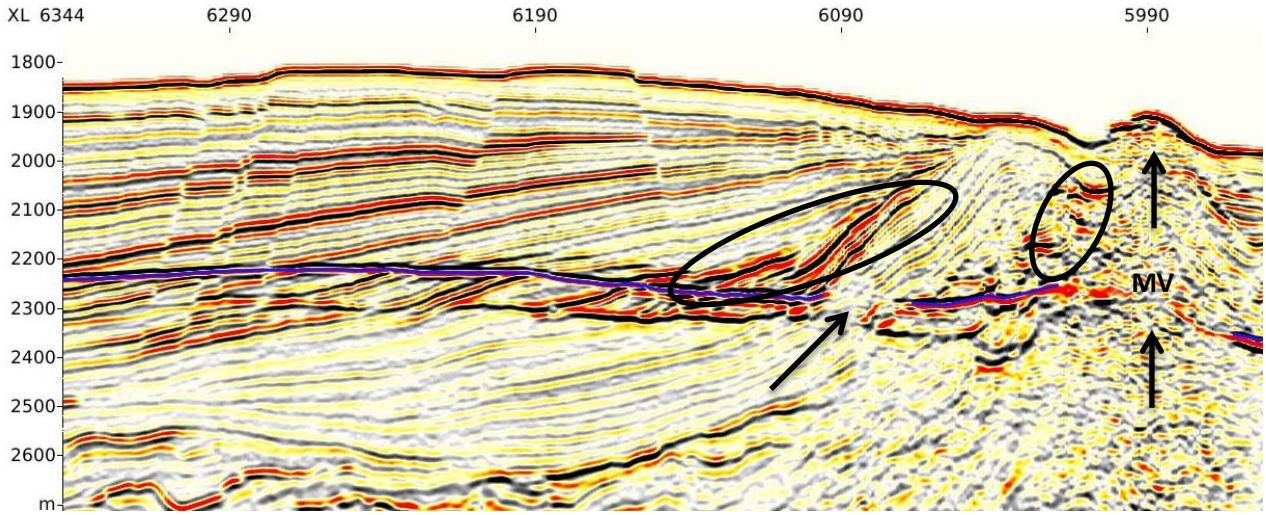

Figure 6.14 - High HF Zone 6b IL2219

High HF Zone 7 is a beautiful example of a BSR that does not correspond to the base of gas hydrate stability. The BSR here is ~323.8 mbsf and occurs beneath a region > 11km across where a significant amount of material has been removed. Bangs et al. (2010) referred to the V-shaped surface topography as a “notch” that is 3-4 km w and 300-400 m deep extending 35 km in length (Fig. 6.14). The seismic data show that the BSR to the left of this notch is very deep (see Low HF Zone 5), and under the notch is very shallow, but overall the trend of the BSR relative to the seafloor is in excellent agreement.

Bangs et al. (2010) proposed that there was a massive release of methane at the time the material was removed as a result of a pressure perturbation association with sediment unroofing. We contend that such a scenario is highly unlikely. First, for this to be the case would require that pore pressure conditions were not hydrostatic, because in the case of hydrostatic pressure conditions, even with the removal of material, hydrostatic pore pressures would persist (e.g., Bouriak et al., 2000). Second, the upper “paleo-BSR” which we have labeled UBSR-2, appears as an expansive feature and also occurs in regions where there is almost no-removal of material at all, which suggests that the UBSR-2might not be related to the removal of material, but rather marks the top of a gas hydrate concentration zone. If this is the case, it would inappropriate to use the UBSR as a baseline for extrapolating out paleo-seafloor

topography. Further, any free gas and interstitial water beneath the paleo-BGSZ would have been suddenly exposed to environmental conditions even more favorable to hydrate formation due to the introduction of very cold bottom waters. The exposure to very cold bottom water temperatures has clearly resulted in a deepening of the BGSZ as indicated by the downward pluming primary-BSR. Liao et al. (2014) also noted deep BSRs in the South China Sea in regions where cold seawater invasion appears to invade and reduce rock temperatures. We deem that the high amplitude reflections (box 1) which change polarity across the BSR are saturated with hydrates. The recovery of the BSR beneath the notch is evidence that there is an efficient supply of gas with stable hydrate above coming up from depth. The BSR is likely shallower beneath the notch because of the focusing effect of heat flow over regions of concave topography (Tao et al., 2014) and the perhaps from the increase in surface heat flow from erosion (Martin et al., 2004).

The topographic disturbance is not negligible here and could be introducing errors in the heat flow estimate for this zone. At site C0006, the rough surface topography resulted in necessary correction factors as high as 16% (Harris et al., 2011). Further, we cannot determine the kinetics of BSR adjustment here because there are simply too many unknowns. The time that it takes for a BSR to correspond to the actual BGSZ following perturbation depends on the timing of the disturbance event, the tectonic/sedimentary stability of the region on order of tens of thousands of years, the thermal diffusivity of the sediments, and the gas composition. Thermal adjustment to the removal of mater may still be ongoing

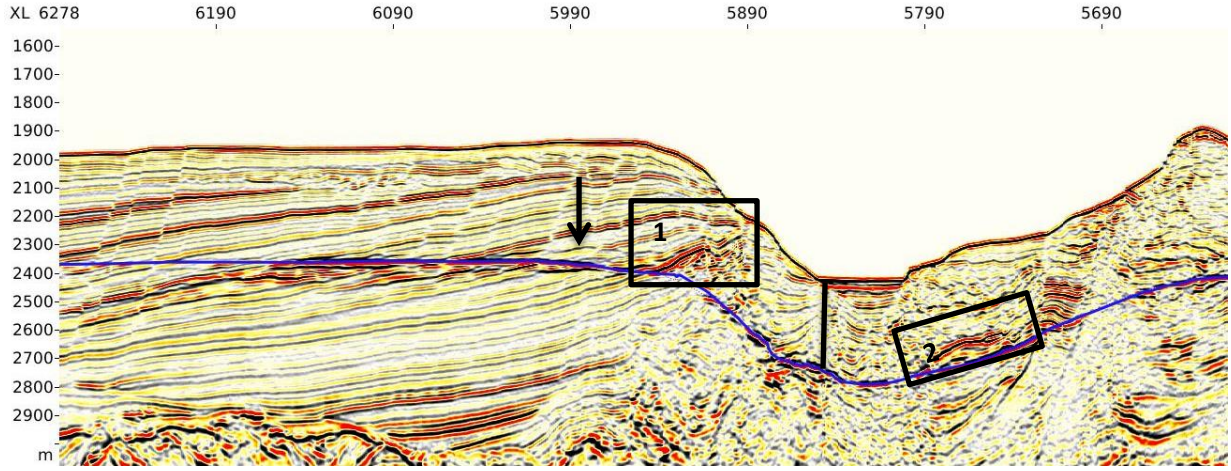

Figure 6.15 - High HF Zone 7 IL2601 BSR Depth 323.78

6.2.2 Analysis of Low Heat Flow Regions

There are five regions of low heat flow defined by values of 44 mWm^{-2} or less. Areas of lower heat flow correspond to deeper BSR depths, thicker GHSZs, and generally occur over surface topographic highs, regions where the BSR has been perturbed, and with increasing distance from the trench.

Low HF Zone 1 registers the lowest heat flow values within the basin, which supports the notion that heat flow should decrease with increasing distance from the trench because of thickening in the underlying accretionary prism (Harris et al. 2013). This zone is >50 km from the trench, and both the surface topography and the underlying accretionary prism are flat. Further, recent sedimentation rates are high which is related to the landward migration of the depocenter noted in Chapter 2. Grevemeyer et al. (2009) estimated that rapid sedimentation rates could lower heat flow by as much as 10-30%. The BSR is on average ~ 423.4 mbsf, and likely corresponds to the BGSZ. There are no deep cutting faults or fracture networks apparent in the seismic data (Fig. 62). The BSR is truncated and disappears in the landward direction, likely as a result of gas migration in the up-dip, seaward direction. Without a sufficient delivery of gas to support an overlying seal from hydrate formation, along with an accumulation of free gas below, a BSR will not be imaged.

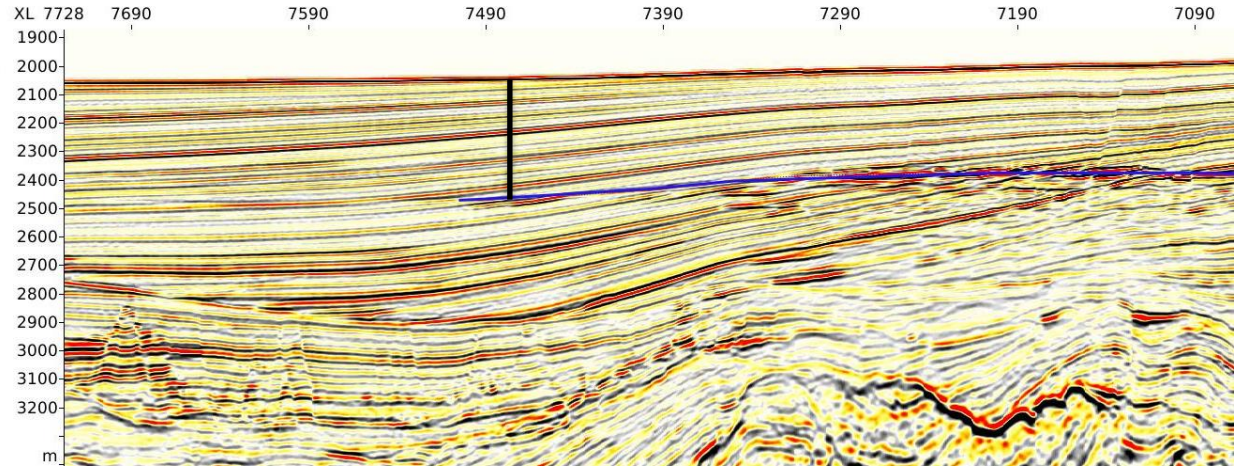

Figure 6.16 - Low HF Zone 1, IL2200, BSR depth 423.36 mbsf

Low HF Zone 2 is about 7 km wide and 5 km across and is the result of a BSR that is on average ~427.5 mbsf. The surface topography here is flat, and this region is characterized by a very thick layer of sediments filling an underlying syncline in the accretionary prism. The BSR likely corresponds to the BGHS. We interpret this to be a regional pocket of a thick sediment column with an overall lower heat flow character (Fig. 63). The patchy nature of this anomaly is due to errors in BSR picking as a result of decreases in BSR amplitudes across perfectly parallel strata.

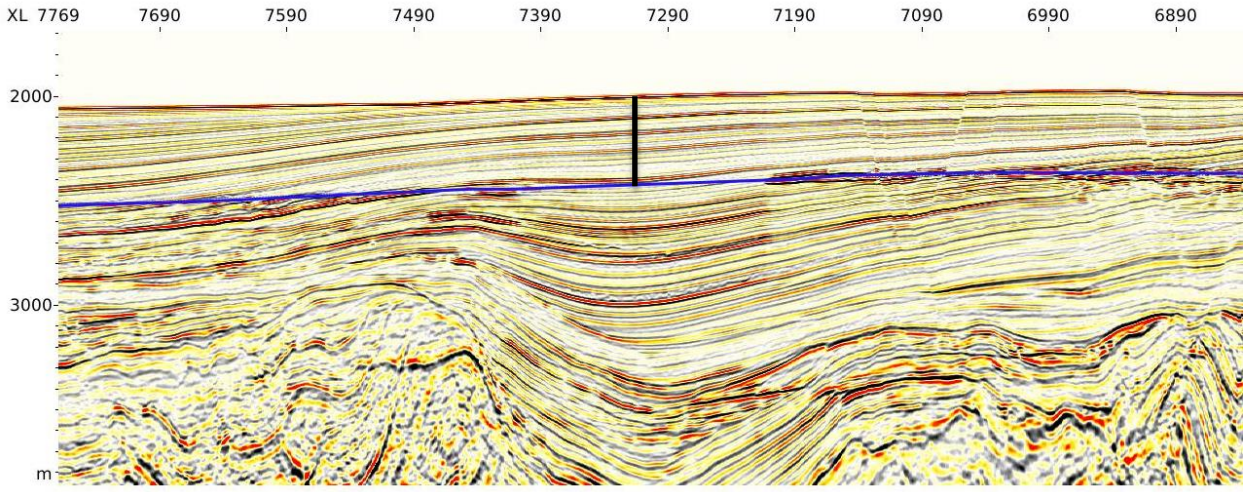

Figure 6.17 - Low HF Zone 2, IL2577, BSR depth 427.44 mbsf

Low HF Zone 3 occurs in the southwest margin of the basin and is cut off by our survey perimeter. It is a well-defined low heat flow region surrounded by concentric zones of stepped increases in heat flow values (Fig. 6.18). The seismic data reveal a primary-BSR, an upper-BSR, and a lower-BSR. The primary-BSR (blue horizon) is deepest at ~ 435.91 mbsf (black line) and shoals upward to 330.01 mbsf (red line) over a zone of chaotic reflections. The upper-BSR is the same polarity as the seafloor, is approximately 330.01 mbsf, or 58.9 meters above the primary BSR (green line). The lower double BSR is a second reversed polarity reflection at 532.8 mbsf which is 99.73 meters below the primary BSR. The many BSRs and their character, testify to the complexities of the geological history of this region. The UBSR is interpreted to be the top of a gas hydrate concentration zone (HCZ), the LBSR corresponds to a s-II hydrate phase boundary, the gap in the LBSR and weak amplitude of the primary-BSR crossing the most heavily tilted package of sediments suggest the release of gas or a lack of gas accumulation. The pluming nature of the primary-BSR indicates an elevated heat flow relative to surrounding environment.

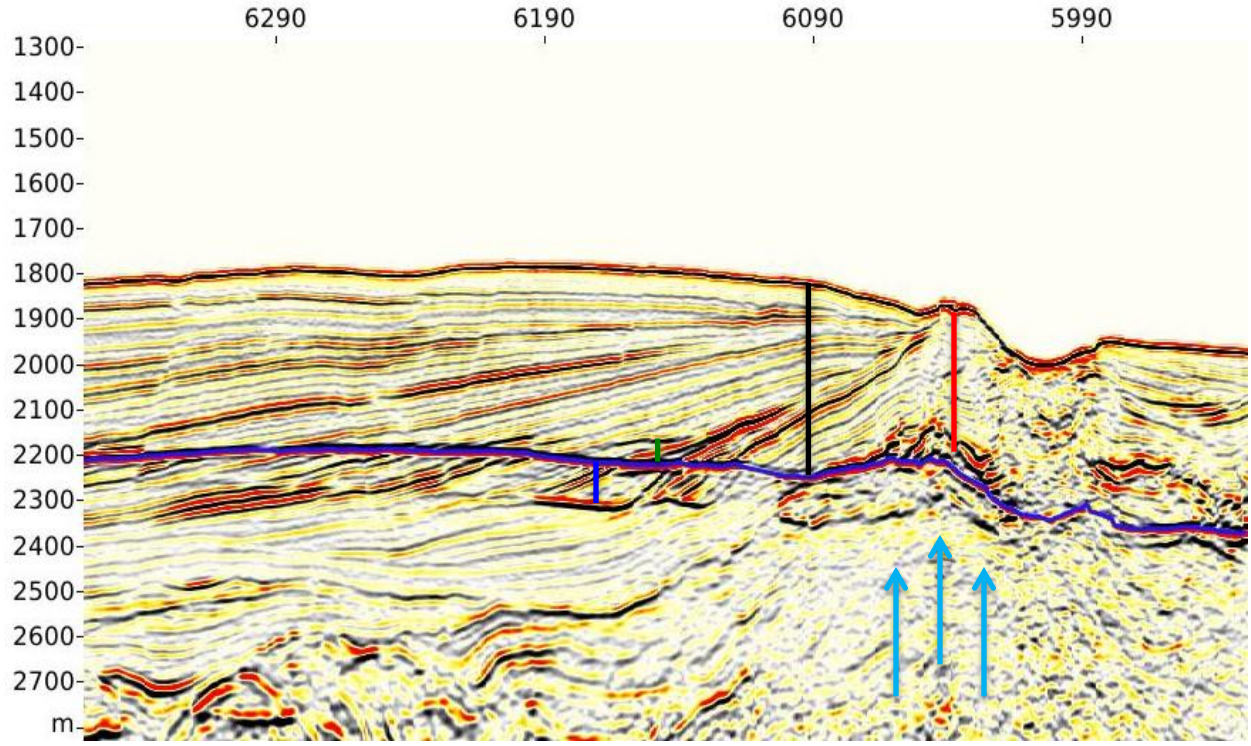

Figure 6.18 - Low HF Zone 3, Inline 2150, BSR (black) 435.91 mbsf. BSR (red) 330.01 mbsf 660 meters apart dBSR (blue) 99.73 meters below the main BSR and 532.80 mbsf uBSR 58.90 meters above the main BSR and 430.60 mbsf.

Low HF Zone 4 appears between 33.30-33.27 lat. to 136.63-136.70+ at the outer arc edge of the basin (Fig. 65). This zone parallels High HF Zone 6, and is likely the result of thermal perturbation to the BGHS from the removal of surface material near the outer arc and nearby infiltration of cold seawater. The UBSR is interpreted here to be a remnant BSR that closely mirrors the pattern of the seafloor. The primary BSR now shoals away from the seafloor, tilting deeper in the sediments up to about 470 mbsf the closer it gets to V-shaped notch.

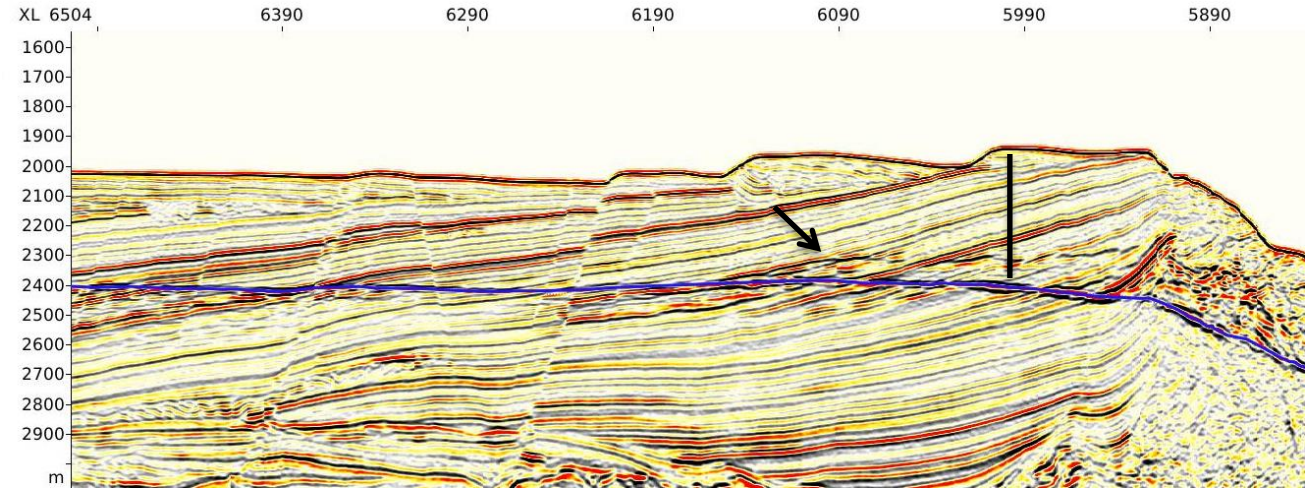

Figure 6.19 - Low HF Zone 4, IL2707, BSR 470.00 mbsf

Low HF Zone 5 corresponds to a block of old accretionary prism that was brought up along one of the splay fault branches, and as such, is part of the frontal prism outside of the boundaries of the Kumano basin (Fig. 6.20). The BSR here is very deep at ~517 mbsf and is related to a hydrate system operating under different parameters than within the Kumano Basin.

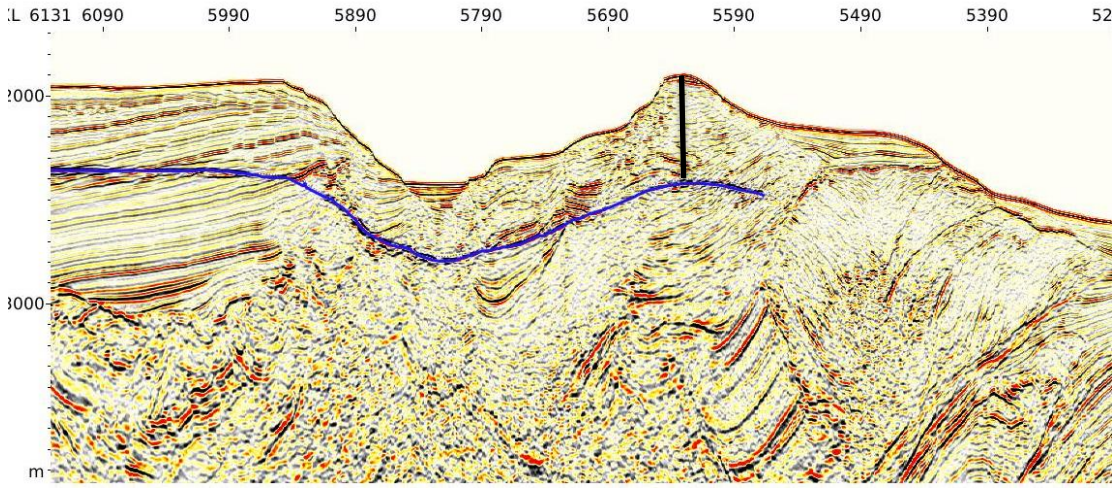

Figure 6.20 - Low HF Zone 5, IL2614, BSR at the black line is at 517.46 mbsf

Exploration of the spatial relationship between BSR-derived heat flow relative to surface and basement features, shows that deviations are reflecting both variations in local geothermal character as well as zones where BSRs are potentially out of alignment with the present BGHS as a result of stress placed on hydrate stability conditions. The underlying basement topography is the main control on heat flow in the landward half of the survey which is characterized by a flat seafloor with few sedimentary disturbances, and a thinner sedimentary cover. Heat flow on the seaward edge reflects agitations from seafloor disturbances including large MTDs, erosion, and compressional tectonic events including fluid expulsion. Thus, we conclude that heat flow in the Kumano Basin is affected by combined along-strike variations in geomorphological structures in the accretionary prism; deformation and associated fracturing leading to increased permeability and fluid flow from depth; and surface processes including erosion and mass wasting. Diffuse, elevated heat flow is observed in sediments above topographic highs in the accretionary prism in High HF Zones 1 and 2. The faults/fracture networks in these zones may act as a favorable pathway for methane migration from depth while focused, advective heat flow is observed only in High HF Zone 6 which is located near an apparently active mud volcano feature. The other four high heat flow zones are each related to surface features including the large removal of material and over the toe of surface landslides. Low heat flow regions are found to correspond to surface topographic highs, and in the case of low heat flow Zone 5, to a large thermal perturbation event.

The heat flow values presented in our model are all <60 mWm^{-2} indicating that heat transfer is primarily conductive, and that the velocity of fluid flow into basin sediments from the underlying accretionary prism is too low to effectively affect heat transfer. Leg 131 further westward in the Nankai Trough also found heat flow consistent with conductive cooling models (Taira et al., 1991). Tectonic activity such as faulting may affect the BSR and hydrate stability by acting as a conduit for warm fluids from depth which would raise the heat flow. Thrust faults that are not delivering fluids by carry colder sediments to deeper depths, should depress the BSR. Our analyses shows that rapid focused fluid advection from depth up deep cutting normal

faults is not reflected in the BSR-derived heat flow. Therefore, if focused advection does occur along these faults, it is likely episodic in relation to seismicity.

Overall, the BSR-derived heat flow reveals the combined effects of surface sedimentation, erosion, and basement topography on heat transfer in the basin (Fig. 6.21). Higher heat flow values are associated with underlying basement topographic highs and regions of recent surface erosion; particularly in respect to large surface MTDs. Lower heat flow values (deeper BSRs) are associated with basement synclines, thick sedimentary packages, regions of surface sediment deposition. GHOZ estimates only considering BSR depths relative to seafloor topography may have significant errors depending on the underlying topography and stratigraphy.

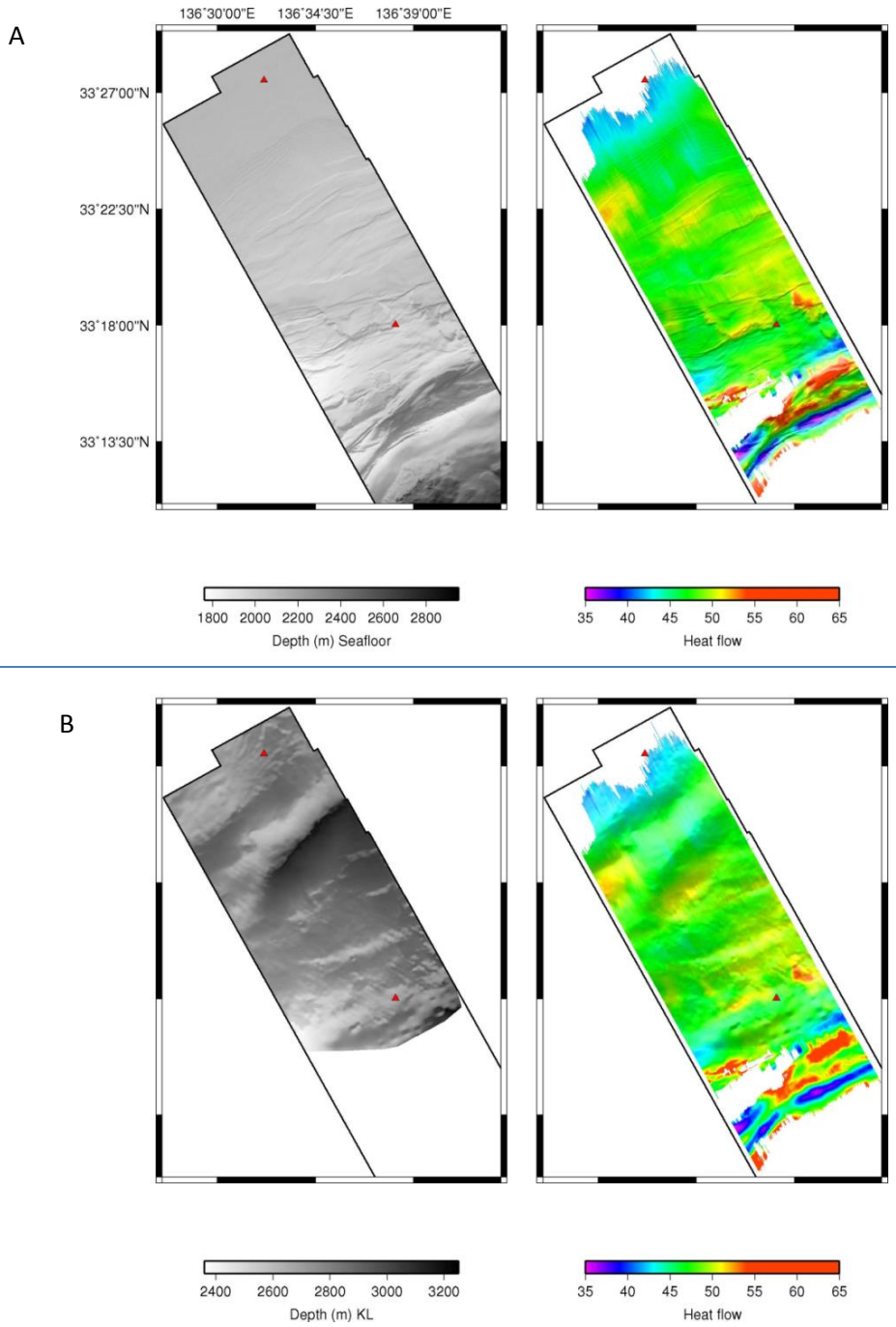

Figure 6.21 – A. Seafloor relief plotted on top of the heat flow map. B. Basement relief plotted on top of heat flow map. A and B show the combined influence that both the basement and seafloor have on BSR depths and corresponding heat flow values.

Chapter 7

Integrated Hydrate Petroleum System Model and Gas in Place Resource Assessment

"It is not really difficult to construct a series of inferences, each dependent upon its predecessor and each simple in itself. After doidoing so, one may produce a startling effect." – Sherlock Holmes

The Adventure of the Dancing Men, Sir Arthur Conan Doyle

7. Hydrate Petroleum System Model & Resource Assessment

7.1 Gas Hydrate System Analysis

The most pressing advancements needed in order to move towards viewing hydrates as an economically recoverable resource (and thus useful) are: 1) better geologic characterization of gas hydrate reservoirs to identify regions with the highest potential for steady flow rates and 2) the ability to run long term production trials in order to fully understand the extent of possible gas flow rates. These advancements demand that we improve our understanding of the dynamic processes involved in gas hydrates systems in nature that lead to the formation of hydrate concentration zones. Furthermore, as industry led exploration for energy resources moves into deeper waters, there is an increased need for risk and reservoir production potential assessments which can benefit from approaching the GH system as a hydrocarbon system (e.g. Collett et al., 2009; Boswell and Saeki, 2010) with a source of gas (taking methane solubility behavior into consideration), identifiable gas migration routes into the hydrate stability field, some constraint on the trapping mechanism whereby gas can accumulate and hydrates can form in concentrated deposits, and methods for detecting and evaluating those concentrated deposits. At the exploration stage, a bottom simulating reflection remains the strongest indicator of the presence of gas hydrates and can be used in conjunction with seismic amplitude, attributes, velocity, or advanced AVO analysis to guide exploration. Constraints from wells, and ideally pressure cores, are an essential second step.

In this chapter, we apply a petroleum systems approach to synthesize the datasets and interpretations from Chapters 2 through 6 to build a conceptual model demonstrating the structural control of geomorphological features and faults, and the sedimentary controls of sand-bearing permeable layers on fluid migration into the GHSZ. Migration pathways and gas accumulation zones were identified by using proxies including the BSR-derived heat flow map and seismic attribute analysis. We then proceed to present an isopach map of gas hydrate concentration zones occurring above the BSR and discuss the possible trapping mechanisms for

both the free gas and gas hydrate reservoirs. Two gas hydrate concentration zones (HCZs) were identified, and a volumetric probability assessment is employed to estimate the amount of gas in place locked up in these HCZs.

7.1.1 Gas Source

Natural gas in a marine environment can be produced by three primary mechanisms: (1) *in situ* production as a microbial byproduct of organic matter degradation; (2) thermal cracking of organic matter via burial and heating; and (3) through abiotic fluid-rock interaction (e.g., Solomon et al., 2014; Johnson et al., 2015). Abiotic methane production is generally rare, and not believed to contribute to the methane pool in our study region because any methane source from subduction related serpentinization would occur far outside the possible fluid delivery pathways into the basin sediments. Thus we will consider biogenic and thermogenic gas production only. The amount of methane that can generated *in situ* in the upper sediment column is limited by the amount of bioavailable organic carbon that escapes oxidation via rapid burial, while thermal cracking demands temperatures of >80 °C which would be equivalent to ~2 kmbsf at Site C0002 or ~3.5 kmbsf at Site C0009 given their respective geothermal gradients.

The TOC at Site C0002 is generally low (between 0.4-0.8 with an average of 0.5 wt%) with a small peak corresponding to the lower basin sediments. This package of lower basin sediments is very thin at C0002 (depth), but is significantly thicker in other regions more landward in the basin (Fig. XX). Very high TOC content was found in the same sequence at C0009 (5.0 wt%) depth (Doan et al., 2011). HARs present within the organic rich package and stemming from the accretionary prism are geophysical evidence for gas charge fluid delivery from deep within basin sediments and from the accretionary prism. Together geophysical and geochemical data from NanTroSEIZE drilling support both biogenic and thermogenic gas contributions to the methane pool that sustains the NGH system in the basin.

7.1.1.1 Geophysical Evidence

The presence of gas appears in seismic data as reductions in acoustic impedance, which strengthens the reflectivity coefficient and results in either enhanced reflections (high amplitude reflections (HARs)), a polarity change (Brown 2004, Avseth et al. 2005), or as anomalous low velocity, low coherency zone. Other seismic indicators of gas-charged fluids include flat spots, bright spots, and dim spots, which are each known as "direct hydrocarbon indicators" (DHIs), and are thus important features to identify when prospecting for gas (Spence et al., 2010; Brown, 2010). In the event of a fluid contact, gas-water, gas-oil, or water-oil, a flat spot will occur at the boundary between the two constituents (Brown, 2004). We assume that oil is not present in the Kumano Basin given that the organic matter found during drilling is predominantly woody material, and therefore flat spots are a direct indication of gas-water contacts. Bright spots commonly occur as an acoustic impedance contrast between a caprock (in this scenario gas hydrates) overlying a gas saturated sand, while dim spots are low acoustic impedance common to gas-saturated rock. Gas can also produce seismic turbidity which appears as a visual distortion of seismic horizons (e.g., Jones et al. 2010).

Flat spots and HARs appear frequently at and well beneath (100s of meters) the BSR in our seismic data. Bright spots likely indicating gas-saturated sands cluster along anticlinal hinges (Fig. 7.1), within tilted strata, and within an erosional feature at the seaward edge of the basin. There are three thick low velocity zones that appear as a plume over basement topographical highs (Fig. 5.1, 5.2). In the amplitude volume these same regions appear as discontinuous, patchy reflections also referred to as seismic turbidity. The acoustic turbidity, corresponding low velocity, the depth, and spatial distribution of these gas signatures in the seismic data indicates that gas is migrating up from depth and is trapped beneath the primary BSR (Fig. 7.2) suggesting an efficient hydrate seal. If that seal is fractured it could result in the release of the deeply sourced gas into the GHSZ. Any gas released from hydrate dissociation following the upward shift of the BGHS will mix with this pool of underlying gas. The low velocity signature spills over the BSR in the center of the survey corresponding to high heat flow

1 (Fig. 6.6) indicates that the release of gas into the hydrate stability zone was recent and that both free gas and NGHs co-exists above the BSR.

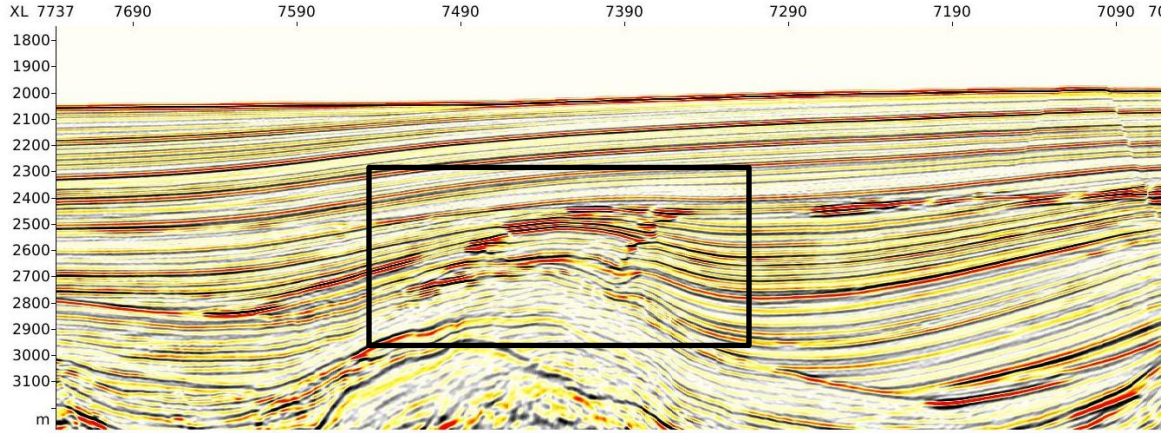

Figure 7.1 - Inline 2407 Gas traps along anticlinal hinges above an underlying topographic high in the accretionary prism. Similar HARS along anticlinal hinges have also been observed in the gas hydrate-bearing regions of the Hikurangi (Barnes et al., 2010) and the Makran (Smith et al., 2014).

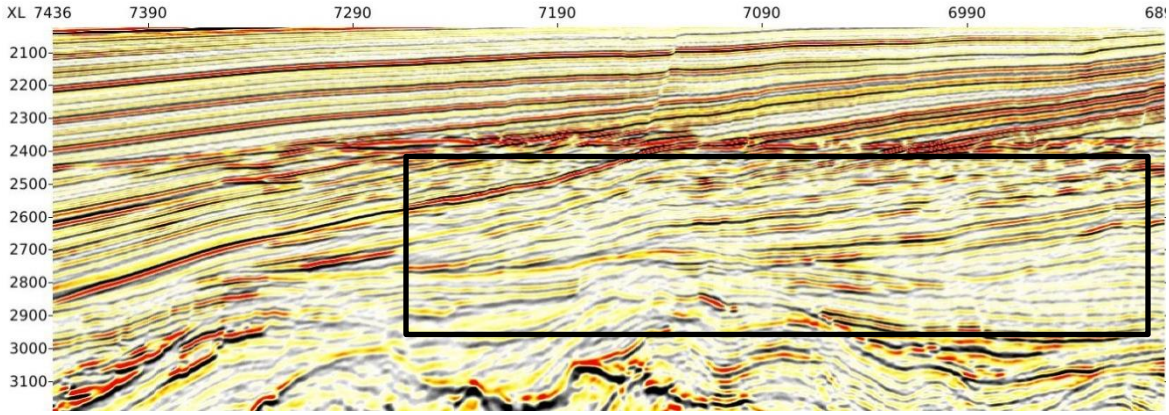

Figure 7.2 - Inline 2178. Example of acoustic turbidity (discontinuous acoustic reflectors inside the black box)as a result of gas accumulation beneath the BSR.

7.1.1.2 Geochemical Evidence

The origin of methane in marine sediments is typically determined by using the C_1 (methane) to C_{2+} (higher hydrocarbon) ratio (Claypool and Kvenvolden, 1993) and from the stable carbon isotopic composition (Witicar, 1999). Thermogenic methane is enriched in ^{13}C (-

30 ‰ to -50‰ V-PDB) and will have a higher concentration of ethane relative to methane than microbial gas ($\delta^{13}C$ of -90 ‰ to -60 ‰). However, it should be noted that more than 90% of gas is lost during core recovery (Paull et al., 2000), isotope fractionation of ^{13}C can occur during migration and hydrate incorporation, and C_{3+} hydrocarbons which often accompany thermogenic gas are potentially selectively removed during migration (Hachikubo et al., 2007; Pape et al., 2010).

It is presumed from the C_1/C_{2+} ratios in the headspace gas measurements taken at Site C0002 and Site C0009 that the methane is primarily biogenic in origin (e.g. Toki et al., 2012) based on the distinction between a biogenic gas and a thermogenic gas using carbon isotope analysis; a $\delta\ ^{13}C$ value above -60‰ (VPDB) is considered to be biogenic. At C0002 the methane/ethane ratio was on average 1000 while the $\delta\ ^{13}C$ ranged from -50‰ to -80‰ (VPDB) implying a microbial source (Strasser, 2012). At C0009 methane/ethane ratio was typically >500. However, the hard distinction between biogenic gas and thermogenic gas based on carbon isotopic values without consideration of mixing is a flawed assumption. The $\delta\ ^{13}C$ value become more enriched with depth and most of the $\delta\ ^{13}C$ curve lies near -60‰ which could mean that a component of thermogenic gas is mixing with microbial gas. The presence of mud volcanism, bright spots over anticlinal structures and ethane in increasing concentrations with depth are supportive evidence of thermogenic gas migration upward into the basin sediments. Further, recent isotope analyses of samples collected from the production trial site in the eastern Nankai Trough determined there was a component of hydrate bound thermogenic gas (ethane) with increasing depth (Kida et al., 2015) and a minor component of thermogenic gas was detected near the Kumano-nada mud volcanos (Uchida et al., 2009). Data plots from Expedition 348 and 338 are shown in figures 7.3 and 7.4. It is clear from the C_1/C_{2+} plotted against the $\delta\ ^{13}C$ of CH_4 values that there is a component of thermogenic and microbial gas mixing. This mixing is more apparent in the 348 data which drilled down into the accretionary prism, which is not surprising given that microbial methane should be more abundant in the shallower sediments as is expressed in Expedition 338's plot.

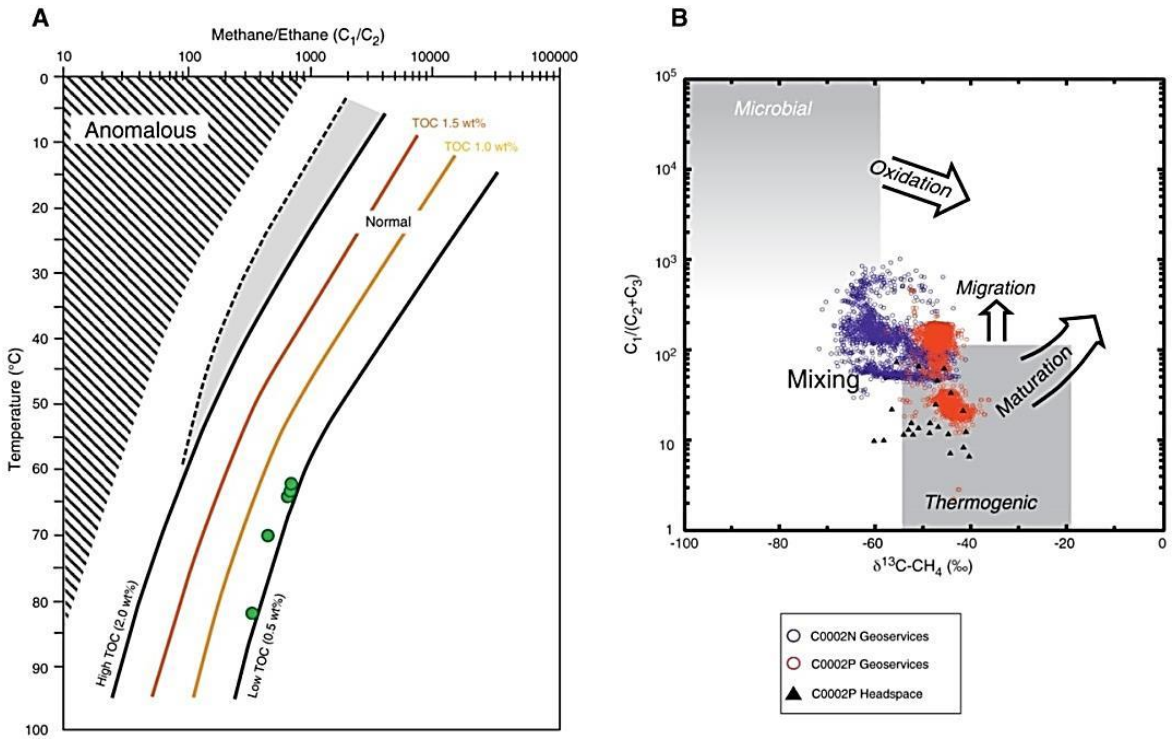

Figure 7.3 - A. Total gas, methane, ethane, and propane in mud gas, Holes C0002F, C0002N (838-2330mbsf) , and C0002P (1954-3058mbsf) B. Bernard plot ($C_1/[C_2 + C_3]$) vs. carbon isotopes of methane gas for mud gas and headspace gas, Holes C0002N and C0002P. Image from IODP Expedition 348 Preliminary Report: shows an onset of thermogenic regime at ~1700 mbsf with a clear thermogenic signature at ~2325 mbsf.

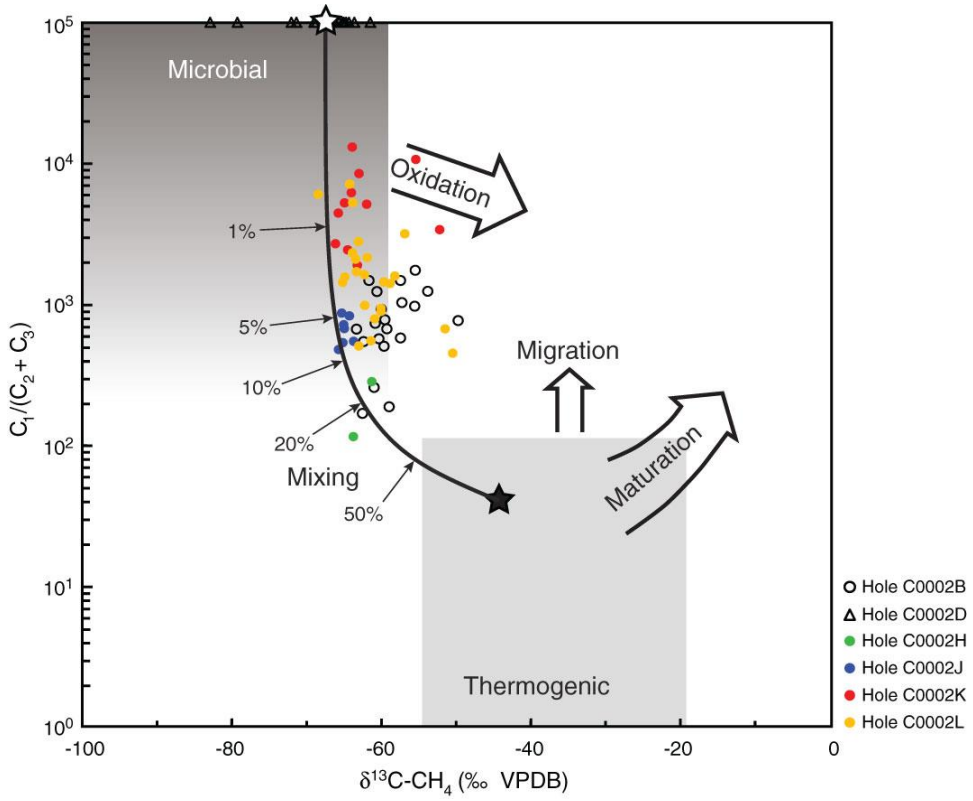

Figure 7.4 - Relationship between the $C_1/(C_2 + C_3)$ ratios and $\delta^{13}C\text{-}CH_4$ in headspace gas, Site C0002 from Figure F77 (Strasser et al., 2014). Open star = end-member of microbial methane, solid star = end-member of thermogenic methane, presumed so that the mixing line between the two end-members best fits the observed data. Solid curve = mixing line between the two end-members. Percent values indicate the contribution of thermogenic methane. VPDB = Vienna Peedee belemnite.

There are potential errors related to using isotopically light methane as a diagnostic indicator of gas from biogenic origins which need to be considered. First, the gas sampled may have undergone post-formation isotopic alterations such as secondary biogenic modification of thermogenic gas from within the poorly studied deep biosphere (Colwell et al., 2004; Smith and D'Hondt, 2006) or from diffusive migration which would result in an enrichment of lighter carbon isotopic values despite being thermogenic in origin (Prinzhofer and Pernaton, 1997). Further, shipboard gas measurements were taken from void space and headspace samples or during mud gas monitoring (Hammerschmidt et al., 2014). Void space gas would provide more indicative measurements for the composition of hydrate-bound gas which the headspace samples would better reflect the background gas composition within sediments, but in either case, 99% of gas is lost during core recovery (Paull et al., 1998; Paull et al., 2000) Given the fact

that ethane and pentane are preferentially lost during recovery over methane as noted by Expedition 348 Scientists (2014), the signature of thermogenic gas at site C0002 could be diluted.

The seismic data supports the geochemistry data showing a component of migration and mixing between deep (potentially thermogenic) and biogenic gas sources. Thermal cracking to produce higher hydrocarbons could be taking place on the incoming plate where higher heat flow is prevalent (Harris et al., 2013) prior to subduction, being transported with the deeply sourced fluids coming from the underlying accretionary prism. While other studies have also proposed that gas forms at depth and migrates up-dip towards the seaward edge of the basin near Site C0002, based on the higher gas hydrate saturation values and the presence of free gas at C0002 relative to C0009 (Doan et al., 2011; Barnes, 2013), our seismic analysis reveals the spatial distribution of these processes; there are four zones where gas is being sourced from depth and contributing to concentrated hydrate deposits above (Fig. 4.33).

7.1.2 Migration Mechanisms

Gas migration in marine sediments can proceed as a short-range and/or long range process (Malinverno and Goldberg, 2015). Short-range migration is the mechanism by which *in situ* methane produced as a byproduct of microbial metabolism diffuses from one sediment layer to the next. Usually, this means from a fine-grained interval where it is difficult to form hydrates because of the Gibbs-Thomson effect on methane solubility in fine grain sediments, to an adjacent coarse grain layer with larger pore spaces which act to lower gas solubility, creating a favorable chemical potential scenario that facilitates hydrate nucleation (Daigle and Dugan, 2011; Torres et al., 2008). NGH recycling is a second example of a short-range migration mechanism. In this case, gas released from NGH dissociation following an upward shift in the BGHS diffuses back into the GHSZ and is potentially reincorporated into a new hydrate structure (in addition to any new gas produced *in situ)* (Paull et al., 1994*)*. Long-range migration on the other hand involves the transfer of free gas and gas-charged fluids into the GHSZ from

depth, usually along pressure gradients via diffuse porous flow through permeable layers, or as focused advection along highly permeability outlets including faults, fractures and fluid escape structures such as pipes, vents, or mud volcanoes (e.g., Hyndman and Davis, 1992)

In the Kumano Basin, there is evidence for both short and long range migration and gas mixing between microbial gas produced *in situ*, and thermogenic gas migration from depth as opposed to the long-range only model presented by Daigle and Dugan (2011) and the short-range only migration reaction-transport model presented by Malinverno and Goldberg (2015). Using Site C0002 TOC and logging data, Malinverno and Goldberg's study (2015) found that *in situ* biogenic methane production could support a NGH system, however, this process alone could not account for the large thickness of hydrate-bearing sands just above the BGHS. From their model, *in situ* production alone would result in a 14% hydrate saturation compared to the 70% hydrate saturation determined from the well log data. They proposed that gas bubbles from hydrate dissociation move up dip through permeable strata. We contend that the seismic evidence supports migration from much deeper than just the hydrate recycling zone. As discussed previously, the dewatering of the subducting wedge is a transient process (Tyron et al., 2002), and the expulsion of fluids from an overpressured accretionary prism or during seismic events could carry gas generated at depth into the GHSZ (Kvenvolden and Kastner, 1990).

Migration behavior is investigated in this study by: (1) utilizing seismic amplitude, velocity, and attribute analyses constrained by borehole data; and (2) considering BSR behavior and heat flow across the basin. Gas migration manifests itself in the seismic data as highly reflective units similar to those observed by Crutchley et al. (2015) along the Hikurangi margin. Because gas attenuates high-frequency seismic waves, the instantaneous frequency attribute is often employed to identify gas occurrence; however, we found the instantaneous frequency was very sensitive to thin-beds, and too noisy to be useful for interpretations of this survey. Through trial and error, with depth constraints on the gas layer beneath the BSR at Site C0002 Zone B, we determined that the signal envelope attribute most clearly images the presence of free gas (Fig.

7.5). Investigations using the signal envelope attribute and velocity volume in concert with the amplitude data allows us to get a better sense of how gas is being distributed in terms of the sedimentary structures and where it potentially originates from.

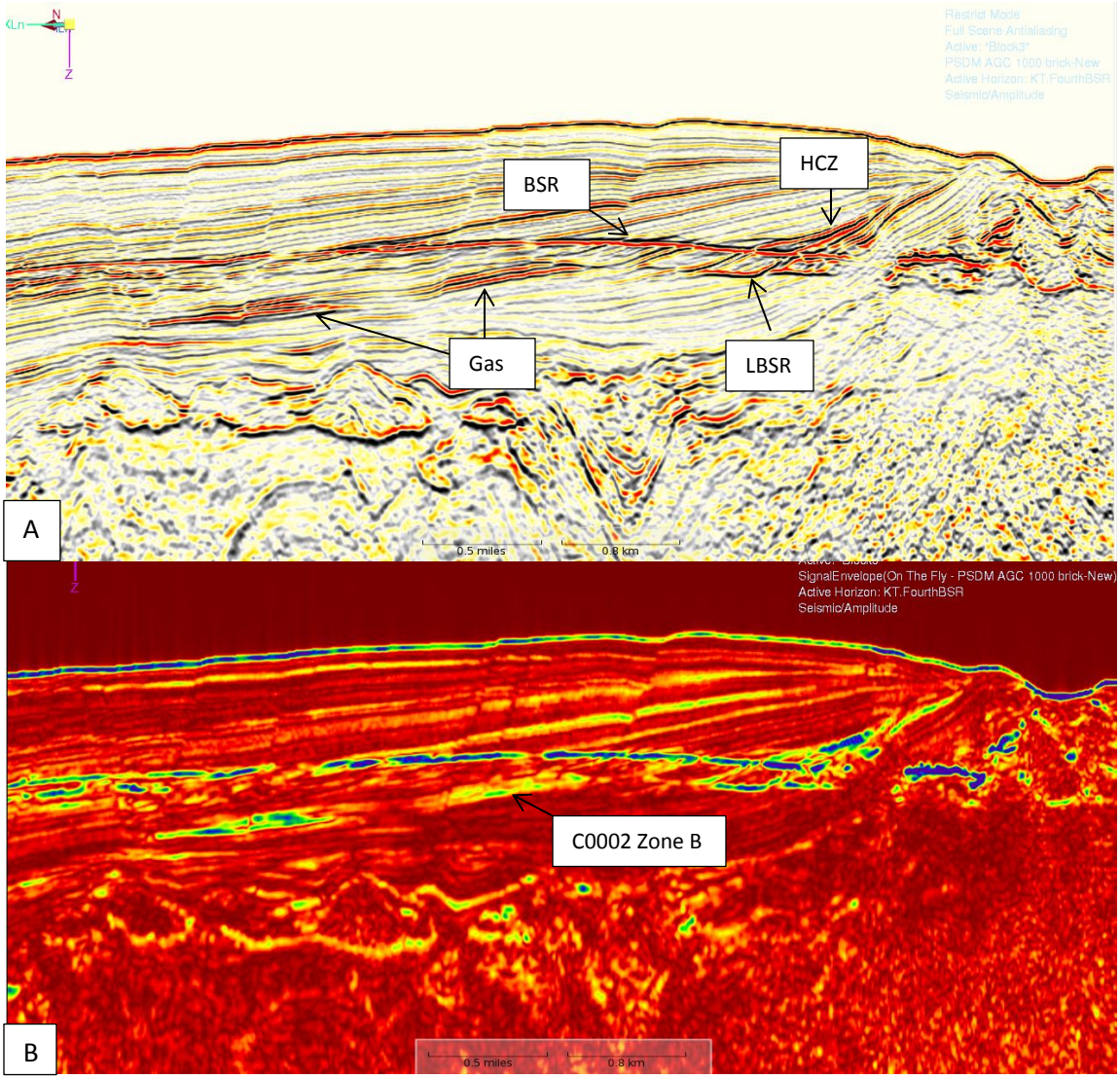

Figure 7.5: Inline 2185. A. amplitude volume, B signal envelope volume. Representative cross section showing the primary BSR with an underlying LBSR approximately 70 m deeper in the sediments. HARs interpreted to be gas migrating up permeable dipping strata in the amplitude volume (A) is visually easier to identify as bright greens and blues (high reflection strength) in the signal envelope volume (B).

By tying the borehole data collected at C0002 and C0009 (Chapter 4.1) to the gas proxies in the 3D seismic data, we determined that gas migrates into the GHSZ by means of three primary mechanisms: (1) transport along permeable dipping strata sandwiched between less permeable clays; (2) episodically through faults, factures and mud volcanism; and (3) by diffusion following BGHS shifts and concomitant hydrate decomposition/recycling.

7.1.2.1 Diffuse Fluid Flow along Permeable Strata

Gas migration up landward-dipping strata is particularly evident (1) by high amplitude reflections found at the seaward edge of the basin where sedimentary units were subjected to ~5-8 degrees of tilt and (2) by the branching off of both LVZ-1 and LVZ-2 in the center of the basin towards the seaward direction. The sand layers in turbidites in the eastern Nankai Trough were found to have permeability two to three orders of magnitude greater than that of mudstones present in the same core (Suzuki and Narita, 2010), and it is reasonable to extend that assumption to the Kumano Basin sediments meaning that highly permeable, tilted sand layers occurring between low permeable mudstone act as effective migration pathways (Suess and von Huene, 1988; Hyndmann and Davis, 1992; Milkov and Sassen, 2002; Riedel et al., 2011; Herbozo et al., 2013). Thus, the structure of the tilted layers serves to more efficiently facilitate and channelize upward gas migration (Figs. 7.5, 7.6).

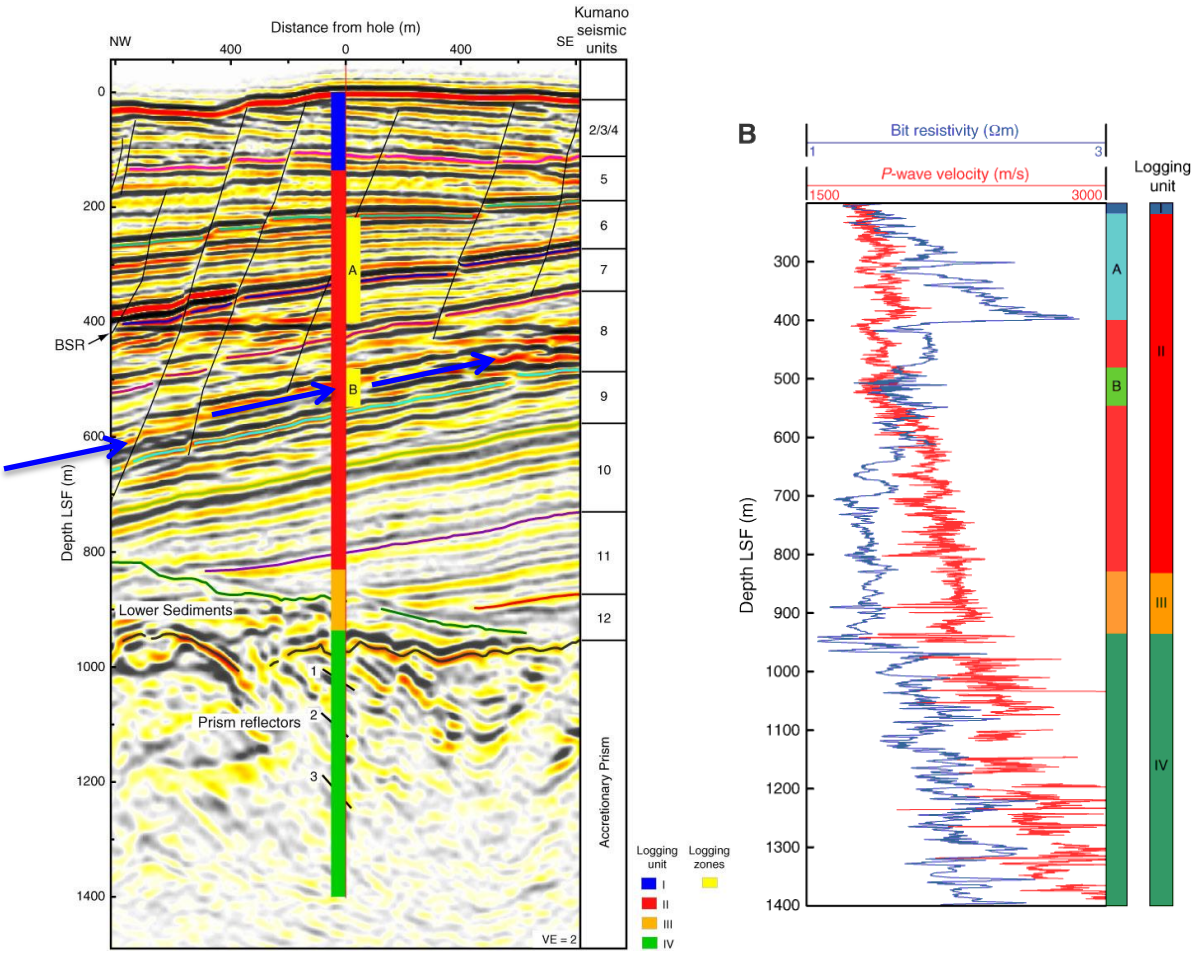

Figure 7.6 - . Logging Units I–IV and Zones A and B superimposed on check shot–corrected prestack depth-migrated seismic profile through Hole C0002A. Seismic Units Kumano 2–12, Lower Sediments, and Accretionary Prism from Gulick et al. (2007). LSF = LWD depth below seafloor, VE = vertical exaggeration. Zone B comprised of >50 sand layers with low P-wave velocity values indicating free gas may be migrating updip. Zone A is characterized by high resistivity spikes suggesting the presence of gas hydrates. Blue arrows indicate gas migration updip in permeable sands between clay at Zone B. Modified F14 and F26 from IODP Expedition 314 Proceedings (2009).

7.1.2.2 Hydrate Recycling

The base of the GHSZ fluctuates over time and this fluctuation results in hydrate dissociation, migration of released gas and the potential reincorporation into the hydrate structure. This process is known as “hydrate recycling” and is most evident in the central region of the basin. During tectonic uplift, perhaps related to thrust movement, Haacke et al. (2007) demonstrated that a free gas zone can exist below the BGHS in the Nankai region because the process of

hydrate recycling stimulated by tectonic uplift during accretion produces gas faster than the rate of free-gas depletion; however his model also shows that this free gas zone beneath the BGHS should be thin because of a competition between free gas generated from recycling and depletion from advection-dispersion from the upward flow of sub-saturated fluids. The seismic data reveal that the free gas zone beneath the BSR is of variable thickness across the basin, and cannot be explained by rapid hydrate recycling only. For example, there are two thick low velocity zones which is similar to Hydrate Ridge where hydrate recycling is rapid and fluids migrating from depth and are rich in methane (Suess et al., 1999) exceeding saturation. Thus, we proposed that hydrate recycling, combined with deeply sourced methane-rich fluids and low fluid flow velocity would explain the thick gas zone beneath the BGHS.

7.1.2.3 Focused Fluid Flow along Faults, and Fluid Escape Structures

Faults and facture networks can either act as a barrier to fluid flow when sealed or as an escape route for gas to bypass into, and even through, the GHSZ. Whether or not a fault behaves as a seal or migration pathway depends on the stress state, host lithology, and chemical processes related to water rock interactions and hydrate formation (Caine et al., 1996;; Davies, 2003; Madrussani et al., 2010). As discussed in Chapter Six, the BSR behavior and reflection strength surrounding faults can illuminate whether a fault is active and can further help to pinpoint focused fluid flow pathways.

Faults were not observed to significantly offset the primary BSR, and very few of the deep cutting normal faults were associated with reduced BSR amplitude strength which could be interpreted as a lack of gas from gas escape, or a lack of GH accumulation as a result of active fluid advection. These particular faults occur within the seaward half of the basin, offset the seafloor, and were proposed by Moore et al., (2013) to be active. The heat flow data surrounding these faults are not abnormally high, nor is there any shoaling of the BSR in vicinity of these faults. So if indeed they are functioning as active conduits for fluids from depth, the flow velocity must be very low. It is more likely that these faults acted as a gas escape pathway

in the recent past in response to episodic seismic events. Further, fluid advection is also known to alternate between diffuse and focused flow over time depending on changes in the stress field (Saffer and Screaton, 2003; Solomon et al., 2009; Yamada et al., 2014). Hammerschmidt et al.'s (2014) analysis of drilling mud gas samples for ^{222}RN along with helium (He) concentration and He isotope ratios supports the notion of episodic fluid flow in the Kumano Basin. Their research found a strong contribution of primordial helium in the upper part of the accretionary prism, but fluid flow velocities too low to support the elevated gas concentrations, and thus they concluded that fluid migration in the upper part of the accretionary prism, which would be transferred to the overlying sediment column, is episodic. Barnes (2013) proposed that faults in the Kumano Basin act as a seal as a result of shearing clay particles and thus the preferential fluid flow pathway would be up permeable, dipping strata layers. We cannot fully disprove Barnes' hypothesis, we would like to add that as found at Woosley Mound in the Gulf of Mexico (Simonetti et al., 2013; Macelloni et al., 2015) hydrates formed during periods of active fluid advection, rather than sheared clay particles, could be acting as a temporary fault seals (e.g., Wood et al., 2002). As such, faults can dually act as gas migration pathways and gas hydrate reservoirs (Fig. 7.7). To test these ideas regarding the roles of faults in the basin we turn our attention to the seismic data.

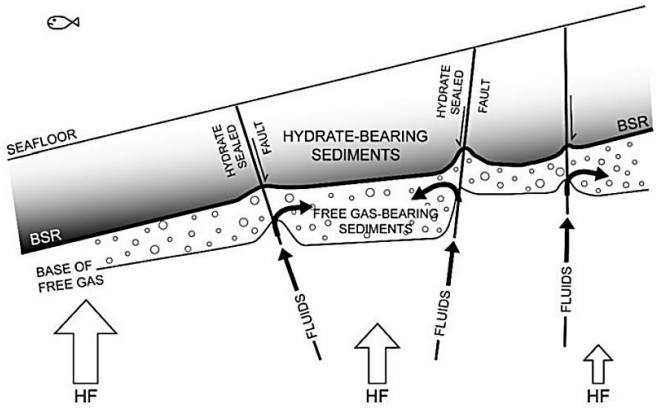

Figure 7.7: Figure from Madrussani et al., 2010. Schematic cross-section illustrating inferred relationship between upward fluid migration, gas hydrate stability and faults. Faults act as a pathway deeper in the sediments, and become barriers to fluid flow within the hydrate stability zone.

The seismic velocity data show the LVZ-1 spilling over above the BSR into the central region associated with numerous faults and fractures. This region correlates to high heat flow zone 1 (Fig. 6.6). The low velocity signature of gas piles up in the updip direction against the normal faults and is capped by positive crosscutting reflections in the amplitude volume interpreted to be the top of hydrate concentration zones. Thus, it appears that pockets of free gas and gas hydrate co-exist above the BSR. Miyakawa et al. (2014) also reported the co-occurrence of free gas and GH in the Kumano Basin evidenced by drilling data. We propose that normal fault activity fractured GH bearing sediments and initially act as a migration pathway for free gas into the stability zone which, in addition to the thick free gas zone below, facilitates the precipitation of concentrated GH deposits and GH sealed faults. Hydrate filled fracture networks have been found in numerous sites around the world including in the GoM (Cook et al., 2008; Cook et al., 2014), in the KG Basin offshore India (Collett et al., 2007; Riedel et al., 2010), and at Hydrate Ridge (Weinberger and Brown, 2006).The association of basement topographic highs with fault-controlled fluid flow potentially delivering basement sourced fluids as observed in these seismic data, is a pattern also observed in the hydrate bearing region of the Makran accretionary margin (Smith et al., 2014).

While there is no drilling data to directly support hydrate sealed faults in the Kumano Basin, from the HCZ and free gas related HAR distribution patterns in the seismic data, we can clearly see that the fault geometry acts to compartmentalize gas hydrate and free gas reservoirs. Thus given all lines of evidence from combined drilling and seismic analyses we infer that the deep cutting normal faults dually act as migration pathways and hydrate reservoirs, and teeter between these roles depending on the stress state and corresponding fluid advection in the basin. Regions where the BSR amplitudes are presently reduced across faults likely indicate a recently active pathway that has not yet been replenished with an accumulation of free gas below necessary for producing a BSR event.

Submarine fluid vents including pipes, chimneys, and mud volcanoes (MVs) (see Cartwright and Santamarina, 2015 for a comprehensive summary of fluid escape expressions in seismic

data) are the product of overpressured pore fluid conditions, and are another mechanism by which a substantial amount of natural gas can be released into the GHSZ within marine sediments and into the overlying water column. Kopf (2002) reports that methane in the presence of aqueous fluids acts as the strongest agent driving overpressures, liquefication, and mud extrusion/eruption. Ray et al.'s geochemical and mineralogical investigation of MVs along the Andaman accretionary prism (2013) demonstrated that mud volcanism is an important mechanism for hydrocarbon rich fluid and gas migration in forearcs, and may even be linked to the décollement. Similar to focused fluid advection up deep cutting faults, major expulsion events are closely tied to seismic activity (Chaudhuri et al., 2011; Tsunogai, et al., 2012) and compression (Milkov, 2000).

No seafloor pockmarks are observed in existing bathymetry data taken over the survey region, and very little seismic evidence for active seeps or fluid escape structures, with the exception of a single MV at the seaward edge that breaks through the seafloor with a conical shaped dome. Pipe features (e.g., Yoo et al., 2013; Riboulot et al., 2013; Cartwright and Santamarina, 2015) are not prevalent; however, a few do exist, and most of these are buried/do not breach the seafloor. One pipe feature was found connected to the toe of a surface landslide which is consistent with the pressure gradient being highest at the toe of the slope (Dugan and Flemings, 2000; Riboulot et al., 2013). This pipe feature also corresponds to high heat flow zone 5b (Fig. 6.11). Regarding the single MV, the seismic data expresses hummocky reflections inferred to be the centralized vent, and the BSR does shoal upward, and is truncated as it approaches this vent feature. Together these traits suggest active or very recently active fluid expulsion which prevents hydrate formation and gas accumulation in the vent region. The shoaling of the BSR indicates elevated heat flow surrounding the vent. The occurrence of HARS branching away from the vent suggests that gas has escaped laterally into basin sediments within the GHSZ at weak points along this vent (Fig. 6.14, high heat flow zone 6b). Because these HARs occur well within the GHSZ, we deduce that these seismic features represent hydrate-bearing sediments.

Fluids from twelve analogous mud volcanoes within the Kumano basin further landward were recently sampled and analyzed for hydrocarbon origins (Pape et al., 2014). Gas hydrates were recovered from MVs 2, 4, 5, and 10 and of these, MVs 2, 4, and 10 showed molecular C^1/C^2 ratios >250 and stable carbon isotopic composition $\delta^{13}C$ of methane >-40‰ V-PDB which together are diagnostic of hydrate-bound thermogenic methane originating from between 2300 and 4300 mbsf corresponding to Cretaceous to Tertiary Shimanto belt below the Pliocene/Pleistocene to recent basin sediments (Pape et al., 2014). Interestingly in 2004, coseismic massive methane release was detected at Kumano Knoll 5 following a large M_w 7.5 earthquake (Miyazaki et al., 2009; Tsunogai et al., 2012). Kuramoto et al. (2001) suggested that the origins of seven MVs in the Kumano basin are linked to thrust activity beneath the forearc basin, while five of the seven MVs investigated by "Shinkai 6500" dives were found to be in different stages of fluid venting (Kuramoto et al., 2001).

From the seismic data, the MV in our study region appears to be deeply rooted. Considering the seismic character of the BSR, the hummocky reflections across the vent, the elevated BSR-derived heat flow surrounding this feature, and analogous mud volcano venting in the basin, we propose that this seep is active or recently active and that the clustering of strong HARs extruding latterly from the vent are likely the product of gas hydrates hosting laterally extruded thermogenic gas molecules. Sampling and geochemical analyses would need to be conducted in order to ground-truth this hypothesis. But regardless, by virtue of being a deep seated mud volcano that breaches the seafloor, we know that fluid expulsion from depth has occurred in the recent past.

7.1.2.4 Fluid Flow Obstruction: MTDs

Unlike Yang et al.'s study (2013) where MTDs were associated with facilitating gas migration, MTDs in our seismic data appear to impede gas migration and hydrate recycling near the BSR (Fig. 75). The stacked HARs beneath the BSR which is overlain by an MTD could be

reflecting overpressure conditions which would imply that the MTD is acting as a barrier to fluid flow.

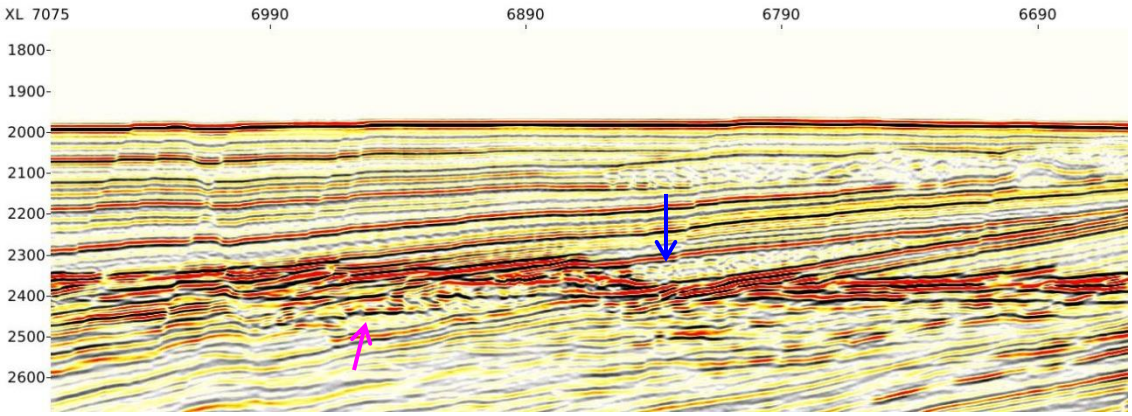

Figure 75: IL2471 MTD appears to suppress gas hydrate recycling. Less HARs above the BSR where the overlying MTD exists (blue arrow) and deeper lower BSRs corresponding to the same unit (pink arrow).

7.1.3 Trapping Mechanisms

The structural and stratigraphic controls on the sub-surface distribution of free gas and gas hydrate is evidenced by the complex distribution of BSRs, variable BSR amplitude strengths and the presence of localized high amplitude reflections both above and below the GHSZ .

7.1.3.1 Gas Traps

Bright spots, a typical seismic signature of the base of a fluid-charged reservoir (e.g., ligtenberg, 2005), are found in the anticlinal-shaped folded sediments, within the syncline between the anticlines, along titled strata, and within filled erosional features beneath the GHSZ. Gas-charged fluids are at least partially confined in stratigraphic traps under the cap of the anticlinal-shaped accreted sediments and within the intercalated synclinal-shaped sediments which corresponds to the ponded slope basins in the early stages of prism growth (Ramirez et al., 2015). Enhanced HARs below the BSR in the seaward half of the basin are concentrated in the tilted sedimentary layers of the gas charged Zone B at C0009. These HARs are interpreted to be the signature of free gas concentrated in erosional features, infilled with

coarse clastic sediments (Fig. 7.9). Similar seismic features were found associated with the Hikurangi Channel (Plaza-Faverola et al., 2012). The gas source, as discussed above, is from the biodegradation of organic material from the thick lower basin sediments and gas from within the accretionary prism that has traveled up deep seated normal faults.

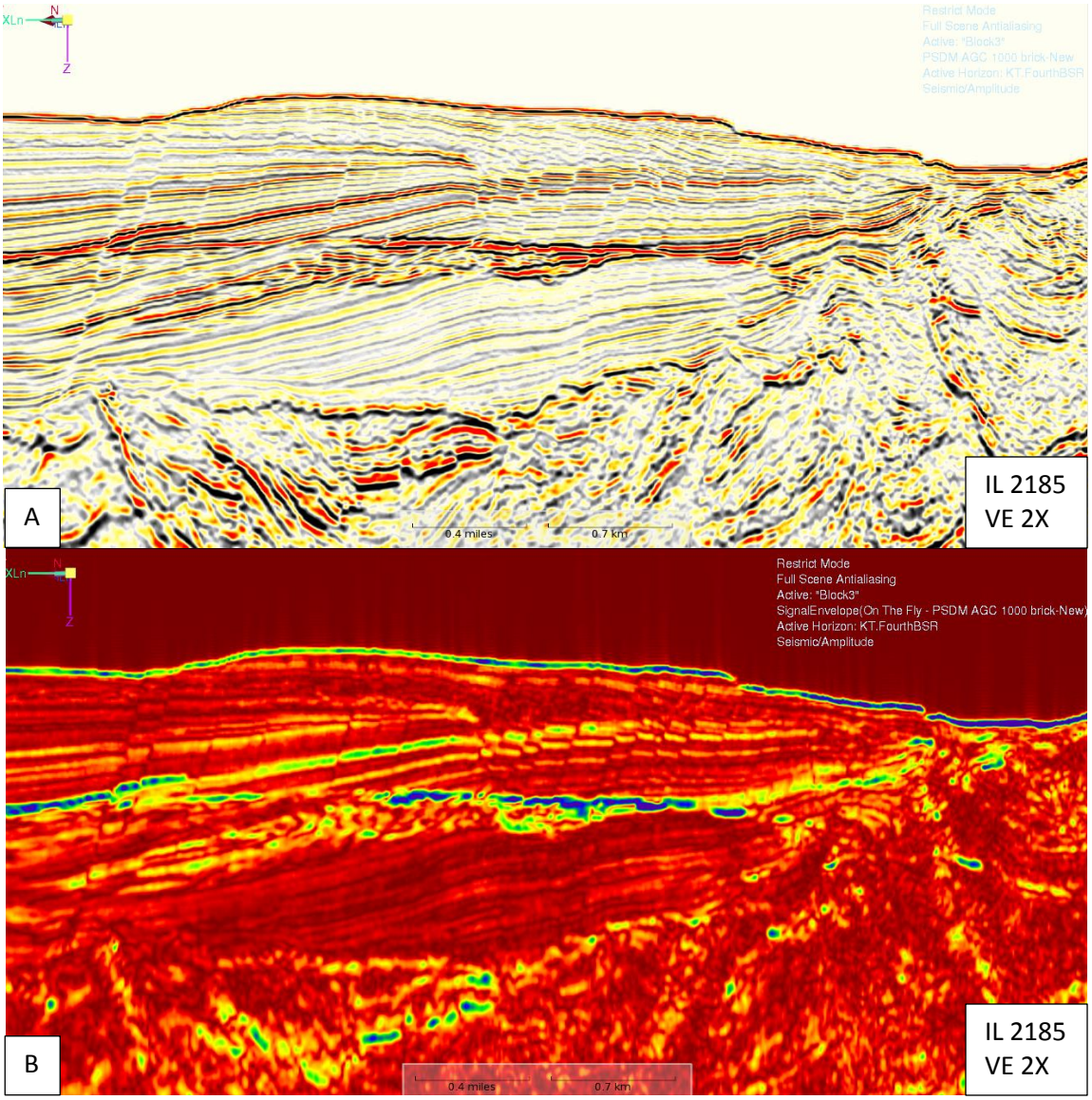

Figure 7.9 - (A) Seismic amplitude display of inline 2185. Shown is the main BSR with negative polarity, the DBSR with positive polarity, and a large low-reflectivity shadow zone. High-amplitude reflections above and below the BSRs are interpreted to be gas and hydrate. Tilted strata related to accretionary tectonics and deep-cutting normal faults may serve as conduits for thermogenic gas migration. (B) Signal envelope display of inline 2185. Display clearly draws out changes in physical properties. High values below the BSR are likely to correspond to gas migrating from depth, updip. Gas fractionation may result in sII hydrate BGHS 70 m below the main BSR. High signal envelope values above the BSR are interpreted as a zone of high gas hydrate concentration. Note the phase change in dipping strata across the BSR.

Many of the stratigraphic horizons below the BSR are enhanced with bright reflections that weaken or terminate at the base of the BSR. This feature can be explained as a change in physical properties at the BSR interface where free gas below the hydrate stability field undergoes a phase change into hydrates within the stability field (Bangs et al., 2005; Boswell et al., 2014). High amplitude reflections that traverse the BSR reverse in phase from a strong positive character in the hydrate stability zone to a strong negative event in the free gas zone. The hydrates act as a seal trapping the free gas below. Further, toward the seaward edge there is a significant reduction in acoustic reflectivity between the BSR and the accretionary prism boundary. This reduced reflectivity could be from diffuse gas accumulation within muds (e.g., Boswell et al., 2012.)

7.1.3.2 Hydrate Traps and Reservoirs

The trapping mechanism for gas hydrates depends on the host sediments and the target hydrate morphology. Dai et al. (2012) demonstrates that pore filling hydrates will form in coarse sand to coarse silt at high effective stress, while nodules form in fine grained sediments at low effective stress. Lenses or veins will form in the direction of the lowest effective stress under intermediate conditions, and disseminated hydrates with low pore space occupancy volume are widespread in fine-grained sediment. There are numerous examples where concentrated GHs have been found in association with submarine mud volcanoes (Reed et al., 1990; Milkov, A.V., 2000; Ben-Avraham et al., 2002; Mazurenko et al., 2003; Ben-Avraham et al., 2005;). It has been proposed that compensation troughs (synclines) surrounding mud volcanoes are proximal weak zones where gas from the upward expulsion can migrate laterally into the hydrate stability zone, and thus the maximum concentration of hydrates in association with MVs is found in compensation troughs (Shnyukov, 2013). Other potential hydrate reservoirs include MTDs (Yang et al., 2013) and fault/facture networks such as was found in the KG Basin (Collett et al., 2015). Hydrate deposits associated with active faults, fracture, mud volcanoes and cold seeps have been found to occupy 50% of the available pore space (e.g., Milkov and Sassen, 2002; Stoian et al., 2008). In terms of energy exploration, the prime GH

reservoir target is turbidite or channel sands with high porosity and high permeability which are likely to host pore-filling hydrates (Fig. 77) (Boswell et al., 2009; Rose et al., 2014). The logging data, pore water data, and soupy structures in sediment cores collected at Sites C0002 and C0009 have shown that both pore-filling GH in sand layers and disseminated GH in muds are present in the basin. Here we take look closer at the seismic data for a more regional assessment and identify the most highly prospective GH reservoirs.

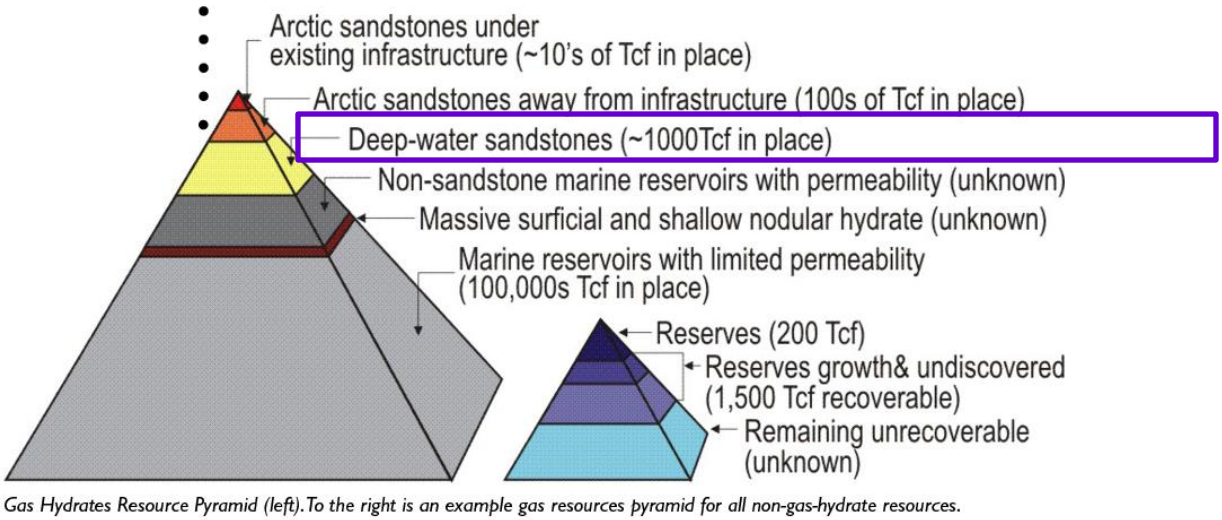

Figure 7.10 - The Gas Hydrates Resource Pyramid from Boswell and Collett FITI Fall 2006. Note largest reservoirs are confined to in fine grained sediments with low permeability, but target resource reservoirs are deep-water sandstones (purple box).

Borehole results from other margin studies have shown that in sand-rich systems, seismic blanking within the GHSZ is characteristic of the reduction of pore space due to low to modest gas hydrate saturation, while modest to high gas hydrate saturation will lead to strong positive amplitudes (Boswell et al., 2011; Shelander et al.,2012; Fohrmann et al. 2012). Both types of seismic responses are observed within the GHSZ in this study. Holbrook et al., 1996 noted that zones of acoustic blanking within the GHSZ, if not associated with homogeneous facies, are likely the product of low gas hydrate saturations. An extended package of tilted, low amplitude reflections in the seaward half of the basin could be interpreted as homogeneous

sediments, but we know most certainly from the cores collected from Site C0002 that this seismic package comprises alternating sands and muds, and therefore is not at all lithologically homogeneous. Soupy structures were found in both sands and fines (Table 3) suggesting that both pore filling and disseminated hydrates are present. Frequent, moderate resistivity spikes above the BSR correlate to this unit and enhanced seismic reflections below the BSR in association the upper blanking suggests the presence of gas. We infer that this unit hosts gas hydrates in low to moderate saturations, but it is not a resource target. The most prospective targets are gas hydrate concentration zones within sand units which will appear as a strong amplitude response with a positive event at the top of the concentration zone.

Drilling in the Eastern Nankai Trough (Saeki et al., 2008) has confirmed that high gas hydrate concentrations are indeed associated with strong, high amplitude reflections within the GHSZ. MHCZs are characterized by high resistivity in well logs; strong normal polarity, unconformable seismic reflection; high seismic velocity; and tend to occur in permeable turbidite deposits or immediately above the BSR which is a favorable zone for production because it is one region where hydrates are most vulnerable to perturbations. They can further be identified using sedimentary facies analysis or by coring (Yuan et al., 1996; Fujii et al., 2008; Plaza-Faverola et al., 2012; Yoo et al., 2013). The formation of such GHCZ requires large volumes of natural gas. The two primary mechanisms by which sufficient gas can accumulate in the GHSZ to support GHCZs are by upward fluid migration via inter-granular porosity or faults, or by hydrate recycling (e.g., Kvenvolden, 1993; Paull et al., 1994; Haacke et al., 2007; Yamada et al., 2014) both of which were previously discussed and demonstrated to exist this study region. Further, several studies have shown that a FGZ beneath the BGHS, also present in this study region, provides replenishment to support hydrate formation (Haacke et al., 2007; Lui and Flemings, 2007; Haacke et al., 2009; Plaza-Faverola et al., 2012). Most of the methane hydrates found in the eastern Nankai Trough were confined to turbidite sand reservoirs (Takano et al., 2010; Noguchi et al., 2011) with channel-fill and sheet-like turbidite sequences determined to be the best reservoir facies based on hydrate content (Ito et al., 2015). Recent studies on the hydro-bio-geomechanic properties of hydrate bearing sediments collected in the

eastern Nankai Trough using Pressure Core Characterization Tools (PCCTs) found that hydrate saturation ranged from 0.15-0.74 with a significant concentration in silty-sands (Santamarina et al., 2015), and Fujii et al. (2005, 2009b.) reported massive hydrate occurrence in mud co-accompanied by a mixture of biogenic and thermogenic gas at two METI exploratory test well. Similarly, the Kumano Basin data provides evidence of a complex hydrate system in terms of hydrate distribution and varied saturations.

From the drilling data, we know that hydrate-bearing sediments (traps) are turbidite sands which includes a >3 m thick sand layer hosting the highest concentration of gas hydrates directly above the BSR at about 386 mbsf (Strasser et al., 2014). Previous studies analyzing ring resistivity, bit resistivity, and P-wave velocity data from Site C0002 estimated high gas hydrate saturations (>60%) in sandy layers with the presence of free gas identified at several depths (Miyakawa et.al., 2014). These thick sand beds within the GHSZ are potential GH reservoir targets (Fig. 7.11). For the purpose of our first order resource estimate, we will focus on the GHCZ connected to the BSR rather than hydrate-bearing sand layers shallower within the GHSZ.

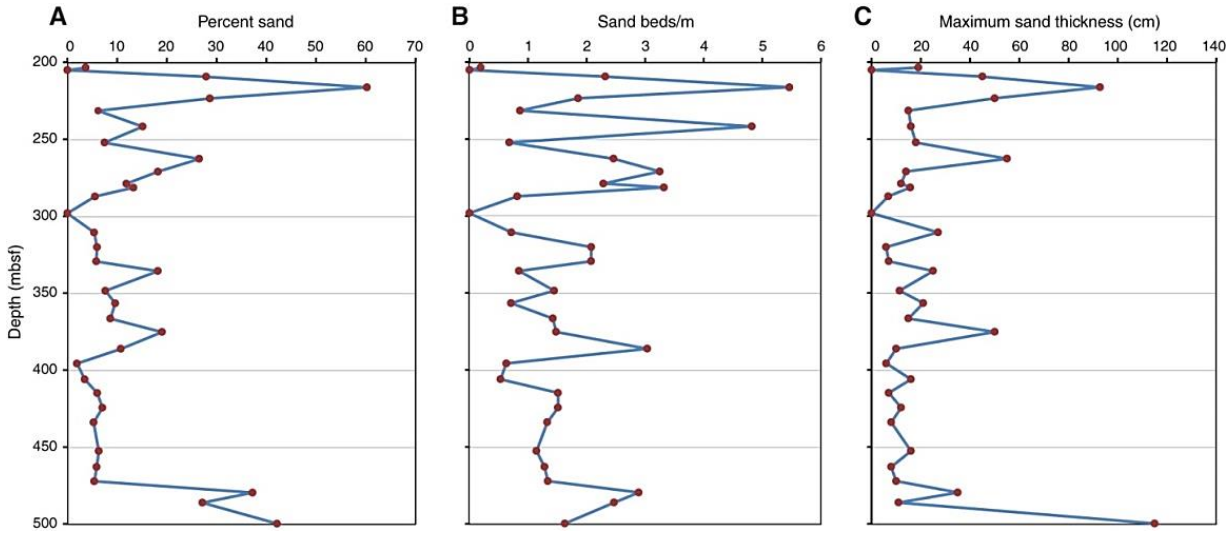

Figure 7.11- Sand occurrences (potential hydrate reservoirs) in Holes C0002K and C0002L with average calculated values plotted. Methane peaks plotted (30, 270), Ethane peak (390-400), Propane peaks (200, 380) Resistivity peaks (270, 295, 370, 390).

7.2 Gas in Place Resource Estimate for the Hydrate Concentration Zones

Extensive resource assessments of MHCZs in the Nankai Trough as part of the 16-year MH exploration program was initiated following the 1999 exploratory wells funded by the Ministry of International Trade and Industry (MITI) (Nakamizu et al., 2004). These exploratory wells located in the eastern Nankai Trough (~100 km northeast of Site C0002) drilled into MH-bearing sand-rich intervals in turbidite fan deposits (Uchida et al, 2004; Fuji et al., 2008), and found MHCZs tens of meters thick occurring immediately above the BSR which were characterized by strong, high amplitude seismic reflections (Fujii et al., 2008; Saeki et al., 2008; Noguchi et al., 2011) (Fig. 79). Following exploration efforts, a depressurization production trial headed by JOGMEC was conducted from March 12th to March 18th, 2013 using the Japanese riser equipped drilling vessel D/V Chikyu. Approximately 120,000 m^3 of methane was produced from the north slope of Dani Atsumi Knoll over the course of the six day trial (Boswell, 2013). The 3D seismic data used for this study provide evidence for two analogous MHCZ. Here we provide the first detailed analysis of MHCZs within our survey region including the 3D extent, gross volume, and gas-in-place estimate.

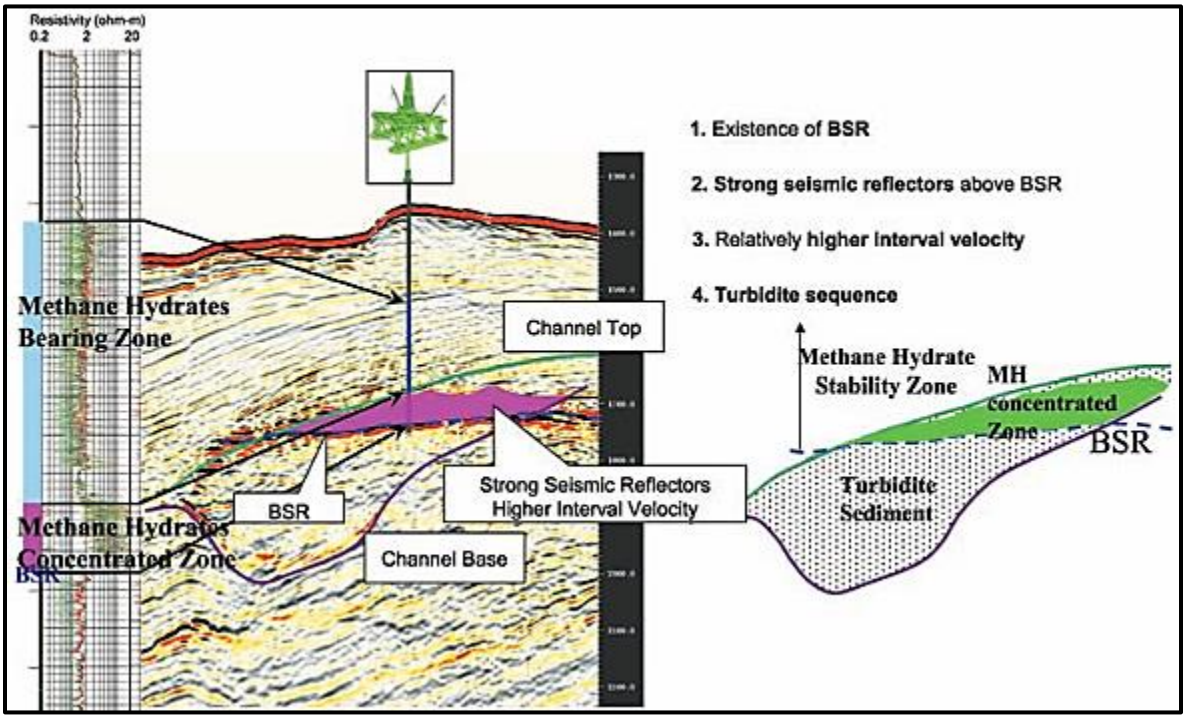

Figure: 79 Example of a resistivity log, seismic line, and sedimentary facies analysis of a confirmed methane hydrate concentration zone in the eastern Nankai Trough. Figure from Saeki et al., 2009; Noguchi et al., 2009.

We define the bottom of the HCZ as the primary BSR. The upper boundary is defined as high amplitude, normal polarity, crosscutting reflections above the BSR. Many of these upper

boundaries terminate against the abundant deep cutting normal faults segmenting the hydrate reservoir lateral continuity with maximum continuity running parallel to the trench. NGH deposits were similarly found to be closely related to large scale structural features in the Ulleung Basin (Yoo et al., 2013), the Gulf of Mexico (Cook et al., 2008; Simonetti et al., 2013) and the KG Basin offshore India (Collett et al., 2015).

The principal MHCZ corresponds to a thick sand unit above the BSR in the center of the basin in association with an intricate fault network and an underlying topographic high in the accretionary prism (High HF Zone 1). A second MHCZ is identified in permeable dipping strata above the BSR toward the seaward edge of the basin near the outer arc high where heat flow was found to be anomalously low as a result of BSR perturbation (Low HF Zone 4 & 6). The significant deepening of the BSR would have resulted in the incorporation of free gas previously beneath the BSR and gas hydrate patches above the BSR into one, continuous layer (Villar-Munox, L. et al., 2014).

Hornbach et al. (2013) proposed that regions of higher BSR-derived heat flow directly correlates to zone of elevated hydrate occurrence because the advection of gas rich fluids associated with warmer temperatures charge the GHSZ with a source of gas. They further went on to say that elevated BSR-derived heat flow could be used in the exploration stage to identify hydrate reservoir targets. Our analysis of the GHCZs in the Kumano Basin clearly demonstrates that Hornbach et al.'s model is far too simplistic. While the GHCZ does correlate with elevated heat flow in the center of the basin, there are regions of high BSR-derived heat flow with no indication of corresponding gas hydrate occurrence, but rather are related to recent erosion at the seafloor, and there is evidence for GHCZs associated with zones of low heat flow. Thus we urge caution in using heat flow analyses as a primary exploration tool for GHCZs.

7.2.1 Estimated Gas in Place Using a Volumetric Method

This resource estimate provides a first order gas in place probability estimate for the hydrate concentration zones above the BSR only. Methane hydrate bearing zones within the

GHOZ are not considered. For consistency, we employ the resource assessment method commissioned by JOGMEC:

$$GIP = GRV * N/G * \phi * MH_{sh} * VR * CO$$

Whereby: GIP- gas in place, GRV - gross rock volume determined by seismic mapping of hydrate concentration zone over the BSR, N/G – Net to gross ratio of sand given as a fraction of 1, ϕ – Porosity, MH_{sh} – % of pore volume occupied by hydrate; VR – Volume Ratio at 0°C, 1 atm., CO – Cage Occupancy.

The gross rock volume was determined by extracting volumetric information from a top and bottom boundary (BSR) picked in the seismic amplitude volume. These two boundaries serve to enclose the methane hydrate concentration zones. Net to gross ratio is the assumed sand to clay ratio within this package based on core data at C0002 and is in favored towards producing a conservative resource estimate. The Net to Gross could range up to 100 percent if the entire rock volume was sand, thus there is room for significant error depending on this varible. Porosity and MH_{sh} are based on shipboard MAD measurements for a sand rich interval at the depth of the BSR (400 mbsf) at Site C0002 during Expedition 338. The porosity value used here is 50% but shipboard data shows that it could range from 40-60%. Post cruise hydrate saturation estimates at the BSR were determined by Miyakawa et al., (2014) and we are confident in the accuracy of this value. However, there could be errors with extrapolating MHsh from C0002 to the center of the basin. Void ratio assumes a pore-filling hydrate model. Cage occupancy is set at a minimum of 0.90, mode of 0.96 a maximum, 1.0 based on observations from recovered natural gas hydrates collected in cores around the world.

Table 6 - Volumetric assessment of gas in place locked up in the hydrate concentrated zones.

MH Resource Assessment Kumano Basin MH Concentrated Zones						
Parameters						Methane in Place (MMcf)
GRV (MMcf)	N/G (frac.)	Φ (frac.)	MH_{sh} (frac.)	VR (STP)	CO (frac.)	
955,940	0.38	0.50	0.60	164	0.90	16,085,028.82
					0.96	17,157,364.07
					1.0	17,872,254.24

1 billion cubic feet is equivalent to 1.027 trillion Btu. Thus, at the low end of our estimate of 16,085,028.82 MMcf., the gas hydrate concentration zones in the Kumano Basin hosts ~16 trillion Btu of natural gas, or approximately 3.135 million barrels of oil equivalent (BP Statistical Review, 2015). . To put this in perspective, as of March 2015, Japan's import cost for natural gas was $8/mmBTU (METI) thus this reservoir is worth ~132 million dollars. The implications are that these HCZ deposits are a highly prospective target. However, these reservoirs are clearly heterogeneous and zones of high hydrate concentrations are laterally segmented by normal faults, but are continuous for long distances along strike parallel to the trench. Multiple production wells would need to be drilled in order to fully exploit these HCZ. Laboratory trials have shown that gas hydrate reservoirs with an underlying free gas, high gas saturation and low water saturation as observed in this study, are the most suitable for recovery via CH_4-CO_2 exchange using liquefied CO_2 (Yuan et al., 2012). Further, the CO_2 swap could help to maintain sediment mechanical strength while reducing the volume of co-produced water and sands (Hyodo et al., 2014) which together proved to be problematic during the Japanese production trial of 2013.

Chapter 8

Conclusion & Summary of Significant Findings

"It was easier to know it than to explain why I know it." –Sherlock Holmes

A Study in Scarlet, Sir Arthur Colan Doyle

By integrating results from 3D seismic mapping and seismic attribute analyses supported by drilling data collected at Sites C0002 (Kinoshita et al., 2009; Strasser et al., 2014) and C0009 (Saffer et al., 2010), this study provides a basin-scale analysis of a NGH system using a petroleum system approach. The significant findings from this study are:

- BSR analysis of upper, primary, and lower BSRs provided a window into the basin's heat flow structure and the complicated interplay between surface sedimentation and underlying deformation processes exert on the depths of the BGHS. Upper BSRs are believed to mark paleo-BGHZs and the top of hydrate concentrated zones. Lower BSRs may also mark paleo-BGHZs, but BGHS modeling provides compelling evidence that LBSRs are a sII methane-ethane BGHS beneath a sI methane boundary

- Seismic attribute analysis was used to identify proxies for gas beneath the BGHS which allowed us to infer the fluid flow pathways and mechanisms in the basin. Gas charged fluids migrate into basin sediments from four points connected to anticlinal features in underlying accretionary prism, and then continues to migrate through the sediments as diffuse fluid flow updip permeable sands sandwiched by less permeable clays, or through faults and fractures up to the point of GHS. Active fluid advection is not evidenced by the BSR character which means at present the faults in the HSZ are likely sealed with hydrates.

- Localized regions of free gas (identified by seismic indicators) appear beneath the primary BSR in dipping beds, along anticlinal hinges, within erosional/channel like features.

- 4 large gas clouds exist beneath the HCZs as evidenced in the velocity volume as a low velocity signature and in the amplitude volume as acoustic turbidity.

- Hydrate recycling at the BSR is evidenced by stacked BSR, and appears to be impeded by the presence of overlying MTDs. The process of recycling provides an accumulation of gas that can be incorporated into hydrates during times of BGHS lowering. Thermogenic gas from depth likely mixes with buried biogenic gas at the recycling interval.

- Two highly prospective zones of concentrated hydrates were mapped across the basin.

The implication of these findings significant for hydrate prospecting and resource assessments are that a source of gas charge from depth along with the fluid conduit model of permeable layers may be a prerequisite for forming resource-grade concentrated hydrate deposits. Free gas accumulates and is integrated into hydrates independently from its point of origin (upward fluid migration or gas recycling) and thus the stratigraphic architecture and potential pathways must be a primary consideration. The HCZs identified in this study should be considered highly prospective as they are analogous to the 2013 Japanese production site at Daini Atsumi Knoll.

Appendix

Table 1.1 Ratio of gas molecule diameter with hydrate cavity diameter (from Sloan and Koh, 2007).

Molecule	Guest diameter Å	Structure I		Structure II	
		5^{12}	$5^{12}6^2$	5^{12}	$5^{12}6^4$
N_2	4.10	0.80	0.70	0.82	0.62
CH_4	4.36	0.86	0.74	0.87	0.65
H_2S	4.58	0.90	0.78	0.91	0.69
CO_2	5.12	1.00	0.83	1.02	0.77
C_2H_6	5.50	1.08	0.94	1.10	0.83
C_3H_8	6.28	1.23	1.07	1.25	0.94
i-C_4H_{10}	6.50	1.27	1.11	1.29	0.98
n-C_4H_{10}	7.10	1.39	1.21	1.41	1.07

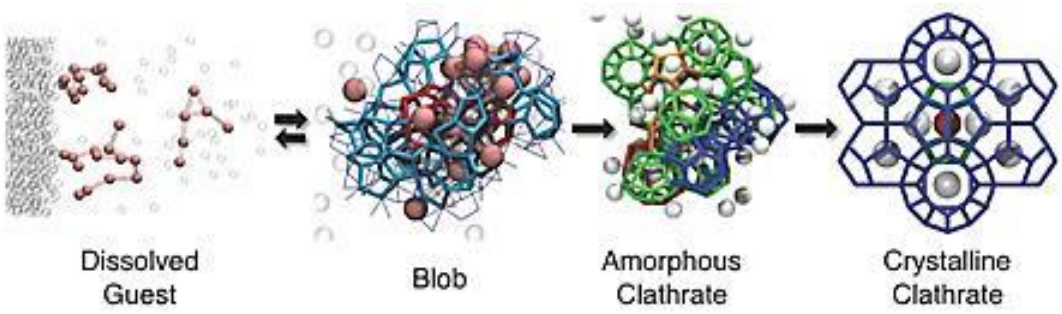

Nucleation and growth of clathrates hydrates from http://www.chem.utah.edu/directory/molinero.php

Conventional gas consumption and reserves in the world in 2012 [44].

Country	Conventional gas consumption (billion cubic meter)	Conventional gas reserve (trillion cubic meter)
US	722.1	8.5
Canada	100.7	2.0
Taiwan	16.3	–
Japan	116.7	–
India	54.6	1.3
China	143.8	3.1
World	3,314.4	187.3

Table 10
Gas hydrate reserves and usage years in major countries.

Country	Gas hydrate (trillion cubic meter)	Usage year
US	9060	12,547
Canada	43.6–809	433–8034
Taiwan	50–230	50–230
Japan	4.7–7.4	40–63
India	1894–14,572	34,689–266,886
China	107.7	749
World	20,000	6034

BP. BP Statistical Review of World Energy June 2013. April 17, 2014.

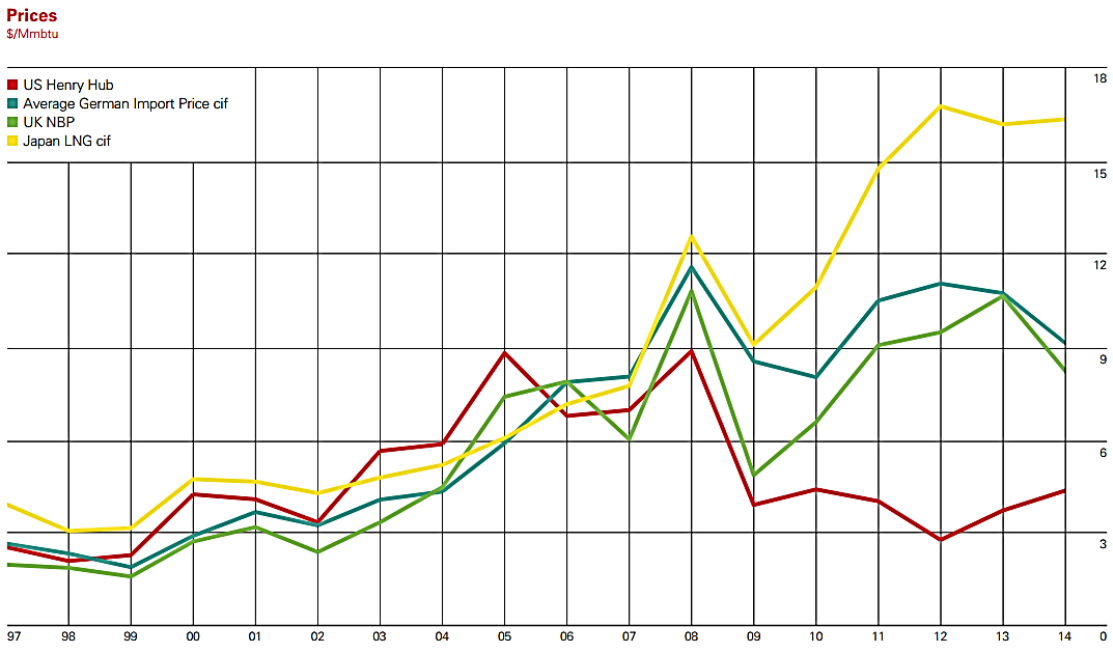

BP Natural Gas Statistical Review June 2015

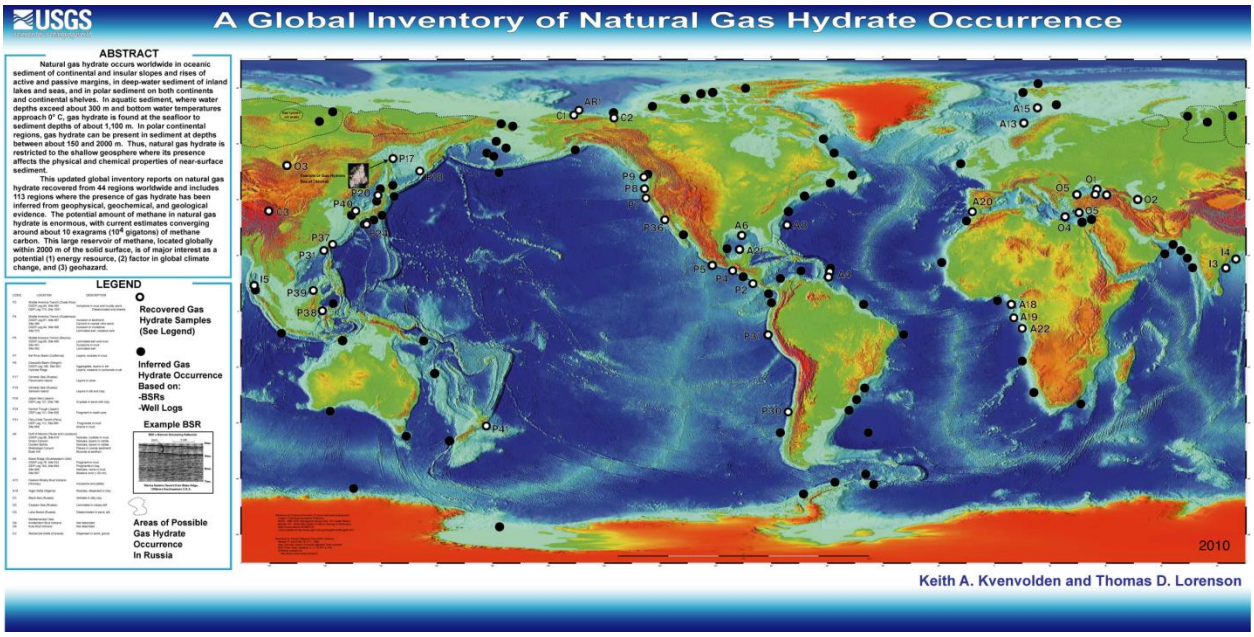

USGS Global Inventory Map

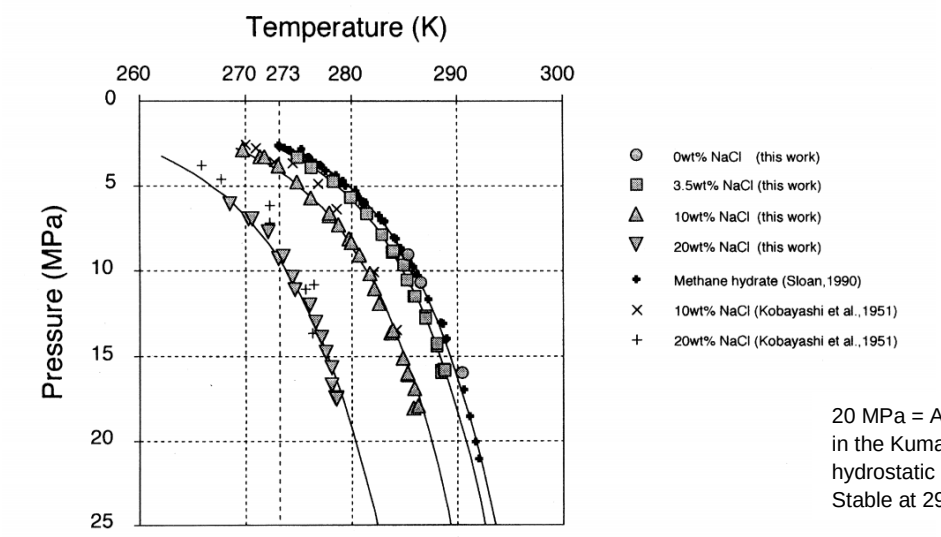

20 MPa = Average pore pressure in the Kumano Basin assuming hydrostatic pressure conditions. Stable at 291 K (blue dot)

Maekawa's Stability Phase Diagram Pressure and temperature conditions for methane hydrate dissociation in sodium chloride solutions. Solid curves are fitted to equation (1) of methane hydrate dissociation conditions for respective concentrations of sodium chloride. From Maekawa et al. 1995. This image shows the difference between the base of hydrate stability in saline water and a pure water system with the depth to the base of saline water shallower than that of a pure water system equal to 20m at 2000m water depths assuming a 50°C/km geothermal gradient and a 1°C seafloor temperature Dissociation pressure of methane hydrate increases and the dissociation temperature decreases as the concentrations of sodium chloride increases.

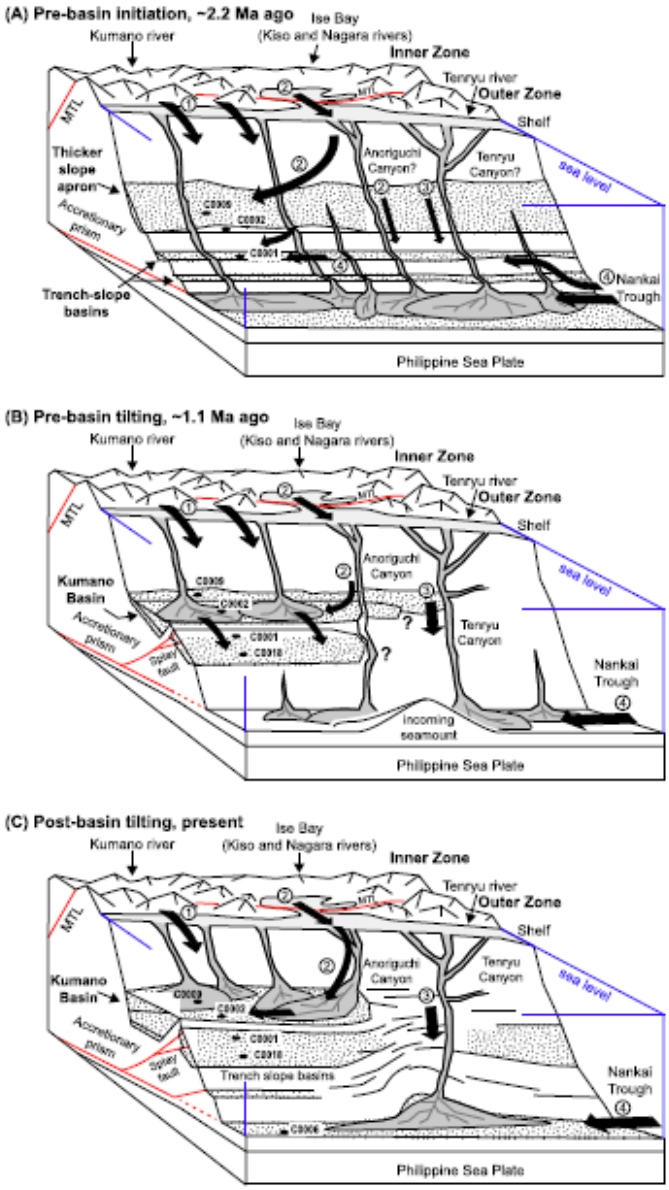

Fig. 8. Summary diagram showing evolution of the Kumano Basin and nearby forearc area from (A) ~0.3 Ma before the basin initiation, to (B) early basin setting, and (C) present. Black arrows show sediment flow patterns determined based on the composition of detrital pyroxenes (1 = Kumano river source, 2 = Inner Zone source, 3 = Tenryu river source, and 4 = Collision Zone source). Important results include recognition of: (i) material from Collision Zone source at site C0001 ~ 2.2 Ma ago, which does not occur at other sampled drill sites during the Quaternary; and (ii) only limited longitudinal transport of sediments in the Kumano Basin, without supply from the Outer Zone further NE of the Ise Bay (e.g., Tenryu river source). MTL = Median Tectonic Line. Full explanation is given under Section 5.

Figure from Buchs et al., 2015

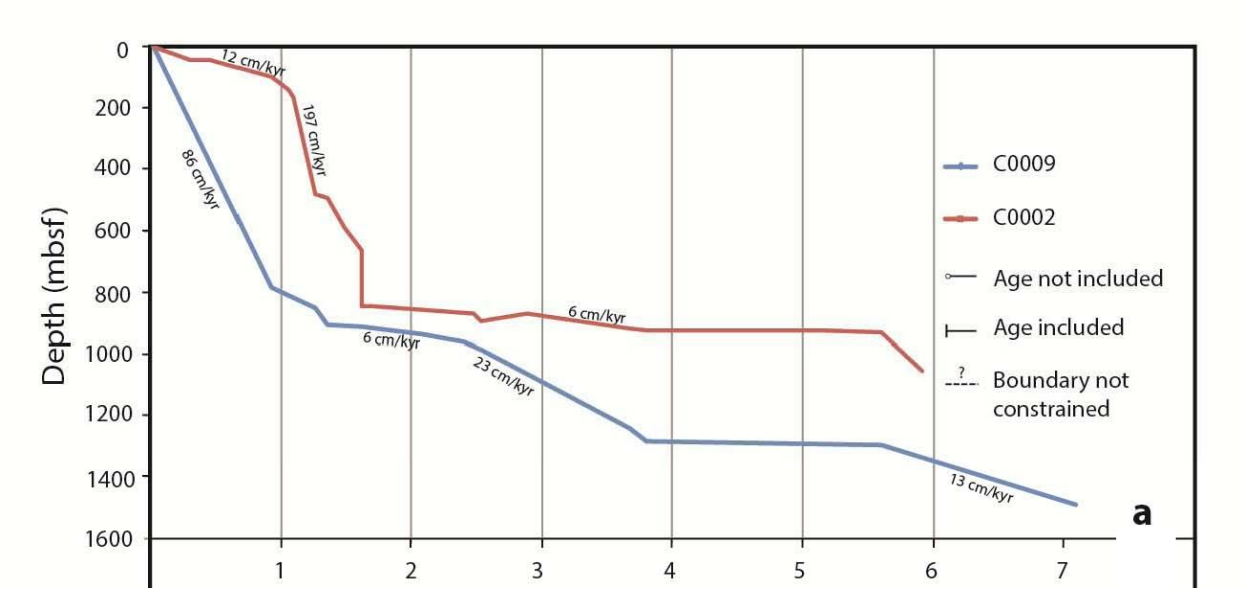

C0002 and C0009 Sedimentation rates

Age Ma

Table 1 Logging units and zones at Site C0002 (Expedition 314 Scientists, 2009). LSF = LWD depth below seafloor

Depth (m LSF)	Logging unit	Zone	Interpreted lithology	Description
0–135.5	I		Unconsolidated sandy/silty mud	Basin sediments
135.5–218.1	II		Hemipelagic	
218.1–400.4		A	Hydrate-bearing zone mud and	
400.4–481.6			silty/sand	
481.6–547.1		B	Potential gas zone turbidites	
547.1–830.4				
830.4–935.6	III		Mudstone	
935.6–total depth	IV		Deformed sand/silty turbidites	Accretionary prism

Age-Depth Relationship. From Saffer et al., 2009

BGHS Modeling

40 C/Km

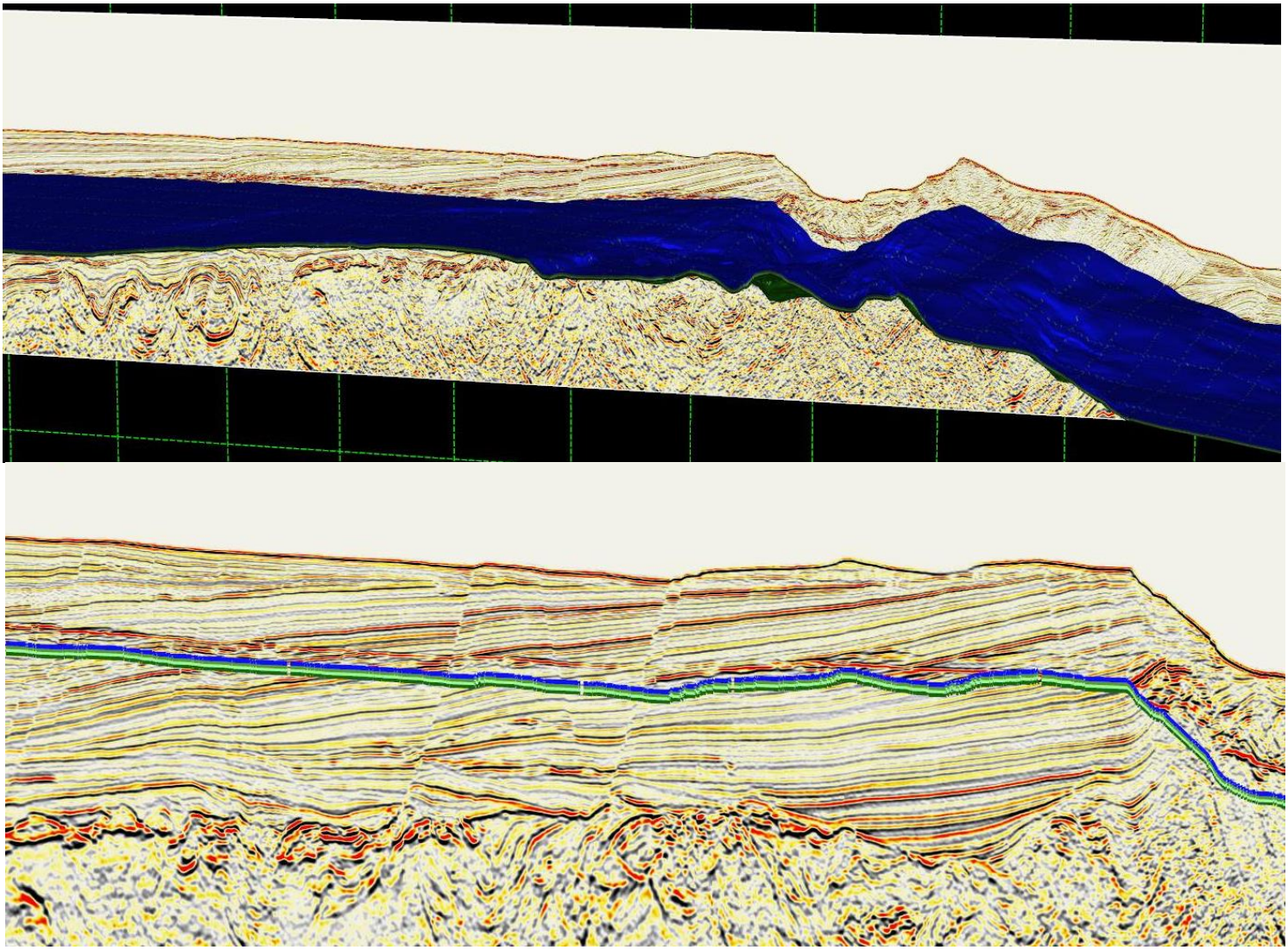

43 C/km

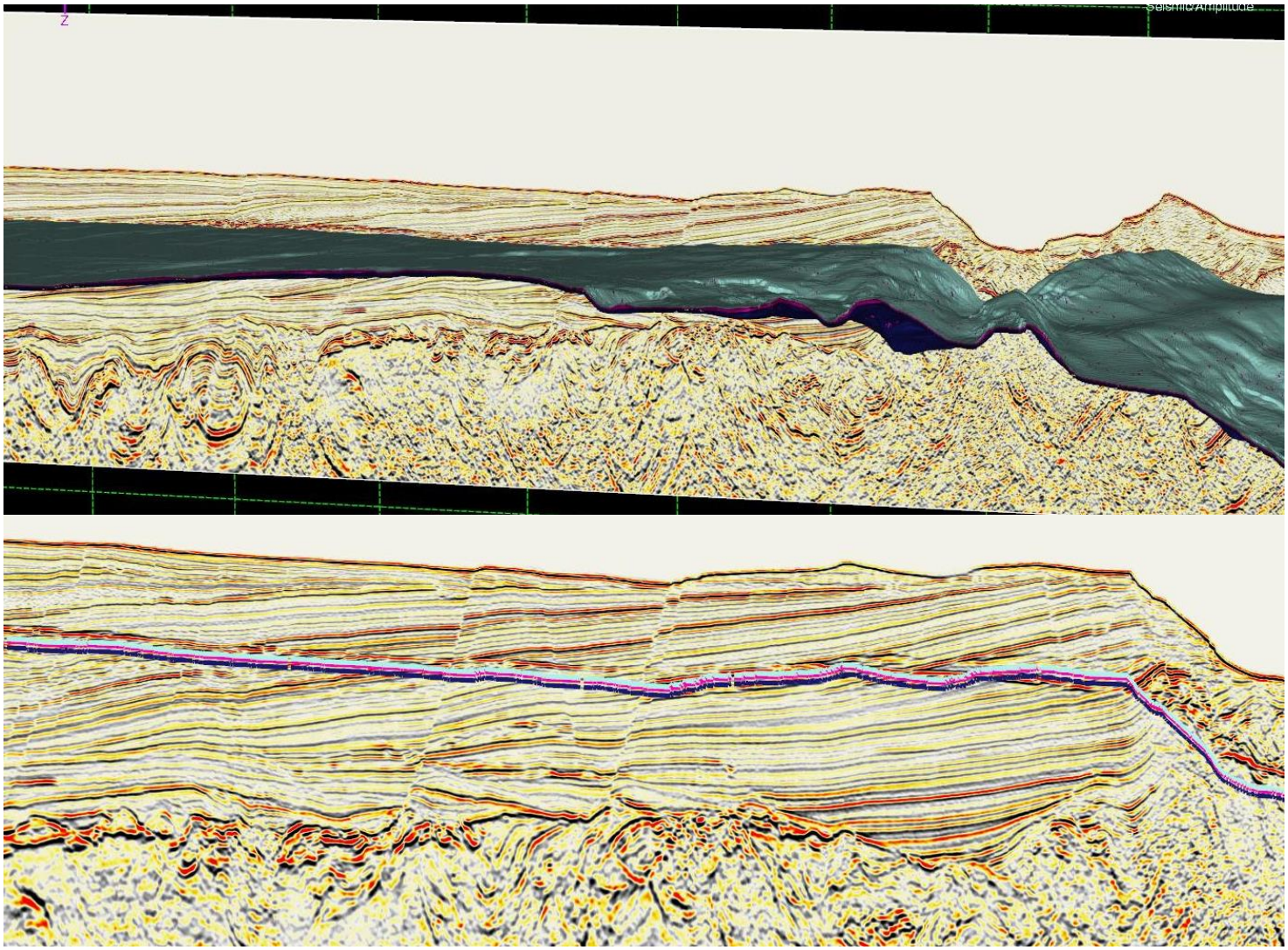

References

Abu-Khader, M.M., 2006. Recent progress in CO_2 capture/sequestration: a review. Energy Sources, Part A: Recovery, Utilization and Environmental Effects 28(14), 1261-1279. doi: 10.1080/009083190933825.

Aloisi, G., Pierre, C., Rouchy, J.-M., Foucher, J.-P., Woodside, J., the MEDINAUT Scientific Party, 2000. Methane-related authigenic carbonates of eastern Mediterranean Sea mud volcanoes and their possible relation to gas hydrate destabilization. *Earth and Planetary Science Letters* 184, 321-338.

Anderson, K., Bhatnagar, G., Crosby, D., Hatton, G., Manfield, P., Kuzmicki, A., Fenwick, N., Pontaza, J., Wicks, M., Socolofsky, S., Brady, C., Svedeman, S., Sum, A.K., Koh, C., Levine, J., Warzinski, R.P., Shaffer, F., 2012. Hydrates in the ocean beneath, around, and above production equipment. Energy & Fuels American Chemical Society, 26, 4167-4176. doi: 10.1021/ef300261z

Anderson, R., Llamedo, M., Tohidi, B., Webber, J.B.W., 2009. Gas hydrate growth and dissociation in narrow pore networks: Capillary inhibition and hysteresis phenomena, *Geology Society Special Publication* 319, 145-159. doi: 10.1144/SP319.12.

Andreassen, K., Hart, P.E., Grantz, A., 1995. Seismic studies of a bottom simulating reflection related to gas hydrate beneath the continental margin of the Beaufort Sea. Journal of Geophysical Research, 100, 12659-12673.

Andreassen, K., Mienert, J., Bryn, P., Singh, S.C., 2000. A Double Gas-Hydrate Related Bottom Simulating Reflector at the Norwegian Continental Margin. GAS HYDRATES: CHALLENGES FOR THE FUTURE. Annals of the New York Academy of Sciences, 912, 126-135. doi: 10.1111/j.1749-6632.2000.tb06766.x.

Ando, M., 1975. Source mechanism and tectonic significance of historical earthquakes along the Nankai Trough, Japan. *Tectonophysics* 27, 119-140.

Antler. G., Turchyn, A. V., Rennie, V., Herut, B., Sivan, O., 2013. Coupled sulfur and oxygen isotope insight into bacterial sulfate reduction in the natural environment. *Geochimica et Cosmochimica Acta* 118, 98-117.

Archer, D., 2007. Methane hydrate stability and anthropogenic climate change. Biogeosciences 4, 521-544.

Archer, D., Buffett, B., Brovkin, V., 2009. Ocean methane hydrates as a slow tipping point in the global carbon cycle. *Proceedings of the National Academy of Sciences* 106(49), 20596-20601.

Ashi, J., Kuramoto, S.i., Morita, S., Tsunogai, U., Goto, S., Kojima, S., Okamoto, T., Ishimura, T., Ijiri, A., Toki, T., Kudo, S., Asai, S., Utsumi, M., 2002 Structure and cold seep of the Nankai accretionary prism off Kumano - Outline of the off Kumano survey during YK01-04 Leg 2 Cruise-. JAMSTEC J. Deep Sea Res. 20.

Ashi, J., Taira, A., 1993. Thermal structure of the Nankai accretionary prism as inferred from the distribution of gas hydrate BSRs, in: Underwood, M.B. (Ed.), Thermal evolution of the Tertiary Shimanto Belt, Southwest Japan: an example of ridge-trench interaction. Spec. Paper.- Geol. Soc. Am., 137-149.

Ashi, J., Tokuyama, H., Taira, A., 2002. Distribution of methane hydrate BSRs and its implication for the prism growth in the Nankai Trough. Marine Geology, 187, 177-191.

Ashi, J., S. Lallemant, H. Masago, and the Expedition 315 Scientists (2009), Expedition 315 summary. In Kinoshita, M., H. Tobin, J. Ashi, G. Kimura, S. Lallemant, E.J. Screaton, D. Curewitz, H. Masago, K.T. Moe , and the Expedition 314/315/316 Scientists, *Proc. IODP*, 314/315/316: Washington, DC (Integrated Ocean Drilling Program Management International, Inc.). doi:10.2204/iodp.proc.314315316.121.2009.

Baba, T., and Cummins, P.R., 2005. Contiguous rupture areas of two Nankai Trough earthquakes revealed by high resolution tsunami waveform inversion. *Geophysical Research Letters* 32, L08305. doi:10.1029/2004GL022320.

Baba, K., Yamada, Y., 2004. BSRs and associated reflections as an indicator of gas hydrate and free gas accumulation: an example of accretionary prism and forearc basin system along the Nankai Trough, off central Japan. Resource Geology 54, 11-24.

Bahk,J.-J., Kim, D.-H., Chun, J.-H., Son, B.-K., Kim, J-H., Ryu, B.-J., Torres, M.E., Riedel, M., Schultheiss, P., 2013. Gas hydrate occurrences and their relation to host sediment properties: Results from Second Ulleung Basin gas hydrate drilling expedition, East Sea. Marine and Petroleum Geology 47, 21-29. doi:10.1016/j.marpetgeo.2013.05.006.

Bahk, J.-J., Kim, G.-Y., Chun, J.-H., Kim, J.-H., Lee, J.Y., Ryu, B.-J., Lee, J.-H., Son, B.-K., 2013b. Characterization of gas hydrate reservoirs by integration of core and log data in the Ulleung Basin, East Sea. *Marine and Petroleum Geology* 47, 30-42.

Bahk, J.-J., Uma, I.-k., Holland, M., 2011. Core lithologies and their constraints on gas-hydrate occurrence in the East Sea, offshore Korea: Results from the site UBGH1-9, *Marine and Petroleum Geology* 28, 1943-1952.

Bahr, A., Pape, T., Abegg, F., Bohrmann, G., Van Weering, T., Ivanov, M.K., 2010. Authigenic carbonates from the eastern Black Sea as an archive for shallow gas hydrate dynamics-Results from combination of CT imaging with mineralogical and stable isotope analyses. *Marine and Petroleum Geology* 27(9), 1819-1829.

Bangs, N.L., Hornbach, M.J., Moore, G.F., Park, J.-O., 2010. Massive methane release triggered by seafloor erosion offshore southwestern Japan. Geology 38, 1019-1022.

Bangs, N.L.B., Musgrave, R.J., Tréhu, A.M., 2005. Upward shifts in the southern Hydrate Ridge gas hydrate stability zone following postglacial warming, offshore Oregon. J. Geophys. Res. 110.

Barnes, J.L., 2013. Fluid flow, gas accumulations and gas hydrate formation in the Kumano Forearc basin determined by seismic reflection interpretation and well data correlation. Thesis submitted to the Graduate Division of the University of Hawaii at Manoa.

Barnes, P.M., Lamarche, G., Bialas, J., Henrys, S., Pecher, I., Netzeband, G.L., Greinert, J., Mountjoy, J.J., Pedley, K., Crutchley, G., 2010. Tectonic and geological framework for gas hydrates and cold seeps on the Hikurangi subduction margin, New Zealand. *Marine Geology* 272(1-4), 26-48.

Ben-Avraham, Z., Reshef, M., Smith, G., 2005. Seismic signature of gas hydrate and mud volcanoes of the South African continental margin. In Martinelli, G., Panahi B. (Eds.), *Mud Volcanoes, Geodynamics and Seismicity*, Springer, 17-27.

Ben-Avraham, Z., Smith, G.,Reshef, M., Jungslager, E., 2002. Gas hydrate and mud volcanoes on the southwest African continental margin off South Africa. Geology 30, 927-930. doi: 10.1130/0091-7613(2002)030<0927:GHAMVO>2.0.CO;2.

Bernard, B.B., Brooks, J.M., Sackett, W.M., 1976. Natural gas seepage in the Gulf of Mexico. Earth and Planetary Science Letters 31(1), 48-54. doi: 10.1016/0012-821X(76)90095-9.

Berndt C., Bünz, S., Clayton, T., Mienert, J., Saunders, M., 2004. Seismic character of bottom simulating reflectors: examples from the mid-Norwegian margin. *Marine and Petroleum Geology* 21, 723-733. doi: 10.1016/j.marpetgeo.2004.02.003.

Birchwood, R., Noeth, S., Jones, E., 2008. Safe drilling in gas-hydrate prone sediments: Findings from the 2005 drilling campaign of the Gulf of Mexico Gas Hydrates Joint Industry Project (JIP). USDOE-NETL, Fire in the Ice Newsletter, Winter 2008, 1-4.

Blake, D., Allamandola, L., Sandford, S., Hudgins, D., Freund, F., 1991. Clathrate hydrate formation in amorphous cometary ice analogs in Vacuo. Science 254(5031), 548-551.

Bohrmann, G., Greiner, J., Suess, E., Torres, M., 1998. Authigenic carbonates from the Cascadia subduction zone and their relation to gas hydrate stability. *Geology* 7, 647-650.

Booth, J.S., Winters, W.J., Dillon, W.P., Clennell, M.B., Rowe, M.M., 1998. Major occurrences and reservoir concepts of marine clathrates hydrates: implications of field evidence. In: Henriet, J.-P., and Mienert, J., (Eds.) Gas Hydrates: Relevance to World Margin Stability and Climate Change. Geological Society, London, Special Publications, 137, 113-127. doi:10.1144/GSL.SP.1998.137.01.08.

Borowski, W. S., Paull, C. K., Ussler, W., 1996. Marine pore-water sulfate profiles indicate in situ methane flux from underlying gas hydrate. *Geology* 24, 655-658.

Borowski, W. S., Paull, C. K., Ussler III, W., 1999. Global and local variations of interstitial sulfate gradients in deep-water, continental margin sediments: Sensitivity to underlying methane and gas hydrates. Marine Geology 159, 131-154.

Borowski, W.S., Rodriguez, N.M., Paull, C.K., Ussler, W., 2013. Are 34S-enriched authigenic sulfide minerals a proxy for elevated methane flux and gas hydrates in the geologic record? Marine and Petroleum Geology 43, 381-395. doi:10.1016/j.marpetgeo.2012.12.009.
Boswell, R., 2009. Is gas hydrate energy within reach? *Science* 325, 957-958

Boswell, R., Collett, T.S., 2006. The gas hydrate resource pyramid: Fire in the Ice: Methane Hydrate Newsletter, US Dept. of Energy, Office of Fossil Energy. National Energy Laboratory, Fall Issue, 5-7.

Boswell, R., Collett, T.S., 2011. Current perspectives on gas hydrate resources. Energy Environmental Science 4(4), 1206-1215. doi:10.1039/c0ee00203h.

Boswell, R., Collett, T., Frye, M., Shedd, W., McConnell, R., and Shelander, D., 2012. Subsurface gas hydrates in the northern Gulf of Mexico. *Marine and Petroleum Geology* 34, 4-30. doi:10.1016/j.marpetgeo.2011.10.003.

Boswell, R., and the Technical Coordination Team National Methane Hydrate R&D Program, 2006. An interagency roadmap for methane hydrate research and development. U.S. Department of Energy Office of Fossil Energy, July 2006. Available online at: https://www.netl.doe.gov/File%20Library/Research/Oil-Gas/methane%20hydrates/InteragencyRoadmap.pdf

Boswell, R., Saeki, T., 2010. Motivations for the geophysical investigation of gas hydrates. In: Riedel, M., Willoughby E., Chopra, S., (Eds.), Geophysical Characterization of Gas Hydrates. SEG Geophysical Developments Series, 14, Oklahoma, 23-32.

Boswell, R., Saeki, T., Shipp, C., Frye, M., Shedd, B., Collett, T., Shelander, D., McConnel, D., 2014. Prospecting for gas hydrate resources. Department of Energy, FITI Methane Hydrate Newsletter 14(2), 9-13. Available online at http://www.netl.doe.gov/File%20Library/Research/Oil-Gas/methane%20hydrates/MHNews_2014_July.pdf#page=9

Bottrell, S.H., Parkes, R.J., Cragg, B.A., Raiswell, R., 2000. Isotopic evidence for anoxic pyrite oxidation and stimulation of bacterial sulphate reduction in marine sediments. Journal of the Geological Society, London 157, 711-714.

Bouriak, S., Vanneste, M., Saotkine, A., 2000. Inferred gas hydrate and clay diapirs near the Storegga Slide on the southern edge of the Vøring Plateau, offshore Norway. Marine Geology 163, 125-148.

BP Statistical Review of World Energy, 2015, Natural gas. 64th edition. Available online at: bp.com/statisticalreview.

Brown, A., 2010. Interpretation of three-dimensional seismic data 7th ed. Tulsa.

Brooks, J.M., Field, M.E., Kennicutt, I.M.C., 1991. Observations of gas hydrates in marine sediments, offshore northern California. Mar. Geol. 96, 103-109.

Brown, K.M., Bangs, N.L., Froelich, P.N., Kvenvolden, K.A., 1996. The nature, distribution, and origin of gas hydrate in the Chile Triple Junction region. Earth and Planetary Science Letters 139, 471-483.

Bryan, G., 1974. In situ indications of gas hydrate. *Marine Science* 3, 299-308.

Bryne, T.B., Ling, W., Tsutsumi, A., Yamamoto, Y., Lewis, J.C., Kanagawa, K., Kitamura, Y., Yamaguchi, A., Kimura, G., 2009. An elastic strain recovery revelas extension across SW Japan subduction zone. *Geophysical Research Letters* 36, L23310. doi:10.1029/2009GL040749.

Buchs, D.M., Cukur, D., Masago, H., Garbe-Schönberg, D., 2015. Sediment flow routing during formation of forearc basins: Constraints from integrated analysis of detrital pyroxenes and stratigraphy in the Kumano Basin, Japan. *Earth and Planetary Science Letters* 414, 164-175.

Buffett B., and Archer D., 2004. Global inventory of methane clathrates: sensitivity to changes in the deep ocean. *Earth and Planetary Science Letters* 227, 185-199.

Burwicz, E.B., Rüpke, L.H., Wallman, K., 2011. Estimation of the global amount of submarine gas hydrates formed vial microbial methane formation based on numerical reaction-transport modeling and a novel parameterization of Holocene sedimentation. Geochim Cosmochim Acta 75, 4562-4576. doi:10.1016/j.gca.2011.05.029.

Caine, J.S., Evans, J.P., Forster, C.B., 1996. Fault zone architecture and permeability structure. *Geology* 24, 1025-1028.

Cartwright, J., Santamarina, C., 2015. Seismic characteristics of fluid escape pipes in sedimentary basins: Implications for pipe genesis. Marine and Petroleum Geology 65, 126-140. doi:10.1016/j.marpetgeo.2015.03.023.

Chapman, N., Gettrust, J., Walia, R., Hannay, D., Spence, G., Wood, W., Hyndman, R., 2002. High-resolution, deep-towed, multichannel seismic survey of deep-sea gas hydrates off western Canada. Geophysics 67(4), 1038-1047.

Chaudhuri, H., Ghose, D.F., Bhandari, F.K., Sen, P., Shina,B., 2011. A geochemical approach to earthquake reconnaissance at the Baratang mud volcano, Andaman and Nicobar Island. *Journal of Asian Earth Science* 46, 52-60.

Chong, Z.R., Yang, S.H.B., Babu, P., Linga, P., Li, X.-S., 2015. Review of natural gas hydrates as an energy resource: Prospects and challenges. Applied Energy, In Press. doi:10.1016/j.apenergy.2014.12.061.

Chopra, S., Marfurt, K.J., 2005. Seismic attributes-a historical perspective. *Geophysics* 70 (5), 3SO-28SO. doi: 10.1190/1.209867.

Chopra, S., Marfurt, K.J., 2006. Seismic attribute mapping of structure and stratigraphy. Distinguished Instructor Short Course No.9. Society of Exploration Geophysicists/European Association of Geoscientist & Engineers. 226p.

Claypool, G.E., Kvenvolden, K.A., 1983. Methane and other hydrocarbon gases in marine sediment. *Annual Review Earth and Planetary Science* 11, 299-327.

Clemens, S.C., Kuhnt, W., LeVay, L.J., and the Expedition 353 Scientists, 2015. Indian monsoon rainfall.*International Ocean Discovery Program Preliminary Report,* 353. doi:10.14379/iodp.pr.353.2015

Clift, P.D., Carter, A., Nicholson, U., Masago, H., 2013. Zircon and apatite thermochronology of the Nankai Trough accretionary prism and trench, Japan: sediment transport in an active and collisional margin setting*. Tectonics* 32, 377-395.

Collett, T., 1993. Natural gas hydrates of the Prudhoe Bay and Kuparuk River area, North Slope, Alaska. Am. Association of Petroleum Geology Bulletin, 77(5), 793-812.

Collett, T., 2001. A review of well-log analysis techniques used to assess gas-hydrate-bearing reservoirs. In: Paull, C.K., Dillon, W.P. (Eds), Natural gas hydrates: Occurrence, distribution, and detection: American Geophysical Union Geophysical Monography 124, 184-210. doi: 10.1029/GM124p0189.

Collett, T.S., 2002, Energy resource potential of natural gas hydrates: American Association of Petroleum Geologists Bulletin 86(11), 1971-1992.

Collett, T.S, Boswell, R., eds., 2012. Thematic set on resource and hazard implications of gas hydrates in the northern Gulf of Mexico. *Marine and Petroleum Geology* 34, 223.

Collett, T.S., Boswell, R., et al., NGHP Expedition 01 Scientific Party, 2014. Geologic implications of gas hydrates in the offshore of India: Results of the National Gas Hydrate Program Expedition 01. *Marine and Petroleum Geology* 58, 3-28. doi:10.1016/j.marpetgeo.2014.07.021.

Collett, T.S., et al., 2008. Results of the Indian National Gas Hydrate Program Expedition 01 initial reports, report. Director General of Hydrocarbons, Ministry of Petroleum and Natural Gas, New Delhi.

Collett, T.S., Dallimore, S.R., 2002. Detailed analysis of gas hydrate induced drilling and production hazards: Proceedings of the 4th International Conference on Gas Hydrates, Yokohama, Japan, May 19-23, 2002, 47-52.

Collett, T.S., Johnson, A., Knapp, C., and Boswell, R., 2009. Natural gas hydrates – a review, in Collett T., et al., (Eds) Natural gas hydrates—Energy resource potential and associated geologic hazards: AAPG Memoir 89.

Collett, T., Riedel, M., Cochran, J., Boswell, R., Presley, J., Kumar, P., Sathe, A., Sethi, A., Lall, M., and the NGHP Expedition Scientists, 2015, Indian National Gas Hydrate Program Expedition 01 report: U.S. Geological Survey Scientific Investigations Report 2012–5054, 1442 p.doi:10.3133/sir20125054.

Collett, T.S. and Lee, M.W., 2012. Well log characterization of natural gas-hydrates. *Petrophysics* 53(3), 348-367.

Colwell, F., Matsumoto, R., Reed, D., 2004. A review of the gas hydrates, geology, and biology of the Nankai Trough. Chemical Geology 205, 391-404. doi: 10.1016/j.chemgeo.2003.023.

Consortium for Ocean Leadership and the Methane Hydrate Project Science Team, 2013. Marine methane hydrate field research plan topical report. DOE Award Number DE-FE0010195. Prepared for: United States Department of Energy, National Energy Technology Laboratory, 70p.

Cook, A.E., Goldberg, D., Kleinberg, R.L., 2008. Fracture-controlled gas hydrate systems in the northern Gulf of Mexico. *Marine and Petroleum Geology* 25(9), 932-941. doi: 10.1016/j.marpetgeo.2008.01.013.

Cook, A.E., Goldberg, D., Malinverno, A., 2014. Natural gas hydrates occupying fractures: A focus on non-vent sites on the Indian margin and the northern Gulf of Mexico. Marine and Petroleum Geology 58, 278-292

Crutchley, G.J., Fraser, D.R.A, Pecher, I.A., Gorman, A.R., Maslen, G., Henrys, S.A., 2015. Gas migration into gas hydrate-bearing sediments on the southern Hikurangi margin of New Zealand. *Journal of Geophysical Research: Solid Earth* 120, 725-743. doi: 10.1002/2014JB011503.

Dai, S, Santamarina, J.C., Waite, W.F., Kneafsey, T.J., 2012. Hydrate morphology: physical properties of sands with patchy hydrate saturation. Journal of Geophysical Research 117 (B11).

Daigle, H., Dugan, B., 2011. Capillary controls on methane hydrate distribution and fracturing in advective systems. *Geochemistry, Geophysics, Geosystems* 12, Q01003. doi:10.1029/2010GC003392.

Davie, M.K., Zatsepina, O.Y., Buffett, B.A., 2004. Methane solubility in marine hydrate environments. *Marine Geology* 203, 177-184.

Davies, R.J., 2003. Kilometer-scale fluidization structures formed during early burial of a deep-water slope channel on the Niger Delta. *Geol. Soc. Am*. 31(11), 949-952.

Davies, R.J., Clarke, A.I., 2010. Methane recycling between hydrate and critically pressured stratigraphic traps, offshore Mauritania. *Geology* 38, 963-966.

Davies, R.J., Thatcher, K.E., Armstrong, H., Yang, J., Hunter, S., 2012. Tracking the relict bases of marine methane hydrates using their intersections with stratigraphic reflections. *Geology* 40(11), 1011-1014. doi: 10.1130/G33297.1.

Davis, E.E., Hyndman, R.D., Villinger, H., 1990. Rates of fluid expulsion across the northern Cascadia accretionary prism: constraints from new heat flow and multichannel seismic reflection data. J. Geophys. Res. 95, 8869-8889.

Davy, H., 1811. The Bakerian lecture: On some of the combinations of oxymuriatic gas and oxygene, and on the chemical relations of these principles, to inflammable bodies. Philosophical Transactions of the Royal Society of London (101), 1-35.

Day, S.J., Thompson, S.P., Evans, A., Parker, J.E., 2015. In situ apparatus for the study of clathrates hydrates relevant to solar system bodies using synchrotron X-ray diffraction and Raman spectroscopy (Research Note). Astronomy & Astrophysics

DeMets, C., Gordon, R.G., Argus, D.F., 2010. Geologically current plate motions. Geophysical Journal International 181, 1-80.

Demirbas, A., 2010. Processes for methane production from gas hydrates. Methane Gas Hydrate. London, Springer, 161-181.

Diaconescu, C.C., Kieckhefer, R.M., Knapp, J.H., 2001. Geophysical evidence for gas hydrates in the deep water of the South Caspian Basin, Azerbaijan. Marine and Petroleum Geology 18, 209-221.

Diaconescu, C.C., Knapp, J.H., 2002. Gas hydrates of the South Caspian Sea. Azerbaijan: Drilling hazards and Seafloor Stability. 393-399.

Dickens, G. R., 2001. Sulfate profiles and barium fronts in sediment on the Blake Ridge: present and past methane fluxes through a large gas hydrate reservoir. *Geochimica et Cosmochimica Acta* 65, 529-543.

Dickens, G.R., 2003. Rethinking the global carbon cycle with a large, dynamic, and microbially mediated gas hydrate capacitor. Earth and Planetary Science Letters 213(3), 169-183.

Dickens, G.R., Paull, C.K., Wallace, P., 1997. Direct measurement of in situ methane quantities in large gas hydrate reservoir: Nature 384, 426-428. doi:10.1038/385426a0.

Dickens, G.R., Quinby-Hunt, M.S., 1994. Methane hydrates stability in seawater. *Geophysical Research Letters 21*, 2115-2118. doi:10.1029/94GL01858.

Doan, M.-L., Henry, P., Conin, M., Wiersberg, T., Boutt, D., Buchs, D., Saffer, D., McNeill, L.C., Cukur, D., Lin, W., 2011. Quantification of free gas in the Kumano fore-arc basin detected from borehole physical properties: IODP NanTroSEIZE drilling Site C0009. *Geochemistry, Geophysics, Geosystems* 12, Q0AD06. doi: 10.1029/2010GC003284.

Domenico, S.N., 1976. Effect of brine-gas mixture on velocity in an unconsolidated sand reservoir. Geophysics 42, 882-895.

Dovorkin, J., Helgerud, M.B., Waite, W.F., Kirby, S.H., Nur, A., 2000. Introduction to physical properties and elasticity models, in: Max, M.D. (Ed.), Natural Gas Hydrate in Oceanic and Permafrost Environments. Kluwer Academic Publishers, Dordrecht, pp. 245-260.

Dugan, B., and Flemings, P.B., 2000. Overpressure and fluid flow in the New Jersey continental slope: Implications for slope failure and cold seeps. Science 289,288-291. doi: 10.1126/science.289.5477.288.

Duxbury, N.S., Abyzov, S.S., Romanovsky, V.E., Yoshikawa, K., 2004. A combination of radar and thermal approaches to search for methane clathrates in the Martian subsurface. Planetary and Space Science 52, 109-115. doi:10.1016/j.pss.2003.08.006.

Egawa, K., Furukawa, T., Saeki, T., Suzuki, K., Narita, H., 2013. Three-dimensional paleomorphologic reconstruction and turbidite distribution prediction revealing a Pleistocene confined basin system in the northeast Nankai Trough area. *AAPG Bulletin* 97(5)781-798. doi:10.1306/10161212014

Egawa, K, Nishimura, O., Izumi, S., Fukami, E., Jin, Y, Kida, M, Konno, Y., Yoneda, J., Ito, T, Suzuki, K., Nakatsuka, Y., Nagao, J., Bulk sediment mineralogy of gas hydrate reservoir at the East Nankai offshore production test site. *Marine and Petroleum Geology*. In Press. 9 p. doi: 10.1016/j.marpetgeo.2015.02.039.

Ellis, S., Pecher, I., Kukowski, n., Xu, W., Henrys, S., Greinert, J., 2010. Testing proposed mechanisms for seafloor weakening at the top of gas hydrate stability on an uplifted submarine ridge (Rock Garden), New Zealand. *Marine Geology* 272, 127-140. doi: 10.1016/j.margeo.2009.10.008.

Erzinger, J., Wiersberg, T., Zimmer, M., 2006. Real-time mud gas logging and sampling during drilling. Geofluids 6:225– 233. doi: 10.1111/j.1468-8123.2006.00152.x.

Expedition 314 Scientists, 2009. Expedition 314 Site C0002. *In* Kinoshita, M., Tobin, H., Ashi, J., Kimura, G., Lallemant, S., Screaton, E.J., Curewitz, D., Masago, H., Moe, K.T., and the Expedition 314/315/316 Scientists, *Proc. IODP,* 314/315/316: Washington, DC (Integrated Ocean Drilling Program Management International, Inc.). doi:10.2204/iodp.proc.314315316.114.2009

Expedition 315 Scientists, 2009. Expedition 315 Site C0002. *In* Kinoshita, M., Tobin, H., Ashi, J., Kimura, G., Lallemant, S., Screaton, E.J., Curewitz, D., Masago, H., Moe, K.T., and the Expedition 314/315/316 Scientists, *Proc. IODP,* 314/315/316: Washington, DC (Integrated Ocean Drilling Program Management International, Inc.). doi:10.2204/iodp.proc.314315316.124.2009

Expedition 319 Scientists, 2010. Site C0009. *In* Saffer, D., McNeill, L., Byrne, T., Araki, E., Toczko, S., Eguchi, N., Takahashi, K., and the Expedition 319 Scientists, *Proc. IODP,* 319: Tokyo (Integrated Ocean Drilling Program Management International, Inc.). doi:10.2204/iodp.proc.319.103.2010

Expedition 332 Scientists, 2011. Expedition 332 summary. *In* Kopf, A., Araki, E., Toczko, S., and the Expedition 332 Scientists, *Proc. IODP,* 332: Tokyo (Integrated Ocean Drilling Program Management International, Inc.). doi:10.2204/iodp.proc.332.101.2011

Expedtion 348 Scientists and Scientific Participants, 2014. NanTroSEIZE Stage 3: NanTroSEIZE plate boundary deep riser 3. IODP Preliminary Report, 348. doi: 10.2204/iodp.pr.348.2014.

Fergusson, C.L., 2003. Provanance of Miocene-Pleistocene turbidite sands and sandstones, Nankai Trough. Ocean Drilling Program Leg 190. In: Mikada, H., Moore, G.F., Taira, A., Beker, K., Moore, J.C.,

Fischer, D., Mogollon, J.M., Strasser, M., Pape, T., Bohrmann, G., Fekete, N., Spiess, V., Kasten, S., 2013. Subduction zone earthquake as potential trigger of submarine hydrocarbon seepage. Nature Geoscience 6, 647-651. doi:10.1038/NGEO1886.

Foucher, J.-P., Nouze, H., Henry, P., 2002. Observation and tentative interpretation of a double BSR on the Nankai slope. *Marine Geology* 187, 161-175. doi:10.1016/S0025-3227(02)00264-5.

Fujii, T., et al., 2009a. Resource assessment of methane hydrate by applying probabilistic approach in the eastern Nankai Trough, Japan (English abstract). *Journal of Geography* 118, 814-834. doi:10.5026/jgeography.118.814.

Fujii, T., Namikawa, T., Nakamizu, M., Tsuji, Y., Okui, T., Kawasaki, M., Ochiai, K., 2005. Modes of occurrence and accumulation mechanism of methane hydrate – Results of METI exploratory test wells 'Tokai-Oki to Kumano-Nada'. Proceedings of the Fifth International Conference on Gas Hydrates, June 12-16, 2005, Trondheim, Norway.

Fujii, T., Nakamizu, m., Tsuji, Y., Namikawa, T., Okui, T., Kawasaki, M., Ochiai, K., Nishimura, M., Takano, O., 2009b. Methane-hydrate occurrence and saturation confirmed from core samples, eastern Nankai Trough, Japan. In Collett, T., Johnson, A., Knapp, C., Boswell, R., (eds), Natural gas hydrates-Energy resource potential and associated geologic hazards: AAPG Memoir 89, 385-400.

Fujii, T., Noguchi, S., Takayama, T., Suzuki, K., Yamamoto, k., Saeki, T., 2013. Site selection and formation evaluation at the 1st offshore methane hydrate production test site in the eastern Nankai Trough, Japan. 75th EAGE Conference & Exhibition incorporating SPE EUROPEC, London, UK, 10-13 June 2013. Workshop paper: B10.

Fujii, T., Saeki, T., Kobayashi, T., Inamori, T., Hayashi, M., Takano, O, Takayama, T., Kawasaki, T., Nagakubo, S., Nakamizu, M., Yokoi, K, Japan Oil, Gas and Metals National Corporation (JOGMEC), 2008. Resource Assessment of Methane Hydrate in the Eastern Nankai Trough, Japan. Offshore Tec*hnology Conference Paper, OTC* 19310, 15p.

Ganguly, N., Spence, G.D., Chapman, N.R., Hyndman, R.D., 2000. Heat flow variations from bottom simulating reflectors on the Cascadia margin. Marine Geology 164, 53-68.

Géli, L., Turon, J.-L., Aslanian, D., Balut, Y., Beuzart, P., Cochran, J., Francheteau, J., Harmegnies, F., Landuré, J.-Y., Suavé, R.L., Mazaud, A., Michel, E., Normand, A., Pichon, J.-J., Vlastelic, I., 2001. Deep-penetration heat flow probes raise questions about interpretations from shorter probes. Eos, Trans.-Am. Geophys. Union 82, 317- 320.

Gellatti, R. and Busetti, M., 2010. A double bottom simulating reflector in the western Ross Sea, Antarctica. Journal of Geophysical Research 116, B04101. doi: 10.1029/2010JB007864.

Giavarini, C., Hester, K., 2011. Gas hydrates: Immense energy potential and environmental challenges (Green Energy and Technology). Springer, 178p.

Goldberg, D., and Saito, S., 1998. Detection of gas hydrates using downhole logs. *Geological Society , London, Special Publications* 137(1), 129-132.

Golmshtok, A.Y., Soloviev, V.A., 2006. Some remarks on the thermal nature of the double BSR. *Marine Geology* 229, 187-198. doi:10.1016/j.margeo.2006.03.004.

Goto, S., Mizoguchi, T., Kimura, R., Kinoshita, M., Yamano, M., Hamamoto, H., 2012. Variations in the thermal conductivities of surface sediments in the Nankai subduction zone off Tokai, central Japan. Marine Geophysical Research. doi: 10.1007/s11001-012-9161-5.

Gorman, A.R., Holbrook, W.S., Hornbach, M.J., Hackwith, K.L., Lizarralde, D., Pecher, I., 2002. Migration of methane gas through the hydrate stability zone in a low-flux hydrate province. Geology 30, 327-330.

Grauls, D., 2001. Gas hydrates: importance and applications in petroleum exploration. Marine and Petroleum Geology 18, 519-523.

Grevemeyer, I., Diaz-Naveas, J.L., Ranero, C.R., Villinger, H.W., 2003. Heat flow over the descending Nazca plate in central Chile, 32°S to 41°S: observations from ODP Leg 202 and the occurrence of natural gas hydrates. Earth and Planetary Science Letters 213, 285-298.

Grevemeyer, I., Kaul, N., Kopf, A., 2009. Heat flow anomalies in the Gulf of Cadiz and off Cape San Vicente, Portugal. Marine and Petroleum Geology 26, 795-804.

Grevemeyer, I., Villinger, H., 2001. Gas hydrate stability and the assessment of heat flow through continental margins. Geophys. J. Int. 145, 647- 660.

Gulick, S.P.S., Bangs N.L.B, Moore, G.F., Ashi, J., Martin, K.M., Sawyer, D.S., Tobin, H.J., Kuramoto, S.,

Guo, J., Likos, W.J., Underwood, M.B., Skarbek, R.M., Adamson, N., and Saffer, D., 2011. Data report: consolidation characteristics of sediments from Sites C0002, C0006, and C0007, IODP Expeditions 315 and 316, NanTroSEIZE Stage 1. In Kinoshita, M., Tobin, H., Ashi, J., Kimura, G., Lallement, S., Screaton, E.J., Curewitz, D., Masago, H., Moe, K.T., and the Expedition 314/315/316 Scientists, Proc.

IODP, 314/315/316: Washington, DC (Integrated Ocean Drilling Program Management International, Inc.). doi:10.2204/iodp.proc.314315316.213.2011

Guo, J., and Underwood, M.B., 2011. Data report: refined method for calculating percentages of kaolinite and chlorite from X-ray diffraction data, with application to the Nankai margin of southwest Japan. *In*Kinoshita, M., Tobin, H., Ashi, J., Kimura, G., Lallemant, S., Screaton, E.J., Curewitz, D., Masago, H., Moe, K.T., and the Expedition 314/315/316 Scientists, *Proc. IODP,* 314/315/316: Washington, DC (Integrated Ocean Drilling Program Management International, Inc.). doi:10.2204/iodp.proc.314315316.201.2011

Guo, J., and Underwood, M.B., 2012. Data report: clay mineral assemblages from the Nankai Trough accretionary prism and the Kumano Basin, IODP Expeditions 315 and 316, NanTroSEIZE Stage 1. *In* Kinoshita, M., Tobin, H., Ashi, J., Kimura, G., Lallemant, S., Screaton, E.J., Curewitz, D., Masago, H., Moe, K.T., and the Expedition 314/315/316 Scientists, *Proc. IODP,*314/315/316: Washington, DC (Integrated Ocean Drilling Program Management International, Inc.). doi:10.2204/iodp.proc.314315316.202.2012

Taira, A., 2001. Tectonic evolution of the Japanese arc system. *Annual Reviews Earth Planetary Science* 29, 109–134. doi: 10.1146/annurev.earth.29.1.109

Taira, A., 2010. Rapid forearc basin uplift and megasplay fault development from 3D seismic images of Nankai Margin off Kii Peninsula, Japan. *Earth and Planetary Science Letters* 300 (1-2), 55-62. doi: 10.1016/j.epsl.2010.09.034.

Taira, A., Hill, I., Firth, J.V., et al., 1991. *Proc. ODP, Init. Repts., Leg* 131: College Station, TX (Ocean Drilling Program). doi:10.2973/odp.proc.ir.131.1991.

Haacke, R.R., Westbrook, G.K., Hyndman, R.D., 2007. Gas hydrate, fluid flow and free gas: Formation of the bottom-simulating reflector. *Earth and Planetary Science Letters* 261, 407-420.

Hachikubo, A., Kosaka, T., Kida, M., Krylov, A., Sakagami, H., Takahashi, N., Shoji, H., (2007). Isotopic fractionation of methane and ethane hydrates between gas and hydrate phases. *Geophysical Research Letters*, 34. L21502. doi: 10.1029/2011gc003623.

Haeckel, M., Boudreau, B.P., Wallmann, K., 2007. Bubble-induced porewater mixing: A 3-D model for deep porewater irrigation. Geochimica et Cosmochimica Acta 71, 5135-5154.

Haeckel, M., Suess, E., Wallmann, K., Rickert, D., 2004. Rising methane gas bubbles form massive hydrate layers at the seafloor. Geochimica et Cosmochimica Acta 68(21), 4335-4345. doi: 10.1016/j.gca.2004.01.018.

Hamamoto, H., Yamano, M., Goto, S., 2005. Heat flow measurement in shallow seas through long-term temperature monitoring. Geophys. Res. Lett. 32, 1-5.

Hamamoto, H., M. Yamano, S. Goto, M. Kinoshita, K. Fujino, and K. Wang, 2011. Heat flow distribution and thermal structure of the Nankai subduction zone off the Kii Peninsula. Geochemistry, Geophysics, Geosystems 12(10), Q0AD20. doi: 10.1029/2011GC003623.

Hammerschmidt, S.B., Davis, E.E., Hüpers, A., Kopf, A., 2013. Limitation of fluid flow at the Nankai Trough megasplay fault zone. *Geo-Marine Letters* 33, 405-418. doi: 10.1007/s00367-013-0337-z.

Hammerschmidt, S.B., Wiersberg, T., Heuer, V.B., Wendt, J., Erzinger, J., Kopf, A., 2014. Real-time drilling mud gas monitoring for qualitative evaluation of hydrocarbon gas composition during deep sea drilling in the Nankai Trough Kumano Basin. Geochemical Transactions, 15:15. doi: 10.1118/s1293-014-0015-8.

Handa, Y.P., 1990. Effect of hydrostatic pressure and salinity on the stability of gas hydrates. J. Phys. Chem. 94, 2652-2657.

Harris, R. N., F. Schmidt-Schierhorn, and G. Spinelli, 2011. Heat Flow along the NanTroSEIZE transect: Results from IODP Expeditions 315 and 316 offshore the Kii Peninsula, Japan. Geochemistry, Geophysics, Geosystems, GC003593. doi: 10.1029/2011GC003593.

Hautala, S.L., Solomon, E.A., Johnson, H.P., Harris, R.N., Miller, U.K., 2014. Dissociation of Cascadia margin gas hydrates in response to contemporary ocean warming. Geophysical Research Letters 41, 9p. doi:10.1002/2014GL061606.

Hayman, N.W., Byrne, T.B., McNeill, L.C., Kanagawa, K., Kanamatsu, T., Browne, C.M., Schleicher, A.M., Huftile, G.J., 2012. Structural evolution of an inner accretionary wedge and forearc basin initiation, Nankai margin, Japan. *Earth and Planetary Science Letters* 353-354, 163-172. doi:10.1016/j.epsl.2012.07.040.

He, T., Spence, G.D., Riedel, M., Hyndman, R.D., Chapman, N.R., 2007. Fluid flow and origin of a carbonate mound offshore Vancouver Island: Seismic and heat flow constraints. Marine Geology 239, 83-98.

Hein, J., Scholl, D., Barren, J., Jones, M., Miller, J., 1978. Diagenesis of late Cenozoic diatomaceous deposits and formation of the bottom simulating reflector in the southern Bearing Sea. *Sedimentology* 25, 155-181.

Helgeland, L.R., Kinn, A.A., Kvalheim, O.F., Wenass, A., 2012. Gas Kick due to hydrates in the drilling for offshore natural gas and oil. Dissertation for Department of Petroleum Engineering and Apllied Geophysics NTNU, Trondheim.

Henry, P., Kanamatsu, T., Moe, K.T., Strasser, M., the IODP Expedition 333 Scientific Party, 2012. IODP Expedition 333: Return to Nankai Trough subduction input sites and coring mass transport deposits. *Scientific Drilling* 14, 4-17. doi:10.2204/iodp.sd.14.01.2012.

Henry, P., Thomas, M., Clennell, M.B., 1999. Formation of natural gas hydrates in marine sediments 2. Thermodynamic calculations of stability conditions in porous sediments. Journal of Geophysical Research 104(B10), 23005-23022.

Henrys, S.A., Ellis, S., Uruski, C., 2003. Conductive heat flow variations from bottom-simulating reflectors on the Hikurangi margin, New Zealand. Geophys. Res. Lett. 30, 37-31 - 37-34.

Herbozo, G., Hübscher, C., Kaul, N., Wagner, M., Pecher, I., Kukowski, N., 2013. Influence of recent depositional and tectonic controls on marine gas hydrates in Trujillo Basin, Peru margin. *Marine Geology* 340, 30-48

Hill, I.A., Taira, A., Firth, J.V., al, e., 1993. Sci. Results, 131, Proc. ODP. Ocean Drilling Program, College Station, TX.

Hiruta, A., Wang, L.-C., Ishizaki, O., Matsumoto R., 2014. Last glacial emplacement of methane-derived authigenic carbonates in the Sea of Japan constrained by diatom assemblage, carbon-14, and carbonate content. *Marine and Petroleum Geology* 56, 51-62. doi:10.1016/j.marpetgeo.2014.04.005.

Holbrook, S., W., Hoskins, H., Wood, W.T., Stephen, R.A., Lizarralde, D., 1996. Leg 164 science party, methane hydrate and free gas on the Blake Ridge from vertical seismic profiling. Science 273, 1840-1843

Hong, W. L., Torres, M. E., Kim, J. H., Choi, J., Bahk,J. J., 2014. Towards quantifying the reaction network around the sulfate-methane-transition-zone in the Ulleung Basin, East Sea, with a kinetic model approach. *Geochimica et Cosmochimica Acta* 140, 127-141.

Hong-Li, L., He, T., Spence, G.D., 2014. North Cascadia heat flux and fluid flow from gas hydrates: modeling 3D topographic effects. *J. Geophys. Res. Solid Earth* 119(1), 99-115.

Hornbach, M.J., Saffer, D.M., Holbrook, W.S., Van Avendonk, H.J.A., Gorman, A.R., 2008. Three-dimensional methane hydrate province: Evidence for large, concentrated zones of gas hydrate and morphologically driven advection. *Journal of Geophysical Research* 113, B07101. doi: 10.1029/2007JB005392.

Housen, B.A., and Musgrave, R.J., 1996. Rock magnetic signature of gas hydrates in accretionary prism sediments. *Earth and Planetary Science Letters* 139, 509-519. doi: 10.1016/0012-821X(95)00245-8.

Hydrocarbon Seal Quantification edited by A.G. Koestler and R. Hunsdale. NPF Special Publication 11, pp. 203-219, Published by Elsevier Science B.V., Amsterdam. Norwegian Petroleum Society (NPF), 2002.

Hyndman, R.D., and E.E. Davis (1992), A mechanism for the formation of methane hydrate and seafloor bottom-simulating-reflectors by vertical fluid expulsion, *J. Geophys. Res.*, *97* (B5), 7025–7041.

Hyndman, R.D., Foucher, J.P., Yamano, M., Fisher, A., Scientific Team of Ocean Drilling Program, L., 1992. Deep sea bottom-simulating-reflectors: calibration of the base of the hydrate stability field as used for heat flow estimates. Earth and Planetary Science Letters 109, 289-301.

Hyndman, R.D., Spence, G.D., 1992. A Seismic Study of Methane Hydrate Marine Bottom Simulating Reflectors. J. Geophys. Res. 97, 6683-6698.

Hyodo M., Li, Y., Yoneda, J., Nakata, Y., Yoshimoto, N., Kajiyama, S., et al., 2014. A comparative analysis of the mechanical behavior of carbon dioxide and methane hydrate-bearing sediments. American Mineralogy 99, 178-183.

Ijiri, A., Tsunogai, U., Gamo, T., Ashi, J., Kinoshita, M. and Nakamura, K., 2002. Chemical composition of the pore water obtained from mud diapirs in the Kumano Basin. Abstracts of Geochemical Society of Japan, 49, Page 116. Available online at:
http://earth.kumst.kyotou.ac.jp/prismfluid/proc/no01162517.pdf

Ike, T., Moore, G.F., Kuramoto, S., Park, J., Kaneda, Y., Taira, A., 2008. Variations in sediment thickness and type along the northern Philippine Sea Plate at the Nankai Trough. *Island Arc* 17, 342-357.

Inamori, T., Hato, M., 2004. Detection of methane hydrate-bearing zones from seismic data. *Resource Geology* 54(1), 99-104.

Ito, T., Komatsu, Y., Fujii, T., Suzuki, K., Egawa, K., Nakatsuka, Y., Konno, Y., Yoneda, J., Jin, Y., Kida, M., Nagao, J., Minagawa, H., 2015. *Marine and Petroleum Geology*, In Press.
DoiDoi:10.1016/j.marpetgeo.2015.02.022.

Jiang, W.-T., Chen, J.-C., Huang, B.-J., Chen, C.-J., Lee, Y.-T., Huang, P.-R., Lung, C.-C., Huang, S.-W., 2006. Mineralogy and physical properties of cored sediments from the gas hydrate potential area of offshore southwestern Taiwan. *Terr. Atmos. Ocean. Sci.* 17(4), 981-1007.

Johnson, J.E., Phillips, S.C., Torres, M.E., Piñero, E., Rose, K.K., Giosan, L.,(2014). Influence of total organic carbon deposition on the inventory of gas hydrate in the Indian continental margins. *Marine and Petroleum Geology* 58, 406-424. doi: 10.1016/j.marpetgeo.2014.08.021.

Jones, A.T., et al., 2010 Acoustic and visual characterization of methane-rich seabed seeps at Omakere Ridge on the Hikurangi Margin, New Zealand. Marine Geology 272, 154-169.

Jones, E., Collett, T., Rose, K., Dugan, B., Wood, W., Latham, T., 2008. Site Selection for DOE/JIP Gas Hydrate Drilling in the Northern Gulf of Mexico. *6th International Conference on Gas Hydrates*. Online at:https://circle.ubc.ca//handle/2429/1165.

Kaplan, I.R. (Ed.), 1972. Natural gases in marine sediments. Plenum Press, New York.

Kars, M., and Kodama, K.,2015. Authigenesis of magnetic minerals in gas hydrate-bearing sediments in the Nankai Trough, offshore Japan. *Geochemistry, Geophysics, Geosystems* 16,947-961. doi: 10.1002/2014GC005614.

Kastner, M., 2001. Gas hydrates in convergent margins: formation, occurrence, geochemistry, and global significance. In Paull, C.K., Dillon, W.P., (Eds.) Natural gas hydrates: occurrence, distribution, and detection. AGU Geophysical Monograph 124, 67-86.

Kastner, M. et al, 1993. Geochemical and Isotopic Evidence for Fluid Flow in the Western Nankai Subduction Zone, Japan. Proceedings of the Ocean Drilling Program, Scientific Results. Vol. 131., Pages 397-413

Kastner, M., Kvenvolden, K.A., Whiticar, M.J., Camerlenghi, A., and Lorenson, T.D., 1995a. Relation between pore fluid chemistry and gas hydrates associated with bottom-simulating reflectors at the Cascadia margin, Sites 889 and 892. *In* Carson, B., Westbrook, G.K., Musgrave, R.J., and Suess, E. (Eds.), *Proc. ODP, Sci. Results,* 146 (Pt. 1): College Station, TX (Ocean Drilling Program), 175–187. doi:10.2973/odp.proc.sr.146-1.213.1995.

Kastner, M., Sample, J.C., Whiticar, M.J., Hovland, M., Cragg, B.A., and Parkes, J.R., 1995b. Geochemical evidence for fluid flow and diagenesis at the Cascadia convergent margin. *In* Carson, B., Westbrook, G.K., Musgrave, R.J., and Suess, E. (Eds.), *Proc. ODP, Sci. Results,* 146 (Pt. 1): College Station, TX (Ocean Drilling Program), 375–384.doi:10.2973/odp.proc.sr.146-1.243.1995.

Kastner, M., Solomon, E.A., Harris, R.N., Torres, M.E., 2014. Fluid origins, thermal regimes, and fluid and solute fluxes in the forearc of subduction zones. In: Stein, R., Blackman, D., Inagaki, F., Larsen, H.-C., (Eds.) Earth and Life Processes Discovered from Subseafloor Environments, Volume 7: A Decade of Science Achieved by the Integrated Ocean Drilling Program (IODP). *Developments in Marine Geology* 7, 671-733.

Kaul, N., Rosenberger, A., Villinger, H., 2000. Comparison of measured and BSR-derived heat flow values, Makran accretionary prism, Pakistan. Marine Geology 164, 37-51.

Kawasaki, M., Umezu, S., Yasuda, M., 2006. Pressure temperature core sampler (PTCS). *Journal of the Japanese Association for Petroleum Technology* 71(1), 139-137 (English abstract).

Kida, M., Jin, Y., Watanabe, M., Konno, Y., Yoneda, J., Egawa, K., Ito, T., Nakatsuka, Y., Suzuki, K., Fujii, T., Nagao, J., 2015. Chemical and crystallographic characterizations of natural gas hydrate recovered from a production test site in the Eastern Nankai Trough. Marine and Petroleum Geology, In Press.

Kim, Y.-G., Lee, S.-M., Jin, Y. K., Baranov, B., Obzhirov, A., Salomatin, A., Shoji, H., 2013. The stability of gas hydrate field in the northeastern continental slope of Sakhalin Island, Sea of Okhotsk, as inferred from analysis of heat flow data and its implications for slope failures. *Marine and Petroleum Geology* 45, 198-207. doi: 10.1016/j.marpetgeo.2013.05.003.

Kim, J.-H., Jou, H.-T., Kang, S.-G., Lee, G.-H., Yi, B.-Y., Yoo, D.-G., Ryu, B.-J., Shin, C., 2013. Seismic characterization and imaging of a gas hydrate deposit in the western part of the Ulleung Basin, East Sea (Japan Sea). *Marine and Petroleum Geology 47,* 214-221. doi: 10.1016/j.marpetgeo.2013.05.019.

Kim, J.-H, Torres, M., Hong, W.-L., Choi, J., Riedel, M., Bahk, J.-J., Kim, S.-H., 2013. Pore fluid chemistry from the Second Gas Hydrate Drilling Expedition in the Ulleung Basin (UBGH2): Source, mechanisms and consequences of fluid freshening in the central part of the Ulleung Basin, East Sea. *Marine and Petroleum Geology* 47, 99-112. doi: 10.1016/j.marpetgeo.2012.12.011.

Kimura, G., Moore, G.F., Strasser, M., Screaton, E., Curewitz, D., Steiff, C., Tobin, H., 2011. Spatial and temporal evolution of the megasplay fault in the Nankai Trough. *Geochemistry, Geophysics, Geosystems* 12(3), Q0A008. doi: 10.1029/2010GC003335.

Kimura, J.-I., Stern, J., Yoshida, T., 2005. Reinitiation of subduction and magmatic responses in SW Japan during Neogene time. Geol. Soc. Am. Bull. 117(7-8), 969-986. doi: 10.1130/B25565.1.

Kinoshita, M., T. Kanamatsu, K. Kawamura, T. Shibata, H. Hamamoto, and K. Fujino (2008), Heat flow distribution on the floor of Nankai Trough off Kumano and implications for the geothermal regime of subducting sediments, *JAMSTEC Rep. Res. Dev.*, *8*, 13–28.

Kinoshita, M., G.F. Moore and Y.N. Kido (2011), Heat flow estimated from BSR and IODP borehole data: Implication of recent uplifting of the imbricate thrust zone in the Nankai Trough off Kumano, *Geochem. Geophys. Geosyst*., *12*,

Kinoshita, M., Tobin, H., Ashi, J., Kumura, G., Lallemant, S., Screaton, E.J., Curewitz, D., Masago, H., Moe, K.T., and the Expedition 314/315/316 Scientists. Proceedings IODP 314/315/316: Washington, DC, Integrated Ocean Drilling Program Management International, Inc. doi:10.2204/iodp.proc.314315316.114.2009.

Kirscheke, S., et al., 2013. Three decades of global methane sources and sinks. Nature Geoscience 6, 813-823. doi:10.1038/NGEO1955.

Kitajima, H., Chester, F.M., and Biscontin, G., 2012. Mechanical and hydraulic properties of Nankai accretionary prism sediments: effect of stress path.*Geochem., Geophys., Geosyst.,* 13(10):Q0AD27. doi:10.1029/2012GC004124

Klauda, J.B., and Sandler, S.I, 2005. Global distribution of methane hydrate in ocean sediments. Energy Fuels 19, 459-470.

Klaus, A. (eds) *Proceedings of the Ocean Drilling Program, Scientific Report 190/196.* Integrated Ocean Drilling Program Management International Inc., Washington, 1-28.

Kobayashi, K., 2002 Tectonic significance of the cold seepage zones in the eastern Nankai accretionary wedge- and outcome of the 15 year KAIKO projects. *Marine Geology* 187, 3-30.

Komatsu, H., Ota, M., Smith, R.L.Jr., Inomata, H., 2013. Review of CO_2-CH_4 clathrate hydrate replacement reaction laboratory studies – properties and kinetics. *Journal of the Taiwan Institute of Chemical Engineers* 44, 517-537. doi: 10.1016/j.jtice.2013.09.010.

Kopf, A.J., 2002. Significance of mud volcanism. Reviews of Geophysics 40, 1005. doi:10.1029/2000rg000093.

Kopf, A., Strasser, M., Monsees, N., Underwood, M.B., and Guo, J., 2011. Data report: particle size analysis of sediments recovered during IODP Expeditions 315 and 316, Sites C0001–C0008, Nankai Trough forearc, off Japan. *In* Kinoshita, M., Tobin, H., Ashi, J., Kimura, G., Lallemant, S., Screaton, E.J., Curewitz, D., Masago, H., Moe, K.T., and the Expedition 314/315/316 Scientists, *Proc. IODP,* 314/315/316: Washington, DC (Integrated Ocean Drilling Program Management International, Inc.).doi:10.2204/iodp.proc.314315316.207.2011

Kopp, H., 2002. BSR occurrence along the Sunda margin: evidence from seismic data. *Earth and Planetary Science Letters* 197, 225-235.

Korup, O., Hayakawa, Y., Codilean, A.T., Matsushi, Y., Saito, H., Oguchi, T., Matsuzaki, H., 2014. Japan's sediment flux to the Pacific Ocean revisited. *Earth-Science Reviews* 135, 1-16. doi: 10.1016/j.earscirev.2014.03.004.

Kumar, D., Dash, R, Dewanga, P., 2009. Methods of gas hydrate concentration estimation with field examples. *Geohorizons*, 76-86.

Kuramoto, S., Ashi, J., Greinert, J., Gulick, S., Ishimura, T., Morita, S., Nakamura, K., Okada, M., Okamoto, T., Rickert, D., Saito, S., Suess, E., Tsunogai., U., Tomosugi, T., 2001. Surface observations of subduction related mud volcanoes and large thrust sheets in the Nankai Subduction Margin; Report on YK00-10 and YK01-04 cruises. *JAMSTEC J. Deep Sea Research* 19, 131-139.

Kuramoto, S., Tamaki, K., Langseth, M.G., Nobes, D.C., Tokuyama, H., Pisciotto, K.A., Taira, A., 1992. Can opal-A/opal-CT BSR be an indicator of the thermal structure of the Yamato Basin, Japan Sea? Proceedings of the Ocean Drilling Program Scientific Results 127,128 Pt.2, 1145-1156.

Kvenvolden, K.A., 1993. Gas hydrates-geological perspective and global change. Reviews of Geophysics 31, 173-188.

Kvenvolden, K.A., 1995. A review of the geochemistry of methane in natural gas hydrate. Organic Geochemistry 23, 997-1008.

Kvenvolden, K.A., 1998. A primer on the geological occurrence of gas hydrate. In Henriet, J., Mienert, J., (Eds.), Gas Hydrates: Relevance to World Margin Stability and Climatic Change. The Geological Society, 9-30.

Kvenvolden, K.A., Barnard, L.A., 1983. Hydrates of natural gas in continental margins, in: Watkins, J.S., Drake, C.L. (Eds.), Studies in Continental Margin Geology. Am. Assoc. Petrol. Geol. Memoir, pp. 631-640.

Kvenvolden, K.A., Ginsberg, G.D., Soloviev, V.A., 1993. Worldwide distribution of subaquatic gas hydrates. *Geo-Marine Letters* 13 (1) 32-40.

Kvenvolden, K.A., Kastner, M., 1990. Gas hydrates of the Peruvian outer continental margin, in: Suess, E., von Huene, R. (Eds.), Proceedings of the Ocean Drilling Program, Scientific Results. Ocean Drilling Program, College Station, TX, pp. 517-526.

Kvenvolden, K.A., and Lorenson, T.D., 2001. The global occurrence of natural gas hydrate. In: *Natural Gas Hydrates: Occurrence, Distribution, and Detection* (eds. C.K. Paull and W.P. Dillion). Geophysics Monogram 124, 3-18

Laberg, J.S., Andreassen, K., 1996. Gas hydrate and free gas indications within the Cenozoic succession of the Bjørnøya Basin, western Barents Sea. Marine and Petroleum Geology 13, 921-940.

Laird, A.P., Morley, C.K., 2011. Development of gas hydrates in a deep-water anticline based on attribute analysis from three-dimensional seismic data. Geosphere 7(1), 240-259. doi: 10.1130/GES00598.1

Lee, M.W., Collett, T.S., 2006. Gas hydrate and free gas saturations estimated from velocity logs on Hydrate Ridge offshore Oregon, USA. In Tréhu, A.M., Bohrmann, G., Torres, M.E., Colwell, F.S. (Eds.), Proc. ODP, Science Results, 204, 1-25. Online at: http://www.odp.tamu.edu/publications/204_SR/VOLUME/CHAPTERS/103.PDF.

Lee, M., Dillion, W., 2001. Amplitude blanking related to the pore-filling of gas hydrate in sediments. Marine Geophysical Research. Volume 22, Issue 2, Pages 101-109.

Lee, J. Y., Santamarina, J.C., Ruppel,C., 2010, Volume change associated with formation and dissociation of hydrate in sediment. *Geochem. Geophys. Geosyst.* 11, Q03007.doi:10.1029/2009GC002667.

Li, H.-L., He, T., Spence, G.D., North Cascadia heat flux and fluid flow from gas hydrates: Modeling 3-D topographic effects. Journal of Geophysical Research: Solid Earth 119, 99-115. doi: 10.1002/2013JB010101.

Liao, W.-Z., Lin, A.T., Liu, C.-S., Oung, J.-N., Wang, Y., 2014. Heat flow in the rifted continental margin of the South China Sea near Taiwan and its tectonic implication. Journal of Asian Earth Sciences 92, 233-244. doi: 10.1016/j.jseaes.2014.01.003.

Ligtenberg, H., 2005. Detection of fluid migration pathways in seismic data: implications for fault seal analysis. Basin Research 17, 141-153.

Lim, D., Choi, J., Xu, Z., Kim, M., Choi, D., Jung, H., Lee, P., 2009. Methane-derived authigenic carbonates from the Ulleung basin sediments East Sea of Korea. Continental Shelf Research 29, 1588-1596. doi: 10.1016/j.csr.2009.04.013.

Lim, Y. C., Lin, S., Yang, T. F., Chen Y, G., Liu, C. S., 2011. Variations of methane induced pyrite formation in the accretionary wedge sediments offshore southwestern Taiwan. *Marine and Petroleum Geology* 28, 1829-1837.

Liu, C.–S., P. Schnürle, Y. Wang (2006), Distribution and Characters of Gas Hydrate Offshore of Southwestern Taiwan, *Terr. Atmos. Ocean. Sci.*, *17*, 615-644.

Liu, X., and Flemings, P.B., 2006. Passing gas through the hydrate stability zone at southern Hydrate Ridge, offshore Oregon. *Earth and Planetary Science Letters* 241, 211-226. doi:10.1016/j.epsl.2005.10.026.

Liu, X., and Flemings, P.B., 2007. Dynamic multiphase flow model of hydrate formation in marine sediments. *Journal of Geophysical Research* 112, B03101. doi:10.1029/2005JB004227.

Liu, X., and Flemings, P.B., 2011. Capillary effects on hydrate stability in marine sediments. *Journal of Geophysical Research* 116, B07102. doi: 10.1029/2010JB008143.

Lodolo, E., Camerlenghi, A., Brancolini, G., 1993. A bottom simulating reflection on the South Shetland margin, Antarctic Peninsula. Antarctic Science 5, 207-210.

Lodolo, E., Camerlenghi, A., Madrussani, G., Tinivella, U., Rossi, G., 2002. Assessment of gas hydrate and free gas distribution on the South Shetland margin (Antarctica) based on multichannel seismic reflection data. Geophysical Journal International 148, 103-119.

Long, D., Lovell, M.A., Rees, J.G., Rochelle, C.A., 2009. Sediment-hosted gas hydrates: New insights on natural and synthetic systems. Geological Society Special Publication, Geological Society of London, 319th edition, 368p.

Lu, S.-M., 2015. A global survey of gas hydrate development and reserves: specifically in the marine field. Renewable and Sustainable Energy Reviews 41, 884-900. doi: 10.1016/j.rser.2014.08.063.

Lu, Z., Sultan, N., 2008. Empirical expressions for gas hydrate stability law, its volume fraction and mass-density at temperatures 273.15k to 290.15k. Geochemical Journal 42, 163-175.

Lucazeau, F., Brigaud, F., Bouroullec, J.L., 2004. High-resolution heat flow density in the lower Congo basin. Geochemistry Geophysics Geosystems 5, 24.

Macelloni, L.,Lutken, C.B., Garg S., Simonettie, A., D'Emidio, M., Wilson, R.M., Sleeper, K., Lapham, L.L., Lewis, T., Pizzi, M., Knapp, J.H., Knapp, C.C., Brooks, J., McGee, T.M., 2015. Heat-flow regimes and the hydrate stability zone of a transient thermogenic, fault-controlled hydrate system (Woolsey Mound northern Gulf of Mexico). Marine and Petroleum Geology 59, 491-504. doi:10.1016/j.marpetgeo.2014.09.010.

MacKay, M.E., Jarrard, R.D., Westbrook, G.K., Hyndman, R.D., 1994. Origin of bottom-simulating reflectors: Geophysical evidence from the Cascadia accretionary prism. Geology 22, 459-462.

Madrussani, G., Rossi, G., Camerlenghi, A., 2009. Gas hydrates, free gas distribution and fault pattern on the west Svalbard continental margin. Geophysical Journal International 180, 666-684.

Maekawa, T., Itoh, S., Sakata, S., Igari, S.-I., Imai, N., 1995. Pressure and temperature conditions for methane hydrate dissociation in sodium chloride solutions. *Geochemical Journal* 29, 325-329.

Magalhaes, V.H., Pinheiro, L.M., Ivanov, M.K., Kozlova, E., Blinova, V., Koganova, J., Vasconcelos, C., McKenzie, J.A., Bernasconi, S.M., Kopf, A.J., Diaz-del-Rio, V., Gonzalez, F.J., Somoza, L., Formation process of methane-derived authigenic carbonates from the Gulf of Cadiz. *Sedimentary Geology* 243-244, 155-168. doi: 10.1016/j.sedgeo.2011.10.013.

Malinverno, A., Goldberg, D.S., 2015. Testing short-term migration of microbial methane as a hydrate formation mechanism: Results from Andaman Sea and Kumano Basin drill sites and global implications. *Earth and Planetary Science Letters* 422, 105-114. doi:10.1016/j.epsl.2015.04.019.

Malinveron, A., Kastner, M., Torres, M.E., Wortmann, U.G., 2008. Gas hydrate occurrence from pore water chlorinity and downhole logs in a transect across the northern Cascadia margin (IODP 311). *Journal of Geophysical Research* 113, B081023. doi: 10.1029/2008JB005702.

Marcaillou, B., Spence, G., Collot, J.-Y., Wang, K., 2006. Thermal regime from bottom simulating reflectors along the north Ecuador–south Colombia margin: Relation to margin segmentation and great subduction earthquakes. J. Geophys. Res. 111, 16.

Martin, V., Henry, P., Nouze, H., Noble, M., Ashi, J., Pascal, G., 2004. Erosion and sedimentation as processes controlling the BSR-derived heat flow on the Eastern Nankai margin. Earth and Planetary Science Letters 222, 131-144.

Maslin, M., Owen, M., Betts, R., Day, S., Dunkley-Jones, T., Ridgwell, A., 2010. Gas hydrates: past and future geohazard? Phil. Trans. Royal Soc. A 368, 2369-2393.

Matsumoto, R., Borowski, W.S., 2000. Gas hydrate estimates from newly determined oxygen isotopic fractionation and $\delta^{18}O$ anomalies of the interstitial waters: Leg 164, Blake Ridge. In: Paull, C.K.,

Matsumoto, R., Wallace, P.J., and Dillon, W.P. (Eds.), Proceedings of the Ocean Drilling Program, Scientific Results 164, 59-66.

Matsumoto, R., Tomaru, H., Lu, H., 2004. Detection and evaluation of gas hydrates in the eastern Nankai Trough by geochemical and geophysical methods. *Resource Geology* 54(1), 53-67.

Matsushima, J., 2006. Seismic wave attenuation in methane hydrate-bearing sediments: Vertical seismic profiling data from the Nankai Trough exploratory well, offshore Tokai, central Japan. *Journal of Geophysical Research* 111, B10101. doi: 10.1029/2005JB004031.

Max, M.D., 2001. Terrestrial methane hydrate: A potentially universal planetary attribute. Is hydrate a key to human habitation of other planetary bodies? Conference on the Geophysical Detection of Subsurface Water on Mars, 7035

Max, M.D., 2012. Natural gas hydrate: In oceanic and permafrost environments. Springer Science & Business Media. doi: 10.1007/978-94-011-4387-5.
Max, M.D., Johnson, A.H., Dillon, W.P., 2006. Economic geology of natural gas hydrate: Coastal systems and continental margins. *Dodrecht*, Springer 9, 341p. doi:10.1007/1-4020-3972-7_1

Mazurenko, L.L., Soloviev, V.A., Gardner, J.M., Ivanov M.K., Gas hydrates in the Ginsburg and Yuma mud volcano sediments (Moroccan Margin): results of chemical and isotopic studies of pore water. *Marine Geology* 195, 201-210.

McCarthy, K., Niemann, M., Palmowski, D., Peters, K., Stankiewicz, A., 2011. Basic petroleum geochemistry for source rock evaluation. *Schlumberger Oilfield Review Summer 2011* 23(2), 32-43.

McConnell, D. and Kendall, B., 2002. Images of the base of gas hydrate stability, northwest Walker Ridge. *Offshore Technology Conference Paper* 14103. 10p.

Milkov, A.V., 2004. Global estimates of hydrate-bound gas in marine sediments: how much is really out there? *Earth Science Reviews* 66, 183-197.

McConnell, D., Collett, T., Boswell, R., Frye, M., Shedd, W., Dufrene, R., Godfriaux, P., Mrozewski, S., Guerin, G., Cook, A., Jones, E., 2010. Gulf of Mexico Gas Hydrate Joint Industry Project Leg II: Results from the Green Canyon 955 Site. Proc. OTC, 14. OTC 20801.

McConnell, D., Zhang, Z., Boswell, R., 2012. Review of progress in evaluating gas hydrate drilling hazards. *Marine and Petroleum Geology* 17(9), 981-991.

McIver,R.D., 1982. Role of naturally occuring gas hydrates in sediment transport. *American Association of Petroleum Geologists* Bulletin 66,789.

Meister, P., Gutjahr, M., Frank, M., Bernasconi, S.M., Vasconcelos, C., McKenzie, J.A., 2011. Dolomite formation within the methanogenic zone induced by tectonically driven fluids in the Peru accretionary prism. *Geology* 39(6), 563-566. doi: 10.1130/G31810.1.

Mikada, H., Kinoshita, M., Becker, K., Davis, E.E., Meldrum, R.D., Flemings, P., Gulick, S.P.S., Matsubayashi, O., Morita, S., Goto, S., Misawa, N., Fujino, K., Toizumi, M., 2003. Hydrogeological and Geothermal studies around Naikai Trough (KR02-10 Nankai Trough Cruise Report). JAMSTEC J. Deep Sea Res. 22, 125-171.

Milkov, A.V., 2000. Worldwide distribution of submarine mud volcanoes and associate gas hydrates. *Marine Geology* 167, 29-42.

Milkov, A.V., 2004. Global estimates of hydrate-bound gas in marine sediments:how much is really out there? Earth Science Review 66, 183-197.

Milkov, A.V., Claypool, G.E., Lee, Y-J., Xu, W., Dickens, G.R., Borowski, W.S., and the Ocean Drilling Program Leg 204 Scientific Party, 2003, In situ methane concentrations at Hydrate Ridge, offshore Oregon: New constraints on the global gas hydrate inventory from active margins: *Geology*, v. 31, no. 10, p. 833-83.

Milkov, A.V., and Sassen 2002. Economic geology of offshore gas hydrate accumulations and provinces. *Marine and Petroleum Geology* 19, 1-11Miyazaki, S.I., Heki, K., 2001. Crustal velocity field of southwest Japan: Subduction and arc-acr collision. *Journal of Geophysical Research* 106(3), 4305-4326.

Minshull, T.A., Bartolome, R., Byrne, S., Danobeitia, J., 2005. Low heat flow from young oceanic lithosphere at the Middle America Trench off Mexico. Earth and Planetary Science Letters 239, 33.

Miyakawa, A., Saito, S., Yamada, Y., Tomaru, H., Kinoshita, M., Tsuji, T., 2014. Gas hydrate saturation at Site C0002, IODP Expeditions 314 and 315, in the Kumano Basin, Nankai Trough. Island Arc 23(2), 142-156.

Miyoshi, T., Mastoshi, I., Ohmura, R., Yasuoka, K., 2007. Thermodynamic stability of type-I and type-II clathrates hydrates depending on the chemical species of the guest substances. *The Journal of Chemical Physics* 129, 234506. doi: 10.1063/1.2746324.

Moore, G.F., Bangs, N.L., Taira, A., Kuramoto, S., Pangborn, S., Tobin, H.J., 2007. Three-dimensional splay fault geometry and implications for tsunami generation. *Science* 318, 1128-1131. doi:10.1126/science.1147195.

Moore, G.F., Boston, B.B., Sacks, A.F., Saffer, D.M., 2013. Analysis of normal fault populations in the Kumano Forearc Basin, Nankai Trough, Japan: 1. Multiple orientations and generations of faults from 3-D coherency mapping. *Geochemistry, Geophysics, Geosystems* 14(6), 1989-2002. doi: 10.1002/ggge.20119.

Moore, G.F., Boston, B.B., Strasser, M., Underwood, M.B., Ratliff, R.A., 2015. Evolution of tectono-sedimentary systems in the Kumano Basin, Nankai Trough forearc. *Marine and Petroleum Geology*, in press.

Moore, G.F., Kanagawa, K., Strasser, M., Dugan, B., Maeda, L., Toczko, S., and the Expedition 338 Scientists, 2013. NanTroSEIZE Stage 3: NanTroSEIZE plate boundary deep riser 2. *IODP Prel. Rept.*, 338. doi:10.2204/iodp.pr.338.2013Moore, G., Kanagawa, K., Strasser, M., Dugan, B., Maeda, L., and Toczko, S., 2014. IODP Expedition 338: NanTroSEIZE Stage 3: NanTroSEIZE plate boundary deep riser 2. *Sci. Drill.,* 17:1–12. doi:10.5194/sd-17-1-2014

Moore, G.F., Park, J.-O., Bangs, N.L., Gulick, S.P., Tobin, H.J., Nakamura, Y., Saito, S., Tsuji, T., Yoro, T., Tanaka, H., Uraki, S., Kido, Y., Sanada, Y., Kuramoto, S., and Taira, A.,, 2009. Structural and seismic stratigraphic framework of the NanTroSEIZE Stage 1 transect, in: Kinoshita, M., Tobin, H., Ashi, J., Kimura, G., Lallemant, S., Screaton, E.J., Curewitz, D., Masago, H., Moe, K.T., and the Expedition 314/315/316 Scientists (Ed.), Proc. IODP. Integrated Ocean Drilling Program Management International, Inc., College Station, TX.

Moore, G.F., Taira, A., Becker, L., Boeckel, B., Cragg, B.A., Dean, A., Fergusson, C.L., Henry, P., Hirano, S., Hisamitsu, T., Hunze, S., Kastner, M., Maltman, A.J., Morgan, J.K., Murakami, Y., Saffer, D.M., Sanchez-Gomez, M., Screaton, E.J., Smith, D.C., Spivack, A.J., Steurer, J., Tobin, H.J., Ujiie, K., Underwood, M.B., Wilson, M., 2001. New insights into deformation and fluid flow processes in the Nankai Trough accretionary prism: Results of Ocean Drilling Program Leg 190. *Geochemistry Geophysics Geosystems* 2, 2001GC000166. Moore, G.F., Taira, A., Klaus, A., Becker, K., Becker, L., Boeckel, B., Cragg, B.A., Dean, P.A., Fergusson, C.L., Henry, P., Hirano, S., Hisamitsu, T., Hunze, S., Kastner, M., Maltman, A.J., Morgan, J.K., Murakami, Y., Saffer, D.M., Sanchez-Gomez, M., Screaton, E.J., Smith, D.C., Spivack, A.J., Steurer, J., Tobin, H.J., Ujiie, K., Underwood, M.B., Wilson, M., 2001a. Initial Report Leg 190. Proc. Ocean Drill. Program

Moore, G.F., Taira, A., Klaus, A., Becker, L., Boeckel, B., Cragg, B.A., Dean, A., Fergusson, C.L., Henry, P., Hirano, S., Hisamitsu, T., Hunze, S., Kastner, M., Maltman, A.J., Morgan, J.K., Murakami, Y., Saffer, D.M., Sanchez-Gomez, M., Screaton, E.J., Smith, D.C., Spivack, A.J., Steurer, J., Tobin, H.J., Ujiie, K.,Underwood, M.B., Wilson, M., 2001b. New insights into deformation and fluid flow processes in the Nankai Trough accretionary prism: Results of Ocean Drilling Program Leg 190. *Geochemistry Geophysics Geosystems* 2 (10), 2001GC000166.

Moore, J.C., 1989. Tectonics and hydrogeology of accretionary prisms: role of the decollement zone.Journal of Structural Geology 11, 95-106.

Moore, J.C., Barrett, M., and Moe, K.T., 2013. Fluid pressures and fluid flows from boreholes spanning the NanTroSEIZE transect through the Nankai Trough, SW Japan. *Tectonophysics,* 600:108–115. doi:10.1016/j.tecto.2013.01.026

Moore, J.C., Silver, E., 2002. Fluid flow in accreting and eroding convergent margins. JOIDES Journal 28, 91-96.

Moore, J.C., Vrolijk, P., 1992. Fluids in accretionary prisms. Reviews of Geophysics 30, 113-135.

Moridis, G., Collett, T., Boswell, R., Kurihara, M., Reagan, M., Koh, C., and Sloan, D., 2009. Toward production from gas hydrates: Current status, assessment of resources, and simulation-based evaluation of technology and potential, SPE Reservoir Eval. and Eng., v. 12 (5), p. 745-771.

Morita, S., Ashi, J., Aoike, K., Kuramoto, S.i., 2004. Evolution of Kumano Basin and Sources of Clastic Ejecta and Pore Fluid in Kumano Mud Volcanoes, Eastern Nanaki Trough International Symposium on Methane Hydrates and Fluid Flow in Upper Accretionary Prisms (PrismFluid 2004), Shirankaikan, Kyoto, Japan.

Mosher, D.C., 2011. A margin-wide BSR gas hydrate assessment: Canada's Atlantic margin. *Marine and Petroleum Geology* 28, 1540-1553.

Mountjoy, J., Pecher, I., Henrys,S., Barnes, P., Plaza-Faverola, A., 2013. Creeping deformation mechanisms for mixed hydrate-sediment submarine landslides. EGU General Assembly, held 7-12 April, 2013 in Vienna, Austria. Abstract id:EGU2013-3489.

Mousis, O., Chassefiere, E., Holm N.G., Bouquet, A., Waite, J.H., Geppert, W.D., Picaud, S., Aikawa, Y., Ali-Dib, M., Charlou, J.L., Rousselot, P., 2015. Methane clathrates in the solar system. Astrobiology 15(4). doi:10.1089/st.20174.1189.

Mousis, O., Alibert, Y., 2005. On the composition of ices incorporated in Ceres. Mon. Not. R. Astron. Soc. 358, 188-192. doi:10.1111/j.1365-2966.2005.08777.x.

Mousis, O., Lunine, J.I., Picaud, S., Cordier, D., 2010. Volatile inventories in clathrates hydrates fromed in the primordial nebula. Astro-ph.EP, arXiv:1011.4171v1.

Murshed, M.M., and Kuhs, W.F., 2009. Kinetic studies of methan-ethane mixed gas hydrates by neutron diffraction and raman spectroscopy. Journal of Physical Chemistry 113, 5172-5180. doi: 10.1012/jp810248s.

Musgrave, R.J., Bangs, L.N., Larrasoaña, J.C., Gràcia, E., Hollamby, J.A., Vega, M.E., 2006. Rise of the base of the gas hydrate zone since the last glacial recorded by rock magnetism. *Geology* 34, 117-120. doi: 10.1130/G22008.1.

Nakamizu, M., Namikawa, T., Ochiai, K., Tsuji, Y., 2004. Efforts heading for production of methane from methane hydrate resources-An outline of METI exploratory test well "Nankai Trough" and future research program and development plan. *Journal of the Japanese Association for Petroleum Technology* 69, 214-221 (English abstract).

Nagakubo, S., 2009. Methane hydrate as a domestic energy resource: Japan's methane hydrate R&D program (English Abstract). *Journal of Geography* 118, 758-775. doi:10.5026/jgeography.118.758.

Navalpakam, R.S., Pecher, I.A., Stern, T., 2012. Weak and segmented bottom simulating reflections on the Hikurangi Margin, New Zealand – Implications for gas hydrate reservoir rocks. *Journal of Petroleum Science and Engineering* 88-89, 29-40. doi:10.1016/j.petrol.2012.01.008.

Noguchi, S., Shimoda, N., Takano, O., Oikawa, N., Inamori, T., Saeki, T., Fujii, T., 2011. 3-D internal architecture of methane hydrate-bearing turbidite channels in the eastern Nankai Trough, Japan. *Marine and Petroleum Geology* 28, 1817-1828. doi:10.1016/j.marpetgeo.2011.02.004.

Ojha, M., 2012. Quantitative assessment of gas hydrates from seismic data. LAP LAMBERT Academic Publishing, 124p.

Omura, A., Ikehara, K., Sugai, T., Shirai, M., Ashi, J., 2012. Determination of the origin and processes of deposition of deep-sea sediments from the composition of contained organic matter: An example from two forearc basins on the landward flank of the Nankai Trough, Japan. *Sedimentary Geology* 249-250, 10-25. doi: 10.1016/j.sedgeo.2012.01.005.

Osegovic, J.P., Tatro, S.R., Holman, S.A., 2006. Physical chemical characteristics of natural gas hydrate. In: Max, M.D. et al., (Eds.), Economic Geology of Natural Gas Hydrate, Springer, 45-105.

Ota, M., Abe, Y., Watanabe, M., Smith, R.L.Jr., Inomata, H., 2005. Methane recovery from methane hydrate using pressurized CO2. Fluid Phase Equilibrium 228-229, 553-559.

Pape, T., Bahr, A., Rethemeyer, J., Kessler, D., Sahling, H., Hinrichs, K.U., Klapp, S.A., Reeburgh, W.S., Bohrmann, G., 2010. Molecular and isotopic partitioning of low-molecular weight hydrocarbons during migration and gas hydrate precipitation in deposits of a high-flux seepage site. *Chemical Geology* 269(3-4), 350-363. doi:10.1016/j.chemgeo.2009.10.009.

Pape, T., Geprags, P., Hammerschmidt, S., Wintersteller, P., Wei, J., Fleischmann, T., Bohrmann, G., Kopf, A.J., 2014. Hydrocarbon seepage and its sources at mud volcanoes of the Kumano forearc basin, Nankai Trough subduction zone. *Geochemistry, Geophysics, Geosystems* 15, 2180-2194. doi:10.1002/2013GC005057.

Park, J.-O., Tsuru, T., Kodaira, S., Cummins, P.R., Kaneda, Y., 2002. Splay fault branching along the Nankai subduction zone. Science 297, 1157-1160.

Paull, C.K., Dillion, W.P., 2001. Natural Gas Hydrates Occurrence, Distribution, and Detection. Edited Volume. Geophysical Monograph. American Geophysical Union. Washington DC

Paull, C.K., Lorenson, T.D., Dickens, G., Borowski, W.S., Ussler, W., III, and Kvenvolden,

K., 2000. Comparisons of in situ and core gas measurements in ODP Leg 164 boreholes. Ann. New York Acad. Sci., 912:23–31.

Paull, C.K., Matsumoto, R., Wallace, P.J., et al., 1996. *Proc. ODP, Init. Repts.,* 164: College Station, TX (Ocean Drilling Program). doi:10.2973/odp.proc.ir.164.1996

Paull, C.K., Matsumoto, R., 2000b. Leg 164 Overview. Section 1 in Paull, C.K., Matsumoto, R., Wallace, P.J., and Dillon, W.P. (Eds.)2000, *Proceedings of the Ocean Drilling Program, Scientific Results*, Vol 164.

Paull, C.K., Ussler III, W., Borowski, W.A., 1994. Sources of biogenic methane to form marine gas-hydrates: In situ production or upwards migration? In: E. Dendy Sloan, J., Happel, J., A., M. (Eds.), The New York Academy of Science, Annals, pp. 392-409.

Pecher, I.A., Henrys, S. A., Wood, W.T., Kukowski, N., Crutchley , G.J., Fohrmann, M., Kilner, J., Senger, K., Gorman, A.R., Coffin, R.B., Greinert, J., Faure, K., 2010. Focused fluid flow on the Hikurangi Margin, New Zealand- Evidence from possible local upwarping of the base of gas hydrate stability. Marine Geology 272, 99-113.

Pecher, I.A., Kukowski, N., Huebscher, C., Greinert, J., Bialas, J., 2001. The link between bottom-simulating reflections and methane flux into the gas hydrate stability zone- new evidence from Lima Basin, Peru Margin. *Earth and Planetary Science Letter* 185 (3-4), 343-354.Pecher, I.A., Minshull, T.A.,

Peckmann, J., Reimer, A., Luth, U., Luth, C., Hasen, B. T., Heinicke, C., Hoefs, J., Reitner, J., 2001. Methane-derived carbonates and authigenic pyrite from the northwestern Black Sea. *Marine Geology* 177, 129-150.

Peketi, A., Mazumdar, A., Joshi, R. K., Patil, D. J., Srinivas, P. L., Dayal, A. M., 2012. Tracing the Paleo sulfate-methane transition zones and H2S seepage events in marine sediments: An application of C-S-Mo systematics. *Geochemistry Geophysics Geosystems* 13, Q10007. doi:10.1029/2012GC004288.

Peltzer, E.T., Brewer, P.G., 2000. Practical Physical Chemistry and Empirical Predictions of Methane Hydrate Stability. Chapter 3 in: Max, M.D. (Ed.), Natural Gas Hydrate in Oceanic and Permafrost Environemnts, 17-28.

Phrampus, B.J., Hornbach, M.J., 2012. Recent changes to the Gulf Stream causing widespread gas hydrate destabilization. Nature/Letter 490, 527-530. doi: 10.1038/nature11528.

Pierre, C., Rouchy, J.M., Gaudichet, A., 2000. Diagenesis in the gas hydrate sediments of the Blake Ridge: Mineralogy and stable isotope compositions of the carbonate and sulfide minerals. In: Paull, C.K.,

Piñero E., Gràcia, E., Martíne-Ruiz, F., Larrasoaña, J.C., Vizcaino, A., Ercilla, G., 2007. Gas hydrate disturbance fabrics of southern Hydrate Ridge sediments (ODP Leg 204): Relationship with texture and physical properties. Geo-Mar Lett 27, 279-288. doi: 10.1007/s00367-007-0077-z.

Pisciotto, K.A., 1981. Diagenetic trends in the siliceous facies of the Monterey Shale in the Santa Monica region, California. *Sedimentology* 28, 547-571.Matsumoto, R., Wallace, P.J., and Dillon, W.P. (Eds.), *Proceedings of the Ocean Drilling Program Scientific* Results 164, 139-146.

Plaza-Faverola, A., Brünz, S., Mienert, J., 2012. The free gas zone beneath gas hydrate bearing sediments and its link to fluid flow: 3-D seismic imaging offshore mid-Norway. *Marine Geology* 291-294, 211-226. doi:10.1016/j.margeo.2011.07.002.

Plaza-Faverola, A., Klaeschen, D., Barnes, P., Pecher, I., Henrys, S., Mountjoy, J., 2012. Evolution of fluid expulsion and concentrated hydrate zones across the southern Hikurangi subduction margin, New Zealand: An analysis from depth migrated seismic data. *Geochemistry, Geophysics, Geosystems* 13(8), Q08018. doi: 10.1029/2012GC004228.

Pohlman, J.W., Kaneko, M., Heuer, V.B., Coffin, R.B., Whiticar, M., 2009. Methane sources and production in the northern Cascadia margin gas hydrate system. *Earth and Planetary Science Letters* 287, 504-512. doi: 10.1016/j.epsl.2009.08.037.

Popescu, I., De Batist, M., Lericolais, G., Nouzé, H., Poort, J., Panin, N., Versteeg, W., Gillet, H., 2006. Multiple bottom-simulating reflections in the Black Sea: Potential proxies of past climate conditions. *Marine Geology* 227(3-4), 163-176. doi: 10.1016/j.margeo.2005.12.006.

Posewang, J., Mienert, J., 1999. The enigma of double BSRs: indicators for changes in the hydrate stability field? *Geo-Marine Letters* 19, 157-163.

Prieto-Ballesteros, O., Kargel, J.S., Fernandez-Sampedro, M., Selsis, F., Martinez, E.S., Hogenboom, D.L., 2005. Evaluation of the possible presence of clathrates hydrates in Europa's icy shell or seafloor. ICARUS 177, 491-505. doi:10.1016/j.icarus.2005.02.021.

Prinzhofer, A., Pernaton, E., 1997. Isotopically light methane in natural gas: bacterial imprint or diffusive fractionation? Chemical Geology 142, 193-200.

Raiswell, R., Canfield, D. E., 1998. Sources of iron for pyrite formation in marine sediments. *American Journal of Science* 298, 219-245.

Rajput, S., Müller, T. M., Clennell, M.B., Rao, P.P., Thakur, N.K., 2012. Constraints on seismic reflections and mode conversions at bottom simulating reflectors associated with gas hydrates. *Journal of Petroleum Science and Engineering* 88-89. 48-60. doi:10.1016/j.petrol.2012.01.022.

Rajput, S., Thakur, N.K., Rao P.P., Joshi, A., 2010. AVO response for a complex double bottom simulating reflectors model. Current Science. Vol. 98, No. 10, p. 1354-1358

Rao, I., Koh, C.A., Sloan,D., Sum, A.K., 2013. Gas hydrate deposition on a cold surface in water-saturated gas systems. Idustrial & Engineering Chemistry Research 52, 6262-6269. doi: 10.1021/ie400493a.

Ramirez, S.G., Gulick, S.P., Hayman, N.W., 2015. Early sedimentation and deformation in the Kumano forearc basin linked with Nankai accretionary prism evolution, southwest Japan. *Geochemistry, Geophysics, Geosystems,* Accepted Manuscript. doi: 10.1002/2014GC005643.

Reed, D.L., Silver, E.A., Tagudin, J.E., Shipley, T.H., Vrolijk, P., 1990. Relations between mud volcanoes, thrust deformation, slope sedimentation and gas hydrates, offshore north Panama. *Marine and Petroleum Geology* 7, 44-54.

Rehder, G., Kirby, S.H., Durnham, W.B., Stern, L.A., Peltzer, E.T., Pinkston, J., Brewer, P.G., 2004. Dissolution rates of pure methane hydrate and carbon dioxide hydrate in undersaturated seawater at 1000-m depth. *Geochimica et Comochimica Acta* 68, 285-292.

Rempel, A.W., 2011. A model for the diffusive growth of hydrate saturation anomalies in layered sediments. *Journal of geophysical Research* 116, B10105. doi: 10.1029/2011/JB008484.

Revil, A., 2000. Thermal conductivity of unconsolidated sediments with geophysical applications. J. Geophysical Research 105, 16749- 16768.

Riboulot, V., Cattaneo, A., Sultan, N., Garziglia, S., Ker, S., Imbert, P., Voisset, M., 2013. Sea-level change and free gas occurrence influencing a submarine landslide and pockmark formation and distribution in deepwater Nigeria. Earth and Planetary Science Letters 375, 78-91. doi: 10.1016/j.epsl.2013.05.013.

Riedel, M., Bahk, J.-J., Kim, H.-S., Yoo, D.-G., Kim, W.-S., Ryu, B.-J., 2013. Seismic facies analyses as aid in regional gas hydrate assessments. Part-I: Classification analyses. Marine and Petroleum Geology 47, 248-268. doi: 10.1016/j.marpetgeo.2013.04.011.

Riedel, M., Collett, T.S., Hyndman, R.D., 2005. Gas hydrate concentration estimates from chlorinity, electrical resistivity and seismic velocity. Geological Survey of Canada, Open File 4934, 28p.

Riedel, M., Collett, T.S., Kumar, P., Sathe, A.V., Cook, A., 2010. Seismic imaging of a fractured gas hydrate system in the Krishna-Godavari Basin offshore India. *Marine and Petroleum Geology* 27, 1476-1493. doi: 10.1016/j.marpetgeo.2010.06.002.

Riedel, M., Collett, T.S., Malone,M., Expedition 311 Scientists, 2005. Cascadia margin gas hydrates. *Proceeding of the International Ocean Drilling Program* 311.

Riedel, M., Collett, T.S., Malone, M.J., and the Expedition 311 Scientists, 2010. *Proc. IODP,* 311: Washington, DC (Integrated Ocean Drilling Program Management International, Inc.). doi:10.2204/iodp.proc.311.213.2010

Riedel, M., Collett, T.S., Shankar, U., 2011. Documenting channel features associated with gas hydrates in the Krishna-Godavari Basin, offshore India. *Marine Geology* 279, 1-11.

Riedel, M., Willoughby E., Chopra, S., (Eds.),2010. Geophysical Characterization of Gas Hydrates. SEG Geophysical Developments Series, 14, Oklahoma.

Riedinger, N., and Brunner, B., 2014. Data report: concentration and sulfur isotope composition of iron monosulfide and pyrite from sediments collected during IODP Expedition 316. *In* Kinoshita, M., Tobin, H., Ashi, J., Kimura, G., Lallemant, S., Screaton, E.J., Curewitz, D., Masago, H., Moe, K.T., and the Expedition 314/315/316 Scientists, *Proc. IODP,* 314/315/316: Washington, D.C. (Integrated Ocean Drilling Program Management International, Inc.). doi:10.2204/iodp.proc.314315316.223.2014

Ritger, S., Carson, B., Suess, E., Methane-derived authigenic carbonates form by subduction-induced pore-water expulsion along the Oregon/Washington margin. *Geol. Soc. Am. Bull*. 98, 147-156.

Rodrigo, C., González-Fernádez, A., Vera, E., 2009. Variability of the bottom-simulating reflector (BSR) and its association with tectonic structure in the Chilean margin between Arauco Gulf (37°S) and Valdivia (40°S). *Marine Geophysical Research* 30, 1-19. doi: 10.1007/s11001-009-9064-2.

Ruppel, C., Boswell, R., Jones, E., 2008. Scientific results from Gulf of Mexico Gas Hydrates Joint Industry Project Leg 1 drilling: introduction and overview. Marine and Petroleum Geology 25(9), 819-829. doi:10.1016/j.marpetgeo.2008.02.007

Ryu, Byong-Jae, et. al., 2013. Scientific results of the second gas hydrae drilling expedition in the Ulleung Basin (UBGH2). Marine and Petroleum Geology 47, 1-20.

Sacks, A., Saffer, D.M., Fisher, D., 2013. Analysis of normal fault poplations in the Kumano forearc basin, Nankai Trough, Japan: 2. Principle axes of stress and strain from inversion of fault orientations. *Geochemistry, Geophysics, Geosystems* 14(6), 1973-1988. doi:10.1002/ggge.20118.

Saeki , T., Fujii, T., Inamori, T., Kobayashi, T., Hayashi, M., Nagakubo, S., Takano, O., 2007. Extraction of methane hydrate concentrated zone for resource assessment in the eastern Nankai Trough, Japan. *Proceedings of 2008 Offshore Technology Conference Houston, Texas*, OTC19311.

Saeki, T., Fujii, T., Inamori, T., Kobayashi, T., Hayashi, M., Nagakubo, S., and Takano, O., 2008. Extraction of methane hydrate concentrated zone for resource assessment in the eastern Nankai Trough, Japan. Offshore Technology Conference Paper 19311. 8 p.

Saffer, D.M., Bekins, B.A., 1998. Episodic fluid flow in the Nankai accretionary complex: Timescale, geochemistry, flow rates, and fluid budget. Journal of Geophysical Research 103, 30,351–330,370.

Saffer, D., McNeill, L., Byrne, T., Araki, E., Toczko, S., Eguchi, N., Takahashi, K., and the Expedition 319 Scientists, 2010. Site C0009. *Proc. IODP,* 319: Tokyo (Integrated Ocean Drilling Program Management International, Inc.). doi:10.2204/iodp.proc.319.103.2010

Saffer, D.M., Screaton, E.J., 2003. Fluid flow at the toe of convergent margins: interpretation of sharp pore-water geochemical gradients. *Earth and Planetary Science Letters* 213(3-4), 261-270.

Saffer, D.M., Tobin, H.J., 2011. Hydrogeology and mechanics of subduction zone forearcs: fluid flow and pore pressure. *Annual Review Earth and Planetary Science* 39(1), 157-186. doi: 10.1146/annurev-earth-040610-133408.

Sain, K., Minshull, T.A., Singh, S.C., Hobbs, R.W., 2000. Evidence for a thick free gas layer beneath the bottom simulating reflector in the Makran accretionary prism. Marine Geology 164, 3-12.

Saito, S., Miyakawa, A., Yamada, Y., and Kinoshita, M., 2010. Methane hydrate occurrence estimated from downhole logging at IODP Site C0002, Kumano Basin. *Sekiyu Gijutsu Kyokaishi,* 75(1):54–58. doi:10.3720/japt.75.54

Saito, H., Suzuki, N., and Tsunogai, U., 2013. Data report: carbon isotope compositions of methane in void gas samples from IODP Expedition 315 Site C0001, Nankai Trough, offshore Japan. *In* Kinoshita, M., Tobin, H., Ashi, J., Kimura, G., Lallemant, S., Screaton, E.J., Curewitz, D., Masago, H., Moe, K.T., and the Expedition 314/315/316 Scientists, *Proc. IODP,* 314/315/316: Tokyo (Integrated Ocean Drilling Program Management International, Inc.). doi:10.2204/iodp.proc.314315316.209.2013

Santamarina, J.C., Dai, S., Terzariol, M., Jang, J., Waite, W.F., Winters, W.J., Nagao, J., Yoneda, J., Konno, Y., Fugii, T., Suzuki, K., 2015. Hydro-bio-geomechanical properties of hydrate-bearing sediments from Nankai Trough. *Marine and Petroleum Geology* In Press, 1-17. doi: 10.1016/j.marpetgeo.2015.02.033.

Sasaki, K., Okuda, Y., Kato, S., 1992. Petroleum geology of the Pacific side of southwest Japan. In: Association of Natural Gas Mining and Association for offshore Petroleum Exploration (eds.) Petroleum and Natural Gas Resources of Japan. Tokyo: Association of Natural Gas Mining and Association for Offshore Petroleum Exploration, 225-246.

Satyavani, N., Sain, K., Lall, M., Kumar B.J.P., 2008. Seismic attribute study for gas hydrates in the Andaman offshore India. Marine Geophysical Research 29, 167-175.

Sauter, E.J., Muyakshin, S.I., Charlou, J.-L., Schlüter, M., Boetius, A., Jerosch, K., Damm, E., Foucher, J.-P., Klages, M., 2006. Methane discharge from a deep-sea submarine mud volcano into the upper water column by gas hydrate-coated methane bubbles. *Earth and Planetary Science Letters* 243, 354-356.

Scholz, N.J., Hyndman, R.D., Dugan, B., Pohlman, J., Hamilton, T., 2011. Do dissociating gas hydrates play a role in triggering submarine slope failures? A case study from the northern Cascadia margin. Proceedings of the 7th International Conference on Gas Hydrates (ICGH 2011), Edinburgh, Scotland, United Kingdom, July 17-21.

Schmitt, D.R., Mwenifumbo, C.J., Pfug, K.A., Meglis, I.L., 2003. Geophysical logging for elastic properties in hard rock: a tutorial In: *Eaton, D.W., Milkereit, B., Salisbury, M.H., (eds.). Hardrock seismic exploration. Society of Exploration Geophysicists Geophysical Development Series* 10, p. 14.

Schultheiss, P., Holland, M., Rack, F., 2010. Borehole pressure coring techniques and core analysis at in situ pressure. In: Riedel, M., Willoghby, E.C., Chopra, S., (Eds.) Geophysical Characterization of Gas Hydrates. Society of Exploration Geophysicists Geophysical Developments No. 14, 263-278.

Seno, T., Stein, S., Gripp, A.E., 1993. A model for the motion of the Philippine Sea plate consistent with NUVEL-1 and geological data. J. Geophys. Res. 98, 17941-17948.

Shedd, W., Boswell, R., Frye, M., Godfriaux, P., Kramer, K., 2012. Occurrence and nature of "bottom simulating reflectors" in the northern Gulf of Mexico. Marine and Petroleum Geology 34, 31-40. doi:10.1016/j.marpetgeo.2011.08.005.

Shelander, D., Dai, J., Bunge, G., 2010. Predicting saturation of gas hydrates using pre-stack seismic data, Gulf of Mexico. *Marine Geophysical Research* 31, 39-57.

Shelander, D., Dai, J., Bunge, G., Singh, S., Eissa, M., and Fisher, K., 2012. Estimating saturation of gas hydrates using conventional 3-D data, Gulf of Mexico Joint Industry Project Leg II. J. Mar. Pet. Geo. 34, 96-110.

Shipley, T.H., Houston, M.H., Buffler, R.T., Shaub, F.J., McMillen, K.J., Ladd, J.W., Worzel, J.L., 1979. Seismic evidence for widespread possible gas hydrate horizons on continental slopes and rises. Am. Assoc. Pet. Geol. Bull. 63, 2204-2213.

Shnyukov, E.F., 2013. Mud Volcanoes of the Black Sea as a prospecting Indicator of methane hydrates. *Lithology and Mineral Resources* 48(2), 114-121. doi:10.1134/S0024490213010045.

Simonetti, A., Knapp, J.H., Sleeper, K., Lutken, C.B., Macelloni, L., Knapp, C., 2013. Spatial distribution of gas hydrates from high-resolution seismic and core data, Woolsey Mound, Northern Gulf of Mexico. *Marine and Petroleum Geology* 44, 21-23. doi: 10.1016/j.marpetgeo.2013.04.004.

Singh, S.C., Huene, R.v., 1996. Velocity structure of a bottom simulating reflector offshore Peru: Results from full waveform inversion. Earth and Planetary Science Letters 139, 459-469.

Sloan, D.E., 1998. Clathrate hydrates of natural gases, second edition, revised and expanded (Chemical Industries Book 73). CRC Press, 705p.

Sloan, D.E., Koh, C., 2007. Clathrate hydrates of natural gases, third edition (Chemical Industries). CRC Press, 752p.

Sloan, E.D., Koh, C.A., Sum, A.K., 2010. Gas hydrate stability and sampling: The future as related to the phase diagram. *Energies* 3, 1991-2000. doi: 10.3390/en312991.

Smith, D.C., D'Hondt, S., 2006. Exploration of life in deep subseafloor sediments. Oceanography 19(4), 58-70.

Smith, G.L., McNeill, L.C., Henstock, T.J., Arraiz, D., Spiess, V., 2014. Fluid generation and distribution in the highest sediment input accretionary margin, the Makran. *Earth and Planetary Science Letters* 403, 131-143. doi:10.1016/j.epsl.2014.06.030.

Sohl, F., Choukroun M., Kargel, J., Kimura, J., Pappalardo, R., Vance, S., Zolotov, M., 2010. Subsurface water oceans on icy satellites: Chemical composition and exchange processes. Space Science Review 153, 485-510.

Solomon, E.A., Kastner, M., Wheat, G., Jannasch, H.W., Robertson, G., et al., 2009. Long-term hydrogeochemical records in the oceanic basement and forearc prism at the Costa Rica subduction zone. *Earth and Planetary Science Letters* 282, 240-251.

Solomon, E.A., Kastner, M., Jannasch, H., Robertson, G., Weinstein, Y., 2008. Dynamic fluid flow and chemical fluxes associated with a seafloor gas hydrate deposit on the northern Gulf of Mexico slope. *Earth and Planetary Science Letters* 270, 95-105.

Somaza, L., León R., Medialdea, T., Pérez, L.F., González, F.J., Maldonado,A., 2014. Seafloor mounds, craters and depressions linked to seismic chimneys breaching fossilized diagenetic bottom simulating reflectors in the central and southern Scotia Sea, Antarctica. *Global and Planetary Change*. doi:10.1016/j.gloplacha.2014.08.004.

Spence, G.D., Haacke, R.R., Hyndman, R.D., 2010. Seismic indicators of Natural Gas Hydrate and underlying free gas. In Riedel, M., Willoughby, E.C., Chopra, S., (Eds.) Geophysical Characterization of Gas Hydrates, SEG Geophysical Developments 14, 39-71.

Spinelli, G.A., and Harris, R.N., 2011. Thermal effects of hydrothermal circulation and seamount subduction: temperatures in the Nankai Trough Seismogenic Zone Experiment transect, Japan. *Geochem., Geophys., Geosyst.,* 12(12). doi:10.1029/2011GC003727

Stoian, I., Park, K.-P., Yoo, D.-G., Haacke, R.R., Hyndman, R.D., Riedel, M., Spence, G., 2008. Siesmic reflection blank zones in the Ulleung Basin, offshore Korea, associated with high concentrations of gas hydrates. Proceedings of the 6th International Conference on Gas Hydrates (ICGH 2008). Vancouver, BC, Canada, July 6-10.

Strasser, M., Dugan, B., Kanagawa, K., Moore, G.F., Toczko, S., Maeda, L., and the Expedition 338 Scientists, 2014. Proc. IODP, 338: Yokohama, *Integrated Ocean Drilling Program.* doi:10.2204/iodp.proc.338.2014.

Strasser, M., Moore, G.F., Kimura, G., Kitamura, Y., Kopf, A.J., Lallemant, S., Park, J.-O., Screaton, E.J., Su, X., Underwood, M.B., Zhao, X., 2009. Origin and evolution of a splay fault in the Nankai accretionary wedge. *Nat. Geosci*. 2, 648-652. doi:10.1038/NGEO609

Strasser, M., Moore, G.F., Kimura, G., Kopf, A.J., Underwood, M.B., Guo, J., Screaton, E.J., 2011. Slumping and mass-movement deposition in the Nankai forearc: Evidence from IODP drilling and 3-D reflection seismic data. Geochemistry, Geophysics, Geosystems 12, Q0AD13. doi:10.1029/2010GC003431.

Stoll, R.D., 1974. Effects of gas hydrates in sediments, in: Kaplan, I.R. (Ed.), Natural Gases in Marine Sediments. Plenum, New York, 235-247.

Subrahmanyam, D., Rao, P.H., 2008. Seismic attributes-A review. *7th International Conference & Exposition on Petroleum Geophysics.* Hyderabad, P-398.

Suess, E., Torres, M.E., Bohrmann, G., Collier, R.W., Greinert, J., Linke, P., Rehder, G., Tréhu, A.M., Wallmann, K., Winckler, G., Zuleger, E., 1999. Gas hydrate destabilization: enhanced dewatering, benthic material turnover and large methane plumes at the Cascadia convergent margin. *Earth and Planetary Science Letters* 170, 1-15.

Suess, E., von Huene, R., (Eds.), 1988. Proceedings of the Ocean Drilling Program, Initial Reports Leg 112, College Station, Texas, 1,015 p.

Sultan, N., 2007. Excess pore pressure and slope failures resulting from gas-hydrates dissociation and dissolution. Offshore Technology Conference Houston, Texas, April 30-May 3, 2007. OTC18532.

Sultan, N., Cochonat, P., Foucher, J.P., Mienert, J., 2004. Effect of gas hydrates melting on seafloor slope instability. *Marine Geology* 213(1-4), 379-401

Sugihara,T., Kinoshita, M., Eichiro, A., Toshinori, K., Masanori, K., Yasuhiro, N., Yukari, K., Yoshinori, S., Moe, T., 2014. Re-evaluating the temperature at the updip limit of locked portion of Nankai megasplay inferred from IODP Site C0002 temperature observatory. Earth, Planets and Space 66(1), 1-14. doi: 10.1186/1880-5981-66-107.

Sun, Y., Wu, S., Dong, D., Lüdmann, T., Gong, Y., 2012. Gas hydrates associated with gas chimneys in fine-grained seiments of the northern South China Sea. Marine Geology 311-314, 32-40. doi: 10.1016/j.margeo.2012.04.003.

Suzuki, K., Schultheiss, P., Nakatsuka, Y., Ito, T., Egawa, K., Holland, M., Yamamoto, K., 2015. Physical properties and sedimentological features of hydrate-bearing samples recovered from the first gas hydrate production test site on Daini-Atsumi Knoll around eastern Nankai Trough. *Marine and Petroleum Geology*: In Press. doi: 10.1016/j.marpetgeo.2015.02.025.

Suzuki, K., Narita, H., 2010. Estimation of permeability of methane hydrate-bearing strata of Nankai Trough, in comparison to core measurement vs. CMR analysis. Journal of the Japanese Association for Petroleum Technology 75(1), 98-105. doi:10.3720/japt.75.98.

Taira, A., Curewitz, D., Hashimoto, T., Ibusuki, A., Kuramoto, S.i., Okano, T., Tanaka, H., 2005. Nankai Trough Seismogenic Site Survey: Kumano Basin Seismic Survey, Philippine Sea, Offshore Kii Peninsula, Japan, in: Taira, A., Daniel, C. (Eds.), CDEX Technical Report Volume 1, p. 64.

Takahashi, H., Tsuji, Y., 2005. Multi-well exploration program 2004 for natural hydrate in the Nankai-Trough offshore Japan. *Proceedings of 2005 Offshore Technology Conference Houston, Texas*, 2-5 May 2005, OTC17162.

Takahashi, H., Yonezawa, T., Takedomi, Y., 2001. Exploration for natural hydrate in Nankai-Trough wells offshore Japan. *Proceedings of Offshore Technology Conference* 2001, OTC13040.

Takahashi, M., 2006. Tectonic development of the Japanese islands controlled by Philippine Sea Plate motion. *Journal of Geography* 115, 116-123.

Takano, O., Fujii, T., Saeki, T., Shimoda, N., Noguchi, S., Nishimura, M., Takayama, T., Tsuji, T., 2010. Applications of sedimentological methodology to the methane-hydrate exploration project in the eastern Nankai Trough area (English Abstract and Figure Labels). *Journal of the Japanese Association for Petroleum Technology* 75(1), 30-41.

Takano, O., Itoh, Y., Kusumoto, S., 2013. Variations in forearc basin configuration and basin filling depositional systems as a function of trench slope break development and strike-slip movement: Examples from the Cenozoic Ishikari-Sanriku-Oki and Tokai-Oki-Kumano-Nada forearc basins, Japan. In: *Mechanism of sedimentary basin formation- multidisciplinary approach on active plate margins, InTech,* Chapter 1. doi: 10.5772/56751.

Taladay, K.T., Expedition 353 Scientists, 2015. Pore water evidence for Methane Hydrates and Fluid Origins in the Mahanadi Basin, Offshore India. Goldschmidt 2015, Prague. Abstract:5915.

Taladay, K.T., Moore, G.F., 2015. Fire in the Ice 15 (1): Methane Hydrate Newsletter, US Dept. of Energy, Office of Fossil Energy. National Energy Laboratory, 1-4. http://www.netl.doe.gov/research/oil-and-gas/methane-hydrates/fire-in-the-ice.

Tanahashi M., Submarine surface geology and methane hydrate in the Nankai Trough available online at: http://earth.kumst.kyoto-u.ac.jp/prismfluid/proc/01162515(rev).pdf

Tay, J.S., Kumar, A., Sudheer, A.K., Deshpande, R.D., Rao, D.K., Patil, D.J., Awasthi, N., Bhutani, R., Bhushan, R., Dayal, A.M., 2013. Origin of gases and water in mud volcanoes of Andaman accretionary prism: implications for fluid migration in forearcs. *Chemical Geology* 347, 102-113.

Tanner, M.T., 2001. Seismic attributes. Can. Soc. Exploration Geophysical Research 26(9), 48-45.

Teichert, B.M.A., Johnson, J.E., Soloman, E.A., Goisan, L., Rose, K., Kocherla, M., Connoly, E.C., Torres, M.E., 2014. Composition and origin of authigenic carbonates in the Krishna-Godavari and Mahanadi Basins, eastern continental margin of India. *Marine and Petroleum Geology* 58, 438-460. doi:10.1016/j.marpetgeo.2014.08.023.

Teichert, B.M.A., Torres, M.E., Bohrmann, G., Eisenhauer, A., 2005. Fluid sources, fluid pathways and diagenetic reactions across an accretionary prism revealed by Sr and B geochemistry. Earth and Planetary Science Letters 239, 106.

Thakur, N.K., Rajput, S., 2010. Exploration of gas hydrates: Geophysical techniques. *Springer Science & Business Media*, Technology & Engineering, 292p.

Tinivella, U., Giustiniani, M., 2011. Gas hydrate, free gas and overpressure. *Proceedings of the 7th International Conference on Gash Hydrates (ICGH).* 4p.

Tinivella, U., Giustiniani, M., 2013. Variations in BSR depth due to gas hydrate stability versus pore pressure. Global and Planetary Change 100, 119-128. doi: 10.1016/j.gloplacha.2012.10.012.

Tobin, H.J., Kinoshita, M., 2006. NanTroSEIZE: The IODP Nankai Trough Seismogenic Zone Experiment. *Scientific Drilling* 2, 23-27. doi: 10.2204/iodp.sd.2.06.2006.

Toki, T., Tsunogai, U., Gamo, T., Kuramoto, S., Ashi, J., 2004. Detection of low-chloride fluids beneath a cold seep field on the Nankai accretionary wedge off Kumano, south of Japan. Earth and Planetary Science Letters 228, 37.

Toki, T., Uehara, Y., Kinjo, K., Ijiri, A., Tsunogai, U., Tomaru, H., Ashi, J., 2012. Methane production and accumulation in the Nankai accretionary prism: Results from IODP Expedition 345 and 316. Geochemical Journal 46, 89-106.

Tomaru, H., Fehn, U., 2015. Movement of fluids in the Nankai trough area: Insights from ^{129}I and halogen distributions along the IODP NanTroSEIZE transect. *Geochimica et Cosmochimica Acta* 149, 64-78. doi: 10.1016/j.gca.2014.10.028.

Tomaru, H., Torres, M.E., Matsumoto, R., Borowski, W., 2006. Effect of massive gas hydrate formation on the water isotopic fractionation of gas hydrate system at Hydrate Ridge, Cascadia margin, offshore Oregon. Geochemistry, Geophysics, Geosystems 7(1), Q10001. doi:10.1029/2005GC001207.

Torres, M.E., Tréhu, A.M., Cespedes, N., Kastner, M., Wortmann, U.G., Kim, J-H, Long, P., Malinverno, A., Pohlman, J.W., Riedel, M., Collett, T.S., 2008. Methane hydrate formation in turbidite sediments of northern Cascadia, IODP Expedition 311. Earth and Planetary Science Letters 271, 170-180. doi:10.1016/j.epsl.2008.03.061.

Tréhu, A.M., Long, P.E., Torres, M.E., et al., 2004. Three-dimensional distribution of gas hydrate beneath southern Hydrate Ridge: constraints from IODP Expedition 311. *Earth and Planetary Science Letters* 222, 846-862. doi: 10.1016/j.epsl.2004.03.035.

Tréhu, A.M., Torres, M., Moore, G.F., Suess, E., Bohrmann, G., 1999. Temporal and spatial evolution of a gas-hydrate-bearing accretionary ridge on the Oregon continental margin. Geology 27, 939-942.

Tsuji, Y. et al., 2009. Methane hydrate occurrence and distribution in the eastern Nankai Trough, Japan: Findings of the Tokai-oki to Kumano-nada methane hydrate drilling program; in Collett, T. et al., eds., Natural gas hydrates—Energy resource potential and associated geologic hazards: AAPG Memoir 89.

Tsuji, Y., Ishida, H., Nakamizu, M., Matsumoto, R., Shimizu, S., 2004. Overview of the METI Nankai Trough wells: A milestone in evaluation of methane hydrate resources. *Resource Geology* 54(1), 3-10.

Tsuji, T., Kamei, R., Pratt, R.G., 2014. Strike-slip motion of a megasplay fault system in the Nankai subduction zone. *Earth, Planets and Space* 66(1), 120. doi: 10.1186/1880-5981-66-120.

Tsuji, T., Kamei, R., Pratt, R.G., 2014b. Pore pressure distribution of a mega-splay fault system in the Nankai Trough subduction zone: Insights into the up-dip extent of the seismogenic zone. *Earth and Planetary Science Letters*, 396, 165-178. doi: 10.1016/j.epsl.2014.04.011.

Tsunogai, U., Maegawa, K., Sato, S., Komatsu, D.D., Nakagawa, F., Toki, T., Ashi, J., 2012. Coseismic massive methane release from a submarine mud volcano. *Earth and Planetary Science Letters* 241-244, 79-85. doi:10.1016/j.epsl.2012.06.004.

Tyron, M.D., Brown, K.M., Torres, M.E., 2002. Fluid and chemical flux in and out of sediments hosting methane hydrate deposits on Hydrate Ridge, OR. II: Hydrological processes. *Earth Planetary Science Letters* 201(3-4), 541-557. doi:10.1016/S0012-821X(02)00732-X.

Uchida, T., Hirano, T., Ebinuma, T., Narita, H., Gohara, K., Mae, S., Matsumoto, R., 1999. Raman spectroscopic determination of hydrate number of methane hydrates. AIChE J., 45, 2641–2645, doi:10.1002/aic.690451220

Uchida, T., Takeya, S., Chuvilin, E.M., Ohmura, R., Nagao J., Yakushev, V.S., Istomin, V.A., Minagawa, H., Ebinuma, T., Narita, H., 2004. Decomposition of methane hydrates in sand, sandstone, clays, and glass beads. Journal of Geophysical Research 109, B05206. doi: 10.1029/2003JB002771.

Uchida, T., Waseda, A., Namikawa, T., 2008. Methane accumulation and high concentration of gas hydrate in marine and terrestrial sandy sediments, in Collett, T., Johnson, A., Knapp, C., Boswell, R., eds., Natural gas hydrates: Energy resource potential and associated geologic hazards: *AAPG Special publication*.

Underwood, M.B., Moore, G.F., 2012. Evolution of sedimentary environments in the subduction zone of southwest Japan: recent results from the NanTroSEIZE Kumano transect. In: Busby, C., Azor, A., (Eds.) Tectonics of Sedimentary Basins: Recent Advances. Blackwell Publishing ltd., p. 310-326.

Usman, M.O., Masago, H., Winkler, W., Strasser, M., 2014. Mid-Quaternary decoupling of sediment routing in the Nankai Forearc revealed by provenance analysis of tubiditic sands. *International Journal of Earth Sciences* 103.4, 1141-1161. doi: 10.1007/s00531-014-1011-z.

Ussler III, W., Paull, C.K., 2001. Ion exclusion associated with marine gas hydrate deposits. In: Paull, C.K., Dillon, W.P. (Eds.) Natural Gas Hydrate: Occurrence, Distribution and Detection. American Geophysical Union. Washington DC, p. 41-51.

Vanneste, H., Kastner, M., James, R.H., Connelly, D.P., Fisher, R.E., Kelly-Gerreyn, B.A., Heeschen, K., Haeckel, M., Mills, R.A., 2012. Authigenic carbonates from the Darwin Mud Volcano, Gulf of Cadiz: A record of palaeo-seepage of hydrocarbon bearing fluids. *Chemical Geology* 300-301, 24-39. doi:10.1016/j.chemgeo.2012.01.006.

Vanneste, M., Sultan, N., Garziglia, S., Forsberg, C.F., L'Heureux, J.-S., 2014. Seafloor instabilities and sediment deformation processes: The need for integrated, multi-disciplinary investigations. *Marine Geology* 352,183-214. doi:10.1016/j.margeo.2014.01.005.

Von Huene, R., Pecher, I.A., 1999. Vertical tectonics and the origins of BSRs along the Peru margin. Earth and Planetary Science Letters 166, 47-55.

Waite, W.F., Santamarina, J.C., Cortes, D.D., Dugan, B., Espinoza, D.N., Germaine, J., Jang,J., Jung, J.W., Kneafsey, T.J., Shin, H., Soga, K., Winters, W.J., Yun, T-S., 2009. Physical properties of hydrate-bearing sediments. *Reviews of Geophysics* 47(4), RG4003. doi: 10.1029/2008RG000279.

Wallace, P.J., Dickens, G.R., Paull, C.K., Ussler, W., 2000. Effects of core retrieval and degassing on the carbon isotope composition of methane in gas hydrate and free gas-bearing sediments from Blake Ridge. In: Paull, C.K., Matsumoto, R., Wallace, P.J., and Oillon, W.P., (Eds.) *Proceedings of the Ocean Drilling Program, Scientific Results*, College Station.

Walsh, M., Rainey, J.D., Lafond, P.G., Park, D.-H., Beckham, G.T., Jones, M.D., Lee, K.-H., Koh, C.A., Sloan, E.D., Wu, D.T., Sum, A.K., 2011. The cages, dynamics, and structuring of incipient methane clathrates hydrates. *Phys. Chem. Chem. Phys.* 13, 19951-19959. doi: 10.1039/c1cp21899a.

Wang, J., Sain, K., Wang, X., Satyavani, N., Wu, S., 2014. Characteristics of bottom-simulating reflectors for hydrate-filled fractured sediments in Krishna-Godavari basin, eastern Indian margin. *Journal of Petroleum Science and Engineering* 122, 515-523.

Wang, K., Hyndman, R.D., Davis, E.E., 1993. Thermal effects of sediment thickening and fluid expulsion in accretionary prism: model and parameter analysis. *Journal of Geophysical Research* 98, 9975-9984.

Wang, P., Huang, X., Pang, S., Zhu, Y., Zhenquan, L., Zhang, S., Liu, H., Yang, K., Li, B., 2015. Geochemical dynamics of the gas hydrate system in the Qilian Mountain Permafrost, Qinghai, northwest China. *Marine and Petroleum Geology* 59, 72-90. doi:10.1016/j.marpetgeo.2014.07.009.

Wang, X., Lee, M., Collett, T., Yang, S., Guo, Y., Wu, S., 2014. Gas hydrate identified in sand-rich inferred sedimentary section using downhole logging and seismic data in Shenhu area, S. China Sea. Marine and Petroleum Geology 51, 298-306. doi:10.1016/j.marpetgeo.2014.01.002.

Waseda, A., Uchida, T., 2004. The geochemical context of gas hydrate in the eastern Nankai Trough. *Resource Geology* 54, 69-78.

Winters, W.J., Wilcox-Cline, R.W., Long, P., Dewri, S.K., Kumar, P., Stern, L., Kerr, L., 2014. Comparison of the physical and geotechnical properties of gas-hydrate-bearing sediments from offshore India and other gas-hydrate-reservoir systems. *Marine and Petroleum Geology* 58, 139-167. doi:10.1016/j.marpetgeo.2014.07.024.

Witicar, M.J., 1999. Carbon and Hydrogen isotope systematics of bacterial formation and oxidation of methane. *Chemical Geology* 161, 291-314.

Weinberger, J.L., Brown, K.M, 2006. Fracture networks and hydrate distribution at Hydrate Ridge, Oregon. *Earth and Planetary Science Letters* 245, 123-136.

Weinberger, J.L., Brown, K.M., Long, P.E., 2005. Painting a picture of gas hydrate distribution with thermal images. Geophysical Research Letters 32(4), L074609. doi: 10.1029/2004GL021437.

Wenqing, L., Jing, G., Xiaofang, L., Jiankui, Z., Yaorong, F., Da, Y., 2013. A study of hydrate plug formation in subsea natural gas pipeline using a novel high-pressure flow loop. Petroleum Science 10, 97-105. doi:10.1007/s12182-013-0255-8.

Wood, W.T., Gettrust, J.F., Chapman, N.R., Spence, G.D., Hyndman, R.D., 2002. Decreased stability of methane hydrates in marine sediments owing to phase-boundary roughness. Nature 420, 656-660.

Wu, N., Zhang, H., Yang, S., Zhang, G., Liang, J., Lu, J., Su, X, Schultheiss, P., Holland, M., Zhu, Y., 2011. Gas Hydrate System of Shenhu Area, Northern South China Sea: Geochemical Results. Journal of Geological Research. doi:10.1155/2011/370298.

Xie, L., Wang, J. S., Wu, N. Y., Wu, D. D., Zhou, W., Zhu, X. W., Hu, J., Chen, H. R., Lin, Q., 2013. Characteristics of authigenic pyrites in shallow core sediments in the Shenhu area of the northern South China Sea: Implications for a possible mud volcano environment. *Science China: Earth Science* 56, 541-548.

Yamada, Y., Baba, K., Miyakawa, A., Matsuoka, T., 2014. Granular experiments of thrust wedges: Insights relevant to methane hydrate exploration at the Nankai accretionary prism. *Marine and Petroleum Geology* 51, 34-48. doi: 10.1016/j.marpetgeo.2013.11.008.

Yamano, M., Foucher, J.P., Kinoshita, M., Fisher, A., Hyndman, R.D., ODP Leg 131 Shipboard Scientific Party, 1992. Heat flow and fluid flow regime in the western Nankai accretionary prism. *Earth and Planetary Science Letters* 109, 451-462.

Yamano, M., Kinoshita, M., Goto, S., Matsubayashi, O., 2003. Extremely high heat flow anomaly in the middle part of the Nankai Trough. *Physics and Chemistry of the Earth* 28, 487-497.

Yamano, M., Uyeda, S., Aoki, Y., Shipley, T.H., 1982. Estimates of heat flow derived from gas hydrates. Geology 10, 339-343.

Yang, J., Davies,R.J., Huuse, M., 2013. Gas migration below gas hydrates controlled by mass transport complexes, offshore Mauritania. *Marine and Petroleum Geology* 48, 366-378. doi:10.1016/j.marpetgeo.2013.09.003.

Yefremova, A., Zhizhchenko, B., 1974. Occurrence of crystal hydrates of gases in the sediments of modern marine basins. *Doklady Akademii Nauk SSSR* 214(5), 2397-2400.

Yelisetti, S., Spence, G.D., Riedel, M., 2014. Role of gas hydrates in slope failure on frontal ridge of northern Cascadia margin. Geophysical Journal International 199, 441-458. doi: 10.1093/gji/ggu254.

Yi, B.Y., Lee, G.H., Horozal, S., Yoo, D.G., Ryu, B.J., Kang, N.K., Lee, S.R., Kim, H.J., 2011. Qualitative assessment of gas hydrate and gas concentrations from the AVO characteristics of the BSR in the Ulleung Basin, East Sea (Japan Sea). *Marine and Petroleum Geology* 28, 1953-1966.

Yoo, D.G., Kang, N.K., Yi, B.Y., Kim, Y.G., Ryu, B.J., Lee, K., Lee, G.H., Riedel, M., 2013. *Marine and Petroleum Geology* 47, 236-247. doi: 10.1016/j.marpetgeo.2013.07.001.

Yoshioka, S., Suminokura, Y., Matsumoto, T., Nakajima, J., 2013. Two-dimensional thermal modeling of subduction of the Philippine Sea plate beneath southwest Japan. Tectonophysics 608, 1094-1108. doi: 10.1016/j.tecto.2013.07.003.

Yu, X., Wang, J., Liang, J., Li, S, Zeng, X., Li, W., 2014. Depositional characteristics and accumulation model of gas hydrates in northern South China Sea. *Marine and Petroleum Geology* 56, 74-86.

Yuan, T., Hyndman, R.D., Spence, G.D., Desmons, B., 1996. Seismic velocity increase and deep-sea gas hydrate concentration above a bottom-simulating reflector on the northern Cascadia continental slope. *Journal of Geophysical Research* 101(6), 13655-13671.

Yuan, Q., Sun, C.Y., Yang, X., Ma, P.C., Ma, Z.W., Liu, B., Ma, Q.-L., Yang, L.-Y., Chen, G.-J., 2012. Recovery of methane from hydrate reservoir with gaseous carbon dioxide using a three-dimensional middle-size reactor. *Energy* 40, 47-58.

Zahnle, K. J., Korycansky, D. G., Nixon, C.A., 2014. Transient climate effects of large impacts on Titan. Icarus 229, 378-391. doi:10.1016/j.icarus.2013.11.006.

Zhang, M., Konishi, H., Xu, H., Sun, X., Lu, H., Wu, D. and Wu, N., 2015. Morphology and formation mechanism of pyrite induced by the anaerobic oxidation of methane from the continental slope of the NE South China Sea. Journal of Asian Earth Sciences, 92, 1: 293-301.

Zhang, Y., Xu, Z., 2003. Kinetics of convective crystal dissolution and melting with applications to methane hydrate dissolution and dissociation in seawater. *Earth and Planetary Science Letters* 213, 133-148.

Zhang, Z., Han, D., 2010. Seismic interpretation of gas hydrate based on physical properties of sediments. SEG 2010 Annual Meeting, Denver, CO. Technical Program Expanded Abstract, 1452-1456.

Zwart, G., Moore, J.C., Cochrane, G.R., 1996. Variations in temperature gradients identify active faults in the Oregon accretionary prism. *Earth and Planetary Science Letters* 139, 485-495.